



Sociedad Mexicana de Bioquímica, A.C.

FUNDADA EN 1957

AVE. CIPRESES S/N COL. SAN ANDRÉS TOTOLTEPEC
C.P. 14400 MÉXICO, D.F.
APARTADO POSTAL 70-806, CIUDAD UNIVERSITARIA
TEL. Y FAX. (55)5622-5742
<http://www.smb.org.mx>
Correo Electrónico: smbq@ifc.unam.mx

MESA DIRECTIVA 2015 - 2017

PRESIDENTE
DR. MIGUEL LARA FLORES

VICE-PRESIDENTE
DRA. IRENE BEATRIZ CASTAÑO NAVARRO

SECRETARIA TESORERA
DRA. ELDA GUADALUPE ESPIN OCAMPO

SUB-SECRETARIO TESORERO
DR. JORGE LUIS FOLCH MALLOL

SOCIOS FUNDADORES

Dr. Barbarín Arreguín Lozano
Dr. Edmundo Calva Cuadrilla
Dr. Guillermo Carvajal Sandoval (†)
Dr. Joaquín Cravioto (†)
Dr. Carlos del Río Estrada (†)
Dr. Silvestre Frenk Freund
Dr. Mario García Hernández (†)
Dr. Jesús Guzmán García (†)
Dr. Jesús Kumate Rodríguez
Dr. José Laguna García (†)
Dr. Guillermo Massieu Helguera (†)
Dr. Raúl Oндarza Vidaurreta
Dr. Efraín G. Pardo Codina
Dr. Guillermo Soberón Acevedo

Otorga la presente

CONSTANCIA a:

María Irene Betancourt Conde

Quien asistió y presentó el trabajo:

Leishmanicidal drug design. Induce fit studies to find potential inhibitors against arginase from *Leishmania Mexicana*

Por:

María Irene Betancourt Conde, Alondra Chaidez Avila,
Alejandra Guadalupe Vázquez Raygoza, José Luis Urbán Martínez,
Daniel Enríquez Mendiola, Claudia Isela Avitia Domínguez, Antonio
Romo Mancillas, Alicia Hernández Campos, Alfredo Téllez Valencia

En la modalidad de cartel durante el XXXI Congreso Nacional de Bioquímica del 6 al 11 de noviembre de 2016 en Aguascalientes, Ags.

Atentamente
Por el Comité Organizador

Dr. Miguel Lara Flores
Presidente



American Chemical Society

Membership Division
Department of Meetings & Expositions Services
Nancy C. Todd

1155 SIXTEENTH STREET, N.W.
WASHINGTON, D.C. 20036
Phone: 614-447-3776
Email: maps@acs.org

THIS IS TO CERTIFY THAT

Irene Betancourt

ATTENDED THE

253rd AMERICAN CHEMICAL SOCIETY NATIONAL MEETING
San Francisco, CA, USA
April 2-6, 2017

AND PRESENTED THE FOLLOWING PAPER:

Title: Inhibition of arginase from *Leishmania mexicana* by
benzimidazole derivatives
Number: 227
Session: General Posters
Type: Poster
Program: **Medecinal**
Date: 4/2/2017

Nancy C Todd





Sociedad Mexicana de Bioquímica, A.C.

FUNDADA EN 1957

AVE. CIPRESES S/N COL. SAN ANDRÉS TOTOLTEPEC
C.P. 14400 MÉXICO, D.F.
APARTADO POSTAL 70-606, CIUDAD UNIVERSITARIA
TEL. Y FAX. (55)5622-5742
<http://www.smb.org.mx>
Correo Electrónico: smbq@ifc.unam.mx

MESA DIRECTIVA 2015 - 2017

PRESIDENTE
DR. MIGUEL LARA FLORES

VICE-PRESIDENTE
DRA. IRENE BEATRIZ CASTAÑO NAVARRO

SECRETARIA TESORERA
DRA. ELDA GUADALUPE ESPIN OCAMPO

SUB-SECRETARIO TESORERO
DR. JORGE LUIS FOLCH MALLOL

SOCIOS FUNDADORES

Dr. Barbarín Arreguín Lozano
Dr. Edmundo Calva Cuadrilla
Dr. Guillermo Carvajal Sandoval (†)
Dr. Joaquín Cravioto (†)
Dr. Carlos del Río Estrada (†)
Dr. Silvestre Frenk Freund
Dr. Mario García Hernández (†)
Dr. Jesús Guzmán García (†)
Dr. Jesús Kumate Rodríguez
Dr. José Laguna García (†)
Dr. Guillermo Massieu Helguera (†)
Dr. Raúl Ondarza Vidaurreta
Dr. Efraín G. Pardo Codina
Dr. Guillermo Soberón Acevedo

Otorga la presente

CONSTANCIA a:

Mara Ibeth Campos Almazán

Quien asistió y presentó el trabajo:

**Effect of *Moringa oleifera* extract on glutaminase-1 activity in
a breast cancer murine model**

Por:

Mara Ibeth Campos Almazán, Jessica Lizbeth Hernández Rivera,
Jaime Abraham de Lira Sánchez, Erick Sierra Campos, Mónica Andrea
Valdez Solana, Claudia Isela Avitia Domínguez, Alfredo Téllez Valencia

En la modalidad de cartel durante el XXXI Congreso Nacional de
Bioquímica del 6 al 11 de noviembre de 2016 en Aguascalientes, Ags.

Atentamente
Por el Comité Organizador

Dr. Miguel Lara Flores
Presidente

Otorga la presente

CONSTANCIA a:

Mara Ibeth Campos Almazán

Quien asistió y presentó el trabajo:

Computational approach to optimize the PTP1B inhibitor JM151

Por:

Mara Ibeth Campos Almazán, Alfredo Téllez Valencia, María Alicia Hernández Campos,
Antonio Romo Mancillas, Erick Sierra Campos, Mónica Andrea Valdez Solana,
Claudia Isela Avitia Domínguez

En la modalidad de presentación oral durante el
XXXII Congreso Nacional de Bioquímica
4 - 9 de noviembre de 2018, Ixtapa Zihuatanejo, Gro.

Atentamente



Dra. Irene B. Castaño Navarro
Presidente

SOCIEDAD MEXICANA DE BIOQUIMICA A.C.

Otorga la presente

CONSTANCIA a:

Daniel Isaac Enríquez Mendiola

Quien asistió y presentó el trabajo:

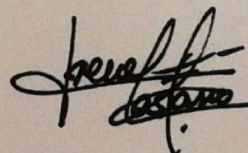
Structural similarity search and biochemical characterization of methicillin resistant *Staphylococcus aureus* shikimate dehydrogenase inhibitors

Por:

Daniel Isaac Enríquez Mendiola; Alfredo Téllez Valencia; Mónica Andrea Valdez Solana, Erick Sierra Campos, Claudia Isela Avitia Domínguez

En la modalidad de presentación oral durante el
XXXII Congreso Nacional de Bioquímica
4 - 9 de noviembre de 2018, Ixtapa Zihuatanejo, Gro.

Atentamente



Dra. Irene B. Castaño Navarro
Presidente



MESA DIRECTIVA 2017 - 2019

PRESIDENTE
DRA. IRENE BEATRIZ CASTAÑO NAVARRO

VICEPRESIDENTE
DR. DAVID RENÉ ROMERO CAMARENA

SECRETARIO TESORERO
DR. JORGE LUIS FOLCH MALLÓL

SUBSECRETARIA TESORERA
DRA. MARÍA SOLEDAD FUNES ARGÜELLO

SOCIOS FUNDADORES

Dr. Barbarín Arreguín Lozano
Dr. Edmundo Calva Cuadrilla
Dr. Guillermo Carvajal Sandoval (†)
Dr. Joaquín Cravioto (†)
Dr. Carlos del Río Estrada (†)
Dr. Silvestre Frenk Freund
Dr. Mario García Hernández (†)
Dr. Jesús Guzmán García (†)
Dr. Jesús Kumate Rodríguez
Dr. José Laguna García (†)
Dr. Guillermo Massieu Helguera (†)
Dr. Raúl Ondarza Vidaurreta
Dr. Efraín G. Pardo Codina
Dr. Guillermo Soberón Acevedo

Otorga la presente

CONSTANCIA a:

Luis Enrique Pérez Del Castillo

Quien asistió y presentó el trabajo:

**Exploring chemical space to find potential inhibitors
of protein tyrosine phosphatase 1B**

Por: Luis Enrique Pérez del Castillo, Claudia Isela Avitia Domínguez,
Marcelo Gómez-Palacio Gastelum, Jorge Cisneros Martínez,
Alfredo Téllez Valencia

En la modalidad de cartel durante el
XXXII Congreso Nacional de Bioquímica
4 - 9 de noviembre de 2018 en Ixtapa, Zihuatanejo, Gro.

Atentamente
Por el Comité Organizador

Dra. Irene B. Castaño Navarro
Presidente

Targeting *Plasmodium* Metabolism to Improve Antimalarial Drug Design

Claudia Avitia-Domínguez¹, Erick Sierra-Campos², Irene Betancourt-Conde¹, Miriam Aguirre-Raudry¹, Alejandra Vázquez-Raygoza¹, Artemisa Luevano-De la Cruz¹, Alejandro Favela-Candia¹, Marie Sarabia-Sanchez¹, Lluvia Ríos-Soto¹, Edna Méndez-Hernández¹, Jorge Cisneros-Martínez¹, Marcelo Gómez Palacio-Gastélum³, Mónica Valdez-Solana², Jessica Hernández-Rivera², Jaime De Lira-Sánchez², Mara Campos-Almazán² and Alfredo Téllez-Valencia^{1,*}

¹Facultad de Medicina y Nutrición, Universidad Juárez del Estado de Durango, Av. Universidad y Fanny Anitua S/N, Durango. Dgo. México, C.P. 34000; ²Facultad de Ciencias Químicas, Universidad Juárez del Estado de Durango, Av. Artículo 123 S/N Fracc. Filadelfia, Gómez Palacio, Durango, CP. 35010, México; ³Facultad de Odontología, Universidad Juárez del Estado de Durango, Predio Canoas S/N, Colonia Los Ángeles, Durango. Dgo. México, C.P. 34070

Abstract: Malaria is one of the main infectious diseases in tropical developing countries and represents high morbidity and mortality rates nowadays. The principal etiological agent *P. falciparum* is transmitted through the bite of the female Anopheles mosquito. The issue has escalated due to the emergence of resistant strains to most of the antimalarials used for the treatment including Chloroquine, Sulfadoxine-Pyrimethamine, and recently Artemisinin derivatives, which has led to diminished effectiveness and by consequence increased the severity of epidemic outbreaks. Due to the lack of effective compounds to treat these drug-resistant strains, the discovery or development of novel anti-malaria drugs is important. In this context, one strategy has been to find inhibitors of enzymes, which play an important role for parasite survival. Today, promising results have been obtained in this regard, involving the entire *P. falciparum* metabolism. These inhibitors could serve as leads in the search of a new chemotherapy against malaria. This review focuses on the achievements in recent years with regard to inhibition of enzymes used as targets for drug design against malaria.

Keywords: Malaria, *Plasmodium falciparum*, enzyme inhibition, drug design.

1. INTRODUCTION

Malaria is the most important disease caused by a parasite. According to the last WHO report [1], malaria affects 104 countries, and 3.4 billion people are at risk, an estimated 627 000 deaths occurred and 207 million of new cases were presented in 2012. Africa was the most affected by the 80% of the cases and the 90% of the deaths, children under 5 years were the majority of them (77%). Five species of the genus *Plasmodium* cause malaria, *P. knowlesi*, *P. vivax*, *P. falciparum*, *P. malariae*, and *P. ovale*. Although *P. vivax* is more widely distributed than *P. falciparum* worldwide, most of the deaths are due to *falciparum*.

Uncomplicated malaria courses with symptoms that could be confused with another type of common diseases, these include abdominal discomfort, irregular fever, fatigue, vague absence of well-being, and muscle aches, and frequently, vomiting, nausea and orthostatic hypotension are present. Conversely, severe malaria caused by *P. falciparum*

affects different organs in a very important manner such as cerebral malaria, pulmonary edema, jaundice, acidosis, hypoglycemia, severe anemia, and acute kidney injury. In addition, cases of severe malaria caused by *P. vivax* have been reported in several countries recently [2].

Malaria treatment includes a variety of drugs, such as Dihydroartemisinin, Artemether, Artesunate, Piperaquine, Sulfadoxine, Lumefantrine, Chloroquine, Quinine, Atovaquone, Mefloquine, Pyrimethamine, Primaquine, Proguanil, Amodiaquine, and Pyronaridine [3]. Because of the development of resistance to these antimalarials by *P. falciparum* strains [4] WHO recommended the use of a combination therapy named ACT (Artemisinin based combination therapy) that includes one Artemisinin derivative plus another drug. Generally, it was an excellent strategy saving thousands of lives around the world. However, resistance to ACT or Artemisinin derivatives has been reported [1, 5]. This situation raises the necessity to find new drugs against malaria. To this end, different macromolecules from *P. falciparum* have been used as targets for drug discovery. These are quite diverse and include enzymes of the respiratory chain in the parasite mitochondria [6], several transport proteins [7], enzymes in the fatty acid synthetic pathway [8], glycolysis pathway [9], a number of proteases [10], and DNA replication and regula-

*Address correspondence to this author at the Facultad de Medicina y Nutrición, Universidad Juárez del Estado de Durango, Av. Universidad y Fanny Anitua S/N, Durango. Dgo. México, C.P. 34000; Tel:/Fax: (+52)6188121687; E-mail: atellez@ujed.mx

tion [11]. Drug-resistant malaria parasites are believed to emerge through mutations in the active sites of drug targets [12] or from biochemical changes in the drug receptors. This review will focus specifically on the achievements on enzymes used for this matter, both belonging to a metabolic pathway, as well as working alone (Fig. 1).

2. GLYCOLYTIC PATHWAY AND LACTATE DEHYDROGENASE

Glycolysis is of great importance for *Plasmodium* during the intraerythrocytic stage, the parasite depends on the glucose as an energy source for ATP production [13]. In addition, infected red blood cells consumption of glucose increases substantially at 50-100 times [14], therefore enzymes from this pathway are excellent drug targets for the search of new inhibitors [15]. Some of the enzymes that have been

used include hexokinase [16, 17], phosphoglucose isomerase [18], triose phosphate isomerase [19], lactate dehydrogenase [20, 21], and enolase [22].

Hexokinase is the first enzyme of glycolysis; it is involved in the glucose phosphorylation [14, 23]. The *P. falciparum* HK (PfHK) has a molecular weight of 55.3 kDa and has 24% identity with the human HKs [16]. Therefore, it has been considered a drug target (Fig. 1) [16, 23]. In this context, PfHK inhibitors were identified from a small library of HK inhibitors [16]. Some of these compounds, such as 856002 (Fig. 1, Table 1), exhibited an $IC_{50} < 1 \mu M$, in addition *in vitro* studies showed that various of these compounds inhibited the parasite growth, with an $EC_{50} < 10 \mu M$. Hence, they suggested the great potential of isobenzothiazoline scaffold for the development of a therapeutic agent against *Plasmodium falciparum*.

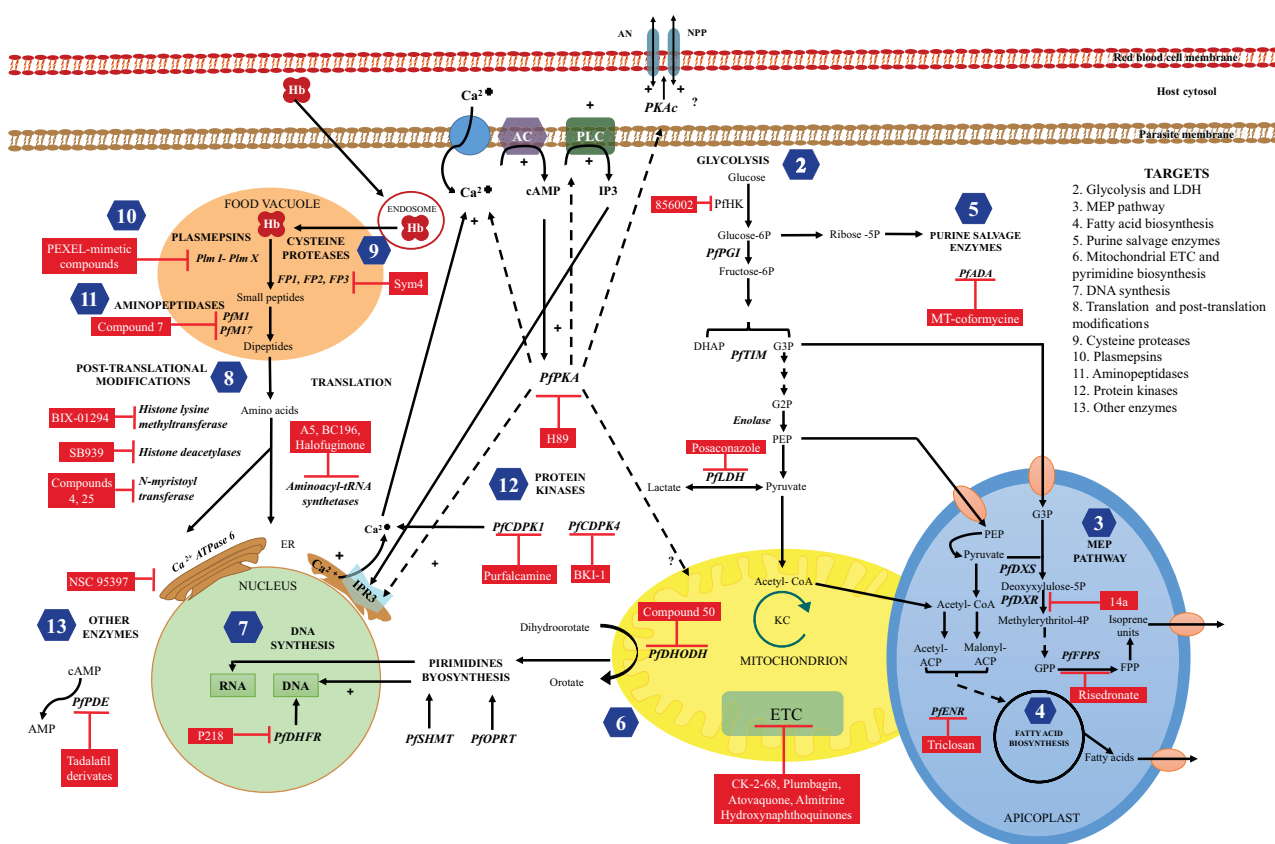


Fig. (1). Overview of metabolic pathways in *P. falciparum*. The targets are indicated by numbers in the hexagons, as they were mentioned in the text. 2) Glycolysis and LDH, 3) MEP pathway, 4) Fatty acid biosynthesis, 5) Purine salvage enzymes, 6) Mitochondrial ETC and pyrimidine biosynthesis, 7) DNA synthesis, 8) Translation and post-translation modification, 9) Cysteine proteases, 10) Plasmepsins, 11) Aminopeptidases, 12) Protein kinases, 13) Other enzymes. The inhibitors are marked in the red boxes. Abbreviations: Pf, *Plasmodium falciparum*; AN, anion channels; NPP, new permeation pathway; PKAc, cAMP dependent protein kinase A; AC, adenylate cyclase; PLC, phospholipase C; IP3, inositol 1,4,5, triphosphate; Hb, haemoglobin; KC, Krebs cycle; MEP, 2 C-methyl-d-erythritol-4-phosphate; PfM1, PfM17, aminopeptidases family 1 and 17; PfPDE, phosphodiesterase; PfCDPK1, PfCDPK4, calcium-dependent protein kinases; ER, endoplasmic reticulum; ETC, electron transport chain; DHAP, dihydroxyacetone phosphate; GPP, geranyl pyrophosphate; FPP, farnesyl pyrophosphate; AMP, adenosine monophosphate; cAMP, cyclic adenosine monophosphate; Plm I, Plm X, plasmepsins family; FP1, FP2, FP3, falcipains family; PfHK, hexokinase; PfPGL, phosphoglucose isomerase; PfTIM, triose phosphate isomerase; PEP, phosphoenolpyruvate; G3P, glyceraldehyde 3-phosphate; G2P, glyceralate 2-phosphate PfLDH, lactate dehydrogenase; PfADA, adenosine deaminase; PfDHODH, dihydroorotate dehydrogenase; PfOPRT, orotate phosphoribosyltransferase; PfDHFR, dihydrofolate reductase; PfSHMT, serine hydroxymethyltransferase; PfDXS, 1-deoxy-D-xylulose 5-phosphate synthase; PfDXR, 1-deoxy-D-xylulose 5-phosphate reductoisomerase; PfFPPS, farnesyl diphosphate synthase; PfENR, enoyl-ACP reductase.

Lactate dehydrogenase (LDH) performs an anaerobic alternative pathway of glucose oxidation. It catalyzes the conversion of pyruvate to lactate. *P. falciparum* enzyme (PfLDH) has multiple structural and kinetic differences compared to human LDH [24, 25] suggesting that this enzyme is an attractive drug target (Fig. 1). Moreover, in the pursuit of PfLDH inhibitors, docking studies using NADH analogues have been performed as well [20]. Itraconazole, atorvastatin, and posaconazole showed the best binding energy and were selected and assessed for antimalarial activity against *P. falciparum* and *P. berghei* in mice. Results showed that these molecules were active against *P. falciparum* clone W2 which is resistant to Chloroquine. In enzyme immunoassays with anti-PfLDH and monoclonal antibodies anti-HRP2 (histidine-rich protein 2), compounds inhibited parasite growth at low doses and the most active was posaconazole (Fig. 1, Table 1).

Recently, traditional Indian herbal extracts, which are employed for the treatment of recurrent fever and symptomatic malaria [21], were evaluated on the recombinant LDH of *P. falciparum* and *P. vivax* strains; the aqueous extract of *Phyllanthus amarus* and the chloroform extract of *Murraya koenigii* showed an inhibitory effect on both recombinant enzymes with an IC₅₀ of 0.1 and 11.2 µg/ml, respectively. Furthermore, these extracts showed *in vitro* antiplasmodial activity in sensitive and Chloroquine resistant strains of *P. falciparum*.

3. MEP PATHWAY

The 2 C-methyl-D-erythritol-4-phosphate (MEP) pathway, also known as non-mevalonate route, was recently discovered. It is present in plants, many bacteria, algae and apicomplexan parasites such as *P. falciparum* [26-28]. Through MEP, organisms synthesize isoprenoids (Fig. 1), compounds that participate in a variety of biological functions such as electron transport, cell signaling, apoptosis, biosynthesis of glycoproteins, protein degradation and membrane structure. The pathway consists of eight steps and involves eight enzymes which are excellent targets for development of herbicides, antimicrobials, and antimalarials. In addition, the non-mevalonate pathway is not found in animals [29].

Studies have shown several enzymes from this pathway as excellent pharmaceutical targets against *P. falciparum*. A metabolic flux study revealed the importance of 1-deoxy-D-xylulose 5-phosphate reductoisomerase (DXR) and 1-deoxy-D-xylulose 5-phosphate synthase (DXS) which have a high flux control coefficient; conversely, the 2-C-methyl-D-erythritol 2,4-cyclodiphosphate synthase (MECPPS) and 1-hydroxy-2-methyl-2- (E) -butenyl 4- diphosphate synthase (HMBPPS) which increase the accumulation of toxic metabolites [30].

1-deoxy-D-xylulose 5-phosphate reductoisomerase (DXR; EC 1.1.1.267) is the second enzyme in this pathway. It catalyzes the conversion of 1-deoxy-D-xylulose 5-phosphate (DXP) to 2- C-methyl-D-erythritol 4-phosphate [31] and is considered a key enzyme in the MEP pathway, therefore, many researchers have focused their interest in DXR [32, 33]. Through a structure-based approach, analogues of Fosmidomycin were designed and their evaluation over the parasite growth was performed. The analogues 14a

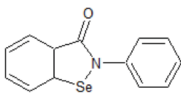
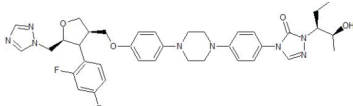
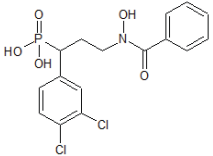
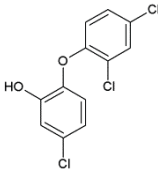
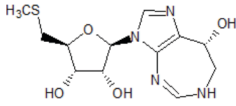
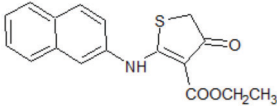
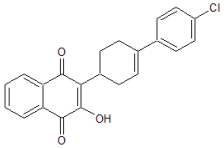
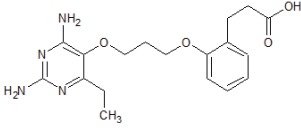
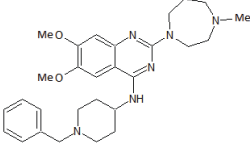
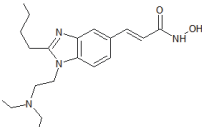
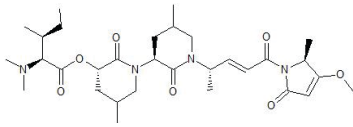
(Fig. 1, Table 1) and 14k showed *in vitro* inhibition in *P. falciparum* 3D7 strain with an IC₅₀ of 0.04 µM and 0.19µM, respectively [34]. In another study, five potential inhibitors of PfDXR were identified through virtual screening using the ZINC database. The compound ZINC00200163 presented the best binding energy (-6.43 KJ/mol) and showed no toxic properties, the inhibitors showed lesser binding energy than Fosmidomycin, Artemether, Quinidine and Mefloquine, which were taken as reference in this study [32]. Therefore the molecules can serve as a guide in the design of new drugs against *P. falciparum* and several reverse analogs of Fosmidomycin were synthesized and evaluated against PfDXR. Two compounds (2a and 2c) showed inhibition within the nanomolar range, and one of them (2c), presented activity blocking parasite growth as well [35].

Otherwise, the farnesyl diphosphate synthase from *P. falciparum* (FPPS) is considered a good target as it differs from its counterpart in humans. The FPPS is involved in the methyl erythritol phosphate pathway that produces essential compounds as ubiquinone [36]. In the search of inhibitors, several bisphosphonate derivatives, previously synthesized and tested as both *P. falciparum* cultures [37] and *P. vivax* FPPS inhibitors [38], were used to carry out 3D-QSAR studies to design a pharmacophore model and looking for potential inhibitors in the SPECS database. Three molecules were found that could serve as starting point to obtain a new class of antimalarials [39].

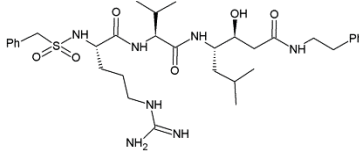
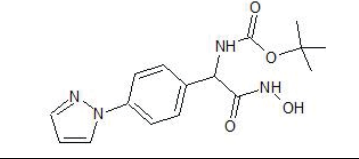
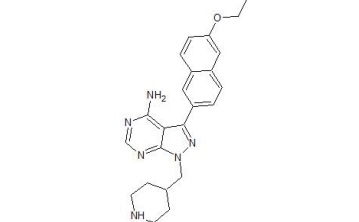
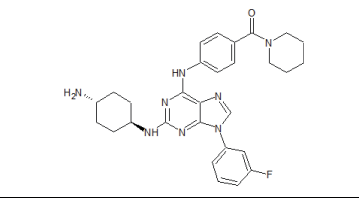
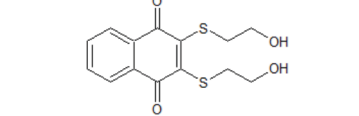
4. FATTY ACID BIOSYNTHESIS

Phospholipids constitute an important part in membrane building; their synthesis involves a series of cycle chemical reactions that implies condensation, reduction, and dehydration of carbon-carbon bonds in the lipid structure. In *P. falciparum*, different from higher eukaryotes where a multifunctional protein (Type I pathway) catalyzes the synthesis of these macromolecules, its process is realized by a dissociated Type II fatty acid synthase (Type II FAS, Fig. 1), a characteristic that makes this enzyme a good target for species-specific inhibition [40, 41]. Previous studies have identified hexachlorophene and analogues as inhibitors with low micromolar IC₅₀ values for PfKAR (an enzyme that participates in the elongation cycle of the acyl-ACP product) [42]. The natural product thiolactomycin (TLM) inhibits the growth of *P. falciparum* with an IC₅₀ value of 50 µM [43]. In addition, TLM analogs have been reported that inhibited parasite growth at low micromolar concentrations [43, 44]. While farnesyl diphosphate synthase (PfFENR) has been validated as an effective antimalarial target, two research groups showed that the growth of *P. falciparum* is inhibited by triclosan with an IC₅₀ value of approximately 1 µM [45]. Triclosan (Fig. 1, Table 1) is known to inhibit PfFENR in a nanomolar range, as well as to prevent, at micromolar concentrations, the growth of *P. falciparum* in the blood-stage [46]. Recently, using virtual screening based on two crystal structures of PfFENR, a structurally novel class of Type II FAS inhibitors was identified [47]. Two amide-containing salicylic acid derivatives were shown to inhibit PfFENR and displayed IC₅₀ values of 1.7 and 3.0 µM and to led to a more prominent developmental attenuation of liver-stage parasites than the Primaquine (gold-standard drug).

Table 1. Some inhibitors described in this review.

Compound name	Compound number and chemical structure	Target enzyme (IC ₅₀ or Ki)	Activity in parasite cultures	Activity <i>in vivo</i>	REF.
856002	1 	PfHK IC ₅₀ =0.01 μM	Yes EC ₅₀ =6.8 ± 1.25 μM	ND	[16]
Posaconazole	2 	PfLDH IC ₅₀ =2.6 μM	Yes EC ₅₀ =0.04 μM	Yes (<i>P. berghei</i>)	[20]
14a	3 	PfDXR 100% inhibition [100 μM]	Yes EC ₅₀ =0.04 μM	ND	[34]
Triclosan	4 	PfENR IC ₅₀ =0.073 ± 0.002 μM	Yes EC ₅₀ =0.80 ± 0.02 μM	ND	[155]
MT-coformycin	5 	PfADA Ki=0.25 nM	YES	ND	[52]
Compound 50	6 	PfDHODH IC ₅₀ =0.006 ± 0.001 μM	YES EC ₅₀ =0.015 ± 0.002 μM	YES	[70]
Atovaquone	7 	DHO-cytochrome c reductase IC ₅₀ =0.052 μM	Yes (* <i>P. berghei</i>)	Yes (* <i>P. berghei</i>)	[156]
P218	8 	PfDHFR-TS Ki=0.54 ± 0.12 nM	YES EC ₅₀ =4.6 ± 1.9 nM	YES ED ₅₀ =0.3 mg/kg ED ₉₀ =1 mg/kg	[11]
BIX-01294	9 	Histone lysine methyltransferase	Yes EC ₅₀ =3.1 ± 1.2 μM	Yes (* <i>P. berghei</i>)	[96, 97]
SB939	10 	Histone deacetylases	Yes EC ₅₀ =0.08 ± 0.03 μM	Yes (* <i>P. berghei</i>)	[100]
Sym4	11 	Falcpains FP1 IC ₅₀ =140 ± 23 nM FP2/2 IC ₅₀ =8.5 ± 1.3 nM FP3 IC ₅₀ =22 ± 8 nM (in crude extract)	ND	ND	[108]

(Table 1) contd....

Compound name	Compound number and chemical structure	Target enzyme (IC ₅₀ or Ki)	Activity in parasite cultures	Activity <i>in vivo</i>	REF.
WEHI-916	12 	Pf Plm V IC ₅₀ = 20nM	EC ₅₀ = 2.5-5 μM	ND	[117]
Compound 7	13 	PfM1 Ki=0.8 μM PfM17 Ki=0.03 μM	Yes EC ₅₀ = 783±86.6 nM	NR	[129]
BKI-1	14 	PfCDPK4 IC ₅₀ =4 nM	Yes EC ₅₀ =0.0349 μM	NR	[141]
Purfalcamine	15 	PfCDPK1 IC ₅₀ =17 nM	Yes EC ₅₀ =230 nM EC ₉₀ =414 nM	Yes	[139]
NSC 95397 (Compound 18)	16 	PfATPase 6 IC ₅₀ =1.0 ± 0.6 μM	Yes EC ₅₀ =3.1 ± 1.2 μM	NR	[154]

Note: ND, not determined; IC₅₀, half maximal inhibitory concentration; Ki, inhibitory constant; EC₅₀, half maximal effective concentration; ED₅₀ and ED₉₀, effective dose 50 and 90, respectively; NR, not reported.

5. PURINE SALVAGE ENZYMES

Purines are necessary for the synthesis of several cofactors and nucleic acid precursors [11, 48]. Although this metabolic pathway is present in both the parasite and human, many of the purine salvage temporary interruptions do not have adverse effects on human health; knowledge of these enzymes may reveal very useful information to design selective drugs against *P. falciparum* [49], some of them positioned as pharmaceutical targets such as adenosine deaminase.

Adenosine deaminase (ADA, EC 3.5.4.4) catalyzes the irreversible hydrolysis of adenosine to inosine or 2-deoxyadenosine to ammonia; besides *P. falciparum* ADA (pfADA) deaminates the 5'-methylthioadenosine (MTA) [50]. Several inhibitors have been characterized and can be divided into two categories: a) substrate inhibitors, whose structures are similar to adenosine and b) transition state analogue inhibitors that resemble the tetrahedral form of Meisenheimer intermediate [51]. The 5-methylthioformycin (MT-coformycin) is an analogue of the specific transition state from plasmodial ADAs. MT-coformycin (Fig. 1, Table 1) is a subnanomolar PfADA inhibitor twenty thousand

times more selective regarding to human ADA [52]. A recent study found, by computational molecular modeling and an *in vitro* tests, a weak inhibitor, the EHNA compound. It was sixty times less potent against PfADA, being even more potent for PvADA (Ki = 1.9 μM) and binds with higher affinity in the mutant D172A PvADA (Ki = 0.9 μM) [53].

6. MITOCHONDRIAL ELECTRON TRANSPORT CHAIN AND PYRIMIDINE BIOSYNTHESIS

The supply of electrons in the ETC (electron transport chain), is started by dehydrogenase (complex I) and continued through the other complexes (III and IV), using as electron carriers coenzyme Q and cytochrome *c*, respectively. In contrast to the mammalian enzyme, there is no evidence that ATP synthase in parasite synthesize ATP; instead, it could serve as a proton leak for the ETC [54].

Targeting the ETC of the human malaria parasite has already been shown to be a successful chemotherapeutic strategy. The Complex III (or *bc₁* complex) is a key mitochondrial enzyme that catalyzes the transfer of electrons maintaining the membrane potential of mitochondria. Hydroxynaphthoquinones inhibit the mitochondrial respiration

of *P. falciparum* by binding to the bc_1 complex (complex III) at the CoQ site. Furthermore, Atovaquone (Fig. 1, Table 1), is an inhibitor of bc_1 complex, it has a mode of action involving competitive inhibition of the Qo site of the bc_1 complex [55]. The IC_{50} of Atovaquone against *P. falciparum* was 3.79 μ M [56]. However, resistance to it was reported due to diverse mutations in the quinone binding site of the cytochrome b gene of *Plasmodium spp* [57]. In other study, Siregar *et al.* [58], suggested that Y268C and Y268N mutations play an important role in atovaquone resistance in *P. falciparum*. Actually, WR249685 was found to inhibit the *Plasmodium* complex III (IC_{50} = 3 nM) with far superior selectivity than other bc_1 inhibitors; therefore, it has the potential for development as antimalarial therapeutic [59]. In addition, complex V also is considered like a drug-development target. It has been shown that almitrine, originally developed as a respiratory stimulant, has activity against *Plasmodium* ATP synthase and the parasite [60].

Pyrimidines, which are needed for nucleic acids biosynthesis, must be obtained by the *novo* biosynthetic metabolic route in *P. falciparum*. Dihydroorotate dehydrogenase (DHODH, EC 1.3.5.2) is a flavoenzyme that catalyzes the fourth reaction and is the limiting step in the *novo* pyrimidine synthesis pathway [61], this enzyme oxidizes the L-dihydroorotate to orotate; there are two isoforms of the enzyme, the first is cytosolic and requires fumarate or NAD^+ as electron acceptor, it is found in *Saccharomyces* and certain protozoans [62]. The second type is expressed in *P. falciparum* and humans, this is a protein bound to membrane and uses ubiquinone as electron acceptor [63].

There are inhibitors reported for DHODH, obtained through virtual screening and high throughput screening, which consist in a triazolopyrimidine, they are able to inhibit the parasite growth in animal models [64, 65]. Compounds Genz-667348, Genz-668857, and Genz-669178 showed an *in vitro* nanomolar potency against DHODH from *P. falciparum*, *P. vivax*, and *P. berghei*, and activity against strains of *P. falciparum* with good tolerability and oral exposure in mice [66]; some of these compounds are under studies to determine their possible clinical utilization. The compound Genz-669178 was optimized and obtained the IDI-6273 inhibitor, which was even more powerful with an EC_{50} value of 2.3 nM against *P. falciparum* [67]. In other studies, the DSM161 and DSM190 compounds obtained an IC_{50} of 0.13 μ M and 0.19 μ M, respectively, to inhibit *P. falciparum* DHODH [65], the DSM265 compound was a potent inhibitor of *P. vivax* DHODH, it revealed an IC_{50} of 0.073 μ M [68]. These inhibitors exhibited excellent bioavailability in mouse models. Conversely, an *in silico* study determined that the affinity of the triazolopyrimidines-based inhibitors for DHODH was due to the formation of hydrogen bonds and important stacking interactions, that strengthen the bond with the PfDHODH [69]. There are other types of inhibitors, the dihydrothiophenone analogues, such as compound 50 (Fig. 1, Table 1), which are also potent against both the isolated enzyme as well as *P. falciparum* strains and report good bioavailability in mice models [70].

Orotate phosphoribosyltransferase (OPRT, EC 2.4.2.10) catalyzes the formation of orotidine 5'-monophosphate, thereafter, it is converted to uridine monophosphate (UMP)

by OMP decarboxylase (orotidine 5'-monophosphate decarboxylase). OPRT can exist as a monomeric enzyme (prokaryotes and lower eukaryotes), or as a dimer fused to OMP decarboxylase (eukaryotes) [71, 72]. Through the study of transition state analogues, potent inhibitors of PfOPRT were discovered, crucial components were identified for inhibitor binding into the active site of PfOPRT. However, no inhibition of *P. falciparum* cultures was found [73].

Serine hydroxymethyltransferase (SHMT, EC 2.1.2.1) belongs to pyrimidine biosynthesis pathway in malaria parasites. Two types of SHMT has been described, a mitochondrial (mSHMT) and cytosolic (cSHMT) isoforms. The former was evidenced to be essential for parasite, indicating it as a valid target for development of novel antimalarials. SHMT catalyzes the reversible interconversion of serine and tetrahydrofolate (THF) to glycine and 5,10-methylenetetrahydrofolate, this enzyme is dependent on ubiquitous pyridoxal phosphate. The SHMT expression improvement during the multiplication of *Plasmodium* cell [74]. A recent study, demonstrated that Cys125 and Cys364 (in redox state) regulates the PfSHMT activity. This residues act as a redox switch: the oxidized form decrease the enzymatic activity while the enzymatic function is recovered in the reduced form [75].

7. DNA SYNTHESIS

Dihydrofolate reductase (DHFR, EC 1.5.1.3) is the most used enzyme as therapeutic target, because is a key enzyme in the nucleic acid pathway and is essential in *Plasmodium* for the DNA synthesis (Fig. 1). DHFR reduces dihydrofolate to tetrahydrofolate and it needs NADH for the catalysis. Nowadays, Sulfadoxine-Pyrimethamine, an inhibitor of dihydrofolate synthase and dihydrofolate synthase reductase, is used as treatment and prophylaxis of malaria. *P. falciparum* DHFR activity is located in the N-terminal portion of the bifunctional protein dihydrofolate reductase-thymidylate synthase (DHFR-TS), while these activities are present in two independent enzymes in human. *P. falciparum* DHFR-TS catalyzes two essential reactions, the synthesis of dTMP and the conversion of dihydrofolate to methylenetetrahydrofolate [76].

The resistance in *P. falciparum* is due to a punctual mutation in the active site residues Ala16, Ile51, Cys59, Ser108 and Ile164 of DHFR [77]. Recently, two inhibitors 4,6-diamino-1,2-triazine (WR99210) and pyrimethamine showed an IC_{50} of 0.57 and 58 nM, respectively, but both were not selective. However, two WR99210 analogues, P65 and P218 (Fig. 1, Table 1), were synthesized and showed high selectivity for DHFR-TS, with an IC_{50} of 229 and 4.6 nM respectively [11].

8. TRANSLATION AND POST-TRANSLATION MODIFICATIONS

Aminoacyl-tRNA synthetases. The protein translation machinery in *P. falciparum* has been located as molecular targets in the pursuit of new drugs because of its vital importance for the parasite (Fig. 1) [78]. Part of this machinery are the aminoacyl-tRNA synthetases (aaRSs), these enzymes function charging amino acids to their cognate t-RNAs for protein synthesis; this action is carried out in two steps. First,

the aaRSs catalyze activation of the amino acid and subsequently the aminoacyl-adenylate intermediate is transferred to tRNA [79, 80]. *P. falciparum* belongs to phylum apicomplexan; like most members in this group it has three active translation compartments: the cytosol, mitochondria, and the apicoplast [81]. *P. falciparum* aaRSs has been suggested to be mainly distributed between the cytoplasm and apicoplast [82].

The aaRSs have been well-established molecular targets for the development of antimicrobial and antifungal for years, but only recently they were considered in parasites such as *Plasmodium*, *Trypanosoma* and *Brugia* [79, 83]. In these efforts antibiotics, such as Mupirocin, an inhibitor of bacterial aaRSs, showed a nanomolar range inhibition of *P. falciparum* targeting apicoplastic isoleucyl t-RNA and Thia-isoleucine, an isoleucine analog, had activity against this parasite, targeting cytosolic isoleucyl t-RNA synthetase as well [84]. Furthermore, fungal secondary metabolite Cladosporin, which inhibit liver and blood stages of parasite, was found to act selectively against cytosolic lysyl t-RNA synthase [85]. Another effort to inhibit aaRSs has been focused on the design of aminoacyl adenylate intermediate analogues [86-88]. Incidentally through a designed chemical library, a group of selective inhibitors of apicoplastic aaRS were discovered, these compounds showed antimalarial activity as well [79]. However, the challenge to avoid inhibiting the human homologs occurs. In fact research has focused on the specific aaRSs in the apicoplast since their cyanobacterial origin; it makes them evolutionarily distant from human aaRSs; or inhibiting both, the cytosolic and apicoplastic forms, as in the case of Alanyl-tRNA synthetase (PfAlaRS), Threonyl-tRNA synthetase (PfThrRS) and glycyl-tRNA synthetase (PfGlyRS) [89, 90].

A range of inhibitors tested *in silico* has been reported for PfAlaRS and the compound named A5 showed an IC₅₀ of 8 μM in parasite cultures. Furthermore, these molecules showed no toxicity in a fibroblast cell line, at least within the IC₅₀ concentrations [89]. Other option to find new therapies is to modify known structures that inhibit proteins, although it has a problem regarding toxicity or lack of bioavailability. Febrifugine, an inhibitor of prolyl-tRNA synthetase (PfProRS), belongs to this category. This compound was found to be hepatotoxic, but its structure was used to generate the analog halofuginone, that inhibits *P. falciparum* in both, erythrocyte and liver stages, however, it is not specific in respect with its human counterpart [91-93]. Borredelin, another compound toxic to humans, has shown to be a powerful antimalarial agent acting on PfThrRS both cytoplasmic and apicoplastic forms. In an effort to improve the potential of this antimalarial compound, a series of analogs that achieved greater selectivity over the target were developed. Two compounds were found, BD196 and BC220, they had antimalarial activity both *in vitro* and *in vivo*, showing no inhibition in cytosolic human ThrRSa at the concentrations tested (Fig. 1) [94].

Tyrosyl-tRNA synthetase (PfTyrRS) is an enzyme whose function as a target in parasites has not been developed, but taking into account its equivalent in bacteria, it is an area to consider. According to its crystallographic structure, there are differences with its counterpart in human (HsTyrRS).

The most notable feature is the presence of the ELR motif; it is exposed in PfTyrRS whereas HsTyrRS is exposed after the proteolytic anchor and it shows a vulnerable point to search for selective inhibitors [95]. Another strategy that has been used in drug design is to find conformation changes during the action of enzymes and to identify any differences with its counterpart in hosts. This is the case of tryptophanyl-tRNA synthetase (PfTrpRS), which decreases its similarity to its human counterpart from 75% to 55%, in the residues involved in the movement for a conformation change during aminoacylation reaction, this conformation change could be exploited in the search of new antimalarials [80].

Histone lysine methyltransferase. The level of post-translational modification has the transcriptional control of genes involved in immune evasion and erythrocyte invasion in *P. falciparum* [96]. Therefore, the enzymes that participate in DNA methylation and post-translational modification like histone lysine methyltransferase are good drug targets. Histone methyltransferases add methyl groups to arginine or lysine residues. The inhibitor of the human G9a histone methyltransferase (BIX-01294, Fig. 1, Table 1) and one derivative (TM2-115) were assessed in culture of *P. falciparum* strains. Both exhibited strong antimalarial activity; TM2-115 had an IC₅₀ values of ~100 nM in culture of *P. falciparum* 3D7 strain. Both compounds showed an irreversible effect of the parasite growth in the intraerythrocytic life cycle. Moreover, these compounds reduced the concentration of the trimethyl histone H3 lysine 4 (H3K4me3) levels in culture of parasites. Therefore, these results could be an evidence that the activity of parasite histone methyltransferase is inhibited [97].

In other work, the design and synthesis of new diaminoquinazoline derivatives based on the interactions reported among the inhibitor BIX01294 and the human histone methyltransferase were made. These compounds were tested in a SAR analysis probing their activity against human cell lines and *P. falciparum* cultures. The data showed that some of these analogs exhibited antimalarial activity at nanomolar concentration. Besides, two compounds were found to be relied upon to generate a new series of compounds so as to make them more specific to parasite histone lysine methyltransferase [96].

Histone deacetylases. The histone deacetylases (HDACs) act in post-translational modifications altering the acetylation state of lysine residues in proteins. This was confirmed by a study using apicidin, a HDACs inhibitor. This inhibitor was tested at different stages of intraerythrocytic development of *P. falciparum*. Significant changes in gene activation and repression in rings, trophozoites and schizonts were obtained. It also produced a higher acetylation in histones, therefore, it can be concluded that the HDAC is an important point in the regulation of transcription [98]. With respect to inhibition of HDACs, Andrews and co-workers tested 14 new derivatives of L-cysteine in cultured parasites, these compounds showed an IC₅₀ in the nanomolar range and a higher level of acetylation was found as well, suggesting HDACs inhibition [99]. Conversely, compound SB939 (Fig. 1, Table 1) had an important effect on the growth of the asexual stages of the parasite with an EC₅₀ between 100-200 nM, and caused elevation in the level of acetylation of his-

tones; additionally this inhibitor was tested in mice models obtaining a good antimalarial activity [100].

N-myristoyltransferase. The enzyme *N-myristoyltransferase* (NMT) has been considered a good target due to its fundamental role in many organisms [101]. Structurally, NMT is a monomer that catalyzes the co-translational or post-translational transfer of myristate to a glycine residue in several eukaryotic proteins [102]. In the search of NMT inhibitors, two compounds (4 and 25) showed activity against enzyme and parasite cultures (Fig. 1), besides, were selective over human counterpart [103], making these molecules a good leads to develop new and more potent inhibitors.

9. CYSTEINE PROTEASES

The cysteine proteases or falcipains are implicated in the hemoglobin degradation. The amino acids derived from this process are incorporated into the parasite proteins, or used for the energy metabolism and are expressed in the intraerythrocytic phase of the life cycle [104].

Falcipain-2 and falcipain-3 are promising targets for the development of new drugs against malaria. A series of dihydroartemisinin derivatives based on a thiosemicarbazone structure, were designed and synthesized as potential falcipain-2 inhibitors, showing an excellent inhibitory activity in the *in vitro* assays, with an IC_{50} in a 0.29-10.63 μ M range. Otherwise, docking studies evaluating the binding energy and interactions, showed that the ligand binding pocket was formed by residues Trp206, Cys42, His174, Gly82, Gly83, Leu172, Asp234 and Gln171, and hydrogen bonds with Cys42 and Gly83 were formed with the most potent compound [105]. In a virtual screening for other inhibitors, leupeptine analogues were submitted into the falcipain-2 and falcipain-3 active sites. From the 104 analogues, the compound named as result_037 showed the best binding energy, and another two, result_044 and result_042 had a similar binding energy as E64 in falcipain-2 [10].

Conversely, a total of 69 hits from the Chembridge and Asinex companies obtained by virtual screening, were rehearsed prioritizing the choice based on docking calculations. This compounds that contained a 1,2,3,4 tetrazol were experimentally evaluated against falcipain-2. Out of these 69 compounds, 28 inhibited the enzyme with an IC_{50} in a range of 5-48 μ M; some of these also had acted against parasite cultures with an IC_{50} less than 10 μ M [106].

In the case of falcipain-3, leupeptine analogues had a better binding energy than those inhibitors reported against falcipain-3 on PDB [107]. Therefore, these leupeptine analogues are promising inhibitors for an antimalarial treatment [10]. In the same context, the action mechanism of symprostataine 4 (Sym4, Fig. 1, Table 1), a secondary metabolic product of a cyanobacterium *Symploca sp.* was widely characterized. The data demonstrated that this molecule was an inhibitor of falcipains of *P. falciparum* at nanomolar concentrations [108].

10. PLASMEPSINS

Plasmodium falciparum exports over 450 proteins into the human host [109, 110], this mechanism requires the

Plasmodium Export Element (PEXEL) [111]. Among the exported proteins are aspartic proteases, such as plasmepsins, which are classified from Plm-I to Plm-X [112]. PlmI, PlmII, HAP (histoaspartic protease) and PlmIV reside in the digestive vacuole [113]. The formation of a digestive vacuole (DV) is in charge of processing nutrients from the circulatory system [114]. Their importance lies in their ability to degrade hemoglobin, a catabolic function in the intraerythrocytic stage of the parasite, necessary for survive. Therefore, these proteases have been considered as a potential target for drug design [115].

One of the plasmepsins, Plm-V, is responsible for cleavage, in the endoplasmic reticulum, at the PEXEL motif, which is located at the N-terminal region of some proteins and needs to be removed for protein exportation [116]. To inhibit this enzyme, a PEXEL-mimetic compound WEHI-916 (Fig. 1, Table 1), was synthesized. This molecule was a potent inhibitor of both Plm-V from *P. falciparum* and *P. vivax*, additionally, PEXEL processing inhibition was found in a dose-dependent manner, in erythrocytes infected with *P. falciparum* and treated with the inhibitor. Furthermore, parasites at the trophozoite stage were killed by this molecule [117].

Different studies have proven that the deletion of PlmI, PlmII or PlmIV decouples the DV, hence, drugs that target plasmepsins should have compounds that are capable of inhibiting more than one of the proteases [118]. Three dimensional structure of this enzyme has been solved through the years, there are more than 19 structures just for PlmII alone, some of them in complex with potential inhibitors [119]. Although the similarity between the plasmepsins is high, a way to inhibit more than one has not been found [120].

11. AMINOPEPTIDASES

P. falciparum has the machinery to synthesize a few amino acids, such as glutamate, asparagine, proline, glutamine, glycine, and aspartate [121]. Therefore, the rest of amino acids come from hemoglobin degradation [88], except for isoleucine, the only amino acid that is absent in hemoglobin and is taken from external sources [122]. Total digestion of hemoglobin requires a combination of different proteases including the aminopeptidases. They catalyze the release of neutral amino acids from the amino-terminus of peptides [123]. In the case of *Plasmodium*, it possesses two neutral aminopeptidases, one from the M1 family of alanyl aminopeptidases (PfM1AAP) and other from the M17 family of leucyl amino peptidases (PfM17LAP). Because of the hemoglobin digestion and supply of free amino acids for parasite survival, these enzymes have been considered as good targets for antimalarial drug design (Fig. 1) [124]. Primary efforts to inhibit both enzymes led to use bestatine, derived from *Streptomyces olivoreticuli*. This compound and other two organophosphorus derivatives, showed activity in the nanomolar range and in parasites cultures at micromolar concentrations [124, 125]. Recently, several hydroxamate derivatives were synthesized and assessed as PfM1 inhibitors. The most potent of them, compound BDM14471, showed an IC_{50} of 6 nM and was selective compared to the mammalian aminopeptidase APN [126]. Additionally, studies testing its effect on parasite growth, indicated that this

molecule inhibit *P. falciparum* cultures with an IC_{50} of 11.0 μM [127] and was not cytotoxic against MRC5 cells [126].

Conversely, a series of phosphonic acid arginine mimetic compounds were synthesized, the best of them (compound 6) showed an IC_{50} of 104 μM and 0.011 μM to PfM1 and PfM17, respectively. Furthermore, the crystal structures of both enzymes alongside with compound 6, revealed important interactions for more potent inhibitor design [128]. Under this perspective, a series of carboxylic and hydroxamic acid derivatives from compound 6 were synthesized. From these studies, compound 7 (Fig. 1, Table 1) was a potent dual PfM1/PfM17 inhibitor, with K_i values of 0.8 and 0.03 μM to PfM1 and PfM2, respectively. From the structure of this compound, other potent dual inhibitors were obtained showing activity against parasite cultures in the nanomolar range [129].

12. PROTEIN KINASES

Kinases are proteins responsible of regulation of the activity of some enzymes by phosphorylation. This process is involved in several intracellular signaling process, including those that control cell growth and division. In this case, *P. falciparum* kinome is formed by four well established groups which include the CMGC, TirK, CAMK, and AGC groups [130]. Some of them that are not included into these groups are the NIMA group and one that has been called "orphan enzymes". Several investigations [131-134] have discovered that between *P. falciparum* kinome and mammal kinome exist significant differences that play an important role in the development of putative targets and specific inhibitors.

The CMGC group (named after initials of some members) is composed by Cyclin-dependent kinases (CDK), Mitogen-activated protein kinases (MAPK), Glycogen synthase kinase (GSK), and Cdc-like kinase (CLK). Within the CDK subgroup, PfPK5 and Pfmrk are kinases involved in DNA repair and transcription, with reported antimalarial potential inhibitors [135]. Furthermore, some chalcones were explored as potentially antimalarial compounds, although there is no evidence of a specific mechanism of action, it has been demonstrated that they possess antimalarial activity, possibly by acting at this level (Fig. 1) as shown by Geyer *et al.*, [136] where a preliminary SAR inhibition study, chalcone derived compounds had a preferential inhibition for the kinases.

The NIMA group (Never in Mitosis gene A) is a family of four kinases involved in cell mitosis and meiosis [137]. One of this kinases, the Pfnek1 (NIMA related kinase of *P. falciparum*) has been demonstrated to be an excellent target for inhibition [134]. Focus on pharmacological investigation, the search of new inhibition compounds included a study with an ethanolic crude extract of *Pseudoceratina* sp., a Vanuatu marine sponge, where compounds like bromotyrosine metabolites were obtained [138]. Also, the homogenetic acid [methyl (2,4-dibromo-3,6-dihydroxyphenyl)acetate] isolated from the sponge inhibited the enzyme with an IC_{50} of approximately 1.8 μM . Then, other set of compounds like the 11,19-dideoxyfistularin-3, 11-deoxyfistularin-3, and dibromoverongiaquinol were identified. However, further studies are necessary to assess and optimize these compounds due to its weak inhibition activity.

The CAMK (Ca^{2+} /calmodulin dependent protein kinases) group involved kinases such PfCDPK1 and PfCDPK4. PfCDPK1 has been proven to be an excellent target for inhibition, due to the fact that it participates in host cell invasion and parasite motility. Several inhibitors of PfPK1 have been previously reported [139, 140], where nanomolar inhibitors of PfCDPK1 were found through virtual screening [140] and a schizont stage inhibitor purfalcamine was reported (Fig. 1, Table 1) [139]. Also, optimization of PfPK1 inhibitors, like imidazopyridazine, yielded compounds with a high effectiveness and an IC_{50} values (< 10 nM) and *in vitro* EC_{50} values < 12 nM. In regard of PfCDPK4, bumped kinase inhibitors (BKIs) were developed, blocking the exflagellation of the parasites microgametocytes with an IC_{50} under nM range and an EC_{50} less than 300 nM. The toxicological activity showed great selectivity low values of toxicity in mice [141].

AGC kinases (cAMP dependent protein kinases) are involved in diverse cellular functions and are potential targets for the treatment of human diseases. The PfPKG, PfPKA and PfPKC are considered promising targets for antimalarial compounds in recent years [142]. Small molecules inhibitors of AGC kinases may also have potential as novel therapeutic approaches against infectious organisms. Adenosine analogue-oligoarginine conjugates (ARC), previously reported to be efficient inhibitors for the mammalian protein kinases, were able to inhibit PfPKG. This study also demonstrated that the ARCs reduced the phosphorylation status of proteins affecting crucial pathways for the parasite, especially compounds ARC 668 and ARC 902 [143].

According to the best of our review of the literature, we found that PfPKA is involved in diverse process such as asexual development of *P. falciparum* during erythrocyte invasion and gametocytogenesis; regulation of intracellular Ca^{2+} influx [144], anion transport through the erythrocyte membrane [145] and mitochondrial protein traffic [144]. Hotta *et al.* [146] observed a relationship between increased cAMP levels and PfPKA activity, suggesting an important role of Ca^{2+} and the cAMP production in the parasite surviving. Therefore, it is reasonable to speculate that Ca^{2+} -dependent signaling pathways may be critical in controlling signaling events (Fig. 1). For instance H89 is a PfPKA inhibitor, which has been demonstrated to block parasite growth at low doses (IC_{50} 3 μM ; [147]).

In the case of PfPKB, the finding of several inhibitors were reported in a study where it was evaluated if the invasion of the parasite was controlled by this signaling cascade. Compound A443654, a molecule belonging to the indazole-pyridine series was the most effective [148]. For the remaining enzymes of this group, there have not been any new studies developed in the search of new inhibitors.

Finally, the *P. falciparum* protein kinase 7 (PfPK7) possess no human homologue; this is the reason why it is considered an excellent target [131]. Studies suggest that this enzyme is involved in pathways that regulate proliferation and development inside the cells [137]. A series of ATP-competitive inhibitors were found in a 568 compounds screening [145]. These molecules inhibited the parasite growth in its asexual stage in blood-stage cultures. K510, K109, K497 and PP2 compounds were excellent inhibitors, with an IC_{50} in the low μM range.

13. OTHER IMPORTANT ENZYMES FOR PARASITE SURVIVAL

Phosphodiesterase. The phosphodiesterase catalyzes the hydrolysis of the 3'-phosphoester bond of cyclic AMP (cAMP) and cGMP. In *P. falciparum* exists four phosphodiesterases (PfPDE α - δ). These are involved in different processes such as gametocytogenesis, ookinete gliding and disease transmission [149, 150], therefore, it can be considered as a valid drug target. It has not been reported the crystallographic structure of the PfPDE since; Howard and co-workers obtained it by homology modeling, they used human phosphodiesterases structures as template, a tridimensional model of the enzyme. Comparison among the human and parasitic enzymes revealed the existence of similarities in the binding site of cGMP. Furthermore, through docking studies with inhibitors like sildenafil and zaprinast, essential information for the design of new inhibitors that were specific to PfPDE was obtained [151]. In other study, 40 analogs of tadalafil, which is an inhibitor of hPDF5, were designed and synthesized. These new compounds were analyzed for their antimalarial activity and cytotoxicity in MRC5 cells, two compounds with an IC₅₀ of ≤ 1 μ M were reported, with an inhibition of 60% of the hydrolysis of cGMP [152].

Ca²⁺ ATPase 6. The Ca²⁺-ATPase 6 from *P. falciparum* (PfATP6) is a membrane transporter, it is localized in the endoplasmic reticulum, and plays a major role in calcium homeostasis making it essential for parasite growth (Fig. 1). Even though there is a controversy over whether or not PfATP6 is sensitive to artemisinin derivatives, it can be considered a pharmaceutical target for the treatment of malaria due to its important role in the parasite's life cycle [153]. In a recent work, a library of 1680 small molecules was tested in recombinant PfATP6, 20 compounds showed inhibition of the enzyme with an IC₅₀ less than 10 μ M, besides some compounds, such as NSC95397 (Fig. 1, Table 1), obtained an EC₅₀ between 2 and 250 μ M in cultures of *P. falciparum*, therefore, these compounds can be optimized to reach higher selectivity on PfATP6 [154].

In summary, inhibitors being developed against enzymes from *Plasmodium* metabolism offer an interesting possibility for the design of new drugs. These molecules will represent a difficult task for the parasite to become resistant. Table 1 shows representative inhibitors, described in this review, that are considered as new chemical scaffold space that is emerging in the fight against malaria.

CONCLUSIONS

While there are numerous attempts to cure or eradicate malaria worldwide it continues to be a great health problem. This might be due to the appearance of resistant *Plasmodium* strains in existing antimalarials. In order to solve this situation, many research groups are working on validation and studies of new targets for drug design. This review describes a number of inhibitors that are emerging, many of them not only with a good ability to inhibit their target enzyme or parasite growth but with encouraging results in *in vivo* assays. Although these data are very promising to find a new chemotherapy against malaria, to reach this goal the constant search for new drugs should continue.

CONFLICT OF INTEREST

The authors confirm that this article content has no conflicts of interest.

ACKNOWLEDGEMENTS

The authors specially thank: Jorge A. Sosa Gutierrez and Eliab M. González-Olvera for their critical reading of this manuscript and helpful suggestions. Financial support from CONACyT, México is acknowledged (Grant No. 128499) to ATV.

REFERENCES

- [1] World Malaria Report 2013. *World Health Organization*, 2013.
- [2] White, N.J.; Pukrittayakamee, S.; Hien, T.T.; Faiz, M.A.; Mokuolu, O.A.; Dondorp, A.M. *Malaria. Lancet*, 2014, 383(9918), 723-735.
- [3] Kumar, S.; Kumari, R.; Pandey, R. New insight-guided approaches to detect, cure, prevent and eliminate malaria. *Protoplasma*, 2015, 252(3), 717-753.
- [4] Fidock, D.A.; Nomura, T.; Talley, A.K.; Cooper, R.A.; Dzekunov, S.M.; Ferdig, M.T.; Ursos, L.M.B.; Naudé, B.; Deitsch, K.W.; Su, X.Z. Mutations in the *P. falciparum* digestive vacuole transmembrane protein PfCRT and evidence for their role in chloroquine resistance. *Mol. Cell*, 2000, 6(4), 861-871.
- [5] Miotto, O.; Almagro-Garcia, J.; Manske, M.; Macinnis, B.; Campino, S.; Rockett, K.A.; Amaratunga, C.; Lim, P.; Suon, S.; Sreng, S.; Anderson, J.M.; Duong, S.; Nguon, C.; Chhor, C.M.; Saunders, D.; Se, Y.; Lon, C.; Fukuda, M.M.; Amenga-Etego, L.; Hodgson, A.V.; Asoala, V.; Imwong, M.; Takala-Harison, S.; Nosten, F.; Su, X.Z.; Ringwald, P.; Arley, F.; Dolecek, C.; Hien, T.T.; Boni, M.F.; Thai, C.Q.; Amambua-Ngwa, A.; Conway, D.J.; Djimde, A.A.; Doumbo, O.K.; Zongo, I.; Ouedraogo, J.B.; Alcock, D.; Drury, E.; Auburn, S.; Koch, O.; Sanders, M.; Hubbard, C.; Maslen, G.; Ruano-Rubio, V.; Jyothi, D.; Miles, A.; O'Brien, J.; Gamble, C.; Oyola, S.O.; Rayner, J.C.; Newbold, C.I.; Berriman, M.; Spencer, C.C.; McVean, G.; Day, N.P.; White, N.J.; Bethell, D.; Dondorp, A.M.; Plowe, C.V.; Fairhurst, R.M.; Kwiatkowski, D.P. Multiple populations of artemisinin-resistant *Plasmodium falciparum* in Cambodia. *Nat. Genet.*, 2013, 45(6), 648-655.
- [6] Biagini, G.A.; Fisher, N.; Berry, N.; Stocks, P.A.; Meunier, B.; Williams, D.P.; Bonar-Law, R.; Bray, P.G.; Owen, A.; O'Neill, P.M. Acridinediones: selective and potent inhibitors of the malaria parasite mitochondrial bc₁ complex. *Mol. Pharmacol.*, 2008, 73(5), 1347-1355.
- [7] Parker, M.D.; Hyde, R.J.; Yao, S.Y.M.; McRobert, L.; Cass, C.E.; Young, J.D.; McConkey, G.A.; Baldwin, S.A. Identification of a nucleoside/nucleobase transporter from *Plasmodium falciparum*, a novel target for anti-malarial chemotherapy. *Biochem. J.*, 2000, 349, 67-75.
- [8] Lindert, S.; Tallorin, L.; Nguyen, Q.; Burkart, M.; McCammon, J.A. *In silico* screening for *Plasmodium falciparum* enoyl-ACP reductase inhibitors. *J. Comput. Aided Mol. Des.*, 2015, 29(1), 79-87.
- [9] Benting, J.; Mattei, D.; Lingelbach, K. Brefeldin A inhibits transport of the glycoprotein-binding protein from *Plasmodium falciparum* into the host erythrocyte. *Biochem. J.*, 1994, 300, 821-826.
- [10] Kesharwani, R.K.; Singh, D.V.; Misra, K. Computation-based virtual screening for designing novel antimalarial drugs by targeting falcipain-III: a structure-based drug designing approach. *J. Vector Borne Dis.*, 2013, 50(2), 93-102.
- [11] Sopitthummakun, K.; Thongpanchang, C.; Vilaivan, T.; Yuthavong, Y.; Chaiyen, P.; Leartsakulpanich, U. *Plasmodium* serine hydroxymethyltransferase as a potential anti-malarial target: inhibition studies using improved methods for enzyme production and assay. *Malaria J.*, 2012, 11, 194-205.
- [12] Vennerstrom, J.; Ager, A.; Andersen, S.; Grace, J.; Wongpanich, V.; Angerhofer, C.; Hu, J.; Wesche, D. Assessment of the antimalarial potential of tetraoxane WR 148999. *Am. J. Trop. Med. Hyg.*, 2000, 62(5), 573-578.

- [13] Sherman, I.W. Carbohydrate metabolism of asexual stages, in *Malaria: Parasite Biology, Pathogenesis and Protection*, Sherman, I.W., Editor. 1998, ASM Press: Washington, D.C. p. 135-143.
- [14] Roth, E.F.J. Malarial parasite hexokinase and hexokinase-dependent glutathione reduction in the *Plasmodium falciparum*-infected human erythrocyte. *J. Biol. Chem.*, **1987**, *262*(32), 15678-15682.
- [15] Lakhdar-Ghazal, F.; Blonski, C.; Willson, M.; Michels, P.; Perie, J. Glycolysis and proteases as targets for the design of new anti-trypanosome drugs. *Curr. Top. Med. Chem.*, **2002**, *2*(5), 439-456.
- [16] Harris, M.T.; Walker, D.M.; Drew, M.E.; Mitchell, W.G.; Dao, K.; Schroeder, C.E.; Flaherty, D.P.; Weiner, W.S.; Golden, J.E.; Morris, J.C. Interrogating a hexokinase-selected small-molecule library for inhibitors of *Plasmodium falciparum* hexokinase. *Antimicrob. Agents Chemother.*, **2013**, *57*(8), 3731-3737.
- [17] Tjhin, E.T.; Staines, H.M.; van Schalkwyk, D.A.; Krishna, S.; Saliba, K.J. Studies with the *Plasmodium falciparum* hexokinase reveal that PfHT limits the rate of glucose entry into glycolysis. *FEBS Lett.*, **2013**, *587*(19), 3182-3187.
- [18] Aoki, K.; Tanaka, N.; Kusakabe, Y.; Fukumi, C.; Haga, A.; Nakanishi, M.; Kitade, Y.; Nakamura, K.T. Crystallization and preliminary X-ray crystallographic study of phosphoglucose isomerase from *Plasmodium falciparum*. *Acta Crystallogr. Sect. F. Struct. Biol. Cryst. Commun.*, **2010**, *66*(Pt 3), 333-336.
- [19] Ullah, M.; Hira, J.; Ghosh, T.; Ishaque, N.; Absar, N. A Bioinformatics Approach for Homology Modeling and Binding Site Identification of Triosephosphate Isomerase from *Plasmodium falciparum* 3D7. *J. Young Pharm.*, **2012**, *4*(4), 261-266.
- [20] Penna-Coutinho, J.; Cortopassi, W.A.; Oliveira, A.A.; Franca, T.C.; Kretzli, A.U. Antimalarial activity of potential inhibitors of *Plasmodium falciparum* lactate dehydrogenase enzyme selected by docking studies. *PLoS One*, **2011**, *6*(7), e21237.
- [21] Keluskar, P.; Ingle, S. Ethnopharmacology guided screening of traditional Indian herbs for selective inhibition of *Plasmodium* specific lactate dehydrogenase. *J. Ethnopharmacol.*, **2012**, *144*(1), 201-207.
- [22] Bhowmick, I.P.; Kumar, N.; Sharma, S.; Coppens, I.; Jarori, G.K. *Plasmodium falciparum* enolase: stage-specific expression and sub-cellular localization. *Malar. J.*, **2009**, *8*, 179.
- [23] Olafsson, A.; Hammerich, M.; Henningsen, J. Photoacoustic spectroscopy of C₂H₄ with a tunable waveguide CO₂ laser. *Appl. Opt.*, **1992**, *31*(15), 2657-2668.
- [24] Sessions, R.B.; Dewar, V.; Clarke, A.R.; Holbrook, J.J. A model of *Plasmodium falciparum* lactate dehydrogenase and its implications for the design of improved antimalarials and the enhanced detection of parasitaemia. *Protein Eng.*, **1997**, *10*(4), 301-306.
- [25] Cameron, A.; Read, J.; Tranter, R.; Winter, V.J.; Sessions, R.B.; Brady, R.L.; Vivas, L.; Easton, A.; Kendrick, H.; Croft, S.L.; Barros, D.; Lavandera, J.L.; Martin, J.J.; Risco, F.; Garcia-Ochoa, S.; Gamo, F.J.; Sanz, L.; Leon, L.; Ruiz, J.R.; Gabarro, R.; Mallo, A.; Gomez de las Heras, F. Identification and activity of a series of azole-based compounds with lactate dehydrogenase-directed antimalarial activity. *J. Biol. Chem.*, **2004**, *279*(30), 31429-31439.
- [26] Rohmer, M. The discovery of a mevalonate-independent pathway for isoprenoid biosynthesis in bacteria, algae and higher plants. *Nat. Prod. Rep.*, **1999**, *16*(5), 565-574.
- [27] Lichtenthaler, H.K. Non-mevalonate isoprenoid biosynthesis: enzymes, genes and inhibitors. *Biochem. Soc. Trans.*, **2000**, *28*(6), 785-789.
- [28] Jomaa, H.; Wiesner, J.; Sanderbrand, S.; Altincicek, B.; Weidemeyer, C.; Hintz, M.; Türbachova, I.; Eberl, M.; Zeidler, J.; Lichtenthaler, H.K.; Soldati, D.; Beck, E. Inhibitors of the non-mevalonate pathway of isoprenoid biosynthesis as antimalarial drugs. *Science*, **1999**, *285*, 1573-1576.
- [29] Hunter, W.N. The non-mevalonate pathway of isoprenoid precursor biosynthesis. *J. Biol. Chem.*, **2007**, *282*(30), 21573-21577.
- [30] Singh, V.K.; Ghosh, I. Methylerythritol phosphate pathway to isoprenoids: kinetic modeling and *in silico* enzyme inhibitions in *Plasmodium falciparum*. *FEBS Lett.*, **2013**, *587*(17), 2806-2817.
- [31] Proteau, P. J. 1-Deoxy-D-xylulose 5-phosphate reductoisomerase: an overview. *Bioorg. Chem.*, **2004**, *32*(6), 483-493.
- [32] Chaudhary, K.K.; Prasad, C.V. Virtual Screening of compounds to 1-deoxy-D-xylulose 5-phosphate reductoisomerase (DXR) from *Plasmodium falciparum*. *Bioinformation*, **2014**, *10*(6), 358-364.
- [33] Goble, J.L.; Johnson, H.; de Ridder, J.; Stephens, L.L.; Louw, A.; Blatch, G.L.; Boshoff, A. The druggable antimalarial target PfDXR: overproduction strategies and kinetic characterization. *Protein Pept. Lett.*, **2013**, *20*(2), 115-124.
- [34] Jansson, A.M.; Wieckowska, A.; Bjorkelid, C.; Yahiaoui, S.; Sooriyaarachchi, S.; Lindh, M.; Bergfors, T.; Dharavath, S.; Desroses, M.; Suresh, S.; Andaloussi, M.; Nikhil, R.; Sreevalli, S.; Srinivasa, B.R.; Larhed, M.; Jones, T.A.; Karlen, A.; Mowbray, S.L. DXR inhibition by potent mono- and disubstituted fosmidomycin analogues. *J. Med. Chem.*, **2013**, *56*(15), 6190-6199.
- [35] Konzuch, S.; Umeda, T.; Held, J.; Hahn, S.; Brucher, K.; Lienau, C.; Behrendt, C.T.; Grawert, T.; Bacher, A.; Illarionov, B.; Fischer, M.; Mordmuller, B.; Tanaka, N.; Kurz, T. Binding modes of reverse fosmidomycin analogs toward the antimalarial target IspC. *J. Med. Chem.*, **2014**, *57*(21), 8827-8838.
- [36] Jordao, F.M.; Gabriel, H.B.; Alves, J.M.; Angeli, C.B.; Bifano, T.D.; Breda, A.; de Azevedo, M.F.; Basso, L.A.; Wunderlich, G.; Kimura, E.A.; Katzin, A.M. Cloning and characterization of bifunctional enzyme farnesyl diphosphate/geranylgeranyl diphosphate synthase from *Plasmodium falciparum*. *Malar. J.*, **2013**, *12*, 184.
- [37] Ghosh, S.; Chan, J.M.; Lea, C.R.; Meints, G.A.; Lewis, J.C.; Tovian, Z.S.; Flessner, R.M.; Loftus, T.C.; Bruchhaus, I.; Kendrick, H.; Croft, S.L.; Kemp, R.G.; Kobayashi, S.; Nozaki, T.; Oldfield, E. Effects of bisphosphonates on the growth of *Entamoeba histolytica* and *Plasmodium* species *in vitro* and *in vivo*. *J. Med. Chem.*, **2004**, *47*(1), 175-187.
- [38] Mukkamala, D.; No, J.H.; Cass, L.M.; Chang, T.K.; Oldfield, E. Bisphosphonate inhibition of a *Plasmodium* farnesyl diphosphate synthase and a general method for predicting cell-based activity from enzyme data. *J. Med. Chem.*, **2008**, *51*(24), 7827-7833.
- [39] Hariharan, S. Pharmacophoric studies of *in vitro* inhibition of *Plasmodium falciparum* growth. *Indian J. Biochem. Biophys.*, **2012**, *49*(2), 101-108.
- [40] Chirala, S.S.; Huang, W.; Jayakumar, A.; Sakai, K.; Wakil, S.J. Animal fatty acid synthase: functional mapping and cloning and expression of the domain I constituent activities. *Proc. Natl. Acad. Sci. USA.*, **1997**, *94*(11), 5588-5593.
- [41] Rock, C.O.; Cronan, J.E. *Escherichia coli* as a model for the regulation of dissociable (type II) fatty acid biosynthesis. *Biochim. Biophys. Acta-Lipids and Lipid Metabolism*, **1996**, *1302*(1), 1-16.
- [42] Wickramasinghe, S.; Inglis, K.; Urch, J.; Muller, S.; van Aalten, D.; Fairlamb, A. Kinetic, inhibition and structural studies on 3-oxoacyl-ACP reductase from *Plasmodium falciparum*, a key enzyme in fatty acid biosynthesis. *Biochem. J.*, **2006**, *393*, 447-457.
- [43] Waller, R.F.; Ralph, S.A.; Reed, M.B.; Su, V.; Douglas, J.D.; Minnikin, D.E.; Cowman, A.F.; Besra, G.S.; McFadden, G.I. A type II pathway for fatty acid biosynthesis presents drug targets in *Plasmodium falciparum*. *Antimicrob. Agents Chemother.*, **2003**, *47*(1), 297-301.
- [44] Jones, S.H.; Urch, J.E.; Brun, R.; Harwood, J.L.; Berry, C.; Gilbert, I.H. Analogues of thiolactomycin as potential anti-malarial and anti-trypanosomal agents. *Bioorg. Med. Chem.*, **2004**, *12*(4), 683-692.
- [45] McLeod, R.; Muench, S.P.; Rafferty, J.B.; Kyle, D.E.; Mui, E.J.; Kirisits, M.J.; Mack, D.G.; Roberts, C.W.; Samuel, B.U.; Lyons, R.E. Triclosan inhibits the growth of *Plasmodium falciparum* and *Toxoplasma gondii* by inhibition of Apicomplexan Fab I. *Int. J. Parasitol.*, **2001**, *31*(2), 109-113.
- [46] Kapoor, M.; Jamal Dar, M.; Surolia, A.; Surolia, N. Kinetic Determinants of the Interaction of Enoyl-ACP Reductase from *Plasmodium falciparum* with Its Substrates and Inhibitors. *Biochem. Biophys. Res. Commun.*, **2001**, *289*(4), 832-837.
- [47] Schrader, F.C.; Glinca, S.; Sattler, J.M.; Dahse, H.; Afanador, G.A.; Prigge, S.T.; Lanzer, M.; Mueller, A.; Klebe, G.; Schlitzer, M. Novel type II fatty acid biosynthesis (FAS II) inhibitors as multistage antimalarial agents. *ChemMedChem.*, **2013**, *8*(3), 442-461.
- [48] Cassera, M.B.; Zhang, Y.; Hazleton, K.Z.; Schramm, V.L. Purine and pyrimidine pathways as targets in *Plasmodium falciparum*. *Curr. Top. Med. Chem.*, **2011**, *11*(16), 2103-2115.
- [49] Ducati, R.G.; Namanja-Magliano, H.A.; Schramm, V.L. Transition-state inhibitors of purine salvage and other prospective enzyme targets in malaria. *Future Med. Chem.*, **2013**, *5*(11), 1341-1360.
- [50] Ting, L.M.; Shi, W.; Lewandowicz, A.; Singh, V.; Mwakwingwe, A.; Birck, M.R.; Ringia, E.A.; Bench, G.; Madrid, D.C.; Tyler, P.C.; Evans, G.B.; Furneaux, R.H.; Schramm, V.L.; Kim, K. Targeting a

- novel *Plasmodium falciparum* purine recycling pathway with specific immucillins. *J. Biol. Chem.*, **2005**, *280*(10), 9547-9554.
- [51] Da Settimo, F.; Primofiore, G.; La Motta, C.; Taliani, S.; Simorini, F.; Marini, A.M.; Mugnaini, L.; Lavecchia, A.; Novellino, E.; Tuscano, D.; Martini, C. Novel, highly potent adenosine deaminase inhibitors containing the pyrazolo[3,4-d]pyrimidine ring system. Synthesis, structure-activity relationships, and molecular modeling studies. *J. Med. Chem.*, **2005**, *48*(16), 5162-5174.
- [52] Ho, M.C.; Cassera, M.B.; Madrid, D.C.; Ting, L.M.; Tyler, P.C.; Kim, K.; Almo, S.C.; Schramm, V.L. Structural and metabolic specificity of methylthioformycin for malarial adenosine deaminases. *Biochemistry*, **2009**, *48*(40), 9618-9626.
- [53] Ivanov, A.; Matsumura, I. The adenosine deaminases of *Plasmodium vivax* and *Plasmodium falciparum* exhibit surprising differences in ligand specificity. *J. Mol. Graph. Model.*, **2012**, *35*, 43-48.
- [54] Nixon, G.L.; Moss, D.M.; Shone, A.E.; Lalloo, D.G.; Fisher, N.; O'Neill, P.M.; Ward, S.A.; Biagini, G.A. Antimalarial pharmacology and therapeutics of atovaquone. *J. Antimicrob. Chemother.*, **2013**, *68*(5), 977-985.
- [55] Kessl, J.J.; Meshnick, S.R.; Trumpower, B.L. Modeling the molecular basis of atovaquone resistance in parasites and pathogenic fungi. *Trends Parasitol.*, **2007**, *23*(10), 494-501.
- [56] Dormoi, J.; Savini, H.; Amalvict, R.; Baret, E.; Pradines, B. *In vitro* interaction of lumefantrine and piperazine by atrovastatin against *Plasmodium falciparum*. *Malaria J.*, **2014**, *13*(1), 189.
- [57] Fisher, N.; Meunier, B. Molecular basis of resistance to cytochrome *bc₁* inhibitors. *FEMS Yeast Res.*, **2008**, *8*(2), 183-192.
- [58] Siregar, J.E.; Kurisu, G.; Kobayashi, T.; Matsuzaki, M.; Sakamoto, K.; Mi-ichi, F.; Watanabe, Y.; Hirai, M.; Matsuoka, H.; Syafruddin, D. Direct evidence for the atovaquone action on the *Plasmodium* cytochrome *bc₁* complex. *Parasitol. Int.*, **2014**, *64*(3), 295-300.
- [59] Barton, V.; Fisher, N.; Biagini, G.A.; Ward, S.A.; O'Neill, P.M. Inhibiting *Plasmodium* cytochrome *bc₁*: a complex issue. *Curr. Opin. Chem. Biol.*, **2010**, *14*(4), 440-446.
- [60] Basco, L.K.; Mitaku, S.; Skaltsounis, A.; Ravelomanantsoa, N.; Tillequin, F.; Koch, M.; Le Bras, J. *In vitro* activities of furoquinoline and acridone alkaloids against *Plasmodium falciparum*. *Antimicrob. Agents Chemother.*, **1994**, *38*(5), 1169-1171.
- [61] Jones, M.E. Pyrimidine nucleotide biosynthesis in animals: genes, enzymes, and regulation of UMP biosynthesis. *Annu. Rev. Biochem.*, **1980**, *49*, 253-279.
- [62] Jordan, D.B.; Bisaha, J.J.; Piccollelli, M.A. Catalytic properties of dihydroorotate dehydrogenase from *Saccharomyces cerevisiae*: studies on pH, alternate substrates, and inhibitors. *Arch. Biochem. Biophys.*, **2000**, *378*(1), 84-92.
- [63] Gutteridge, W.E.; Dave, D.; Richards, W.H. Conversion of dihydroorotate to orotate in parasitic protozoa. *Biochim. Biophys. Acta*, **1979**, *582*(3), 390-401.
- [64] Patel, V.; Booker, M.; Kramer, M.; Ross, L.; Celatka, C.A.; Kennedy, L.M.; Dvorin, J.D.; Duraisingh, M.T.; Sliz, P.; Wirth, D.F.; Clardy, J. Identification and characterization of small molecule inhibitors of *Plasmodium falciparum* dihydroorotate dehydrogenase. *J. Biol. Chem.*, **2008**, *283*(50), 35078-35085.
- [65] Gujjar, R.; Marwaha, A.; El Mazouni, F.; White, J.; White, K.L.; Creason, S.; Shackleford, D.M.; Baldwin, J.; Charman, W.N.; Buckner, F.S.; Charman, S.; Rathod, P.K.; Phillips, M.A. Identification of a metabolically stable triazolopyrimidine-based dihydroorotate dehydrogenase inhibitor with antimalarial activity in mice. *J. Med. Chem.*, **2009**, *52*(7), 1864-1872.
- [66] Booker, M.L.; Bastos, C.M.; Kramer, M.L.; Barker, R.H., Jr.; Skerlj, R.; Sidhu, A.B.; Deng, X.; Celatka, C.; Cortese, J.F.; Guerrero Bravo, J.E.; Crespo Llado, K.N.; Serrano, A.E.; Angulo-Barturen, I.; Jimenez-Diaz, M.B.; Viera, S.; Garuti, H.; Wittlin, S.; Papastogiannidis, P.; Lin, J.W.; Janse, C.J.; Khan, S.M.; Duraisingh, M.; Coleman, B.; Goldsmith, E.J.; Phillips, M.A.; Munoz, B.; Wirth, D.F.; Klinger, J.D.; Wiegand, R.; Sybertz, E. Novel inhibitors of *Plasmodium falciparum* dihydroorotate dehydrogenase with anti-malarial activity in the mouse model. *J. Biol. Chem.*, **2010**, *285*(43), 33054-33064.
- [67] Lukens, A.K.; Ross, L.S.; Heidebrecht, R.; Javier Gamo, F.; Lafuente-Monasterio, M.J.; Booker, M.L.; Hartl, D.L.; Wiegand, R.C.; Wirth, D.F. Harnessing evolutionary fitness in *Plasmodium falciparum* for drug discovery and suppressing resistance. *Proc. Natl. Acad. Sci. U. S. A.*, **2014**, *111*(2), 799-804.
- [68] Coteron, J.M.; Marco, M.; Esquivias, J.; Deng, X.; White, K.L.; White, J.; Koltun, M.; El Mazouni, F.; Kokkonda, S.; Katneni, K.; Bhamidipati, R.; Shackleford, D.M.; Angulo-Barturen, I.; Ferrer, S.B.; Jimenez-Diaz, M.B.; Gamo, F.J.; Goldsmith, E.J.; Charman, W.N.; Bathurst, I.; Floyd, D.; Matthews, D.; Burrows, J.N.; Rathod, P.K.; Charman, S.A.; Phillips, M.A. Structure-guided lead optimization of triazolopyrimidine-ring substituents identifies potent *Plasmodium falciparum* dihydroorotate dehydrogenase inhibitors with clinical candidate potential. *J. Med. Chem.*, **2011**, *54*(15), 5540-5561.
- [69] Deng, X.; Kokkonda, S.; El Mazouni, F.; White, J.; Burrows, J.N.; Kaminsky, W.; Charman, S.A.; Matthews, D.; Rathod, P.K.; Phillips, M.A. Fluorine modulates species selectivity in the triazolopyrimidine class of *Plasmodium falciparum* dihydroorotate dehydrogenase inhibitors. *J. Med. Chem.*, **2014**, *57*(12), 5381-5394.
- [70] Xu, M.; Zhu, J.; Diao, Y.; Zhou, H.; Ren, X.; Sun, D.; Huang, J.; Han, D.; Zhao, Z.; Zhu, L.; Xu, Y.; Li, H. Novel selective and potent inhibitors of malaria parasite dihydroorotate dehydrogenase: discovery and optimization of dihydrothiophenone derivatives. *J. Med. Chem.*, **2013**, *56*(20), 7911-7924.
- [71] Yablonski, M.J.; Pasek, D.A.; Han, B.D.; Jones, M.E.; Traut, T.W. Intrinsic Activity and Stability of Bifunctional Human UMP Synthase and Its Two Separate Catalytic Domains, Orotate Phosphoribosyltransferase and Orotidine-5'-phosphate Decarboxylase. *J. Biol. Chem.*, **1996**, *271*, 10704-10708.
- [72] Suchi, M.; Mizuno, H.; Kawai, Y.; Tsuboi, T.; Sumi, S.; Okajima, K.; Hodgson, M.E.; Ogawa, H.; Wada, Y. Molecular cloning of the human UMP synthase gene and characterization of point mutations in two hereditary orotic aciduria families. *Am. J. Hum. Genet.*, **1997**, *60*(3), 525-539.
- [73] Zhang, Y.; Evans, G.B.; Clinch, K.; Crump, D.R.; Harris, L.D.; Frohlich, R.F.; Tyler, P.C.; Hazleton, K.Z.; Cassera, M.B.; Schramm, V.L. Transition state analogues of *Plasmodium falciparum* and human orotate phosphoribosyltransferases. *J. Biol. Chem.*, **2013**, *288*(48), 34746-34754.
- [74] Nirmalan, N.; Wang, P.; Sims, P.F.; Hyde, J.E. Transcriptional analysis of genes encoding enzymes of the folate pathway in the human malaria parasite *Plasmodium falciparum*. *Mol. Microbiol.*, **2002**, *46*(1), 179-190.
- [75] Chitnumsub, P.; Ittarat, W.; Jaruwat, A.; Noytanom, K.; Amornwatcharapong, W.; Pornthanakasem, W.; Chaiyen, P.; Yuthavong, Y.; Leartsakulpanich, U. The structure of *Plasmodium falciparum* serine hydroxymethyltransferase reveals a novel redox switch that regulates its activities. *Acta Crystallogr. D. Biol. Crystallogr.*, **2014**, *70*(Pt 6), 1517-1527.
- [76] Dasgupta, T.; Anderson, K.S. Probing the role of parasite-specific, distant structural regions on communication and catalysis in the bifunctional thymidylate synthase-dihydrofolate reductase from *Plasmodium falciparum*. *Biochemistry*, **2008**, *47*(5), 1336-1345.
- [77] Volpato, J.P.; Pelletier, J.N. Mutational 'hot-spots' in mammalian, bacterial and protozoal dihydrofolate reductases associated with antifolate resistance: Sequence and structural comparison. *Drug Resist. Updat.*, **2009**, *12*, 28-41.
- [78] Khan, S.; Garg, A.; Camacho, N.; Van Rooyen, J.; Kumar Pole, A.; Belhali, H.; Ribas de Pouplana, L.; Sharma, V.; Sharma, A. Structural analysis of malaria-parasite lysyl-tRNA synthetase provides a platform for drug development. *Acta Crystallogr. D. Biol. Crystallogr.*, **2013**, *69*(Pt 5), 785-795.
- [79] Hoen, R.; Novoa, E.M.; Lopez, A.; Camacho, N.; Cubells, L.; Vieira, P.; Santos, M.; Marin-Garcia, P.; Bautista, J.M.; Cortes, A.; Ribas de Pouplana, L.; Royo, M. Selective inhibition of an apicoplastic aminoacyl-tRNA synthetase from *Plasmodium falciparum*. *Chembiochem.*, **2013**, *14*(4), 499-509.
- [80] Koh, C.Y.; Kim, J.E.; Napoli, A.J.; Verlinde, C.L.; Fan, E.; Buckner, F.S.; Van Voorhis, W.C.; Hol, W.G. Crystal structures of *Plasmodium falciparum* cytosolic tryptophanyl-tRNA synthetase and its potential as a target for structure-guided drug design. *Mol. Biochem. Parasitol.*, **2013**, *189*(1-2), 26-32.
- [81] Jackson, K.E.; Habib, S.; Frugier, M.; Hoen, R.; Khan, S.; Pham, J.S.; Ribas de Pouplana, L.; Royo, M.; Santos, M.A.; Sharma, A.; Ralph, S.A. Protein translation in *Plasmodium* parasites. *Trends Parasitol.*, **2011**, *27*(10), 467-476.
- [82] Bhatt, T.K.; Kapil, C.; Khan, S.; Jairajpuri, M.A.; Sharma, V.; Santoni, D.; Silvestrini, F.; Pizzi, E.; Sharma, A. A genomic

- glimpse of aminoacyl-tRNA synthetases in malaria parasite *Plasmodium falciparum*. *BMC Genomics*, **2009**, *10*, 644.
- [83] Pham, J.S.; Dawson, K.L.; Jackson, K.E.; Lim, E.E.; Pasaje, C.F.; Turner, K.E.; Ralph, S.A. Aminoacyl-tRNA synthetases as drug targets in eukaryotic parasites. *Int. J. Parasitol. Drugs Drug Resist.*, **2014**, *4*(1), 1-13.
- [84] Istvan, E.S.; Dharia, N.V.; Bopp, S.E.; Gluzman, I.; Winzeler, E.A.; Goldberg, D.E. Validation of isoleucine utilization targets in *Plasmodium falciparum*. *Proc. Natl. Acad. Sci. U. S. A.*, **2011**, *108*(4), 1627-1632.
- [85] Hoepfner, D.; McNamara, C.W.; Lim, C.S.; Studer, C.; Riedl, R.; Aust, T.; McCormack, S.L.; Plouffe, D.M.; Meister, S.; Schuierer, S.; Plikat, U.; Hartmann, N.; Staedtler, F.; Cotesta, S.; Schmitt, E.K.; Petersen, F.; Supek, F.; Glynn, R.J.; Tallarico, J.A.; Porter, J.A.; Fishman, M.C.; Bodenreider, C.; Diagana, T.T.; Movva, N.R.; Winzeler, E.A. Selective and specific inhibition of the *Plasmodium falciparum* lysyl-tRNA synthetase by the fungal secondary metabolite cladospirin. *Cell Host Microbe*, **2012**, *11*(6), 654-663.
- [86] Ding, D.; Meng, Q.; Gao, G.; Zhao, Y.; Wang, Q.; Nare, B.; Jacobs, R.; Rock, F.; Alley, M.R.; Plattner, J.J.; Chen, G.; Li, D.; Zhou, H. Design, Synthesis, and Structure-Activity Relationship of *Trypanosoma brucei* Leucyl-tRNA Synthetase Inhibitors as Antitrypanosomal Agents. *J. Med. Chem.*, **2011**, *54*(5), 1276-1287.
- [87] Farrera-Sinfreu, J.; Espanol, Y.; Geslain, R.; Guitart, T.; Albericio, F.; Ribas de Pouplana, L.; Royo, M. Solid-phase combinatorial synthesis of a lysyl-tRNA synthetase (LysRS) inhibitory library. *J. Comb. Chem.*, **2008**, *10*(3), 391-400.
- [88] Liu, J.; Istvan, E.S.; Gluzman, I.Y.; Gross, J.; Goldberg, D.E. *Plasmodium falciparum* ensures its amino acid supply with multiple acquisition pathways and redundant proteolytic enzyme systems. *Proc. Natl. Acad. Sci. U. S. A.*, **2006**, *103*(23), 8840-8845.
- [89] Khan, S.; Sharma, A.; Jamwal, A.; Sharma, V.; Pole, A.K.; Thakur, K.K.; Sharma, A. Uneven spread of cis- and trans-editing aminoacyl-tRNA synthetase domains within translational compartments of *P. falciparum*. *Sci. Rep.*, **2011**, *1*, 188.
- [90] Jackson, K.E.; Pham, J.S.; Kwek, M.; De Silva, N.S.; Allen, S.M.; Goodman, C.D.; McFadden, G.I.; Ribas de Pouplana, L.; Ralph, S.A. Dual targeting of aminoacyl-tRNA synthetases to the apicoplast and cytosol in *Plasmodium falciparum*. *Int. J. Parasitol.*, **2012**, *42*(2), 177-186.
- [91] Derbyshire, E.R.; Mazitschek, R.; Clardy, J. Characterization of *Plasmodium* liver stage inhibition by halofuginone. *ChemMedChem*, **2012**, *7*(5), 844-849.
- [92] Keller, T.L.; Zocco, D.; Sundrud, M.S.; Hendrick, M.; Edenius, M.; Yum, J.; Kim, Y.J.; Lee, H.K.; Cortese, J.F.; Wirth, D.F.; Dignam, J.D.; Rao, A.; Yeo, C.Y.; Mazitschek, R.; Whitman, M. Halofuginone and other febrifugine derivatives inhibit prolyl-tRNA synthetase. *Nat. Chem. Biol.*, **2012**, *8*(3), 311-317.
- [93] Zhou, H.; Sun, L.; Yang, X.L.; Schimmel, P. ATP-directed capture of bioactive herbal-based medicine on human tRNA synthetase. *Nature*, **2013**, *494*(7435), 121-124.
- [94] Novoa, E.M.; Camacho, N.; Tor, A.; Wilkinson, B.; Moss, S.; Marin-García, P.; Azcarate, I.G.; Bautista, J.M.; Miranda, A.C.; Francklyn, C.S.; Varon, S.; Royo, M.; Cortes, A.; Ribas de Pouplana, L. Analogs of natural aminoacyl-tRNA synthetase inhibitors clear malaria *in vivo*. *Proc. Natl. Acad. Sci. U. S. A.*, **2014**, *111*(51), E5508-E5517.
- [95] Bhatt, T.K.; Khan, S.; Dwivedi, V.P.; Banday, M.M.; Sharma, A.; Chandele, A.; Camacho, N.; Ribas de Pouplana, L.; Wu, Y.; Craig, A.G.; Mikkonen, A.T.; Maier, A.G.; Yogavel, M.; Sharma, A. Malaria parasite tyrosyl-tRNA synthetase secretion triggers pro-inflammatory responses. *Nat. Commun.*, **2011**, *2*, 530.
- [96] Sundriyal, S.; Malmquist, N.A.; Caron, J.; Blundell, S.; Liu, F.; Chen, X.; Srimongkolpithak, N.; Jin, J.; Charman, S.A.; Scherf, A.; Fuchter, M.J. Development of diaminoquinazoline histone lysine methyltransferase inhibitors as potent blood-stage antimalarial compounds. *ChemMedChem*, **2014**, *9*(10), 2360-2373.
- [97] Malmquist, N.A.; Moss, T.A.; Mecheri, S.; Scherf, A.; Fuchter, M.J. Small-molecule histone methyltransferase inhibitors display rapid antimalarial activity against all blood stage forms in *Plasmodium falciparum*. *Proc. Natl. Acad. Sci. U. S. A.*, **2012**, *109*(41), 16708-16713.
- [98] Chaal, B.K.; Gupta, A.P.; Wastuwidyaningtyas, B.D.; Luah, Y.H.; Bozdech, Z. Histone deacetylases play a major role in the transcriptional regulation of the *Plasmodium falciparum* life cycle. *PLoS Pathog.*, **2010**, *6*(1), e1000737.
- [99] Andrews, K.T.; Tran, T.N.; Lucke, A.J.; Kahnberg, P.; Le, G.T.; Boyle, G. M.; Gardiner, D.L.; Skinner-Adams, T.S.; Fairlie, D.P. Potent antimalarial activity of histone deacetylase inhibitor analogues. *Antimicrob. Agents Chemother.*, **2008**, *52*(4), 1454-1461.
- [100] Sumanadasa, S.D.; Goodman, C.D.; Lucke, A.J.; Skinner-Adams, T.; Sahama, I.; Haque, A.; Do, T.A.; McFadden, G.I.; Fairlie, D.P.; Andrews, K.T. Antimalarial activity of the anticancer histone deacetylase inhibitor SB939. *Antimicrob. Agents Chemother.*, **2012**, *56*(7), 3849-3856.
- [101] Bowyer, P.W.; Tate, E.W.; Leatherbarrow, R.J.; Holder, A.A.; Smith, D.F.; Brown, K.A. N-Myristoyltransferase: a Prospective Drug Target for Protozoan Parasites. *ChemMedChem*, **2008**, *3*(3), 402-408.
- [102] Wright, M.H.; Clough, B.; Rackham, M.D.; Rangachari, K.; Brannigan, J.A.; Grainger, M.; Moss, D.K.; Bottrill, A.R.; Heal, W.P.; Broncel, M. Validation of N-myristoyltransferase as an antimalarial drug target using an integrated chemical biology approach. *Nat. Chem.*, **2014**, *6*(2), 112-121.
- [103] Yu, Z.; Brannigan, J.A.; Moss, D.K.; Brzozowski, A.M.; Wilkinson, A.J.; Holder, A.A.; Tate, E.W.; Leatherbarrow, R.J. Design and synthesis of inhibitors of *Plasmodium falciparum* N-myristoyltransferase, a promising target for antimalarial drug discovery. *J. Med. Chem.*, **2012**, *55*(20), 8879-8890.
- [104] Arafat, K.; Ferrer, S.; Marti, S.; Moliner, V. Quantum mechanics/molecular mechanics studies of the mechanism of falcipain-2 inhibition by the epoxysuccinate E64. *Biochemistry*, **2014**, *53*(20), 3336-3346.
- [105] Liu, Y.; Cui, K.; Lu, W.; Luo, W.; Wang, J.; Huang, J.; Guo, C. Synthesis and antimalarial activity of novel dihydro-artemisinin derivatives. *Molecules*, **2011**, *16*(6), 4527-4538.
- [106] Shah, F.; Gut, J.; Legac, J.; Shivakumar, D.; Sherman, W.; Rosenthal, P.J.; Avery, M.A. Computer-aided drug design of falcipain inhibitors: virtual screening, structure-activity relationships, hydration site thermodynamics, and reactivity analysis. *J. Chem. Inf. Model.*, **2012**, *52*(3), 696-710.
- [107] Kerr, I.D.; Lee, J.H.; Pandey, K.C.; Harrison, A.; Sajid, M.; Rosenthal, P.J.; Brinen, L.S. Structures of falcipain-2 and falcipain-3 bound to small molecule inhibitors: implications for substrate specificity. *J. Med. Chem.*, **2009**, *52*(3), 852-857.
- [108] Stolze, S.C.; Deu, E.; Kaschani, F.; Li, N.; Florea, B.I.; Richau, K.H.; Colby, T.; van der Hoorn, R.A.; Overkleef, H.S.; Bogoy, M.; Kaiser, M. The antimalarial natural product symplostatin 4 is a nanomolar inhibitor of the food vacuole falcipains. *Chem. Biol.*, **2012**, *19*(12), 1546-1555.
- [109] Deponte, M.; Hoppe, H.C.; Lee, M.C.; Maier, A.G.; Richard, D.; Rug, M.; Spielmann, T.; Przyborski, J.M. Wherever I may roam: protein and membrane trafficking in *P. falciparum*-infected red blood cells. *Mol. Biochem. Parasitol.*, **2012**, *186*(2), 95-116.
- [110] Boddey, J.A.; Cowman, A.F. *Plasmodium* nesting: remaking the erythrocyte from the inside out. *Annu. Rev. Microbiol.*, **2013**, *67*, 243-269.
- [111] Marti, M.; Good, R.T.; Rug, M.; Knuepfer, E.; Cowman, A.F. Targeting malaria virulence and remodeling proteins to the host erythrocyte. *Science*, **2004**, *306*(5703), 1930-1933.
- [112] Gardner, M.J.; Hall, N.; Fung, E.; White, O.; Berriman, M.; Hyman, R.W.; Carlton, J.M.; Pain, A.; Nelson, K.E.; Bowman, S.; Paulsen, I.T.; James, K.; Eisen, J.A.; Rutherford, K.; Salzberg, S.L.; Craig, A.; Kyes, S.; Chan, M.S.; Nene, V.; Shallom, S.J.; Suh, B.; Peterson, J.; Angiuoli, S.; Pertea, M.; Allen, J.; Selengut, J.; Haft, D.; Mather, M.W.; Vaidya, A.B.; Martin, D.M.; Fairlamb, A.H.; Fraunholz, M.J.; Roos, D.S.; Ralph, S.A.; McFadden, G.I.; Cummings, L.M.; Subramanian, G.M.; Mungall, C.; Venter, J.C.; Carucci, D.J.; Hoffman, S.L.; Newbold, C.; Davis, R.W.; Fraser, C.M.; Barrell, B. Genome sequence of the human malaria parasite *Plasmodium falciparum*. *Nature*, **2002**, *419*(6906), 498-511.
- [113] Liu, J.; Gluzman, I.Y.; Drew, M.E.; Goldberg, D.E. The role of *Plasmodium falciparum* food vacuole plasmepsins. *J. Biol. Chem.*, **2005**, *280*(2), 1432-1437.
- [114] Goldberg, D.E. Hemoglobin degradation. *Curr. Top. Microbiol. Immunol.*, **2005**, *295*, 275-291.
- [115] Ersmark, K.; Samuelsson, B.; Hallberg, A. Plasmepsins as potential targets for new antimalarial therapy. *Med. Res. Rev.*, **2006**, *26*(5), 626-666.

- [116] Chang, H.H.; Falick, A.M.; Carlton, P.M.; Sedat, J.W.; DeRisi, J.L.; Marletta, M.A. N-terminal processing of proteins exported by malaria parasites. *Mol. Biochem. Parasitol.*, **2008**, *160*(2), 107-115.
- [117] Sleebs, B.E.; Lopaticki, S.; Marapana, D.S.; O'Neill, M.T.; Rajasekaran, P.; Gazdik, M.; Gunther, S.; Whitehead, L.W.; Lowes, K.N.; Barfod, L.; Hviid, L.; Shaw, P.J.; Hodder, A.N.; Smith, B.J.; Cowman, A.F.; Boddey, J.A. Inhibition of Plasmeprin V activity demonstrates its essential role in protein export, PfEMP1 display, and survival of malaria parasites. *PLoS Biol.*, **2014**, *12*(7), e1001897.
- [118] Omara-Opyene, A.L.; Moura, P.A.; Sulsona, C.R.; Bonilla, J.A.; Yowell, C.A.; Fujioka, H.; Fidock, D.A.; Dame, J.B. Genetic disruption of the *Plasmodium falciparum* digestive vacuole plasmepsins demonstrates their functional redundancy. *J. Biol. Chem.*, **2004**, *279*(52), 54088-54096.
- [119] Valiente, P.A.; Batista, P.R.; Pupo, A.; Pons, T.; Valencia, A.; Pascutti, P.G. Predicting functional residues in *Plasmodium falciparum* plasmepsins by combining sequence and structural analysis with molecular dynamics simulations. *Proteins*, **2008**, *73*(2), 440-457.
- [120] Gil, L.A.; Valiente, P.; Pascutti, P.; Pons, T. Computational Perspectives into Plasmepsins Structure—Function Relationship: Implications to Inhibitors Design. *J. Trop. Med.*, **2011**, *2011*, 657483.
- [121] Payne, S.H.; Loomis, W.F. Retention and loss of amino acid biosynthetic pathways based on analysis of whole-genome sequences. *Eukaryot. Cell*, **2006**, *5*(2), 272-276.
- [122] Martin, R.E.; Kirk, K. Transport of the essential nutrient isoleucine in human erythrocytes infected with the malaria parasite *Plasmodium falciparum*. *Blood*, **2007**, *109*(5), 2217-2224.
- [123] Taylor, A. Aminopeptidases: structure and function. *FASEB J.*, **1993**, *7*(2), 290-298.
- [124] Skinner-Adams, T.S.; Lowther, J.; Teuscher, F.; Stack, C.M.; Grembecka, J.; Mucha, A.; Kafarski, P.; Trenholme, K.R.; Dalton, J.P.; Gardiner, D.L. Identification of phosphinate dipeptide analog inhibitors directed against the *Plasmodium falciparum* M17 leucine aminopeptidase as lead antimalarial compounds. *J. Med. Chem.*, **2007**, *50*(24), 6024-6031.
- [125] McGowan, S.; Oellig, C.A.; Birru, W.A.; Caradoc-Davies, T.T.; Stack, C.M.; Lowther, J.; Skinner-Adams, T.; Mucha, A.; Kafarski, P.; Grembecka, J.; Trenholme, K.R.; Buckle, A.M.; Gardiner, D.L.; Dalton, J.P.; Whisstock, J.C. Structure of the *Plasmodium falciparum* M17 aminopeptidase and significance for the design of drugs targeting the neutral exopeptidases. *Proc. Natl. Acad. Sci. U. S. A.*, **2010**, *107*(6), 2449-2454.
- [126] Deprez-Poulain, R.; Flipo, M.; Piveteau, C.; Leroux, F.; Dassonneville, S.; Florent, I.; Maes, L.; Cos, P.; Deprez, B. Structure-activity relationships and blood distribution of antiplasmodial aminopeptidase-1 inhibitors. *J. Med. Chem.*, **2012**, *55*(24), 10909-10917.
- [127] Flipo, M.; Florent, I.; Grellier, P.; Sergheraert, C.; Deprez-Poulain, R. Design, synthesis and antimalarial activity of novel, quinoline-based, zinc metallo-aminopeptidase inhibitors. *Bioorg. Med. Chem. Lett.*, **2003**, *13*(16), 2659-2662.
- [128] Kannan Sivaraman, K.; Paiardini, A.; Sienczyk, M.; Ruggeri, C.; Oellig, C.A.; Dalton, J.P.; Scammells, P.J.; Drag, M.; McGowan, S. Synthesis and structure-activity relationships of phosphonic arginine mimetics as inhibitors of the M1 and M17 aminopeptidases from *Plasmodium falciparum*. *J. Med. Chem.*, **2013**, *56*(12), 5213-5217.
- [129] Mistry, S.N.; Drinkwater, N.; Ruggeri, C.; Sivaraman, K.K.; Loganathan, S.; Fletcher, S.; Drag, M.; Paiardini, A.; Avery, V.M.; Scammells, P.J.; McGowan, S. Two-pronged attack: dual inhibition of *Plasmodium falciparum* M1 and M17 metalloaminopeptidases by a novel series of hydroxamic acid-based inhibitors. *J. Med. Chem.*, **2014**, *57*(21), 9168-9183.
- [130] Hanks, S.K. Genomic analysis of the eukaryotic protein kinase superfamily: a perspective. *Genome Biol.*, **2003**, *4*(5), 111.
- [131] Ward, P.; Equinet, L.; Packer, J.; Doerig, C. Protein kinases of the human malaria parasite *Plasmodium falciparum*: the kinome of a divergent eukaryote. *BMC Genomics*, **2004**, *5*, 79.
- [132] Anamika; Srinivasan, N.; Krupa, A. A genomic perspective of protein kinases in *Plasmodium falciparum*. *Proteins*, **2005**, *58*(1), 180-189.
- [133] Solyakov, L.; Halbert, J.; Alam, M.M.; Semblat, J.P.; Dorin-Semblat, D.; Reininger, L.; Bottrill, A.R.; Mistry, S.; Abdi, A.; Fennell, C.; Holland, Z.; Demarta, C.; Bouza, Y.; Sicard, A.; Nivez, M.P.; Eschenlauer, S.; Lama, T.; Thomas, D.C.; Sharma, P.; Agarwal, S.; Kern, S.; Pradel, G.; Graciotti, M.; Tobin, A.B.; Doerig, C. Global kinomic and phospho-proteomic analyses of the human malaria parasite *Plasmodium falciparum*. *Nat. Commun.*, **2011**, *2*, 565.
- [134] Dorin, D.; Le Roch, K.; Sallicandro, P.; Alano, P.; Parzy, D.; Poulet, P.; Meijer, L.; Doerig, C. Pfk-1, a NIMA-related kinase from the human malaria parasite *Plasmodium falciparum* Biochemical properties and possible involvement in MAPK regulation. *Eur. J. Biochem.*, **2001**, *268*(9), 2600-2608.
- [135] Xiao, Z.; Waters, N.C.; Woodard, C.L.; Li, Z.; Li, P. Design and synthesis of Pfmrk inhibitors as potential antimalarial agents. *Bioorg. Med. Chem. Lett.*, **2001**, *11*(21), 2875-2878.
- [136] Geyer, J.A.; Keenan, S.M.; Woodard, C.L.; Thompson, P.A.; Gerena, L.; Nichols, D.A.; Gutteridge, C.E.; Waters, N.C. Selective inhibition of Pfmrk, a *Plasmodium falciparum* CDK, by antimalarial 1, 3-diaryl-2-propenones. *Bioorg. Med. Chem. Lett.*, **2009**, *19*(7), 1982-1985.
- [137] Dorin-Semblat, D.; Sicard, A.; Doerig, C.; Ranford-Cartwright, L.; Doerig, C. Disruption of the PFPK7 gene impairs schizogony and sporogony in the human malaria parasite *Plasmodium falciparum*. *Eukaryot. Cell*, **2008**, *7*(2), 279-285.
- [138] Lebouvier, N.; Jullian, V.; Desvignes, I.; Maurel, S.; Parenty, A.; Dorin-Semblat, D.; Doerig, C.; Sauvain, M.; Laurent, D. Antiplasmodial activities of homogenetic acid derivative protein kinase inhibitors isolated from a Vanuatu marine sponge *Pseudoceratina* sp. *Mar. Drugs*, **2009**, *7*(4), 640-653.
- [139] Kato, N.; Sakata, T.; Breton, G.; Le Roch, K.G.; Nagle, A.; Andersen, C.; Bursulaya, B.; Henson, K.; Johnson, J.; Kumar, K.A.; Marr, F.; Mason, D.; McNamara, C.; Plouffe, D.; Ramachandran, V.; Spooner, M.; Tuntland, T.; Zhou, Y.; Peters, E.C.; Chatterjee, A.; Schultz, P.G.; Ward, G.E.; Gray, N.; Harper, J.; Winzler, E.A. Gene expression signatures and small-molecule compounds link a protein kinase to *Plasmodium falciparum* motility. *Nat. Chem. Biol.*, **2008**, *4*(6), 347-356.
- [140] Lemercier, G.; Fernandez-Montalvan, A.; Shaw, J.P.; Kugelstadt, D.; Bomke, J.; Domostoj, M.; Schwarz, M.K.; Scheer, A.; Kappes, B.; Leroy, D. Identification and characterization of novel small molecules as potent inhibitors of the plasmodial calcium-dependent protein kinase 1. *Biochemistry*, **2009**, *48*(27), 6379-6389.
- [141] Ojo, K.K.; Pfander, C.; Mueller, N.R.; Bursstroem, C.; Larson, E.T.; Bryan, C.M.; Fox, A.M.; Reid, M.C.; Johnson, S.M.; Murphy, R.C.; Kennedy, M.; Mann, H.; Leibly, D.J.; Hewitt, S.N.; Verlinde, C.L.; Kappe, S.; Merritt, E.A.; Maly, D.J.; Billker, O.; Van Voorhis, W.C. Transmission of malaria to mosquitoes blocked by bumped kinase inhibitors. *J. Clin. Invest.*, **2012**, *122*(6), 2301-2305.
- [142] Haste, N.M.; Talabani, H.; Doo, A.; Merckx, A.; Langsley, G.; Taylor, S.S. Exploring the *Plasmodium falciparum* cyclic-adenosine monophosphate (cAMP)-dependent protein kinase (PfPKA) as a therapeutic target. *Microbes Infect.*, **2012**, *14*(10), 838-850.
- [143] Lavogina, D.; Budu, A.; Enkvist, E.; Hopp, C.S.; Baker, D.A.; Langsley, G.; Garcia, C.R.; Uri, A. Targeting *Plasmodium falciparum* protein kinases with adenosine analogue-oligoarginine conjugates. *Exp. Parasitol.*, **2014**, *138*, 55-62.
- [144] Wurtz, N.; Desplans, J.; Parzy, D. Phenotypic and transcriptomic analyses of *Plasmodium falciparum* protein kinase A catalytic subunit inhibition. *Parasitol. Res.*, **2009**, *105*(6), 1691-1699.
- [145] Merckx, A.; Echalier, A.; Langford, K.; Sicard, A.; Langsley, G.; Joore, J.; Doerig, C.; Noble, M.; Endicott, J. Structures of *P. falciparum* protein kinase 7 identify an activation motif and leads for inhibitor design. *Structure*, **2008**, *16*(2), 228-238.
- [146] Hotta, C.T.; Gazarini, M.L.; Beraldo, F.H.; Varotti, F.P.; Lopes, C.; Markus, R.P.; Pozzan, T.; Garcia, C.R. Calcium-dependent modulation by melatonin of the circadian rhythm in malarial parasites. *Nat. Cell Biol.*, **2000**, *2*(7), 466-468.
- [147] Syn, C.; Parzy, D.; Traincard, F.; Boccaccio, I.; Joshi, M.B.; Lin, D.T.; Yang, X.M.; Assemat, K.; Doerig, C.; Langsley, G. The H89 cAMP-dependent protein kinase inhibitor blocks *Plasmodium falciparum* development in infected erythrocytes. *Eur. J. Biochem.*, **2001**, *268*(18), 4842-4849.
- [148] Vaid, A.; Thomas, D.C.; Sharma, P. Role of Ca²⁺/calmodulin-PfPKB signaling pathway in erythrocyte invasion by *Plasmodium falciparum*. *J. Biol. Chem.*, **2008**, *283*(9), 5589-5597.

- [149] Taylor, C.J.; McRobert, L.; Baker, D.A. Disruption of a *Plasmodium falciparum* cyclic nucleotide phosphodiesterase gene causes aberrant gametogenesis. *Mol. Microbiol.*, **2008**, *69*(1), 110-118.
- [150] Moon, R.W.; Taylor, C.J.; Bex, C.; Schepers, R.; Goulding, D.; Janse, C.J.; Waters, A.P.; Baker, D.A.; Billker, O. A cyclic GMP signalling module that regulates gliding motility in a malaria parasite. *PLoS Pathog.*, **2009**, *5*(9), e1000599.
- [151] Howard, B.L.; Thompson, P.E.; Manallack, D.T. Active site similarity between human and *Plasmodium falciparum* phosphodiesterases: considerations for antimalarial drug design. *J. Comput. Aided Mol. Des.*, **2011**, *25*(8), 753-762.
- [152] Beghyn, T.B.; Charton, J.; Leroux, F.; Laconde, G.; Bourin, A.; Cos, P.; Maes, L.; Deprez, B. Drug to genome to drug: discovery of new antiplasmodial compounds. *J. Med. Chem.*, **2011**, *54*(9), 3222-3240.
- [153] Arnou, B.; Montigny, C.; Morth, J.P.; Nissen, P.; Jaxel, C.; Moller, J.V.; Maire, M. The *Plasmodium falciparum* Ca²⁺-ATPase PfATP6: insensitive to artemisinin, but a potential drug target. *Biochem. Soc. Trans.*, **2011**, *39*(3), 823-831.
- [154] David-Bosne, S.; Florent, I.; Lund-Winther, A.M.; Hansen, J.B.; Buch-Pedersen, M.; Machillot, P.; le Maire, M.; Jaxel, C. Antimalarial screening via large-scale purification of *Plasmodium falciparum* Ca²⁺-ATPase 6 and *in vitro* studies. *FEBS J.*, **2013**, *280*(21), 5419-5429.
- [155] Kapoor, N.; Banerjee, T.; Babu, P.; Maity, K.; Surolia, N.; Surolia, A. Design, development, synthesis, and docking analysis of 2'-substituted triclosan analogs as inhibitors for *Plasmodium falciparum* Enoyl-ACP reductase. *IUBMB Life*, **2009**, *61*(11), 1083-1091.
- [156] Siregar, J.E.; Kurisu, G.; Kobayashi, T.; Matsuzaki, M.; Sakamoto, K.; Mi-ichi, F.; Watanabe, Y.-i.; Hirai, M.; Matsuoka, H.; Syafruddin, D. Direct evidence for the atovaquone action on the *Plasmodium* cytochrome bc 1 complex. *Parasitol. Int.*, **2015**, *64*(3), 295-300.

RESEARCH ARTICLE

Kinetic and molecular dynamic studies of inhibitors of shikimate dehydrogenase from methicillin-resistant *Staphylococcus aureus*

Daniel Enríquez-Mendiola¹ | Alfredo Téllez-Valencia¹ | Erick Sierra-Campos² |
Mara Campos-Almazán¹ | Mónica Valdez-Solana² | Marcelo Gómez Palacio-Gastélum³ |
Claudia Avitia-Domínguez¹ 

¹Facultad de Medicina y Nutrición, Universidad Juárez del Estado de Durango, Durango, Durango, México

²Facultad de Ciencias Químicas, Universidad Juárez del Estado de Durango, Gómez Palacio, Durango, México

³Facultad de Odontología, Universidad Juárez del Estado de Durango, Durango, Durango, México

Correspondence

Claudia Avitia-Domínguez, Facultad de Medicina y Nutrición, Universidad Juárez del Estado de Durango, Av. Universidad y Fanny Anitúa S/N, Durango, Durango C.P. 34000, México.

Email: avitiaclaudia@gmail.com

Funding information

Consejo Nacional de Ciencia y Tecnología, Grant/Award Number: 257848, 258694 and 623226

Abstract

Due to its resistance to many antibiotics, methicillin-resistant *Staphylococcus aureus* (MRSA) have become a worldwide health problem creating the urgent necessity of developing new drugs against this pathogen. In this sense, one approach is to search for inhibitors of important enzymes in its metabolism. According to this, the shikimate pathway is an important metabolic route in bacteria and its enzymes are considered as great targets for the development of new antibiotic drugs. One of these enzymes is the shikimate dehydrogenase that catalyzes the reversal reduction from 3-dehydroshikimate to shikimate using NADPH as cofactor. In this work, four new compounds were found capable of inhibiting the shikimate dehydrogenase (SDH) from *S. aureus* (SaSDH) activity. A detailed kinetic characterization showed that the most potent inhibitor presented a K_i of 8 and 10 μM with respect to shikimate and NADP^+ , respectively, and a mixed partial inhibition mechanism for both substrates. Molecular dynamics studies revealed that the four inhibitors perturb the structure of SaSDH affecting important domains. Toxicological and physicochemical parameters indicated that these compounds can be considered as potential drugs. Therefore, these compounds are good hits that will help in the process to obtain a new drug against MRSA.

KEYWORDS

drug design, enzyme kinetics, molecular dynamic, MRSA, shikimate dehydrogenase

1 | INTRODUCTION

Bacterial resistance has become a worldwide public health problem due to the loss of efficacy of the treatments, the increment in treatment costs, and hospitalization time. This generates a high impact in the health system and society, creating the urgent necessity to develop new drugs to treat multiresistant bacterial infections and particularly new drugs with new action mechanisms (WHO, 2017). A globally clinical important bacterium is *Staphylococcus aureus*;

this is a gram-positive coccus, commonly found as part of human microbiota (Kloos & Bannerman, 1995), and its clinical interest takes place with the appearance of resistant *S. aureus* strains that have developed different mechanisms to avoid the effects of different types of drugs such as β -lactams, carbapenems, and cephalosporines, between others (Enright et al., 2002; Li et al., 2018). These strains are known as methicillin-resistant *S. aureus* (MRSA) and are responsible for causing different kinds of infections from skin and soft tissues infections such as bulbous impetigo or

abscess and cellulitis, between others, to more dangerous infections such as blood stream infections, bone infections, or toxic shock syndrome (Liu et al., 2011; Pottinger, 2013). Since their appearance, MRSA strains have extended worldwide and incremented in over 300% becoming one of the most important human pathogens (Novales, 2011). Nowadays, most of the drugs used to treat these infections are losing their efficacy or are no longer effective and the appearance of side-effects, as well as new resistant strains, makes harder to treat these infections. All the aforementioned makes necessary to develop new antibiotic with different action mechanisms. In this context, an approach is to search for inhibitors of important enzymes in the pathogen metabolism. According to this, an important metabolic pathway, absent in mammals and vital for plants, fungi, bacteria, and some *Apicomplexa* parasites, is the shikimate pathway that has been considered as an attractive target to develop new drugs (Bentley & Haslam, 1990; Coggins et al., 2003; Roberts et al., 1999).

This pathway binds the metabolism of carbohydrates, the condensation of phosphoenolpyruvate (PEP) from glycolysis and D-erythrose-4-phosphate (E4P) from the pentose phosphate pathway, with the synthesis of aromatic compounds such as vitamin K, folates, ubiquinone, and aromatic amino acids from chorismate, the main product of the pathway (Bentley & Haslam, 1990). The enzymes involved in this pathway are considered as great targets for the development of new antibiotic drugs (Han et al., 2006; Hawkins, Lamb, Moore, Charles, & Roberts, 1993; Peek, Shi, & Christendat, 2014). One of these is the shikimate dehydrogenase (SDH) that catalyzes the fourth step in the pathway, the reversal reduction of 3-dehydroshikimate to shikimate depending on NADPH as cofactor. Structurally, the SDH family presents differences between its members; in bacteria it is found as a monofunctional enzyme (Han et al., 2006, 2009), while in plants it can be found as a bifunctional complex called DHQ-SDH complex that catalyzes the third and fourth steps of the pathway (Bonner & Jensen, 1994), and in fungi SDH takes a place in the pentafunctional AroM component (Duncan, Edwards, & Coggins, 1987).

Particularly in bacteria, SDH can be found as a monomer in practically all the species where it has been studied (Anton & Coggins, 1988; Avitia-Domínguez et al., 2014; Gan et al.,

2007; Han et al., 2006, 2009; Peek et al., 2014), only in *Thermus thermophilus* (Bagautdinov & Kunishima, 2007) and *Methanocaldococcus jannasschi* (Padyana & Burley, 2003) it has been found as a dimer. The enzyme is composed by two α/β domains linked by two α helices, the N-terminal domain supports the substrate binding site and the C-terminal domain that presents a characteristic Rossmann fold where the NADPH binding site is located (Arcuri et al., 2008; Peek & Christendat, 2015; Ye et al., 2003).

Nowadays, different types of bacterial SDH inhibitors have been reported including natural compounds (Avitia-Domínguez et al., 2014; Díaz-Quiroz et al., 2018; Han et al., 2006; Peek et al., 2014). Taking into account the structure of three compounds that inhibit SDH from *S. aureus* (SaSDH) reported by our group previously, four new SaSDH inhibitors were found in this work. The characterization of their inhibition mechanism and molecular dynamic simulations of the enzyme-inhibitor complex were performed. Additionally, studies of their physicochemical and toxicological properties were realized.

2 | METHODS AND MATERIALS

2.1 | Compounds selection

The new SaSDH inhibitors search was realized based on a structural similarity search strategy taking into count the structures of the three SaSDH inhibitors reported, compound **238**, **766**, and **894** (Avitia-Domínguez et al., 2014; Figure 1). The libraries used for the search were the “Fragment Library” from Maybridge (www.maybridge.com), which includes 1,000 compounds that stand by the Lipinski rules (Lipinski, Lombardo, Dominy, & Feeney, 2001) to be considered as potential molecules for drug design, and the “Hit2lead” library from ChemBridge (www.chembridge.com) which includes more than 1,300,000 of small molecules. Compounds were selected using the tool *superposition* in MAESTRO software v. 11.5 (www.schrodinger.com); those molecules with a root-mean-square deviation (RMSD) less than 4.0 in comparison with the structure of inhibitors **238**, **766**, and **894** were selected to be tested in vitro, because after trying with different values, this cut-off allowed us to conserve the principal chemical nucleus of the three inhibitors and basically vary the substituents around the rings during selection.

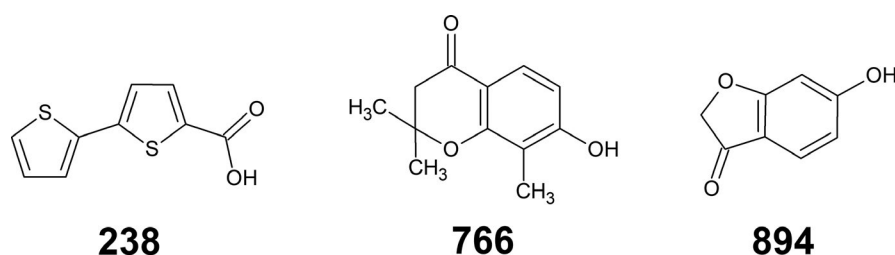


FIGURE 1 Chemical structures of the three SaSDH inhibitors used as starting point for structural similarity search

2.2 | Enzyme activity

The enzyme was purified by affinity chromatography as described elsewhere (Avitia-Domínguez et al., 2014), and the enzymatic activity of the SaSDH was assayed in the reversed direction, monitoring the reduction of NADP⁺ to NADPH at 340 nm and 25°C, and the reaction mix contained 100 mM Tris-HCl pH 8.0, 1 mM shikimate, 1 mM NADP⁺. The reaction was started by the addition of SaSDH (50 ng). The activity of the enzyme was determined spectrophotometrically using the molar extinction coefficient of NADP⁺ ($\epsilon = 6,200 \text{ M}^{-1} \text{ cm}^{-1}$).

2.3 | Inhibition assays

The inhibition percentage was determined measuring the enzymatic activity under conditions described above, adding to the reaction mix each one of the selected molecules (previously dissolved in DMSO) at a concentration of 400 μM , maintaining the DMSO concentration at 10% in the reaction. The inhibition percentage was calculated adjusting the data to Equation :

$$\text{Inhibition \%} = \frac{A_0 - A_1}{A_0} \times 100 \quad (1)$$

where A_0 is the enzymatic activity without inhibitor, and A_1 is the enzyme activity in the presence of inhibitor.

2.4 | Inhibition mechanism characterization

The inhibition mechanism was determined through curves varying one substrate, shikimate or NADP⁺ (10–600 μM), and keeping the other at saturated concentration. Inhibitors were varied in the following manner, inhibitor **1** in a range of 70–150 μM , inhibitor **2** 150–250 μM , inhibitor **3** 10–50 μM , and inhibitor **4** 10–50 μM . All the experiments were performed by quadruplicate. The data obtained were analyzed using SIGMAPLOT v. 12.3 (Systat 2011) fitting them to the mixed full, mixed partial, uncompetitive full, and non-competitive full equations of inhibition modes (Segel, 1975).

$$\text{Mixed full} = \frac{V_{\max}}{\left(\frac{K_m}{S}\right) \left(1 + \frac{I}{K_i}\right) + \left(1 + \frac{I}{\alpha K_i}\right)} \quad (2)$$

$$\text{Mixed partial} = (V_{\max}) \left(\frac{\frac{1 + \beta \left(\frac{I}{\alpha K_i}\right)}{1 + \frac{I}{\alpha K_i}}}{\left(1 + \frac{K_m}{S}\right) \left(1 + \frac{I}{\alpha K_i}\right)} \right) \quad (3)$$

$$\text{Uncompetitive full} = \frac{V_{\max}}{1 + \frac{I}{K_i} + \frac{K_m}{S}} \quad (4)$$

$$\text{Noncompetitive full} = \frac{V_{\max}}{\left(1 + \frac{I}{K_i}\right) \left(1 + \frac{K_m}{S}\right)} \quad (5)$$

where V_{\max} is the maximum velocity, K_m is the Michaelis constant, S is the substrate concentration, I is the inhibitor concentration, K_i is the inhibition constant of an inhibitor, α indicates how many times K_s is modified when the enzyme is saturated with inhibitor, and β that expresses the change of the catalytic constant in the presence of saturating concentrations of inhibitor.

2.5 | Molecular docking

Molecules were built using CHEMSKETCH 11.5 (Spessard, 1998), and the molecular docking was performed in Glide (Friesner et al., 2004), due to the lack of an existing *Staphylococcus aureus* SDH crystal structure, the SaSDH 3D model previously reported (Avitia-Domínguez et al., 2014) was used to carry out the molecular docking studies. The grid box was generated selecting the residues involved in shikimate and NADP⁺ binding sites Ser13, Ser15, Asn58, Ile59, Thr60, Lys64, Glu65, Ala83, Asn85, Asp100, Ala125, Gly126, Gly127, Ala128, Ser129, Lys130, Ile132, Asn148, Arg149, Arg153, Leu166, Thr182, Thr183, Pro184, Met187, Ile194, Ile209, Met235, and Gln239. Hydrogen and atom charges were added using the *Protein Preparation Wizard* tool in Maestro software (www.schrodinger.com), and the energy was minimized with the OPLS3 force field (Harder et al., 2015). Extra precision mode was used in the docking score with the addition of flexible ligand penalization states using EPIK program (Shelley et al., 2007). The poses with the best binding energy of each compound were selected for molecular dynamics studies.

2.6 | Molecular dynamic simulations

Molecular dynamic simulations of the SaSDH-inhibitor complex were carried out with the software GROMACS 5.0.4 (Abraham et al., 2015) using the CHARMM36 force field (Vanommeslaeghe et al., 2010). In each case, the ligand was extracted and parameterized with the SWISSPARAM server (Bjelkmar, Larsson, Cuendet, Hess, & Lindahl, 2010) (<http://www.swissparam.ch>). Once parameterized, the complex was solvated with the transferable intermolecular potential with 3 points (TIP3) water model in a unitary cubic cell of 1 nm in periodic conditions, charges were neutralized with Na⁺ and Cl⁻ ions at a 0.15 mol/L concentration. The prepared complexes were submitted to an energy minimization with 500 steps on a conjugate gradient. Once minimized, canonic (NVT) (Berendsen, van Postma, van Gunsteren, DiNola, & Haak, 1984) and isothermic-isobaric (NPT) (Pastor, Brooks, & Szabo,

1988) simulations were performed (with an isotropic position scale) at 300°K and 1 atm of pressure. Finally, 50 ns molecular dynamic simulations were carried out at 300°K with no restrictions, obtaining 10,000 conformations saved every 5,000 steps. The obtained trajectories were analyzed with matricial analyses for the root-mean-square deviation (RMSD) and root-mean-square fluctuation (RMSF), while size clustering analyses were performed with GROMOS (Daura et al., 1999) to select the most representative conformations from the simulation.

2.7 | Principal component analysis

A principal component analysis (PCA) was performed to extract the principal modes involved in the enzyme-inhibitor complex motion (Amadei, Linssen, & Berendsen, 1993). The covariance matrix was assembled using a simple linear transformation in the Cartesian coordinate space. A vectorial depiction of every single component of the motion indicates the direction of the motion. For this, a set of eigenvectors were derived through the diagonalization of the covariance matrix. Each eigenvector has a corresponding eigenvalue that describes the energetic contribution of each component to the motion (Mesentean, Fischer, & Smith, 2006). The protein regions that are responsible for the most significant collective motions can be acknowledged through PCA. The GROMACS inbuilt to `g_covar` and `g_anaeig` were used to perform PCA (Doss et al., 2014).

2.8 | Physicochemical and toxicological properties

To determine the inhibitors physicochemical and toxicological properties online server PRE-ADMET (Lee, Park, Lee, & No, 2007) (www.preadmet.bmdrc.kr) and DATAWARRIOR 4.07.02 (Sander, Freyss, von Korff, & Rufener, 2015) were used. Both tools predicted important parameters such as drug-like properties based on the Lipinski rules, drug-like rule and drug DB rule. Additionally, ADME properties such as human intestinal absorption, plasma protein binding, blood-brain barrier penetration, and skin permeability were predicted too. Additionally, different toxicological features like their potential to be mutagenic, carcinogenic, irritant, reproduction effects, CYP450 inhibition, and hERG inhibition also were determined. Finally, the evaluation of potential activity against 2,547 human target proteins was explored using the Swiss Target Prediction server (Gfeller et al., 2014).

3 | RESULTS AND DISCUSSIONS

3.1 | New potential inhibitors selection

In a previous report, three SaSDH inhibitors (compounds **238**, **766**, and **894**) were found (Avitia-Domínguez et al.,

2014; Figure 1), with the end to find new inhibitors, but trying to keep their chemical cores, a structure similarity search strategy was applied. In order to do this, two chemical libraries were used, and each compound was structurally compared with the structures of the previously reported inhibitors to obtain its RMSD value. According to this, all molecules with RMSD values lower than 4.0 were selected, the smaller the RMSD value among two structures the greater the similarity. After comparisons, 156 compounds were chosen from the Maybridge library and 50 from ChemBridge library to determine their SaSDH inhibition capability.

3.2 | SaSDH inhibition

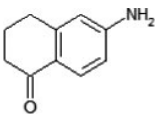
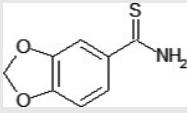
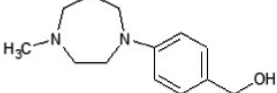
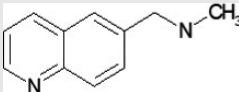
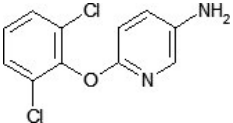
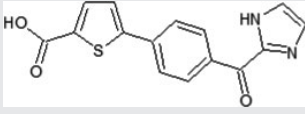
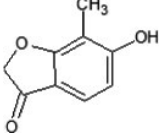
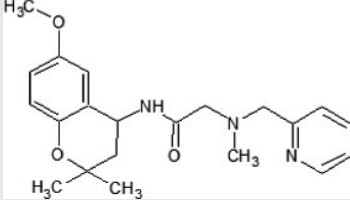
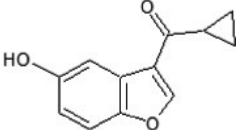
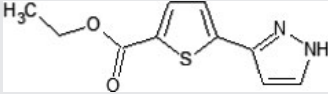
The ten compounds with the highest SaSDH inhibition at 400 μ M are shown in Table 1; the first five correspond to Maybridge and the last five to ChemBridge. The best two compounds from each library were selected to continue with their characterization, named compounds **1**, **2**, **3**, and **4**. These molecules inhibited SaSDH in the same magnitude order as inhibitors reported for SDHs from other bacteria (Han et al., 2006; Peek et al., 2014).

Structurally, the four new inhibitors share characteristics with their predecessors, and compound **1** supports a core very similar to that of inhibitor **766**. In the case of compound **2**, its core is like that of inhibitor **894**, while compound **3** shares a thiophene-carboxylic acid with inhibitor **238**, and finally, compound **4** only changes one substituent with respect to the structure of inhibitor **894**. Interestingly, the other compounds in Table 1 do not share these characteristics and their inhibition capability was lower, suggesting that the presence of these features is crucial to inhibit SaSDH. Therefore, these new four compounds increase the diversity of SDHs inhibitors reported actually (Avitia-Domínguez et al., 2014; Han et al., 2006; Peek et al., 2014).

3.3 | Inhibition mechanism characterization

In previous SDH inhibitors reports, the inhibition mechanism was not specified as partial or full (Avitia-Domínguez et al., 2014; Han et al., 2006; Peek et al., 2014). Therefore, we decided to perform a more detailed characterization of the inhibition mechanisms for inhibitors **1**, **2**, **3**, and **4** in both substrates (shikimate and NADP⁺). In order to do this, double reciprocal plots were constructed and Slope versus Inhibitor replots were used to identify a partial or full inhibition based on the behavior of the curve, where a straight line suggests a complete inhibition and a hyperbolic behavior suggests a partial inhibition. Additionally, $1/\Delta$ intercept or $1/\Delta$ slope versus $1/\text{Inhibitor}$ replots were used to confirm the partial or full inhibition, if the value of the intercept is equal to zero indicates full inhibition and an intercept on the abscises with value under zero refers to partial inhibition (Segel, 1975).

TABLE 1 The ten most potent SaSDH inhibitors found through structural similarity search

Code and name	Structure	Inhibition %
Code: NRB00999 6-amino-1,2,3,4-tetrahydro-naphthalen-1-one (compound 1)		91
Code: CC00075 1,3-benzodioxole-5-carbothioamide (compound 2)		75
Code: CC60309 [4-(4-methylperhydro-1,4-diazepin-1-yl)phenyl]methanol		67
Code: CC04546 <i>N</i> -methyl- <i>N</i> -(quinolin-6-ylmethyl)amine		63
Code: BTB03828 6-(2,6-dichlorophenoxy)pyridin-3-amine		60
Code: 58232223 5-[4-(1 <i>H</i> -imidazol-2-ylcarbonyl)phenyl]thiophene-2-carboxylic acid (compound 3)		98
Code: 4030563 6-hydroxy-7-methyl-1-benzofuran-3(2 <i>H</i>)-one (compound 4)		98
Code: 24996351 <i>N</i> -(6-methoxy-2,2-dimethyl-3,4-dihydro-2 <i>H</i> -chromen-4-yl)- <i>N</i> -(2-methyl-2-(pyridin-2-ylmethyl)glycinamide		34
Code: 5859430 cyclopropyl(5-hydroxy-1-benzofuran-3-yl)methanone		32
Code: 32202032 ethyl 5-(1 <i>H</i> -pyrazol-3-yl)thiophene-2-carboxylate		28

The data showed that for shikimate, compound **1** (Figure 2a–c) and **4** (Figure 2j–l) exhibited a mixed partial inhibition mechanism, while compounds **2** (Figure 2d–f) and **3** (Figure 2g–i) exhibited a mixed full and a uncompetitive full inhibition mechanism, respectively. In the case of NADP⁺, compounds **1** (Figure 3a–c) and **3** (Figure 3g–i) exhibited a mixed full inhibition mechanism, while compounds **2** (Figure 3d–f) and **4** (Figure 3j–l) exhibited a non-competitive full and a mixed partial inhibition mechanism, respectively.

According to the kinetic analysis (Table 2), the data indicated that compound **1** presented a higher affinity for NADP⁺ binding site than for shikimate binding site (K_i of 46 μM versus 106.1 μM). Furthermore, it showed different inhibition mechanism to each substrate, a mixed partial for shikimate and mixed full for NADP⁺. In this context, the α and β values obtained for shikimate suggest that compound **1** prefers de ES complex ($\alpha = 0.61$) and that the ESI complex works 87% lower than the product formation rate in the absence of

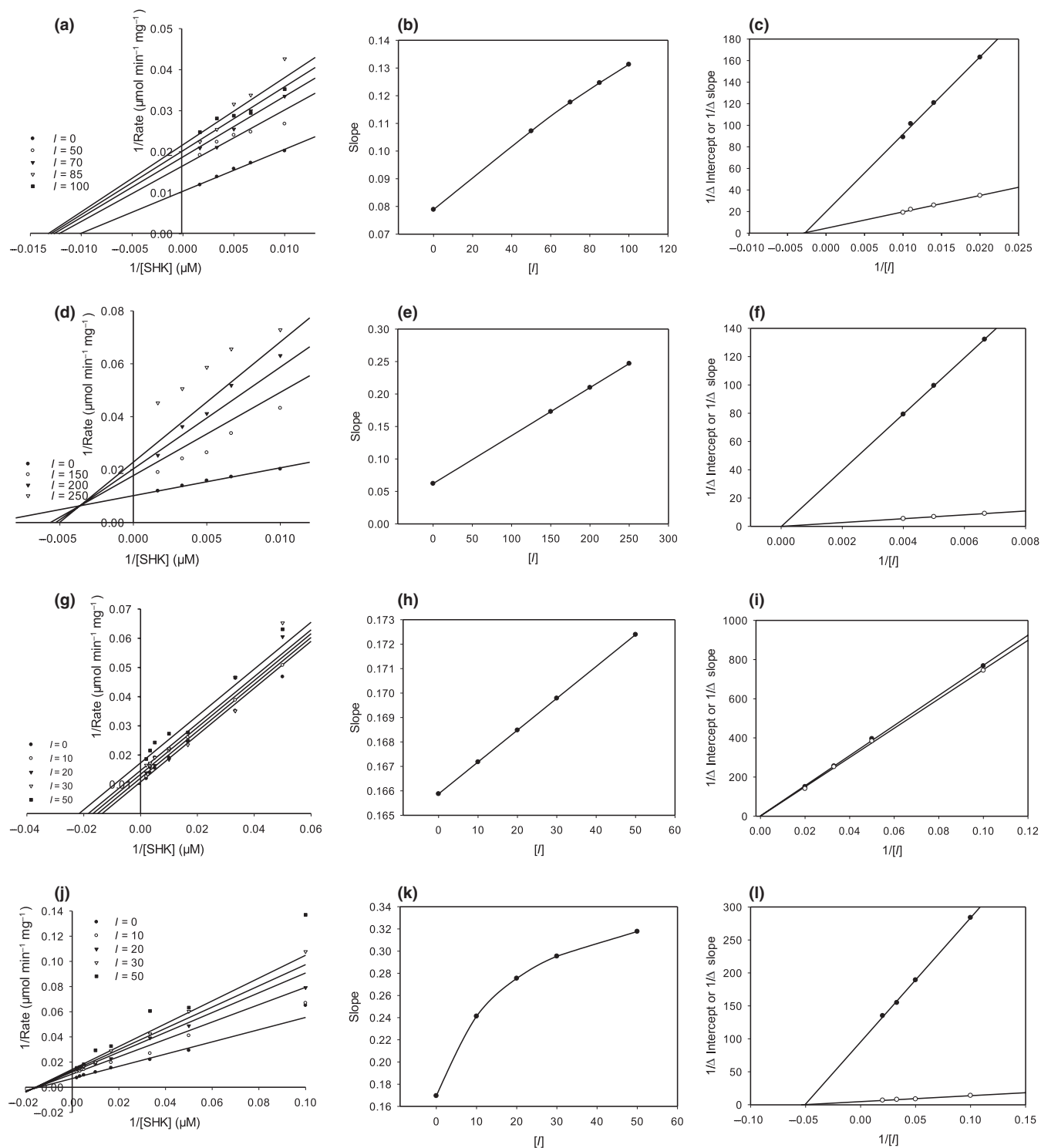


FIGURE 2 Inhibition mechanism for shikimate. (a), (d), (g), and (j), Lineweaver-Burk plots for compounds **1**, **2**, **3**, and **4**, respectively; (b), (e), (h), and (k), Slope versus Inhibitor replot for compounds **1**, **2**, **3**, and **4**, respectively; and (c), (f), (i), and (l), $1/\Delta$ intercept or $1/\Delta$ slope versus $1/\text{inhibitor}$ replot for compounds **1**, **2**, **3**, and **4**, respectively. The data showed represent the mean of four independent assays

inhibitor ($\beta = 0.13$). In the case of NADP^+ , the α value indicated that compound **1** binds 2.3 times better to the free enzyme than ES complex. Compound **2** to the contrary, showed higher affinity for shikimate binding site than for NADP^+ binding site (K_i of $75.3 \mu\text{M}$ versus $246.2 \mu\text{M}$). This inhibitor

presented a mixed full and non-competitive full inhibition mechanism for shikimate and NADP^+ , respectively, and in the case of shikimate, it prefers binding to the free enzyme instead the ES complex. Compound **3** as well as **2**, showed more affinity for shikimate binding site than NADP^+ binding

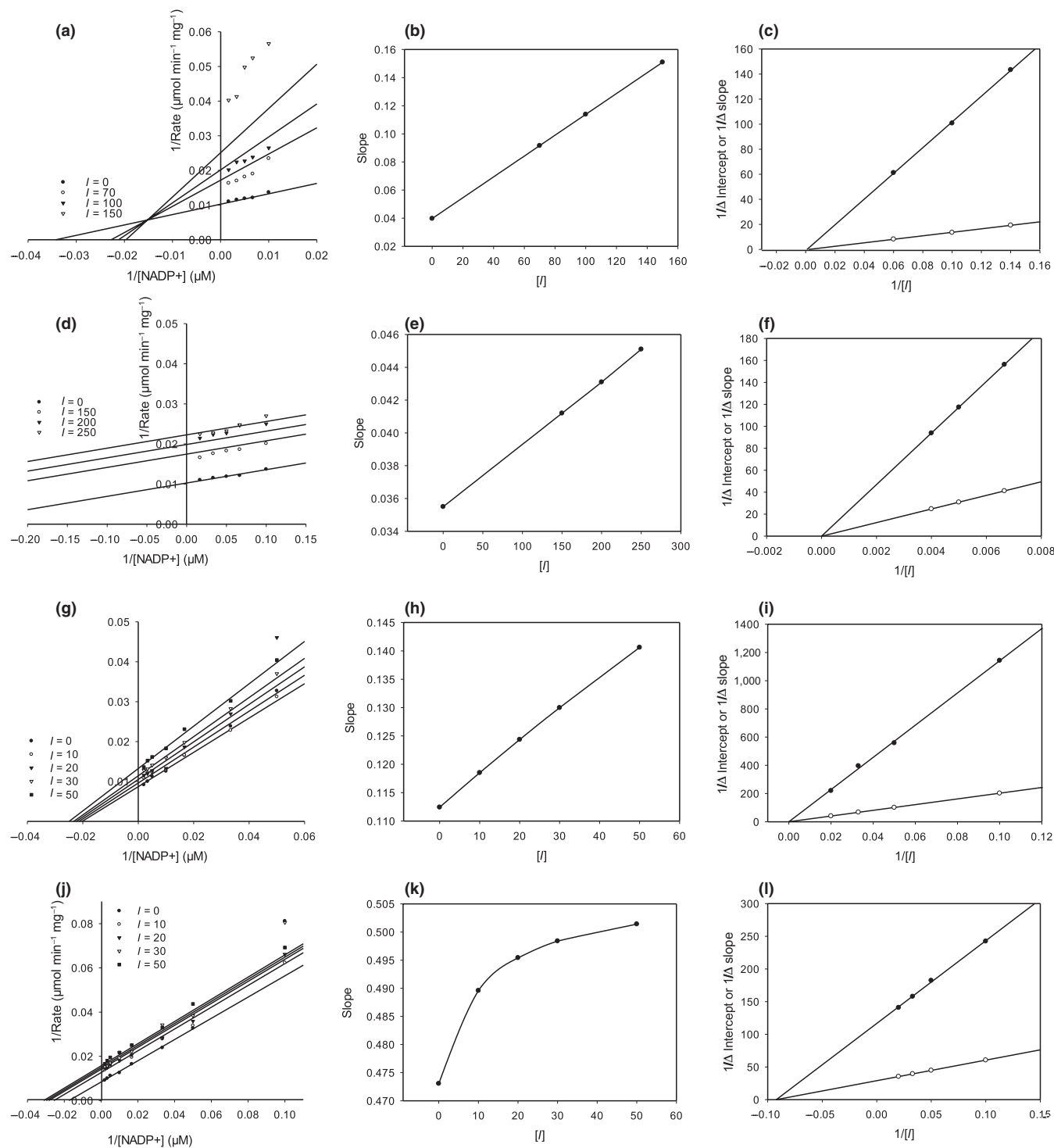


FIGURE 3 Inhibition mechanism for NADP⁺. (a), (d), (g), and (j), Lineweaver-Burk plots for compounds **1**, **2**, **3**, and **4**, respectively; (b), (e), (h), and (k), Slope versus Inhibitor replots for compounds **1**, **2**, **3**, and **4**, respectively; and (c), (f), (i), and (l), 1/Δ intercept or 1/Δ slope versus 1/inhibitor replots for compounds **1**, **2**, **3**, and **4**, respectively. The data showed represent the mean of four independent assays

site (K_i of 83.1 μM versus 212.9 μM). Its inhibition mechanisms were uncompetitive full and mixed full for shikimate and NADP⁺, respectively, presenting, in the case of NADP⁺, a preference for the ES complex. Finally, compound **4** showed the lowest K_i values from the four, with a K_i of 8.3 μM with respect to shikimate and a K_i of 10.3 μM for NADP⁺, which

indicates that it presented the same affinity for both binding sites. In reference to its inhibition mechanisms, compound **4** showed a mixed partial for both substrates. The α value obtained for shikimate suggests that this inhibitor recognizes almost with the same affinity both free enzyme and the ES complex; however, for NADP⁺ there is a clear preference

TABLE 2 Kinetic constants and inhibition mechanism

Compound	K_i (μM)		α value		β value		Inhibition type	
	Shikimate	NADP ⁺	Shikimate	NADP ⁺	Shikimate	NADP ⁺	Shikimate	NADP ⁺
1	106.1 \pm 5.96	46 \pm 5.05	0.61 \pm 0.28	2.3 \pm 0.30	0.13 \pm 0.12	NA	Mixed partial	Mixed full
2	75.3 \pm 13.86	246.2 \pm 10.78	2.7 \pm 0.19	NA	NA	NA	Mixed full	Non-competitive full
3	83.1 \pm 11.63	212.9 \pm 15.06	NA	0.45 \pm 0.36	NA	NA	Uncompetitive full	Mixed full
4	8.3 \pm 1.8	10.3 \pm 2.8	0.89 \pm 0.14	0.51 \pm 0.007	0.41 \pm 0.003	0.48 \pm 0.002	Mixed partial	Mixed partial

Note: NA: not applicable. The data are presented as \pm SD of four independent assays.

for ES complex. The β value was almost the same for both substrates indicating that the ESI complex works at 59% and 52% lower than the product formation rate in the absence of inhibitor.

Interestingly, even with the structural similarity shared with the previously reported inhibitors for the SaSDH (Avitia-Domínguez et al., 2014), the inhibition mechanisms presented were different, and inhibitors **238** and **766** showed a competitive inhibition toward shikimate and an uncompetitive inhibition mechanism toward NADP⁺, while inhibitor **894** showed a mixed competitive inhibition mechanism with respect to shikimate and a mixed uncompetitive inhibition mechanism with respect to NADP⁺. In the case of compound **4** and inhibitor **894** both presented a mixed-type inhibition for both substrates, this can be explained by the high similarity between both structures; for the other three compounds, they do not share as high structural similarity with the inhibitors previously reported. These differences in the inhibition types could be given by the presence of different functional groups and substituents such as amino and sulfur in the structures.

There are other reports of inhibitors of SDH from different bacteria such as *Helicobacter pylori* (Han et al., 2006) and *Pseudomonas putida* (Peek et al., 2014). In the case of *H. pylori*, they report five compounds with either competitive or non-competitive inhibition mechanisms, but do not specify if their inhibition type is full or partial; however, their K_i values are within the same order as those here reported. For *P. putida*, SDH inhibition mechanisms were not reported. This is the first report for SDH inhibitors where the inhibition mechanisms were specified as a full or partial, achieving more information to understand, in a better manner, how the inhibitors work and give important data for further studies.

3.4 | Molecular dynamic simulations

After the kinetic characterization, structural analyses of the enzyme-inhibitor complex were performed through 50 ns molecular dynamics studies. Firstly, the RMSD was determined, this parameter is crucial to analyze the stability of the molecular dynamic trajectories, and the RMSD of the complexes were plotted in function of time (Figure 4). The results indicated that compounds **1** and **3** formed more stable complexes; it was noted from the first 10 ns to the end of the simulations, showing less dispersion in the mean of the RMSD value (1.1 \pm 0.7 and 1.2 \pm 0.4 nm, respectively). In the case of compounds **2** and **4**, both showed a greater dispersion on their RMSD value (2.7 \pm 0.6 nm), presenting greater instability the first 25 ns and after that time it was clearly observed how the complex reach stabilization (Figure 4). Likewise, it was noted that the binding of the compound **1** was stabilized by the formation of hydrogen bonds with catalytic residues Lys64, Asn85, and Ser15 (Peek & Christendat, 2015)

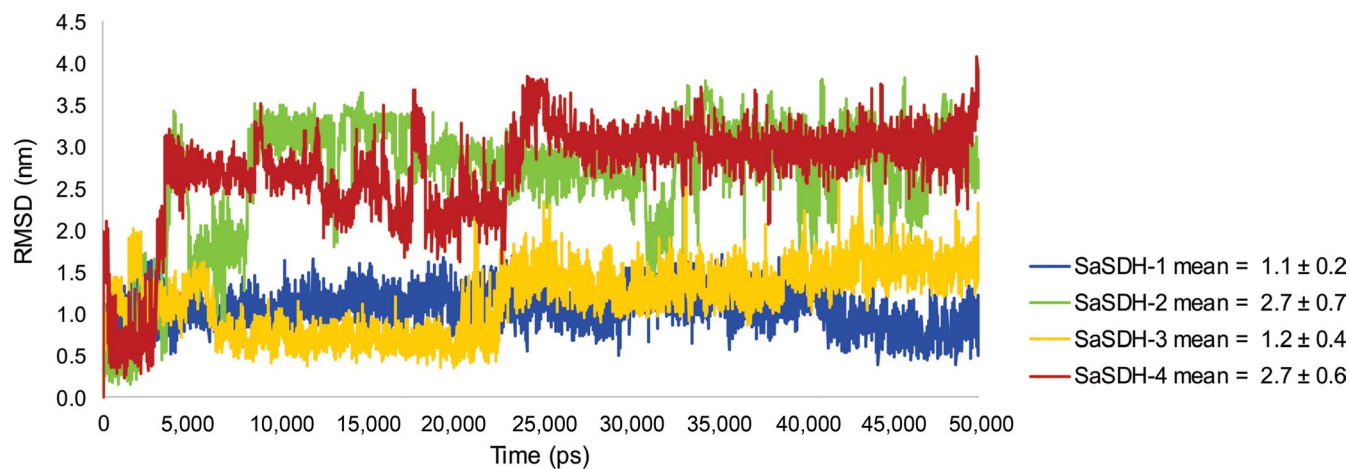


FIGURE 4 Root-mean-square deviation (RMSD) of the SaSDH-inhibitor complexes

(Figure 5a) and compound **3** was stabilized by the formation of hydrogen bonds with the residues Ala128 and Arg149 (Figure 5c); these compounds showed a greater number of hydrogen bonds (an average of 3 hydrogen bonds for both).

Compound **2** was stabilized by the formation of a hydrogen bond with the carboxyl group from the Glu65 (Figure 5b), and compound **4** was stabilized by the formation of hydrogen bonds with the residues Lys64 and Ile209 (Figure 5d). This

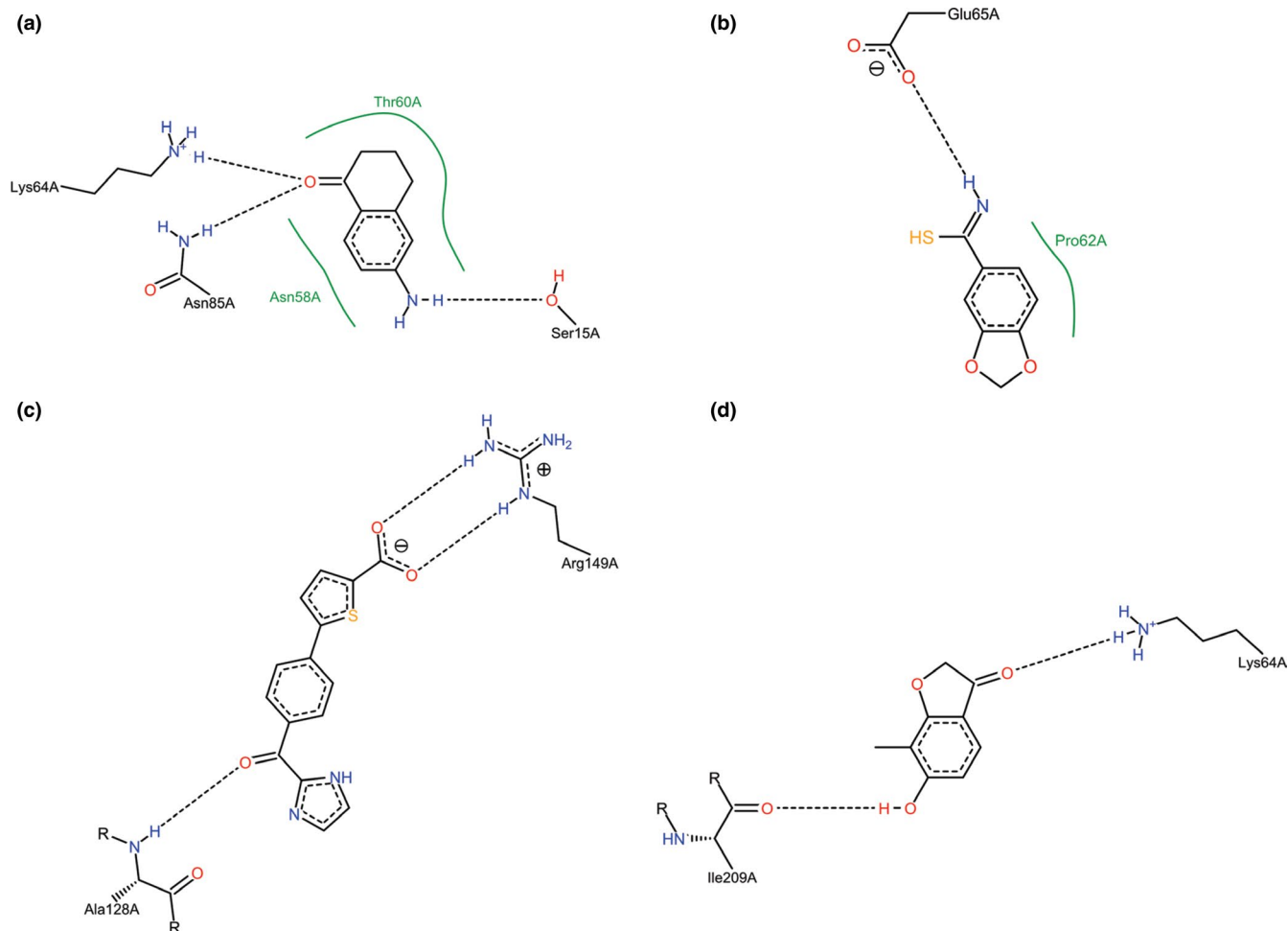


FIGURE 5 Interactions of the complexes (a) SaSDH-1, (b) SaSDH-2, (c) SaSDH-3 and (d) SaSDH-4

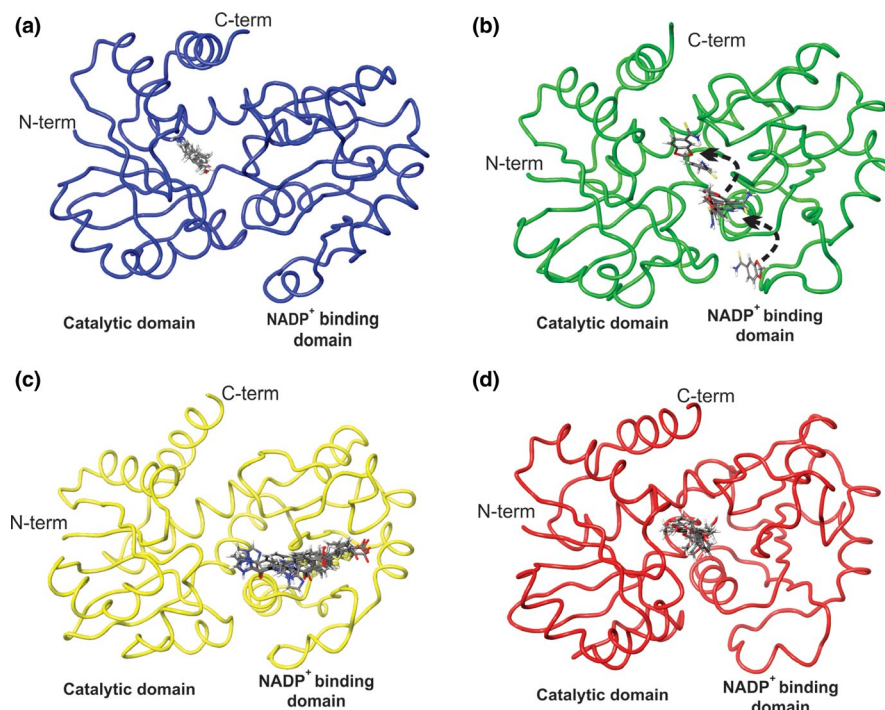


FIGURE 6 Cluster analyses of compounds displacement during molecular dynamic simulation (a) SaSDH-1, (b) SaSDH-2, (c) SaSDH-3 and (d) SaSDH-4

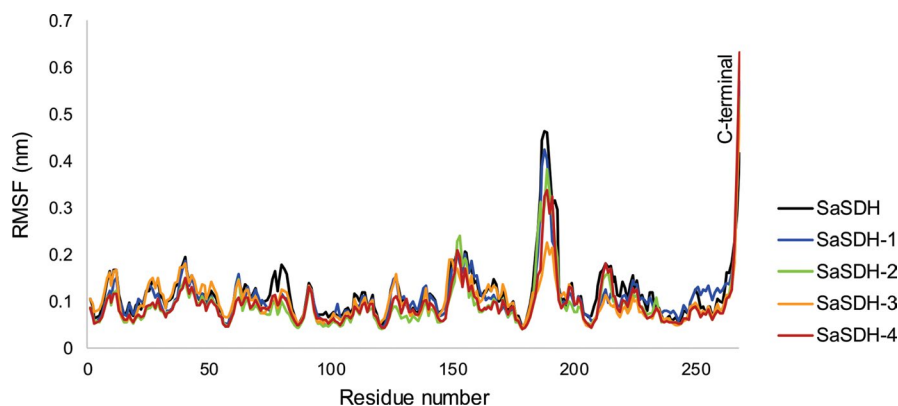


FIGURE 7 Root-mean-square fluctuation (RMSF) of C α atoms with respect to their average position in time

in concordance with the stable behavior observed for compounds **1** and **3** compared with compounds **2** and **4**.

Furthermore, it was interesting to observe that during the molecular dynamic simulations each inhibitor had a very different behavior. At the beginning of the simulation, the inhibitors were found between the shikimate binding site and the NADP⁺ binding site. As the simulation goes on, compound **1** settled into the shikimate binding site (active site, Figure 6a). For compound **2**, three main poses were noted for this compound, at the beginning it was close to the NADP⁺ binding site, then it went into the interface between the NADP⁺ and shikimate binding sites and, finally, it kept closer to the

shikimate binding site (Figure 6b). In the case of compound **3**, it settled into the NADP⁺ binding site (Figure 6c) and compound **4** remains during all simulation in the interface of the NADP⁺ and shikimate binding sites (Figure 6d).

To continue with the analysis, RMSF of the C α atoms were determined, and this parameter was helpful to understand how the binding of these four compounds provoked changes on the flexibility of the SaSDH domains. Results showed that the binding of the inhibitors caused a small decrease on the flexibility of the shikimate (Val5, Ser13, Ser15, Asn58, Ile59, Thr60, Lys64, Asn85, Asp100, Phe236, and Gln239) and NADP⁺ (Lys64, Glu65, Ala83, Ala125, Gly126,

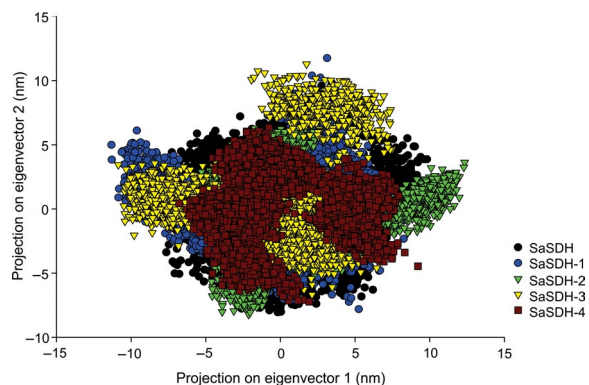


FIGURE 8 Comparison of the essential movements obtained from the 2D projection of the apo-SaSDH and SaSDH-inhibitor complexes from the first two eigenvectors

Gly127, Ala128, Ser129, Lys130, Ile132, Asn148, Arg149, Arg153, Leu166, Thr182, Thr183, Pro184, Met187, Ile194, Ile209, and Met235) binding domains, being the compounds **3** and **4** the ones that had a greater effect on the NADP^+ binding domain (Figure 7).

3.5 | Principal component analysis

A PCA was carried out to explore the most significant collective modes of motion occurring along the simulations of the uncomplexed and complexed SaSDH. The PCA showed a greater fluctuation from the systems corresponding to SaSDH-inhibitor complexes, where an increase in amplitude

of the eigenvector 1 in SaSDH-inhibitor complexes was observed in a plot of eigenvector 2 versus eigenvector 1 (Figure 8). These differences were clearer by the comparison of the movement described by the eigenvector 1 of each molecular dynamic simulation complex (Figure 9). The loop formed by the residues Pro184, Ala185, Gly186, Met187, Ala188, Gly189, Asn190, Asn191, Glu192, Ser193, and Ile194, which is considered as a highly flexible region (Han et al., 2009; Ye et al., 2003), showed greater movements in the case of complexes SDH-1, -2, and -4 (dotted circle). Additionally, in these complexes the catalytic domain kept rigid and the NADP^+ binding domain showed more displacement (Figure 9a,b,d). To the contrary, SaSDH-3 complex not only presented more movement in catalytic domain, but also this compound provoked a general displacement in the entire structure (Figure 9c). Therefore, these perturbations could explain the inhibitory effect of these molecules.

3.6 | Physicochemical and toxicological properties

After kinetic and structural characterization, an important point to know about these inhibitors was their physicochemical and toxicological properties. To this end, the four compounds were analyzed using the PRE-ADMET and DATAWARRIOR 4.07.02 software (Table 3). With respect to the toxicological parameters, compound **1** was the worst evaluated presenting high potential to be carcinogenic and mutagenic, as well as to inhibit the hERG potassium channel and CYP450. For ADME properties, in general, the four inhibitors were well

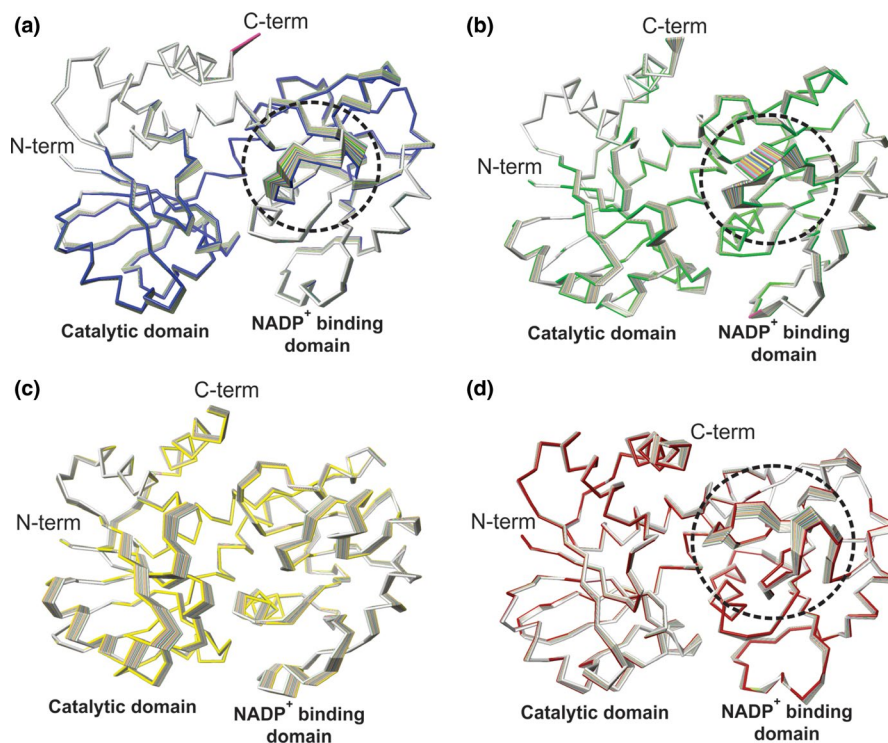


FIGURE 9 Conformational assemble obtained from the principal components analysis. (a) SaSDH-1, (b) SaSDH-2, (c) SaSDH-3, and (d) SaSDH-4

TABLE 3 Predicted toxicological, ADME, and drug-like properties

Parameters	Compound 1	Compound 2	Compound 3	Compound 4
Toxicological				
Irritant ^a	None	None	None	None
Reproductive effects ^a	None	None	None	None
Carcinogenic ^a	High	None	None	None
Mutagenic ^a	High	None	None	None
hERG inhibition ^b	Medium risk	Low risk	Low risk	Medium risk
CYP450 inhibition ^b	2C19, 2C9 and 3A5	2C19, 2C9 and 3A4	2C9 and 3A4	2C9
ADME				
Blood–brain barrier penetration ^b	Low absorption	Low absorption	Low absorption	Low absorption
Human intestinal absorption ^b	Well absorbed	Well absorbed	Well absorbed	Well absorbed
Plasma protein binding ^b	Weakly bound	Weakly bound	Weakly bound	Strongly bound
Caco2 permeability ^b	Middle permeability	Middle permeability	Middle permeability	Middle permeability
Drug like				
Drug-likeness score ^a	−4.967	1.887	−0.24	3.39
CMC-like rule ^b	Qualified	Not qualified	Qualified	Qualified
Lead-like rule ^b	Suitable	Suitable	Suitable	Suitable
Rule of five ^b	Suitable	Suitable	Suitable	Suitable
WDI-like rule ^b	Suitable	Suitable	Suitable	Suitable

^aDetermined by DATAWARRIOR v4.07.02.^bDetermined by PRE-ADMET.

evaluated, only compound **4** presented a strong binding to plasma proteins. In the case of drug-like parameters, all of them reached values to be considered as potential oral drugs, only compound **2** not qualified for CMC rules.

Finally, the potential activity of these molecules against other target proteins was predicted using the Swiss Target Prediction server. The results showed that from the 2,547 proteins analyzed, compound **1** presented cytochrome P450 19A and cholinesterase as the main potential targets. In the case of compound **2**, these were the muscleblind-like protein 1 and the tyrosyl-DNA phosphodiesterase 1. Microtubule-associated protein tau and FAD-linked sulphhydryl oxidase ALR were selected for compound **3**, while microtubule-associated protein tau and the androgen receptor were the main for compound **4**. The probability of these potential activities ranging from 21% to 55%. Therefore, even with the presence of some negative features all of these characteristics can be improved by studying and modifying these structures to make them less toxic and more powerful.

4 | CONCLUSIONS

Through a structural similarity search strategy, four new SaSDH inhibitors were found, and the mixed-type inhibition mechanism showed by them indicated that these compounds

were able to interact with the free enzyme and with the ES complex for both substrates. This characteristic is important because it means that independently of the substrate concentration, there will always be inhibition, in contrast to a classic competitive inhibitor. Furthermore, structural analyses of the SaSDH-inhibitor complexes demonstrated that these compounds interacted with residues important for the enzyme catalysis and that perturbs its structure. Additionally, according to their chemical structure, in general passed the different evaluations realized to be considered as a potential drug. Finally, the detailed data about full or partial inhibition in each case and the structural results highlight important information that will be used to optimize these compounds and serves to design more potent molecules to obtain a new drug against MRSA.

ACKNOWLEDGMENTS

C.A.-D. and A.T.-V. acknowledge Consejo Nacional de Ciencia y Tecnología (CONACyT) for grants Nos. 258694 and 257848, respectively. CONACyT is also acknowledged for the fellowship granted to D.E.-M. (No. 623226).

CONFLICT OF INTEREST

The authors confirm that this article content has no conflict of interest.

ORCID

Claudia Avitia-Domínguez  <https://orcid.org/0000-0002-1017-8609>

REFERENCES

- Abraham, M. J., Murtola, T., Schulz, R., Páll, S., Smith, J. C., Hess, B., & Lindahl, E. (2015). GROMACS: High performance molecular simulations through multi-level parallelism from laptops to supercomputers. *SoftwareX*, *1*, 19–25. <https://doi.org/10.1016/j.softx.2015.06.001>
- Amadei, A., Linssen, A. B. M., & Berendsen, H. J. C. (1993). Essential dynamics of proteins. *Proteins: Structure, Function, and Bioinformatics*, *17*, 412–425. [https://doi.org/10.1002/\(ISSN\)1097-0134](https://doi.org/10.1002/(ISSN)1097-0134)
- Anton, I. A., & Coggins, J. R. (1988). Sequencing and overexpression of the *Escherichia coli* aroE gene encoding shikimate dehydrogenase. *Biochemical Journal*, *249*, 319–326. <https://doi.org/10.1042/bj2490319>
- Arcuri, H. A., Borges, J. C., Fonseca, I. O., Pereira, J. H., Neto, J. R., Basso, L. A., ... de Azevedo, W. F. Jr. (2008). Structural studies of shikimate 5-dehydrogenase from *Mycobacterium tuberculosis*. *Proteins: Structure, Function, and Bioinformatics*, *72*, 720–730. <https://doi.org/10.1002/prot.21953>
- Avitia-Domínguez, C., Sierra-Campos, E., Salas-Pacheco, J. M., Nájera, H., Rojo-Domínguez, A., Cisneros-Martínez, J., & Téllez-Valencia, A. (2014). Inhibition and biochemical characterization of methicillin-resistant *Staphylococcus aureus* shikimate dehydrogenase: An in silico and kinetic study. *Molecules*, *19*, 4491–4509. <https://doi.org/10.3390/molecules19044491>
- Bagautdinov, B., & Kunishima, N. (2007). Crystal structures of shikimate dehydrogenase AroE from *Thermus thermophilus* HB8 and its cofactor and substrate complexes: Insights into the enzymatic mechanism. *Journal of Molecular Biology*, *373*, 424–438. <https://doi.org/10.1016/j.jmb.2007.08.017>
- Bentley, R., & Haslam, E. (1990). The shikimate pathway—a metabolic tree with many branches. *Critical Reviews in Biochemistry and Molecular Biology*, *25*, 307–384. <https://doi.org/10.3109/10409239009090615>
- Berendsen, H. J. C., van Postma, J. P. M., van Gunsteren, W. F., DiNola, A. R. H. J., & Haak, J. R. (1984). Molecular dynamics with coupling to an external bath. *The Journal of Chemical Physics*, *81*, 3684–3690. <https://doi.org/10.1063/1.448118>
- Bjellkmar, P., Larsson, P., Cuendet, M. A., Hess, B., & Lindahl, E. (2010). Implementation of the CHARMM force field in GROMACS: Analysis of protein stability effects from correction maps, virtual interaction sites, and water models. *Journal of Chemical Theory and Computation*, *6*, 459–466. <https://doi.org/10.1021/ct900549r>
- Bonner, C. A., & Jensen, R. A. (1994). Cloning of cDNA encoding the bifunctional dehydroquinase shikimate dehydrogenase of aromatic-amino-acid biosynthesis in *Nicotiana tabacum*. *Biochemical Journal*, *302*, 11–14. <https://doi.org/10.1042/bj3020011>
- Coggins, J. R., Abell, C., Evans, L. B., Frederickson, M., Robinson, D. A., Roszak, A. W., & Laphorn, A. P. (2003). Experiences with the shikimate-pathway enzymes as targets for rational drug design. *Biochemical Society Transactions*, *31*, 548–552. <https://doi.org/10.1042/bst0310548>
- Daura, X., Gademann, K., Jaun, B., Seebach, D., Van Gunsteren, W. F., & Mark, A. E. (1999). Peptide folding: When simulation meets experiment. *Angewandte Chemie International Edition*, *38*, 236–240. [https://doi.org/10.1002/\(ISSN\)1521-3773](https://doi.org/10.1002/(ISSN)1521-3773)
- Díaz-Quiroz, D. C., Cardona-Félix, C. S., Viveros-Ceballos, J. L., Reyes-González, M. A., Bolívar, F., Ordoñez, M., & Escalante, A. (2018). Synthesis, biological activity and molecular modelling studies of shikimic acid derivatives as inhibitors of the shikimate dehydrogenase enzyme of *Escherichia coli*. *Journal of Enzyme Inhibition and Medicinal Chemistry*, *33*, 397–404. <https://doi.org/10.1080/14756366.2017.1422125>
- Doss, G. P., Rajith, B., Chakraborty, C., NagaSundaram, N., Ali, S. K., & Zhu, H. (2014). Structural signature of the G719S-T790M double mutation in the EGFR kinase domain and its response to inhibitors. *Scientific Reports*, *4*, srep05868.
- Duncan, K., Edwards, R. M., & Coggins, J. R. (1987). The pentafunctional arom enzyme of *Saccharomyces cerevisiae* is a mosaic of monofunctional domains. *Biochemical Journal*, *246*, 375. <https://doi.org/10.1042/bj2460375>
- Enright, M. C., Robinson, D. A., Randle, G., Feil, E. J., Grundmann, H., & Spratt, B. G. (2002). The evolutionary history of methicillin-resistant *Staphylococcus aureus* (MRSA). *Proceedings of the National Academy of Sciences*, *99*, 7687–7692. <https://doi.org/10.1073/pnas.122108599>
- Friesner, R. A., Banks, J. L., Murphy, R. B., Halgren, T. A., Klicic, J. J., Mainz, D. T., ... Perry, J. K. (2004). Glide: A new approach for rapid, accurate docking and scoring. 1. Method and assessment of docking accuracy. *Journal of Medicinal Chemistry*, *47*, 1739–1749. <https://doi.org/10.1021/jm0306430>
- Gan, J., Yan, W., Prabakaran, P., Yijun, G., Li, Y., Andrykovitch, M., ... Ji, X. (2007). Structural and biochemical analyses of shikimate dehydrogenase AroE from *Aquifex aeolicus*: Implications for the catalytic mechanism. *Biochemistry*, *46*, 9513–9522. <https://doi.org/10.1021/bi602601e>
- Gfeller, D., Grosdidier, A., Wirth, M., Daina, A., Michielin, O., & Zoete, V. (2014). SwissTargetPrediction: A web server for target prediction of bioactive small molecules. *Nucleic Acids Research*, *42*, W32–W38. <https://doi.org/10.1093/nar/gku293>
- Han, C., Tiancen, H., Dalei, W., Su, Q., Zhou, J., Ding, J., ... Jiang, H. (2009). X-ray crystallographic and enzymatic analyses of shikimate dehydrogenase from *Staphylococcus epidermidis*. *The FEBS Journal*, *276*, 1125–1139. <https://doi.org/10.1111/j.1742-4658.2008.06856.x>
- Han, C., Wang, L., Kunqian, Y., Chen, L., Lihong, H., Chen, K., ... Shen, X. (2006). Biochemical characterization and inhibitor discovery of shikimate dehydrogenase from *Helicobacter pylori*. *The FEBS Journal*, *273*, 4682–4692. <https://doi.org/10.1111/j.1742-4658.2006.05469.x>
- Harder, E., Damm, W., Maple, J., Chuanjie, W., Reboul, M., Xiang, J. Y., ... Knight, J. L. (2015). OPLS3: A force field providing broad coverage of drug-like small molecules and proteins. *Journal of Chemical Theory and Computation*, *12*, 281–296.
- Hawkins, A. R., Lamb, H. K., Moore, J. D., Charles, I. G., & Roberts, C. F. (1993). The pre-chorismate (shikimate) and quininate pathways in filamentous fungi: Theoretical and practical aspects. *Microbiology*, *139*, 2891–2899.
- Kloos, W. E., & Bannerman, T. L. (1995). *Staphylococcus* and *Micrococcus* Murray. In E. J. Baron, M. A. Faller, F. C. Tenover, & R. H.

- Yolken (Eds.), *Manual of clinical microbiology*. Washington, DC: ASM Press.
- Lee, S. K., Park, S. H., Lee, I. H., & No, K. T. (2007). *PreAD-MET Ver. v2. 0*. Seoul, Korea: BMDRC.
- Li, J., Liu, D., Tian, X., Koseki, S., Chen, S., Ye, X., & Ding, T. (2018). Novel antibacterial modalities against methicillin resistant *Staphylococcus aureus* derived from plants. *Critical Reviews in Food Science and Nutrition*, *3*, 1–9.
- Lipinski, C. A., Lombardo, F., Dominy, B. W., & Feeney, P. J. (2001). Experimental and computational approaches to estimate solubility and permeability in drug discovery and development settings. *Advanced Drug Delivery Reviews*, *46*, 3–26. [https://doi.org/10.1016/S0169-409X\(00\)00129-0](https://doi.org/10.1016/S0169-409X(00)00129-0)
- Liu, C., Bayer, A., Cosgrove, S. E., Daum, R. S., Fridkin, S. K., Gorwitz, R. J., ... Murray, B. E. (2011). Clinical practice guidelines by the Infectious Diseases Society of America for the treatment of methicillin-resistant *Staphylococcus aureus* infections in adults and children. *Clinical Infectious Diseases*, *52*, e18–e55. <https://doi.org/10.1093/cid/ciq146>
- Mesentean, S., Fischer, S., & Smith, J. C. (2006). Analyzing large-scale structural change in proteins: Comparison of principal component projection and sammon mapping. *Proteins: Structure, Function, and Bioinformatics*, *64*, 210–218. <https://doi.org/10.1002/prot.20981>
- Novales, M. G. M. (2011). Resistencia antimicrobiana del *Staphylococcus aureus* en México. *Boletín Médico del Hospital Infantil de México*, *68*, 262–270.
- Padyana, A. K., & Burley, S. K. (2003). Crystal structure of shikimate 5-dehydrogenase (SDH) bound to NADP: Insights into function and evolution. *Structure*, *11*, 1005–1013. [https://doi.org/10.1016/S0969-2126\(03\)00159-X](https://doi.org/10.1016/S0969-2126(03)00159-X)
- Pastor, R. W., Brooks, B. R., & Szabo, A. (1988). An analysis of the accuracy of Langevin and molecular dynamics algorithms. *Molecular Physics*, *65*, 1409–1419. <https://doi.org/10.1080/00268978800101881>
- Peek, J., & Christendat, D. (2015). The shikimate dehydrogenase family: Functional diversity within a conserved structural and mechanistic framework. *Archives of Biochemistry and Biophysics*, *566*, 85–99. <https://doi.org/10.1016/j.abb.2014.12.006>
- Peek, J., Shi, T., & Christendat, D. (2014). Identification of novel polyphenolic inhibitors of shikimate dehydrogenase (AroE). *Journal of Biomolecular Screening*, *19*, 1090–1098. <https://doi.org/10.1177/1087057114527127>
- Pottinger, P. S. (2013). Methicillin-resistant *Staphylococcus aureus* infections. *Medical Clinics*, *97*, 601–619.
- Roberts, C. W., Finnerty, J., Johnson, J. J., Roberts, F., Kyle, D. E., Krell, T., ... Tzipori, S. (1999). Reply: Shikimate pathway in apicomplexan parasites. *Nature*, *397*, 220. <https://doi.org/10.1038/16621>
- Sander, T., Freyss, J., von Korff, M., & Rufener, C. (2015). DataWarrior: An open-source program for chemistry aware data visualization and analysis. *Journal of Chemical Information and Modeling*, *55*, 460–473. <https://doi.org/10.1021/ci500588j>
- Segel, I. H. (1975). Enzyme kinetics: Behavior and analysis of rapid equilibrium and steady state enzyme systems.
- Shelley, J. C., Cholleti, A., Frye, L. L., Greenwood, J. R., Timlin, M. R., & Uchimaya, M. (2007). Epik: A software program for pK a prediction and protonation state generation for drug-like molecules. *Journal of Computer-Aided Molecular Design*, *21*, 681–691. <https://doi.org/10.1007/s10822-007-9133-z>
- Spessard, Gary. O. (1998). ACD Labs/LogP dB 3.5 and ChemSketch 3.5. *Journal of Chemical Information and Computer Sciences*, *38*, 1250–1253. <https://doi.org/10.1021/ci980264t>
- Systat. (2011). *SigmaPlot 12*. San Jose, CA: SYSTAT Software, Inc..
- Vanommeslaeghe, K., Hatcher, E., Acharya, C., Kundu, S., Zhong, S., Shim, J., ... Vorobyov, I. (2010). CHARMM general force field: A force field for drug-like molecules compatible with the CHARMM all-atom additive biological force fields. *Journal of Computational Chemistry*, *31*, 671–690.
- WHO (World Health Organization). (2017). *WHO publishes list of bacteria for which new antibiotics are urgently needed*. WHO. <http://www.who.int>
- Ye, S., von Delft, F., Brooun, A., Knuth, M. W., Swanson, R. V., & McRee, D. E. (2003). The crystal structure of shikimate dehydrogenase (AroE) reveals a unique NADPH binding mode. *Journal of Bacteriology*, *185*, 4144–4151. <https://doi.org/10.1128/JB.185.14.4144-4151.2003>

How to cite this article: Enríquez-Mendiola D, Téllez-Valencia A, Sierra-Campos E, et al. Kinetic and molecular dynamic studies of inhibitors of shikimate dehydrogenase from methicillin-resistant *Staphylococcus aureus*. *Chem Biol Drug Des*. 2019;00:1–14. <https://doi.org/10.1111/cbdd.13532>



Biochemical, Kinetic, and Computational Structural Characterization of Shikimate Kinase from Methicillin-Resistant *Staphylococcus aureus*

Alejandro Favela-Candia¹ · Alfredo Téllez-Valencia¹ · Mara Campos-Almazán¹ · Erick Sierra-Campos² · Mónica Valdez-Solana² · Jesús Oria-Hernández³ · Adriana Castillo-Villanueva³ · Hugo Nájera⁴ · Claudia Avitia-Domínguez¹

Published online: 12 February 2019
© Springer Science+Business Media, LLC, part of Springer Nature 2019

Abstract

One of the most widespread pathogens worldwide is methicillin-resistant *Staphylococcus aureus*, a bacterium that provokes severe life-threatening illnesses both in hospitals and in the community. The principal challenge lies in the resistance of MRSA to current treatments, which encourages the study of different molecular targets that could be used to develop new drugs against this infectious agent. With this goal, a detailed characterization of shikimate kinase from this microorganism (SaSK) is described. The results showed that SaSK has a K_m of 0.153 and 224 μM for shikimate and ATP, respectively, and a global reaction rate of 13.4 $\mu\text{mol}/\text{min}/\text{mg}$; it is suggested that SaSK utilizes the Bi–Bi Ping Pong reaction mechanism. Furthermore, the physicochemical data indicated that SaSK is an unstable, hydrophilic, and acidic protein. Finally, structural information showed that SaSK presented folding that is typical of its homologous counterparts and contains the typical domains of this family of proteins. Amino acids that have been shown to be important for SaSK protein function are conserved. Therefore, this study provides fundamental information that may aid in the design of inhibitors that could be used to develop new antibacterial agents.

Keywords MRSA · Shikimate kinase · Enzyme kinetics · Homology modeling · Molecular dynamics

✉ Claudia Avitia-Domínguez
avitiaclaudia@gmail.com

Alejandro Favela-Candia
alejandrofavela3@gmail.com

Alfredo Téllez-Valencia
atellez@ujed.mx

Mara Campos-Almazán
marai_campos@hotmail.com

Erick Sierra-Campos
ericksier@gmail.com

Mónica Valdez-Solana
valdezandyval@gmail.com

Jesús Oria-Hernández
jesus.oria.inp@gmail.com

Adriana Castillo-Villanueva
acastilloinp@gmail.com

Hugo Nájera
hnajerap@gmail.com

- 1 Facultad de Medicina y Nutrición, Universidad Juárez del Estado de Durango, Av. Universidad y Fanny Anitua S/N, C.P. 34000 Durango, Dgo, Mexico
- 2 Facultad de Ciencias Químicas, Universidad Juárez del Estado de Durango, Av. Artículo 123 S/N Fracc. Filadelfia, Gómez Palacio, C.P. 35010 Durango, Mexico
- 3 Laboratorio de Bioquímica Genética, Secretaría de Salud, Instituto Nacional de Pediatría, C.P. 04534 Ciudad de México, Mexico
- 4 Departamento de Ciencias Naturales, Universidad Autónoma Metropolitana, Unidad Cuajimalpa, Delegación Cuajimalpa de Morelos, Av. Vasco de Quiroga 4871, Colonia Santa Fe Cuajimalpa, C.P. 05300 Ciudad de México, Mexico

Introduction

Methicillin-resistant *Staphylococcus aureus* (MRSA) remains one of the most problematic bacterial pathogens worldwide [1]. This microorganism is both a commensal bacterium and a human pathogen, since approximately 30% of the human population is colonized [2, 3]. MRSA provokes severe life-threatening illnesses that affect skin, soft tissues, and blood, and causes serious deep-seated infections; a further issue is the common introduction of these infections through medical devices [3, 4]. The principal challenge lies in the resistance of MRSA to current treatments [5], which creates a need for the investigation of different molecular targets to develop new drugs against this pathogen.

A fundamental metabolic route that is present in bacteria, plants, fungus, and apicomplexan parasites but absent in humans, is the shikimate pathway (SP) [6]. This route comprises seven enzymatic reactions that utilize erythrose-4-phosphate, which is derived from the pentose phosphate pathway, and phosphoenolpyruvate which is generated by glycolysis to obtain chorismate [7]. This metabolite is necessary for the synthesis of aromatic compounds such as tryptophan, tyrosine, and phenylalanine, as well as other compounds, including folates, ubiquinones, mycobactins, menaquinones, and naphthoquinones that are crucial for bacterial survival [6, 8]. Therefore, the enzymes of this pathway are attractive targets for the development of new antimicrobial agents [9].

One of the enzymes in the SP is shikimate kinase (SK), which catalyzes the transfer of the phosphoryl from ATP to shikimate to form shikimate-3-phosphate and ADP [10]. SK is a member of the nucleoside monophosphate kinase (NMP kinase) family, which are enzymes that undergo large conformational changes during catalysis [11, 12] and share a homologous α - β - α fold [13, 14]. The crystal structure of SKs from bacteria and plants has been reported previously [12, 15–18]. Based on the structural data, the enzyme is composed of three domains: the core domain, which is formed by five central parallel β -sheets and a highly conserved phosphate-binding loop (P-loop); the LID domain, which contains important residues for ATP binding and undergoes substantial structural changes upon substrate binding; the NMP-binding domain, which is responsible for the recognition and binding of shikimate [19].

In this study, we performed for the first time a biochemical, kinetic, and structural characterization of shikimate kinase from MRSA (SaSK) using molecular dynamics studies, with the aim of providing fundamental information that could contribute to the design inhibitors that could be developed into new antibacterial agents.

Materials and Methods

Cloning and Expression and Purification of SaSK

Genomic DNA from methicillin-resistant *Staphylococcus aureus* subsp. *aureus* (ATCC® BAA1720™ strain, ATCC®, Manassas, VA, USA) was used for SaSK gen (*aroK*) cloning. A 525 bp DNA fragment was amplified using PCR with the following oligonucleotides: 5'-AATCATGATAAATCACCA-3' (forward) and 5'-CTAATACTGATCACTCGCTT-3' (reverse). The amplification product was digested with *Nde*I and *Bam*HI and inserted into the overexpression vector pET28a (Novagen, Gibbstown, NY). The plasmid containing the gene was introduced via transformation of *E. coli* BL21 (DE3)pLysS cells (Novagen, Madison, WI, USA). Recombinant protein expression was induced in 500 mL of Luria–Bertani broth containing kanamycin (50 μ g/mL). The culture was grown at 37 °C with continuous shaking; once it reached an OD₆₀₀ of 1.0, 0.8 mM β -D-thiogalactopyranoside (IPTG) was added and the culture was incubated for 12 h at 20 °C.

Subsequently, the cells were harvested by centrifugation and resuspended in buffer A (50 mM Tris–HCl, pH 7.5, 300 mM NaCl, 10 mM imidazole, and 10 mM β -mercaptoethanol) containing 300 μ M protease inhibitor (PMSF) and were then lysed via sonication. The cellular debris was removed by centrifugation at 26,000 rpm for 30 min. The supernatant was loaded onto a column containing Ni–NTA resin and the protein was purified using buffer A containing different concentrations of imidazole (10–300 mM). The fractions containing the protein (in 50 mM imidazole) were pooled and concentrated via centrifugation using an Amicon Ultra-15 10K concentrator. Finally, the imidazole was removed by washing the protein with buffer B containing 50 mM Tris–HCl, pH 7.5, 1 mM DTT, and 1 mM EDTA using the same concentrator. The protein concentration was determined using the Bradford method [20].

Activity Assays

The enzymatic activity was measured using a coupled system according to the method described by Millar *et al.* [21], with some modifications. Briefly, a reaction mixture containing 100 mM Tris–HCl, pH 7.6, 10 mM shikimate, 0.4 mM NADH⁺, 100 mM KCl, 25 mM MgCl, 1.6 mM phosphoenolpyruvate, 2 mM ATP, pyruvate kinase (3 μ g/mL), and lactate dehydrogenase (3 μ g/mL) was used. The reaction was initiated via the addition of 0.65 μ g of SaSK. The moles of substrate consumed were measured at

25 °C by monitoring the NADH⁺ consumption at 340 nm ($\epsilon_{340} = 6220 \text{ M}^{-1} \text{ cm}^{-1}$).

Steady-State Kinetics

The kinetic parameters of shikimate and ATP were determined by measuring their initial velocities while varying the concentration of one substrate and maintaining the other substrate at the concentration indicated in activity assays. For shikimate, the concentration varied within the range of 50–1000 μM while that of ATP varied between 50 and 700 μM ; all assays were conducted in quadruplicate. The data were linearized based on a Hanes–Wolf plot [22] and adjusted according to different models of a bisubstrate enzyme (Eq. 1) using SigmaPlot software (v12.3).

$$\frac{V}{V_{\max}} = \frac{[A][B]}{K_{\text{mB}}[A] + K_{\text{mA}}[B] + [A][B]}, \quad (1)$$

where V is the initial velocity, V_{\max} is the maximum velocity, A and B represent the substrates ATP and shikimate, respectively, and K_{mA} and K_{mB} are the Michaelis–Menten constants for each substrate.

Determination of the Oligomeric State and Molecular Weight

The oligomeric state of native shikimate kinase was assayed by size exclusion chromatography using a Superose 6 10/300 GL column (GE Healthcare) coupled to an Äkta FPLC system. The column was equilibrated with 5 column volumes of buffer containing 50 mM Tris–HCl, pH 8.0, and 150 mM NaCl prior to use, and was developed in the same media at 0.5 mL/min. The column calibration was performed using gel filtration standards obtained from Bio-Rad that were supplemented with *Giardia lamblia* aldolase and equine cytochrome C. Shikimate kinase (200 μg) was injected onto the column and the absorbance was monitored at 280 nm. The major peaks were collected and concentrated using Amicon Ultra-0.5 centrifugal filter units that had a nominal molecular weight limit (NMWL) of 3 kDa. The collected fractions, plus a sample of protein not subject to gel filtration, were used for 12% SDS–PAGE according to the method described by Laemmli [23] and were then electroblotted onto an Immobilon-P Millipore PVDF membrane. Thereafter, the membrane was blocked with 5% skim milk in PBS/Tween (PBS-T) for 2 h at 25 °C and washed with PBS-T. The PVDF membrane was then incubated with rabbit IgG anti-His Tag (Santa Cruz Biotechnology, Dallas, TX, USA) at a dilution of 1:2000 overnight at 4 °C with orbital agitation. The membrane was washed 3 times with

PBS-T buffer, once with PBS-T containing 1 M NaCl, and was finally washed once more with PBS-T. Afterward, the membrane was incubated with a goat anti-rabbit IgG-peroxidase conjugate (Sigma–Aldrich) that was diluted 1:2000 for 1 h at 25 °C with orbital agitation and then washed two times with PBS-T. The antigen–antibody interaction was visualized using diaminobenzidine and H₂O₂. The reaction was monitored until bands were clearly visible, at which time the reaction was stopped by withdrawal of the chromogenic solution and washed with PBS-T. The elution volume of the anti-His Tag-positive western blot fraction was interpolated based on a calibration curve generated using gel filtration standards to estimate the molecular mass of native SaSK.

Physicochemical Parameters

Different physicochemical parameters of SaSK, such as the isoelectric point, the amino acid composition, the number of positively charged (Arg + Lys) and negatively charged (Asp + Glu) residues, the molar extinction coefficient, the aliphatic index, and the instability index, were calculated using the ProtParam tool on the ExpASY server [24]. Furthermore, the degree of protein hydrophobicity (GRAVY) was determined using the Protscale tool on the same server [25, 26]. Additionally, the degree of protein thermostability was determined by incubating the enzyme at different temperatures that ranged from 4 to 40 °C for 8 h. Thereafter, an aliquot was withdrawn to measure the activity using the reaction conditions described above.

Homology Modeling

Because this is the first report about SaSK, the structure of this enzyme has never been determined. Therefore, a homology modeling strategy was used to obtain a 3D structure of the enzyme. To this end, two models were generated using the servers Swiss model [30] and (PS)2-V2 [33, 34] that used the crystal structure of SK from *Helicobacter pylori* (PDB ID: 3MUF) [16] as a template, since both enzymes share approximately 26% amino acid sequence identity. The stereochemical characteristics of the models were evaluated using the Swiss-model server [35].

Molecular Dynamics Simulations

Molecular dynamics (MD) simulations were performed using GROMACS (v5.0.4) with the CHARMM36 force field [27, 28]. The enzyme complex containing both substrates (SaSK–SHK–ATP) was built using coordinates reported in two crystallographic structures of SK from *Mycobacterium*

tuberculosis, one of which contains shikimate and the other contains ATP (PDB 2IYQ and 2IYW, respectively) [12]. The substrates were parametrized using the SwissParam server [29, 30]. The complex was immersed in a cubic box using the TIP3P water model. The system charges were neutralized using Na^+ and Cl^- ions. Thereafter, the complex was subject to 500 cycles of steepest-descent algorithmic modeling for the purposes of energy minimization using a conjugate gradient algorithm with a tolerance of 1000 KJ/mol/nm. Afterwards, canonical (NVT) [31] and isothermal–isobaric (NPT) [32] simulations (with isotropic position scaling) at 300 K and 1 atm pressure were performed. Finally, a complete molecular dynamics simulation of 20 ns at 300 K without restrictions was performed, which obtained 2,000 conformations that were saved every 5000 steps.

Principal Component Analysis

The modes of motion of the enzyme-substrate complex were evaluated by performing principal component analyses (PCA) [33]. To this end, a covariance matrix was assembled using a simple linear transformation in Cartesian coordinate space. A vectorial representation of every single component indicated their direction of motion. For this purpose, a set of eigenvectors was derived via the diagonalization of the covariance matrix. Each eigenvector had a corresponding eigenvalue that described the energetic contribution of each component to the motion [34]. The protein regions that are responsible for the most significant collective motions can be revealed using PCA [35]. The GROMACS in-built tools *g_covar* and *g_anaeig* were used to perform the PCA.

Results and Discussion

Cloning and Expression and Purification of SaSK

Genomic DNA from the methicillin-resistant *Staphylococcus aureus* BAA1720 strain was used for amplification of the *aroK* gene that encodes shikimate kinase. Using PCR, a 525 bp product was obtained, which was then sequenced to confirm the identity of the gene and cloned into a pET28a vector for overexpression. The enzyme was purified using affinity chromatography and eluted in 50 mM imidazole; at this concentration, five other proteins that were nonspecifically bound to the resin co-eluted with SaSK (Fig. 1a). To determine its molecular weight and oligomeric state, size exclusion chromatography in native conditions was used. As was expected, the chromatogram contained several peaks (Fig. 1b); therefore, to determine which peak corresponded to SaSK, western blot analysis was used to identify each peak as described in the Materials and Methods. The results

indicated that only one peak was recognized by the anti-His tag antibodies, and this peak corresponded to SaSK (Fig. 1b, inset). According to the calibration curve (Fig. 1c), this peak corresponds to a molecular weight of 18.6 kDa, which is in concordance with that predicted based on the amino acid sequence and the reported masses of other SKs from bacteria such as *B. anthracis* (19.1 kDa) [36], *M. tuberculosis* (18.5 kDa) [37], *S. flexneri* (26.9 kDa) [38], and *H. pylori* (18 kDa) [16]. Additionally, it can be concluded from the oligomeric state analysis that SaSK is monomeric, which is in line with observations based on the crystallographic structure of SKs from *M. tuberculosis* [12], *E. coli* [17], *E. chrysanthemi* [18], *A. baumannii* [15], *H. pylori* [16].

Kinetic Parameters and Reaction Mechanism

The SK shikimate-binding site has been proposed to be a more promising target for drug design than the ATP-binding site due to the diminished likelihood of off-target activity at the shikimate-binding site [15]. Thus, the steady-state kinetic parameters were determined using curves generated by utilizing different fixed concentrations of one substrate and varying the concentration of the other, as described in the “Materials and Methods” section. Hyperbolic data (Fig. 2a, c) were linearized as a function of $[\text{S}]/V_0$ versus $[\text{S}]$ based on a Hanes-Woolf plot [22] (Fig. 2b, d). The data were adjusted based on different kinetic models used for bisubstrate enzymes to obtain K_m values for shikimate and ATP of 0.153 and 224 μM , respectively, and a global reaction rate of 13.4 $\mu\text{mol}/\text{min}/\text{mg}$. In respect to the kinetic parameters reported for other bacterial SKs, the K_m value for ATP was in the same range [39–41]. Nevertheless, the K_m for shikimate was three orders of magnitude less than that reported previously [39, 42]. This discrepancy could be due to the methods used to obtain the parameters, because in the previous reports, data were adjusted independently for each substrate instead of being regarded as a bisubstrate enzyme, which permitted the analysis of the influence of ATP on shikimate binding.

Based on the data, it can be concluded that ATP increases the affinity of SaSK for shikimate. Additionally, the pattern observed in the linear plots (Fig. 2b, d) suggests that SaSK utilizes a Bi–Bi Ping Pong reaction mechanism [43], which is in accordance with that reported for kinases from the NMP family [11]. Therefore, the results suggest that the reaction is initiated by the binding of ATP to SaSK, after which ADP is released, and proceeds via the binding of shikimate to finally produce shikimate-3-phosphate and regenerate the free enzyme. Similar results have been observed in SK from *Erwinia chrysanthemi*; however, with respect to ATP [44], the authors observed a four-fold difference between the K_m (620 μM) and the K_D (2.56 mM), which suggests that the

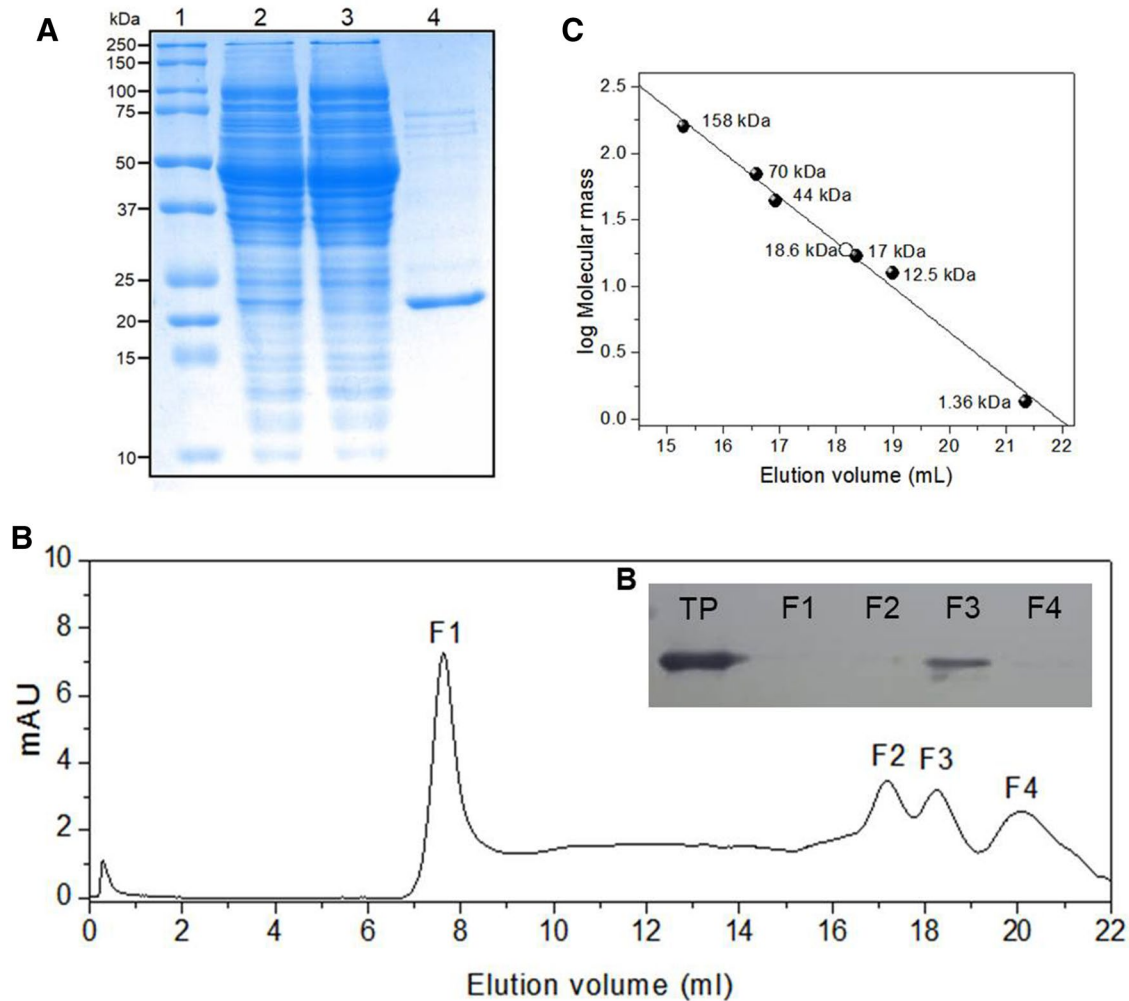


Fig. 1 Purification and molecular weight determination of SaSK. **a** SDS–PAGE (15%) of purified recombinant SaSK; line 1, molecular weight markers; lane 2, supernatant; lane 3, eluate; lane 4, SaSK eluted with 50 mM imidazole. **b** Size exclusion chromatogram in native conditions showing the different peaks that were obtained. The inset shows the results of western blot analysis for each peak.

The TP line corresponds to the protein preparation from which the aliquot was withdrawn to charge into the column; lines F1, F2, and F4 correspond to the different peaks observed in the chromatogram, and F3 corresponds to the peak in which SaSK was eluted. **c** Calibration curve showing the elution volume of different molecular weight standards; the open circle corresponds to that of SaSK

binding of one substrate could positively modify the affinity of the enzyme for the second substrate. However, this is not observed in SK from *M. tuberculosis*, in which no such difference was reported for the K_m (112 μM) and K_D (196 μM) for ATP [42]. In the same study, an inverse effect in respect to shikimate, for which the K_m (650 μM) was almost four-fold higher than the K_D (181 μM), suggested the presence of negative cooperativity between ATP to shikimate binding. Ultimately, the authors proposed the presence of rapid-equilibrium randomness in substrate binding in the reaction mechanism of this enzyme. Based on crystallographic data, a random sequential mechanism has also been proposed [12].

Physicochemical Characterization

Data obtained from the *in silico* prediction of physicochemical parameters indicated that the protein has an acidic character and a theoretical isoelectric point of 5.09, similarly to *B. anthracis* SK (estimated pI of 5.38), but totally unlike *M. tuberculosis* SK (pI of 10.56) [36], which indicates that SK could be acidic or basic; apparently, there is no consensus on this point. Furthermore, a stability index that is greater than 40 classifies the protein as unstable [45]. Based on its negative grand average of hydropathicity (GRAVY) value [46], SaSK can be classified as a hydrophilic protein. These and other representative data are shown in Table 1. The SaSK

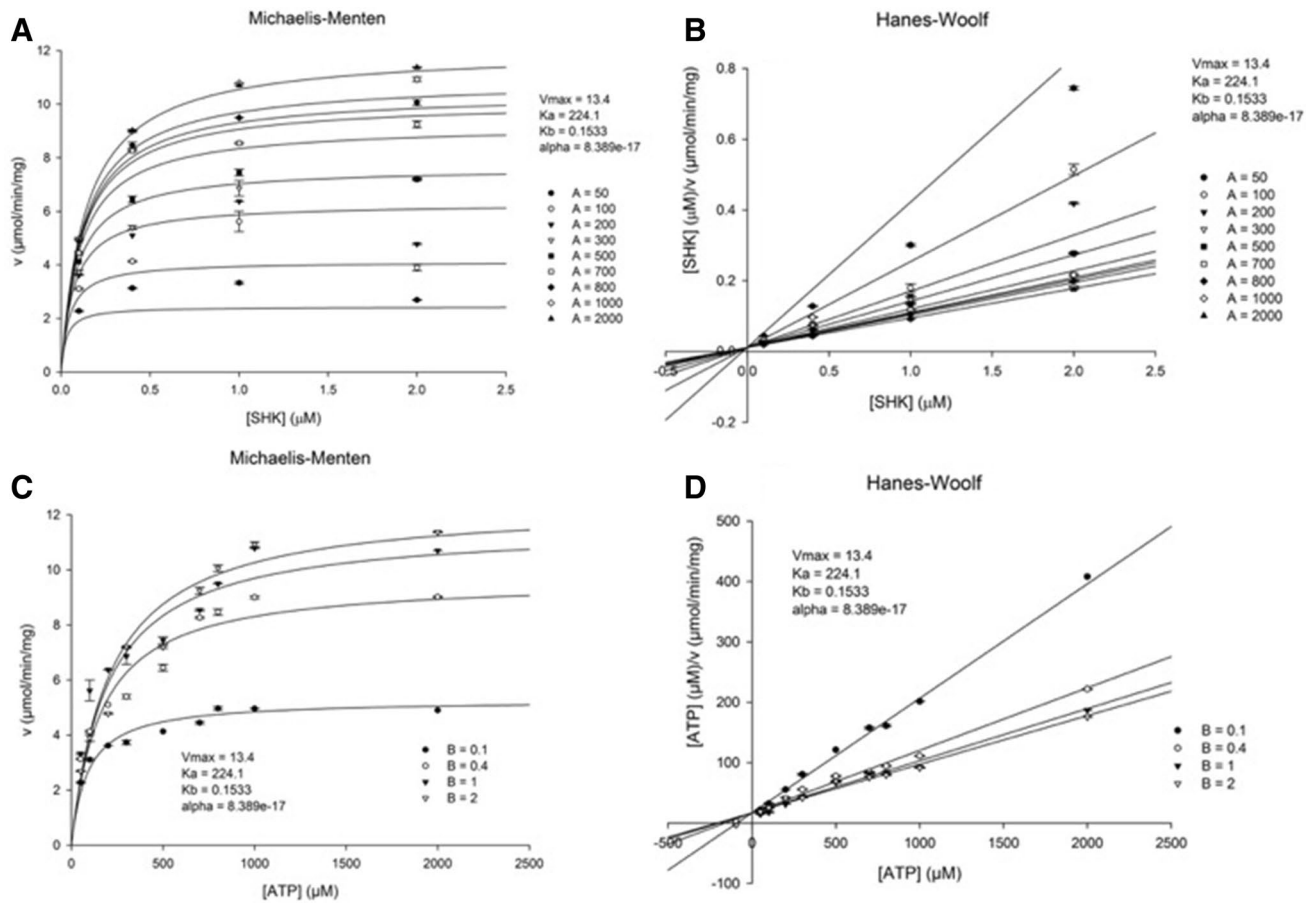


Fig. 2 SaSK kinetics characterization. **a** and **c** Michaelis–Menten plots for shikimate (0.1, 0.4, 1, and 2 mM) and ATP (0.05, 0.1, 0.2, 0.3, 0.5, 0.7, 0.8, 1, and 2 mM), respectively. **b** and **d** Hanes-

Woolf plots for shikimate and ATP, respectively. Plots represent the mean \pm SD of four independent assays

Table 1 Predicted physicochemical properties of the SaSK

Parameter	Value
Theoretical pI	5.09
Extinction coefficients $\text{M}^{-1} \text{cm}^{-1}$ at 280 nm	20,400
Amino acid more frequently (%)	Ile (14.9)
Amino acid less frequently (%)	Trp (0.6)
Total number of positively charged residues (Arg + Lys)	18
Total number of negatively charged residues (Asp + Glu)	25
Instability index	46.69
Grand average of hydropathicity (GRAVY)	-0.303

physicochemical parameters are generally comparable to the published values of characteristics of SKs from *Shigella flexneri* [38] and *Yersinia pestis* [47].

Additionally, the protein thermostability was determined. The results showed that, after 8 h of incubation, the enzyme maintained its maximal activity in a range from 4 to 20 °C, while at 25 and 26 °C, it dropped to 70% and 60%, respectively. A further increase of two degrees

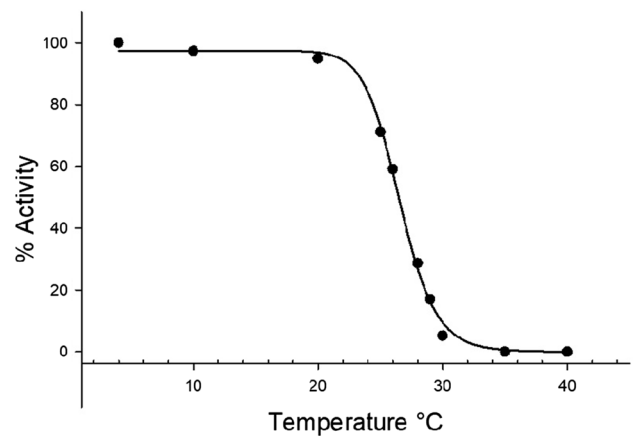


Fig. 3 SaSK thermostability plot

led to the loss of 70% of the maximal activity, and at 30 °C the enzyme was practically inactive (Fig. 3), which is in accordance with its predicted instability index.

Homology Modeling

In view of our interest in investigating the interactions between SaSK and its substrates, selecting the best structure as a template to generate the SaSK 3D model was very important. To achieve this, two main conditions must be accomplished: the structure should be in complex containing both substrates and the LID domain should be in the catalytically closed conformation.

Upon analysis of the nine crystal structures of SKs from different bacterial sources that are available in the Protein Data Bank, only two were of complexes containing both substrates or products: SK from *M. tuberculosis* (shikimate-ADP) [12], and SK from *H. pylori* (shikimate-3-phosphate-ADP) [16], which showed the LID domain in the catalytically closed conformation. An alignment of the sequences from *M. tuberculosis* and *H. pylori* with that of SaSK showed 22% and 26% of identity, respectively. Therefore, the structure of SK from *H. pylori* was selected as the template. Additionally, it is important to mention that, upon comparison to the other crystal structures that are available, the sequence identity ranges from 24 to 30% (data not shown).

The two models that were generated from the Swiss-model and (PS)2-V2 servers had very similar values in terms of evaluation; 94% and 92% of the amino acids were within the favorable region of the Ramachandran plot, respectively. The Q -mean score was -2.7 for Swiss model and -3.9 for (PS)2-V2; this was to be expected due to the lower sequence identity with the template. However, as seen below, the same general folding configuration was maintained. Therefore, to select the correct model, another specific characteristic had

to be taken into account, it was the orientation of the Arg120 side chain, which is involved in ATP binding [40]. To this end, a structural alignment with *M. tuberculosis* SK in complex with shikimate and ADP was performed and the results indicated that the model generated by the (PS)2-V2 server showed the correct orientation of this residue. Therefore, this model was selected for use in further studies (Fig. 4).

Additionally, multiple sequence analysis based on the structure showed that SaSK exhibits the typical structural domains that have been described in other SKs from bacteria (Fig. 5) [14, 17]. The LID is composed of residues Asn115-Thr127. Furthermore, the functional motif Walker A, which forms a P-loop, participates in phosphate binding (residues Gly12-Ser19), and the Walker B motif (residues Ile77-Gly83), which contains Gly82, is involved in shikimate binding [13]. Likewise, amino acid 79, which is an aspartic acid in NMP kinases [48], is an alanine in SaSK and in *E. coli* SK [17], and is a serine in SKs from *M. tuberculosis* and *H. pylori* [12, 16]. The entire shikimate-binding site was encompassed by amino acids I36-E64 [13]. Finally, the catalytic residues correspond to Asp37, Ser19, Lys18, and Arg120 [12].

Molecular Dynamics Simulations

With the goal of gaining structural information relevant to the SaSK catalytic process, molecular dynamics simulations were performed in the presence of substrates for 20 ns. To do this, the SaSK-SHK-ATP complex was built. The data showed that, after 8 ns, the complex was stabilized, which was confirmed via the ligand-protein RMSD measurement.

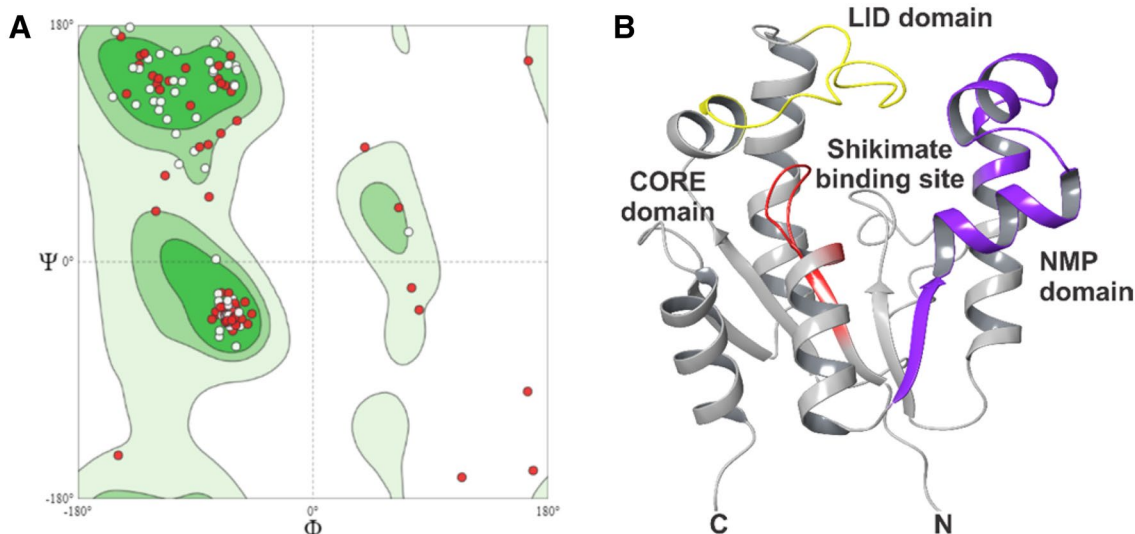


Fig. 4 Stereochemistry evaluation and structural analysis of SaSK. **a** Ramachandran plot for the SaSK 3D model. Dark green, green, and light green represent favored, permitted, and not permitted regions,

respectively. **b** Ribbon representation of the SaSK 3D model indicating the principal domains

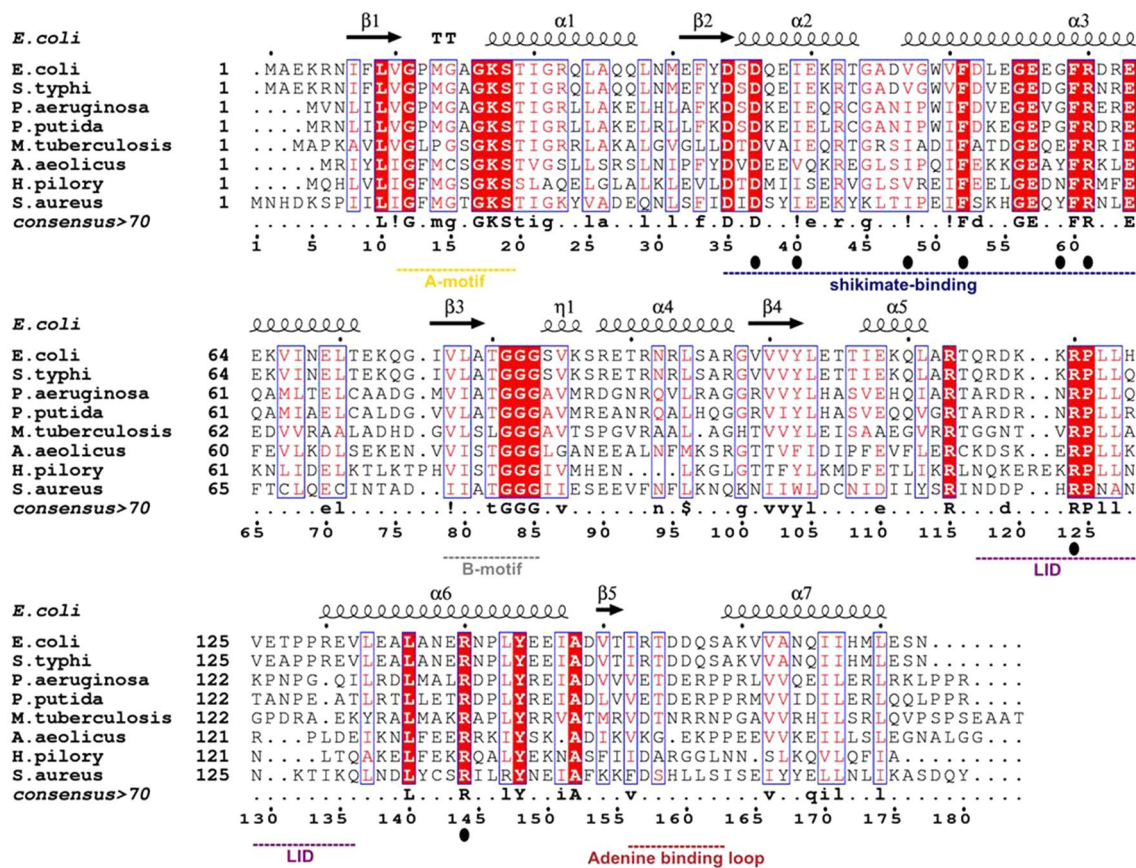


Fig. 5 Multiple sequence analyses of SKs from bacteria. The figure shows the principal structural motifs of SKs. Filled circles indicate residues involved in substrate binding and catalysis. The secondary structure is indicated in the upper part of the sequence alignment; β sheets are depicted as arrows and α -helix as spirals. The sequence identifiers are as follows: *Escherichia coli* (P0A6D7), *Salmonella*

typhi (P63602), *Pseudomonas aeruginosa* (P34003), *Pseudomonas putida* (Q88CV1), *Mycobacterium tuberculosis* (P9WPY3), *Aquifex aeolicus* (O67925), *Helicobacter pylori* (P56073), and *Staphylococcus aureus* (Q6GGG1). The alignments were generated using the CLUSTAL-W web-based server [49] and rendered in ESPrnt [50]

The values of the standard deviation from 8 to 20 ns were 0.09 and 0.1 nm for shikimate and ATP, respectively (Fig. 6).

The PCA analyses revealed that conformational changes occurred in the SaSK–SHK–ATP complex; specifically, the LID and NMP domains were subject to small movements, but the closed conformation of the enzyme was maintained during the entire simulation (Fig. 7). A similar behavior was described in *M. tuberculosis* SK, where small movements in both domains and the preservation of the closed conformation in the enzyme were observed after 10 ns of MD simulation [51]. Additionally, fluctuations were also reported in the SK from *B. anthracis*, different models were constructed with the LID domain in the open or closed conformation as well as using uncomplexed and complexed forms of the enzyme; after 4 ns of MD, more changes in the LID domain were observed in the uncomplexed than in the complexed structure [36].

Furthermore, a time-dependent analysis of the interactions within the SaSK–SHK–ATP complex during 20 ns

of simulation was performed (Fig. 8). In the case of shikimate, hydrogen bonds with Asp37, Gly82, Arg61, and Arg138 were formed at the beginning of the simulation (Fig. 8a). These interactions have been observed in crystal structures [12, 16, 52, 53] and are important for the binding and correct orientation of shikimate; Asp37 orients O1 of SHK, while Arg58 and Arg138 interact with its carboxyl group. However, these interactions varied during simulation. At 10 ns, hydrogen bonds were observed only with Asp37 and Gly83, and these were maintained for the rest of the simulation (Fig. 8a). On the other hand, ATP interacted via hydrogen bonds with Gly15, Gly17, Lys18, Arg113, Ser152, and Ser156 (Fig. 8b). However, after 5 ns, these interactions shifted to Gly15, Gly17, Lys18, Ser19, Thr20, Arg120, and Leu54 (data not shown), and were maintained until the end of the simulation (Fig. 8b). In particular, the interaction with Arg120 is very important because this amino acid may act as a Lewis acid during enzyme catalysis by activating and positioning the

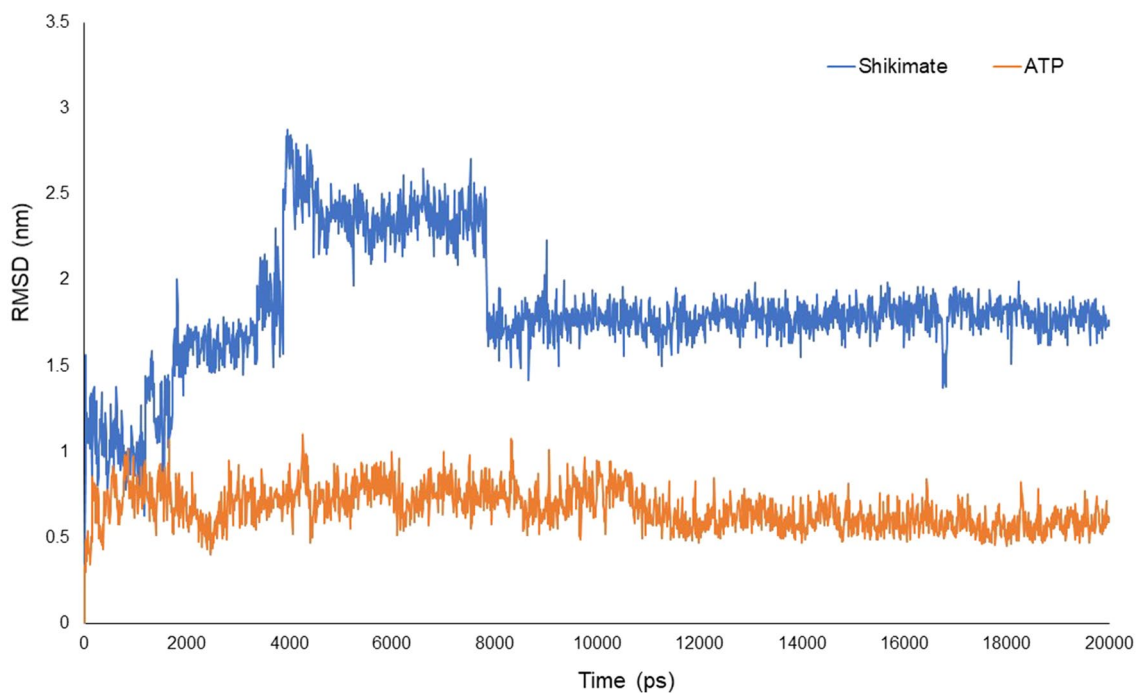


Fig. 6 RMSD plot of shikimate (blue) and ATP (orange) with respect to SaSK. (Color figure online)

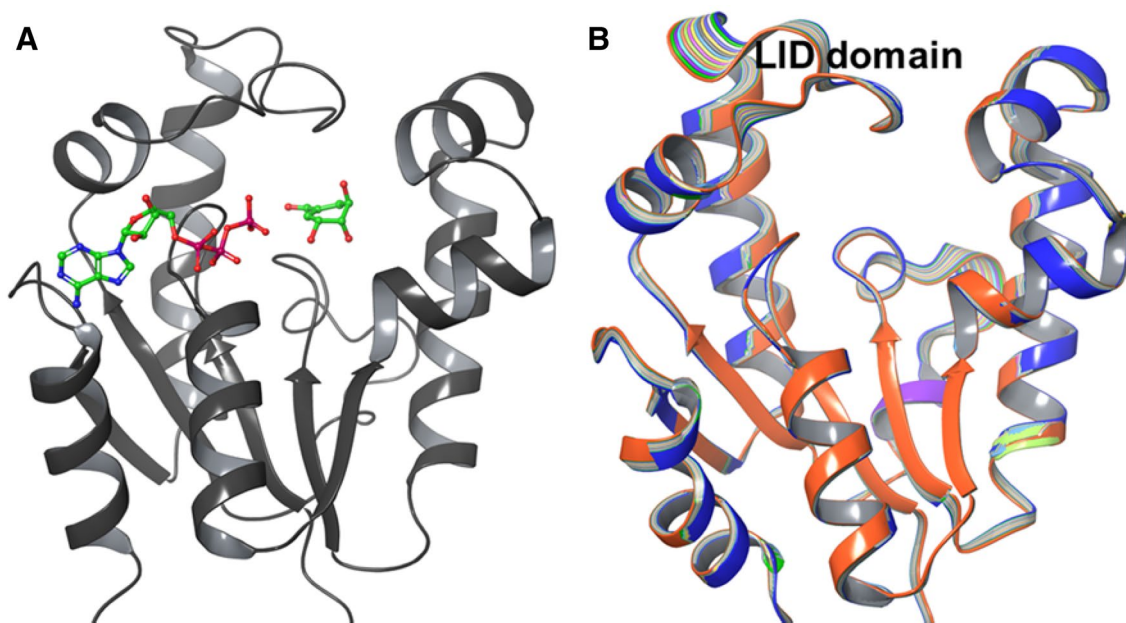


Fig. 7 SaSK–SHK–ATP complex. **a** Binding mode of shikimate and ATP by SaSK. **b** Conformational ensemble obtained from the principal component analysis

phosphoryl group of ATP for nucleophilic attack by the C3 hydroxyl group, as well as by possibly stabilizing the phosphoryl oxygen atoms in the transition state [51, 53].

Additionally, hydrogen bonding with Ser19 contributes to the orientation of both substrates during the phosphoryl

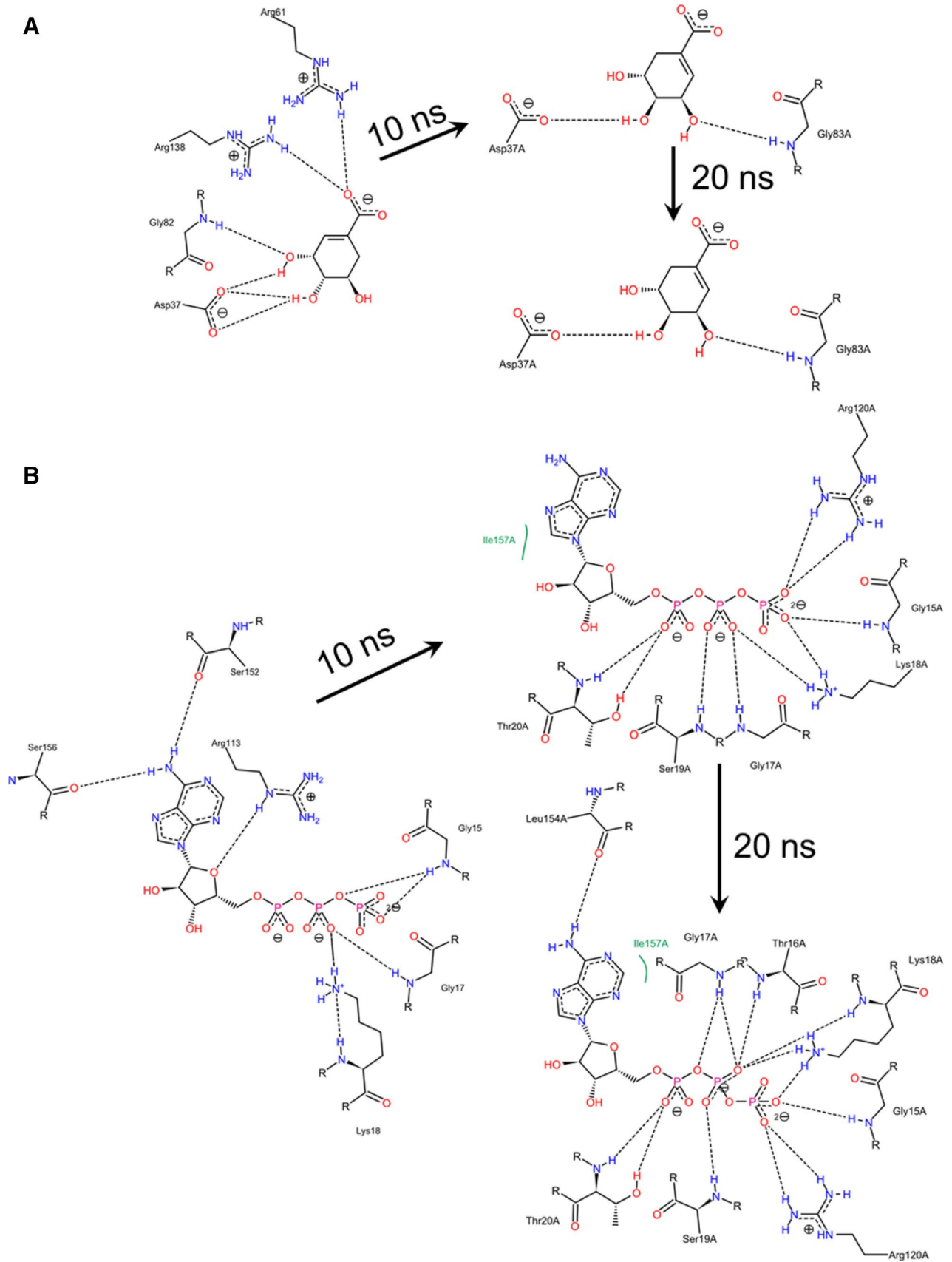


Fig. 8 Maps of the interactions within the SaSK–SHK–ATP complex. **a** shikimate **b** ATP. The image shows the interactions that occurred at different times during the entire dynamics simulation: beginning, 10 ns; final, 20 ns. The dashed lines indicate hydrogen bonds between the protein and ligand. The maps were generated in Server Poseview [54]

transfer reaction [12]; in this case, Ser19 is located next to the β -phosphate of ATP (Fig. 8b).

Conclusion

This work reports, for the first time, a complete biochemical, kinetic, and computational characterization of SK from the nosocomial and community pathogen methicillin-resistant *S. aureus*. In general, the results indicated that the enzyme showed characteristics similar to those reported for other bacterial SKs, as well as those of members of the nucleoside monophosphate kinase family. The data reported here will be useful in the search for inhibitors that serve as guides for the design of new drugs to treat this infectious agent.

Acknowledgements C.A.D. and A.T.V. acknowledge Consejo Nacional de Ciencia y Tecnología (CONACyT) for Grants Nos. 258694 and 257848. CONACyT is also acknowledged for the fellowship granted to A.F.C. (No. 326106).

Compliance with Ethical Standards

Conflict of Interest The authors declare no conflicts of interest.

References

1. Stryjowski, M. E., & Corey, G. R. (2014). Methicillin-resistant *Staphylococcus aureus*: An evolving pathogen. *Clinical Infectious Diseases*, 58, S10–S19.
2. Kluytmans, J., Van Belkum, A., & Verbrugh, H. (1997). Nasal carriage of *Staphylococcus aureus*: Epidemiology, underlying mechanisms, and associated risks. *Clinical Microbiology Reviews*, 10, 505–520.
3. Wertheim, H. F., Melles, D. C., Vos, M. C., van Leeuwen, W., van Belkum, A., Verbrugh, H. A., & Nouwen, J. L. (2005). The role of nasal carriage in *Staphylococcus aureus* infections. *The Lancet Infectious Diseases*, 5, 751–762.
4. King, M. D., Humphrey, B. J., Wang, Y. F., Kourbatova, E. V., Ray, S. M., & Blumberg, H. M. (2006). Emergence of community-acquired methicillin-resistant *Staphylococcus aureus* USA 300 clone as the predominant cause of skin and soft-tissue infections. *Annals of Internal Medicine*, 144, 309–317.
5. Drew, R. H. (2007). Emerging options for treatment of invasive, multidrug-resistant *Staphylococcus aureus* infections. *Pharmacotherapy: The Journal of Human Pharmacology and Drug Therapy*, 27, 227–249.
6. Bentley, R., & Haslam, E. (1990). The shikimate pathway—a metabolic tree with many branches. *Critical Reviews in Biochemistry and Molecular Biology*, 25, 307–384.
7. Herrmann, K. M., & Weaver, L. M. (1999). The shikimate pathway. *Annual Review of Plant Biology*, 50, 473–503.
8. Dewick, P. M. (1995). The biosynthesis of shikimate metabolites. *Natural Product Reports*, 12, 101–133.
9. Kapnick, S. M., & Zhang, Y. (2008). New tuberculosis drug development: Targeting the shikimate pathway. *Expert Opinion on Drug Discovery*, 3, 565–577.
10. Griffin, H. G., & Gasson, M. J. (1995). The gene (*aroK*) encoding shikimate kinase I from *Escherichia coli*. *DNA Sequence*, 5, 195–197.
11. Yan, H., & Tsai, M. D. (1999). Nucleoside monophosphate kinases: Structure, mechanism, and substrate specificity. *Advances in Enzymology and Related Areas of Molecular Biology: Mechanism of Enzyme Action, Part A*, 73, 103–134.
12. Hartmann, M. D., Bourenkov, G. P., Oberschall, A., Strizhov, N., & Bartunik, H. D. (2006). Mechanism of phosphoryl transfer catalyzed by shikimate kinase from *Mycobacterium tuberculosis*. *Journal of Molecular Biology*, 364, 411–423.
13. Cheng, W.-C., Chang, Y.-N., & Wang, W.-C. (2005). Structural basis for shikimate-binding specificity of *Helicobacter pylori* shikimate kinase. *Journal of Bacteriology*, 187, 8156–8163.
14. Pereira, J. H., De Oliveira, J. S., Canduri, F., Dias, M. V., Palma, M. S., Basso, L. A., Santos, D. S., & De Azevedo, W. F. (2004). Structure of shikimate kinase from *Mycobacterium tuberculosis* reveals the binding of shikimic acid. *Acta Crystallographica Section D: Biological Crystallography*, 60, 2310–2319.
15. Sutton, K. A., Breen, J., MacDonald, U., Beanan, J. M., Olson, R., Russo, T. A., Schultz, L. W., & Umland, T. C. (2015). Structure of shikimate kinase, an *in vivo* essential metabolic enzyme in the nosocomial pathogen *Acinetobacter baumannii*, in complex with shikimate. *Acta Crystallographica Section D: Biological Crystallography*, 71, 1736–1744.
16. Cheng, W.-C., Chen, Y.-F., Wang, H.-J., Hsu, K.-C., Lin, S.-C., Chen, T.-J., Yang, J.-M., & Wang, W.-C. (2012). Structures of *Helicobacter pylori* shikimate kinase reveal a selective inhibitor-induced-fit mechanism. *PLoS ONE*, 7, e33481.
17. Romanowski, M. J., & Burley, S. K. (2002). Crystal structure of the *Escherichia coli* shikimate kinase I (*AroK*) that confers sensitivity to mecillinam. *Proteins: Structure, Function, and Bioinformatics*, 47, 558–562.
18. Krell, T., Coyle, J., Horsburgh, M., Coggins, J., & Laphorn, A. (1997). Crystallization and preliminary X-ray crystallographic analysis of shikimate kinase from *Erwinia chrysanthemi*. *Acta Crystallographica Section D*, 53, 612–614.
19. Vornhein, C., Schlauderer, G. J., & Schulz, G. E. (1995). Movie of the structural changes during a catalytic cycle of nucleoside monophosphate kinases. *Structure*, 3, 483–490.
20. Bradford, M. M. (1976). A rapid and sensitive method for the quantitation of microgram quantities of protein utilizing the principle of protein-dye binding. *Analytical Biochemistry*, 72, 248–254.
21. Millar, G., Lewendon, A., Hunter, M., & Coggins, J. (1986). The cloning and expression of the *aroL* gene from *Escherichia coli* K12. Purification and complete amino acid sequence of shikimate kinase II, the *aroL*-gene product. *Biochemical Journal*, 237, 427–437.
22. Hanes, C. S. (1932). Studies on plant amylases: The effect of starch concentration upon the velocity of hydrolysis by the amylase of germinated barley. *Biochemical Journal*, 26, 1406.
23. Laemmli, U. K. (1970) Cleavage of structural proteins during the assembly of the head of bacteriophage T4. *nature*, 227, 680.
24. Gasteiger, E., Gattiker, A., Hoogland, C., Ivanyi, I., Appel, R. D., & Bairoch, A. (2003). ExPASy: The proteomics server for in-depth protein knowledge and analysis. *Nucleic Acids Research*, 31, 3784–3788.

25. Gasteiger, E., Hoogland, C., Gattiker, A., Wilkins, M. R., Appel, R. D., & Bairoch, A. (2005). Protein identification and analysis tools on the ExPASy server (pp. 571–607). In: *The proteomics protocols handbook*. New York: Springer.
26. Walker, J. M. (2005). *The proteomics protocols handbook*. New York: Springer.
27. Best, R. B., Zhu, X., Shim, J., Lopes, P. E., Mittal, J., Feig, M., & MacKerell Jr, A. D. (2012). Optimization of the additive CHARMM all-atom protein force field targeting improved sampling of the backbone ϕ , ψ and side-chain χ^1 and χ^2 dihedral angles. *Journal of Chemical Theory and Computation*, 8, 3257–3273.
28. Vanommeslaeghe, K., Hatcher, E., Acharya, C., Kundu, S., Zhong, S., Shim, J., Darian, E., Guvench, O., Lopes, P., & Vorobyov, I. (2010). CHARMM general force field: A force field for drug-like molecules compatible with the CHARMM all-atom additive biological force fields. *Journal of Computational Chemistry*, 31, 671–690.
29. Bjelkmar, P., Larsson, P., Cuendet, M. A., Hess, B., & Lindahl, E. (2010). Implementation of the CHARMM force field in GROMACS: Analysis of protein stability effects from correction maps, virtual interaction sites, and water models. *Journal of Chemical Theory and Computation*, 6, 459–466.
30. Zoete, V., Cuendet, M. A., Grosdidier, A., & Michielin, O. (2011). SwissParam: A fast force field generation tool for small organic molecules. *Journal of Computational Chemistry*, 32, 2359–2368.
31. Berendsen, H. J., Postma, J. v., van Gunsteren, W. F., DiNola, A., & Haak, J. (1984). Molecular dynamics with coupling to an external bath. *The Journal of Chemical Physics*, 81, 3684–3690.
32. Pastor, R. W., Brooks, B. R., & Szabo, A. (1988). An analysis of the accuracy of Langevin and molecular dynamics algorithms. *Molecular Physics*, 65, 1409–1419.
33. Amadei, A., Linssen, A. B. M., & Berendsen, H. J. C. (1993). Essential dynamics of proteins. *Proteins: Structure, Function, and Bioinformatics*, 17, 412–425.
34. Mesentean, S., Fischer, S., & Smith, J. C. (2006). Analyzing large-scale structural change in proteins: Comparison of principal component projection and sammon mapping. *Proteins: Structure, Function, and Bioinformatics*, 64, 210–218.
35. Hess, B., Kutzner, C., Van Der Spoel, D., & Lindahl, E. (2008). GROMACS 4: Algorithms for highly efficient, load-balanced, and scalable molecular simulation. *Journal of Chemical Theory and Computation*, 4, 435–447.
36. Pauli, I., Caceres, R. A., & de Azevedo Jr, W. F. (2008). Molecular modeling and dynamics studies of Shikimate Kinase from *Bacillus anthracis*. *Bioorganic & Medicinal Chemistry*, 16, 8098–8108.
37. Oliveira, J. S., Pinto, C. A., Basso, L. A., & Santos, D. S. (2001). Cloning and overexpression in soluble form of functional shikimate kinase and 5-enolpyruvylshikimate 3-phosphate synthase enzymes from *Mycobacterium tuberculosis*. *Protein Expression and Purification*, 22, 430–435.
38. Arora, N., Banerjee, A. K., & Murty, U. (2010). *In silico* characterization of Shikimate Kinase of *Shigella flexneri*: a potential drug target. *Interdisciplinary Sciences: Computational Life Sciences*, 2, 280–290.
39. DeFeyter, R. C., & Pittard, J. (1986). Purification and properties of shikimate kinase II from *Escherichia coli* K-12. *Journal of Bacteriology*, 165, 331–333.
40. Gu, Y., Reshetnikova, L., Li, Y., Wu, Y., Yan, H., Singh, S., & Ji, X. (2002). Crystal structure of shikimate kinase from *Mycobacterium tuberculosis* reveals the dynamic role of the LID domain in catalysis. *Journal of Molecular Biology*, 319, 779–789.
41. Chen, K., Dou, J., Tang, S., Yang, Y., Wang, H., Fang, H., & Zhou, C. (2012). Deletion of the *aroK* gene is essential for high shikimic acid accumulation through the shikimate pathway in *E. coli*. *Bioresource Technology*, 119, 141–147.
42. Rosado, L. A., Vasconcelos, I. B., Palma, M. S., Frappier, V., Najmanovich, R. J., Santos, D. S., & Basso, L. A. (2013). The mode of action of recombinant *Mycobacterium tuberculosis* shikimate kinase: Kinetics and thermodynamics analyses. *PLoS ONE*, 8, e61918.
43. Segel, I. H. (1975). *Enzyme kinetics: Behavior and analysis of rapid equilibrium and steady state enzyme systems*. New York: Wiley.
44. Krell, T., Maclean, J., Boam, D. J., Cooper, A., Resmini, M., Brocklehurst, K., Kelly, S. M., Price, N. C., Laphorn, A. J., & Coggins, J. R. (2001). Biochemical and X-ray crystallographic studies on shikimate kinase: The important structural role of the P-loop lysine. *Protein Science*, 10, 1137–1149.
45. Guruprasad, K., Reddy, B. B., & Pandit, M. W. (1990). Correlation between stability of a protein and its dipeptide composition: A novel approach for predicting *in vivo* stability of a protein from its primary sequence. *Protein Engineering, Design and Selection*, 4, 155–161.
46. Kyte, J., & Doolittle, R. F. (1982). A simple method for displaying the hydropathic character of a protein. *Journal of Molecular Biology*, 157, 105–132.
47. Arora, N., Narasu, M., & Banerjee, A. (2016). Shikimate kinase of *Yersinia pestis*: A sequence, structural and functional analysis. *International Journal of Biomedical Data Mining*, 5, 2.
48. Abele, U., & Schulz, G. (1995). High-resolution structures of adenylate kinase from yeast ligated with inhibitor Ap5A, showing the pathway of phosphoryl transfer. *Protein Science*, 4, 1262–1271.
49. Larkin, M. A., Blackshields, G., Brown, N., Chenna, R., McGettigan, P. A., McWilliam, H., Valentin, F., Wallace, I. M., Wilm, A., & Lopez, R. (2007). Clustal W and Clustal X version 2.0. *Bioinformatics*, 23, 2947–2948.
50. Robert, X., & Gouet, P. (2014). Deciphering key features in protein structures with the new ENDscript server. *Nucleic Acids Research*, 42, W320–W324.
51. Blanco, B., Prado, V. n., Lence, E., Otero, J. M., Garcia-Doval, C., Van Raaij, M. J., Llamas-Saiz, A. L., Lamb, H., Hawkins, A. R., & González-Bello, C. n (2013). *Mycobacterium tuberculosis* shikimate kinase inhibitors: Design and simulation studies of the catalytic turnover. *Journal of the American Chemical Society*, 135, 12366–12376.
52. Dhaliwal, B., Nichols, C. E., Ren, J., Lockyer, M., Charles, I., Hawkins, A. R., & Stammers, D. K. (2004). Crystallographic studies of shikimate binding and induced conformational changes in *Mycobacterium tuberculosis* shikimate kinase. *FEBS Letters*, 574, 49–54.
53. Gan, J., Gu, Y., Li, Y., Yan, H., & Ji, X. (2006). Crystal structure of *Mycobacterium tuberculosis* shikimate kinase in complex with shikimic acid and an ATP analogue. *Biochemistry*, 45, 8539–8545.
54. Stierand, K., Maaß, P. C., & Rarey, M. (2006). Molecular complexes at a glance: Automated generation of two-dimensional complex diagrams. *Bioinformatics*, 22, 1710–1716.

Publisher's Note Springer Nature remains neutral with regard to jurisdictional claims in published maps and institutional affiliations.



Structural characterization, biochemical, inhibition and computational studies of *Entamoeba histolytica* phosphoglycerate mutase: finding hits for a new antiamebic drug

Artemisa Luévano-De la Cruz¹ · Elkin Eduardo Sanabria-Chanaga² · Lilián Yépez-Mulia³ · Rafael Castillo² · Alicia Hernández-Campos² · Hugo Nájera⁴ · Claudia Avitia-Domínguez¹ · Erick Sierra-Campos⁵ · Mónica Valdez-Solana⁵ · Alfredo Téllez-Valencia¹ 

Received: 27 October 2017 / Accepted: 23 April 2018 / Published online: 7 May 2018
© Springer Science+Business Media, LLC, part of Springer Nature 2018

Abstract

Entamoeba histolytica is the causative agent of amoebiasis, which infects an estimated 50 million people globally each year. This parasite uses glycolysis as its only source of energy making enzymes of this route such as phosphoglycerate mutase (EhPGAM) excellent targets in the search for new drugs, a continuing necessity due to the adverse effects and unsuccessful cases of treatment that have resulted from the use of available antiparasitic agents. The aim of this work is to present the biochemical and structural characterization of EhPGAM and the results of a search for the first inhibitors of this enzyme. To this end, the activity of purified recombinant EhPGAM was assessed against an in-house chemical library of 200 benzimidazole derivatives. The results showed that seven compounds inhibited this enzyme about 40–70% at 100 μM and molecular dynamics simulations indicated that the two most potent inhibitors (Compound **1** and Compound **2**) form stable complexes and have the highest binding energy. Hence, these inhibitors can be considered good candidates in the search of new drugs to treat amoebiasis.

Keywords Amoebiasis · Phosphoglycerate mutase · Enzyme inhibition · Homology modeling · Molecular dynamics · Benzimidazole derivatives

Introduction

Amoebiasis is the result of infection by the protozoan parasite *E. histolytica* and affects about 50 million people worldwide and causing the death of 100,000 individuals per year (Theel and Pritt 2016). *Entamoeba* infection is universally distributed and is considered a cosmopolitan disease. It is more commonly encountered in tropical areas and warm weather climates, but also more likely to present itself in poorly sanitized areas, where overcrowding and poor management of water and feces prevails (Alam et al. 2014; Bruckner 1992; Ramos et al. 2005). *E. histolytica* has different pathogenic capabilities, being able to maintain a commensal behavior in the human intestine (Espinosa-Cantellano and Martínez-Palomo 2000; Ximenez et al. 2009), or provokes clinical manifestations that include diarrhea, dysentery, and cause abscesses in organs such as the liver, lung and brain (Baxt and Singh 2008).

Metronidazole has been used for over 40 years, and continues to be the leading drug in amoebiasis treatment (Lofmark et al. 2010). Other drugs like nitroimidazole

✉ Alfredo Téllez-Valencia
atellez@ujed.mx

¹ Facultad de Medicina y Nutrición, Universidad Juárez del Estado de Durango Av. Universidad y Fanny Anitúa S/N, Durango CP 34000, Mexico

² Facultad de Química, Departamento de Farmacia, Universidad Nacional Autónoma de México, Ciudad de México CP 04510, Mexico

³ IMSS, Unidad de Investigación Médica en Enfermedades Infecciosas y Parasitarias, Ciudad de México CP 06720, Mexico

⁴ Departamento de Ciencias Naturales, Universidad Autónoma Metropolitana, Unidad Cuajimalpa Av. Vasco de Quiroga 4871, Colonia Santa Fe Cuajimalpa, Delegación Cuajimalpa de Morelos, Ciudad de México CP 05300, Mexico

⁵ Facultad de Ciencias Químicas, Universidad Juárez del Estado de Durango, Av. Artículo 123S/N Fracc. Filadelfia, Gómez Palacio, Durango CP 35010, Mexico

derived compounds, diloxanide furoate, emetine, and diiodohydroxyquin have also been used as alternative treatments (Ali and Nozaki 2007; Saucedo-Mendiola et al. 2012). Nevertheless, these antiamebic drugs have various side effects including dizziness, anorexia, diarrhea, nausea, abdominal discomfort, vomiting, alcohol intolerance, vertigo, and although rarely, encephalopathy or convulsions (Ali and Nozaki 2007; Cudmore et al. 2004; Haque et al. 2003). Furthermore, it is also known that metronidazole is carcinogenic in rodents and mutagenic in bacteria (Bendisky et al. 2002; Roe 1983). Therefore, there is an urgency to identify new drugs for treating amoebiasis.

E. histolytica trophozoites have no typical mitochondria, instead they have mitosomes, organelles that have lost their capacity to synthesize ATP (Tovar et al. 1999). As a result, the glycolysis pathway becomes essential in the generation of ATP for cellular work (Ali and Nozaki 2007). Metabolic flow studies in this parasite also indicate that phosphoglycerate mutase (PGAM) exerts a significant control in glycolytic flow (Moreno-Sanchez et al. 2008; Saavedra et al. 2005; Saavedra et al. 2007); this enzyme catalyzes the interconversion between 3-phosphoglycerate (3-PG) and 2-phosphoglycerate (2-PG).

There are two classes of PGAMs: cofactor-dependent PGAMs (dPGAMs) and cofactor-independent PGAMs (iPGAMs) (Jedrzejewski 2000). PGAM from *E. histolytica* (EhPGAM) belongs to the group of iPGAMs, with a reported molecular weight of 64 kDa and a monomeric structure (Saavedra et al. 2005). It is also important to keep in mind that human PGAM (HsPGAM), on the other hand, is a member of the dPGAMs class, and it is a heterodimeric protein (Wang et al. 2005). Considering that both enzymes support kinetic and structural differences, this makes EhPGAM an attractive target for antiamebic drug design.

So far there are no reported inhibitors of EhPGAM, a fact that lead to our consideration of exploring the antiparasitic activity of benzimidazole derivatives (Flores-Carrillo et al. 2017; Lopez-Vallejo et al. 2011; Soria-Arteche et al. 2013). In this paper, we report the biochemical and structural characterization of EhPGAM together with inhibition studies carried out with our in-house library of benzimidazole derivatives. Moreover, we also report a structural analysis of the EhPGAM-inhibitor complex obtained through docking and molecular dynamics to identify the first structures that could be used as hits in a later hit-to-lead optimization process.

Materials and Methods

Synthesis of benzimidazole derivatives 1–7

Compounds **1** and **3–7** were prepared beginning with a properly substituted *o*-phenyldiamine and carrying out

our synthetic procedure, previously reported for similar benzimidazole derivatives (Velázquez-López et al. 2016; Flores-Carrillo et al. 2017; Soria-Arteche et al. 2013). Compound **2** (1*H*-benzimidazole-5-carboxylic acid) was purchased from Sigma Aldrich (Cat. 296783).

6-Chloro-2-(methylthio)-1*H*-benzimidazole-5-carboxylic acid (**1**)

White solid from ethanol; mp 216–217 °C; ¹H NMR (DMSO-*d*₆; 300 MHz): δ = 7.63 (1 H, s, H-4), 7.39 (1 H, s, H-7), 4.66 (2 H, bs, int. D₂O, NH, OH), 2.67 (3 H, s, S-CH₃); ¹³C NMR (DMSO-*d*₆; 75.3 MHz): δ = 169.41 (C, CO), 154.01 (C, C2), 141.09 (C, C6), 137.63 (C, C7a), 131.27 (C, C5), 123.78 (C, C3a), 114.76 (CH, C4), 114.12 (CH, C7), 13.76 (SCH₃); EIMS *m/z* 242 [M]⁺; HRESIMS *m/z* (pos): 241.9934 C₉H₇O₂N₂ClS (calcd. 241.9917) (Flores-Carrillo et al. 2017).

6-Chloro-2-(4-nitrophenyl)-1*H*-benzimidazole-7-carboxylic acid (**3**)

White solid from ethanol; mp 323–324 °C; ¹H NMR (DMSO-*d*₆; 300 MHz): δ = 13.49 (1 H, bs, -COOH), 8.45 (2 H, d, *J* = 8.6 Hz, H-3', H-5'), 8.38 (2 H, d, *J* = 8.8 Hz, H-2', H-6'), 7.71 (1 H, d, *J* = 8.5 Hz, H-5), 7.35 (1 H, d, *J* = 8.6 Hz, H-4); ¹³C NMR (DMSO-*d*₆; 75.3 MHz): δ = 169.79 (C, COOH), 154.46 (C, C2), 147.06 (C, C4'), 146.69 (C, C7a), 143.17 (C, C1'), 142.64 (C, C3a), 137.37 (C, C6), 131.44 (CH, C2', C6'), 128.41 (CH, C5), 123.89 (CH, C4), 123.09 (CH, C3', C5'), 119.82 (C, C7); Anal. Calcd. for C₁₄H₈ClN₃O₄: C, 52.93; H, 2.54; N, 13.23. Found: C, 53.02; H, 2.28; N, 13.58.

2-(4-Nitrophenyl)-1*H*-benzimidazole-7-carboxylic acid (**4**)

White solid from ethanol/DMF, mp 353–354 °C. ¹H NMR (DMSO-*d*₆; 300 MHz): δ = 12.74 (1 H, bs, NH, -COOH), 8.60 (2 H, d, *J* = 7.9 Hz, H-3', H-5'), 8.37 (2 H, d, *J* = 8.2 Hz, H-2', H-6'), 7.98 (1 H, d, *J* = 7.9 Hz, H-6), 7.87 (1 H, d, *J* = 7.4 Hz, H-4), 7.37 (1 H, t, *J* = 7.7 Hz, H-5); ¹³C NMR (DMSO-*d*₆; 75.3 MHz): δ = 165.87 (C, COOH), 164.26 (C, C2), 149.15 (C, C4'), 142.70 (C, C1'), 140.05 (C, C7a), 133.68 (C, C3a), 129.83 (CH, C4), 129.19 (CH, C2', C6'), 127.18 (CH, C6), 126.29 (CH, C5), 123.54 (CH, C3', C5'), 120.51 (C, C7); ESIMS *m/z* 284 [M + H]⁺.

1-Methyl-2-(methylthio)-1*H*-benzimidazole-5-carboxamide (**5**)

White crystals from methanol, mp 232–233 °C. ¹H NMR (DMSO-*d*₆; 300 MHz): δ = 8.09 (1 H, d, *J* = 1.2 Hz, H-4),

7.92 (1 H, bs, $-\text{NH}_2$), 7.75 (1 H, dd, $J_1 = 8.4$ Hz, $J_2 = 1.5$ Hz, H-6), 7.49 (1 H, d, $J = 8.7$ Hz, H-7), 7.25 (1 H, bs, $-\text{NH}_2$), 3.68 (3 H, s, $\text{N}-\text{CH}_3$), 2.72 (3 H, s, $\text{S}-\text{CH}_3$); EIMS m/z 221 $[\text{M}]^+$ (100), 205 (25), 188 (54).

1-Methyl-2-(methylthio)-*N*-(5-nitro-1,3-thiazol-2-yl)-1*H*-benzimidazole-6-carboxamide (6)

Yellow solid from acetonitrile, mp 306–307 °C. ^1H NMR (DMF- d_7 ; 300 MHz): $\delta = 13.54$ (bs, NH), 8.63 (1 H, s, H-4'), 8.47 (1 H, d, $J = 1.5$ Hz, H-7), 8.10 (1 H, dd, $J = 8.4$ Hz, $J = 1.5$ Hz, H-5), 7.71 (1 H, d, $J = 8.4$ Hz, H-4), 3.83 (3 H, s, NCH_3), 2.84 (3 H, s, SCH_3); ^{13}C NMR (DMSO- d_6 ; 75.3 MHz): $\delta = 167.14$ (C, CO), 163.77 (C, C2'), 162.55 (C, C2), 157.79 (C, C3a), 147.48 (CH, C4'), 142.83 (C, C5'), 137.48 (C, C7a), 124.26 (C, C6), 122.70 (CH, C4), 117.74 (CH, C5), 110.44 (CH, C7), 30.03 (NCH_3), 14.20 (SCH_3); EIMS m/z 349 $[\text{M}]^+$ (18), 205 (100), 177 (30). HRFABMS m/z (pos): 350.0390 $\text{C}_{13}\text{H}_{12}\text{N}_5\text{O}_3\text{S}_2$ (calcd. 350.0376) (Soria-Arteche et al. 2013).

6-Chloro-2-(methylthio)-*N*-(5-nitro-1,3-thiazol-2-yl)-1*H*-benzimidazole-5-carboxamide (7)

Yellow crystal from ethanol/DMF. mp 249–250 °C. ^1H NMR (DMSO- d_6 ; 300 MHz): $\delta = 13.60$ (1 H, bs, $\text{N}-\text{H}$), 13.06 (1 H, bs), 8.67 (1 H, s, H-4'), 7.80 (1 H, s, H-7), 7.65 (1 H, s, H-4), 2.71 (3 H, s, $\text{S}-\text{CH}_3$); ^{13}C NMR (DMSO- d_6 ; 75.3 MHz): $\delta = 167.03$ (C, CO), 162.32 (C, C2'), 158.53 (CH, C4'), 147.07 (C, C2), 143.09 (C, C7a), 142.56 (C, C5'), 137.84 (C, C3a), 133.03 (C, C5), 125.77 (C, C6), 123.94 (CH, C4), 117.96 (CH, C7), 14.20 (SCH_3); EIMS m/z 370 $[\text{M} + \text{H}]^+$; FABMS m/z 370 $[\text{M} + \text{H}]^+$.

Gene expression and protein purification

The amplification of the gene encoding EhPGAM (XM_649090.2) was performed through PCR using genomic DNA extracted from *E. histolytica* HM1 IMSS strain. The oligonucleotides used were 5'CCGCTAGCGAAG-GACTTAAACCAAATA3' (forward) and 5'GCGGATCC TTAATGAACTTAATAAGAGATGG3' (reverse) with *NheI* and *BamHI* restriction sites (underlined) included. The vector PCR BLUNT II® TOPO® (Invitrogen, Carlsbad, CA) was used to clone the PCR product. The plasmid was then introduced by transformation into the host strain *E. coli* DH5 α competent cells (Invitrogen, Carlsbad, CA), and then sequenced. Thereafter, the gene was subcloned into over-expression vector pET28a(+) and transformed in *E. coli* BLR (DE3) competent cells (Novagen, Madison, WI). This procedure allowed the generation of a 6 His-Tag protein in the N-terminus.

Cells harboring the plasmid with the EhPGAM gene were grown in Luria-Bertani medium (500 mL) supplemented with kanamycin (50 $\mu\text{g}/\text{mL}$) at 37 °C. Once the culture reached an O.D.₆₀₀ of 0.8, over-expression was induced with 1 mM of isopropyl thio- β -D-galactoside for 4 h at 37 °C, and then at 25 °C overnight. Cells were harvested by centrifugation and the pellet was washed twice with buffer A (Tris-HCl 50 mM, pH 8). Afterwards, cells were resuspended in a solution of buffer A containing protease inhibitor PMSF at 200 μM . The His-tagged protein was extracted by sonication, the cellular debris was eliminated by centrifugation at 13,000 r.p.m. during 30 minutes and purified by affinity chromatography using a Ni-NTA column. The supernatant was loaded into the column previously equilibrated with phosphate buffer (PBS, pH 8.0). Then, it was washed with PBS plus 50 mM imidazole (100 mL). EhPGAM was eluted with PBS containing 300 mM imidazole (15 mL). Protein concentration was determined using the BCA method (Wiechelman et al. 1988).

Enzyme activity

EhPGAM activity was determined in the forward (glycolytic) reaction, using a UV-1800 SHIMADZU spectrophotometer. The conversion of 3-PG to 2-PG was measured by coupling this reaction to lactate dehydrogenase via enolase and pyruvate kinase, following the decrease of NADH at 340 nm, and using a molar extinction coefficient of 6220 $\text{M}^{-1}\text{cm}^{-1}$. The reaction was carried out at 37 °C (0.7 mL final volume) and contained: assay buffer (0.1 M triethanolamine/HCl (pH 6.0), 1.0 mM MgSO_4 and 0.1% Triton X-100), 5.0 mM MgCl_2 , 1.0 mM ADP, 0.2 mM NADH, 2.0 mM 3-PG (Santa Cruz Biotechnology, Inc.), and the auxiliary enzymes, 1 U enolase (Sigma), 42 μg lactate dehydrogenase (Roche) and 21 μg pyruvate kinase (Roche). The reaction initiated with the addition of EhPGAM (1.74 μg). The decrease in the absorbance at 340 nm was used to determine the moles of substrate consumed. The K_m and V_{max} for 3-PG were determined measuring initial velocities and varying substrate concentration from 0.05 to 3.0 mM.

Molecular weight determination

Size exclusion chromatography in native conditions was carried out at room temperature using a Superdex 75 10/300 GL column in a FPLC system, the column was washed with distilled water (50 mL) followed by 50 mL of elution buffer (50 mM phosphate, pH 7, and 0.15 M KCl) at a rate of 0.5 mL/min. After that, 150 μL of purified EhPGAM (150 $\mu\text{g}/\text{mL}$) was loaded into the column and eluted with elution buffer (20 mL). Molecular weight (MW) was determined by extrapolation of the enzyme elution volume on a calibration curve generated using ribonuclease A, chymotrypsinogen

A, ovalbumin, albumin, aldolase, catalase, ferritin, and thyroglobulin, adjusting the data to the equation:

$$K_{av} = (V_e - V_o)/(V_t - V_o),$$

where K_{av} is the distribution coefficient, V_o is the column void volume, V_e is the protein elution volume and V_t is the total matrix volume, reported elsewhere (Saucedo-Mendiola et al. 2014).

Inhibition assays

The inhibition assays were performed using an in-house library of benzimidazole derivatives and the reaction conditions described above, adding the appropriate compound at a concentration of 100 μ M dissolved in DMSO (10% final concentration) to increase solubility. The percentage of inhibition was obtained using the following equation:

$$\% \text{ Inhibition} = \frac{A_0 - A_1}{A_0} \times 100$$

where: A_0 is the enzyme activity without inhibitor and A_1 is the enzyme activity in the presence of inhibitor.

Homology modeling

The amino acid sequence of EhPGAM (XP_654182) was obtained from NCBI (www.ncbi.nlm.nih.gov) and used to search for homologous proteins using the BLASTp tool (Jacob et al. 2008) to carry out a subsequent selection of the best template. The crystal structure of PGAM from *Leishmania mexicana* (PDB ID: 3IGZ, Nowicki et al. 2009) was selected as the template protein and used to construct the EhPGAM 3D model. At this point, three models were obtained using PRIME from Maestro (Jacobson et al. 2002; Jacobson et al. 2004), Swiss model (Arnold et al. 2006; Biasini et al. 2014), and ESyPred3D (Lambert et al. 2002). The stereochemical quality of the models was evaluated through the structure assessment tool on the Swiss model Server; the best model was selected based on the parameters of Q-mean, Z-score, and Ramachandran plot (Benkert et al. 2011; Laskowski et al. 1993). The final model was submitted for geometric optimization with molecular dynamics (MD) during 10 ns using GROMACS 4.6.7 (Van Der Spoel et al. 2005). The structure with the highest statistical probability in the last 5 ns was chosen for molecular dockings studies.

Molecular docking studies

Ligand preparation

Ligand structures were drawn using ACD/ChemSketch freeware. Subsequently, *Ligand Preparation Wizard* tool

from Maestro (www.schrodinger.com) was used to generate the three-dimensional structures. Each ligand was submitted for a geometry optimization using the semi-empirical method PM6 in Spartan' 10 (Hehre 2003). MGLtools 1.5.4 was used to assign Gasteiger atomic charges to all ligands (Morris et al. 2009). The isomerism of the benzimidazole nucleus was taken into account when it became necessary.

Docking studies

Docking calculations were performed with Autodock 4.2 software (Morris et al. 2009), selecting the catalytic site as the target. The grid map dimensions were selected as 50 points with grid point spacing of 0.375 Å. The conformational search of the ligand was carried out using a Lamarckian genetic algorithm and the best binding mode of each molecule was selected based on the cluster size and the lowest free binding energy.

Molecular dynamics simulation

The lowest binding free energy conformation of each complex was considered as the initial conformation for MD studies. Parameters and molecular topologies for the ligands were generated using the semi-empirical quantum chemistry program SQM of ACPYPE (Sousa da Silva and Vranken 2012; Wang et al. 2006; Wang et al. 2004). All MD simulations of EhPGAM were performed using GRO-MACS 4.6.7. The protein was simulated in aqueous 0.15 M NaCl solution, described using the all-atom Amber99-ILDN force field (Best and Hummer 2009; Hornak et al. 2006; Lindorff-Larsen et al. 2010), and the TIP3P model for water molecules (Jorgensen et al. 1983).

Energy minimization and equilibration of the system were carried out for 100 ps of MD using the NVT and NPT protocols. Thereafter, a 10 ns and a 5 ns MD simulations were performed on the protein-ligand complex and for each ligand, respectively. RMSD and hydrogen bonding also were analyzed during the complete MD simulation. For the binding free energy calculations, the last 3 ns for each MD simulation were used and the estimation of the binding free energy was made with the linear interaction energy (LIE) equation (Aguayo-Ortiz et al. 2013; Aqvist et al. 1994; Punkvang et al. 2010).

$$\Delta G = \alpha[(V_{LJ})_{\text{bound}} - (V_{LJ})_{\text{free}}] + \beta[(V_{\text{CL}})_{\text{bound}} - (V_{\text{CL}})_{\text{free}}] + \gamma$$

In this study the values $(V_{LJ})_{\text{bound}}$ and $(V_{\text{CL}})_{\text{bound}}$ were separated in the energy interaction of the ligands with the protein and with Manganese, this with the purpose of analyzing the contribution of each interaction independently.

Results and discussion

Biochemical characterization

The present study was performed with the aim of characterizing EhPGAM and finding its first inhibitors through a study with in-house benzimidazole derivatives. To this end, the EhPGAM gene was cloned and over-expressed, the enzyme purified and characterized (see experimental section). After cloning, the PCR product was sequenced and the result was used to screen a genomic library, revealing a 100% homology with the sequence XM_649090.2 that corresponded to the EhPGAM gene. The protein eluted as a single band, in SDS-PAGE analysis (Fig. 1a). Size exclusion chromatography in native conditions also showed a chromatogram with a single peak that corresponded to a MW of 57 kDa (Fig. 1b). According to these data, and in correspondence with its amino acid sequence, it can be stated that EhPGAM is a monomer. These results agree with previous reports to other iPGAMs, such as *L. mexicana* PGAM (monomer, 60 kDa) (Guerra et al. 2004) and *T. brucei* PGAM (monomer, 60.5 kDa) (Chevalier et al. 2000). There was a small discrepancy between the MW reported here for EhPGAM and the previous one (64 kDa) (Saavedra et al. 2005), but this is possibly due to differences in the processes of cloning and MW determination.

Additionally, amino acid sequence alignment with others iPGAMs showed that EhPGAM shares 46% identity and 63% similarity to *T. brucei* and *L. Mexicana* PGAMs; it is less related to *B. stearothermophilus* and *B. anthracis* PGAMs (36% identity and 53% similarity). Concerning the catalytic site, amino acids belonging to the domains of phosphatase and transferase (Jedrzejewski et al. 2000a, 2000b) are conserved in EhPGAM (Fig. 2).

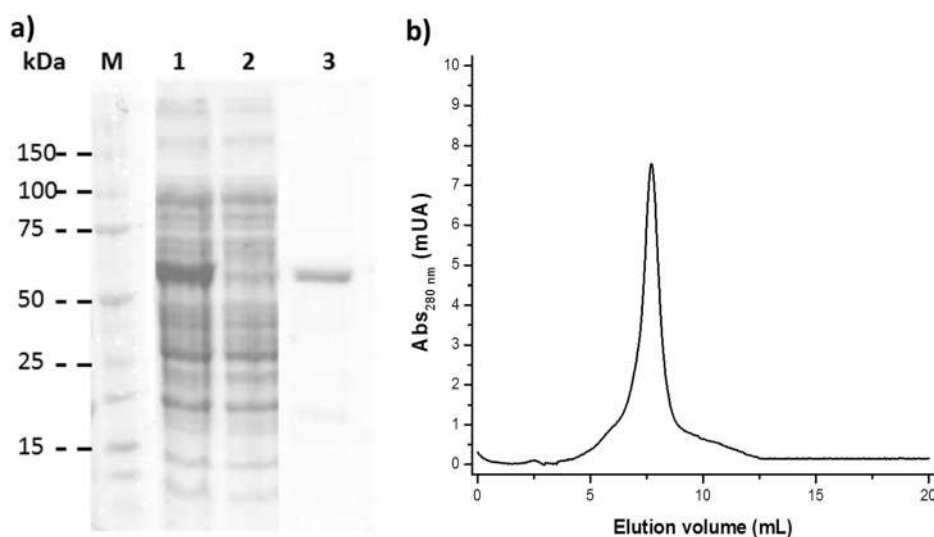
With respect to kinetic parameters, the values obtained for 3-PG were a K_m of 773 μM and a V_{max} of 8.93 $\mu\text{mol}/\text{min}/\text{mg}$. The K_m value was in the same order of that which was reported for other iPGAMs (*L. mexicana* PGAM, K_m of 150 μM (Guerra et al. 2004), and *T. brucei* PGAM, K_m of 270 μM (Chevalier et al. 2000)), including the value reported previously for EhPGAM (Saavedra et al. 2005), K_m of 830 μM . In regards to V_{max} , a velocity six times less than that previously reported by Saavedra et al. 2005 (V_{max} of 53 $\mu\text{mol}/\text{min}/\text{mg}$) was obtained. This difference in results could be attributed to differences in the expression, purification and measurement of the biochemical processes under study.

EhPGAM inhibition

With the enzyme characterized, an in-house library of benzimidazole derivatives was used to test enzyme activity. The data showed that from the 200 compounds assessed, seven of them inhibited EhPGAM activity between 40–70% at 100 μM (Table 1) and according to an analysis of their ADME-Tox properties, all of these compounds also satisfy Lipinski (Lipinski et al. 2001), Egan (Egan et al. 2000), and Veber (Veber et al. 2002) rules. Additionally, according to the in silico analysis, the two most potent compounds (Compound 1 and Compound 2), showed no presence of toxicophores in their structure, and had a drug likeness score in the permitted range (Table 1).

From a structural point of view, it could be said that the simplest effective combination showing EhPGAM inhibition activity consists of a benzimidazole nucleus with a carboxylate group at position 5 (Compound 2). When a methylthio and a chlorine were included at positions 2 and 6, respectively (Compound 1), the potency of

Fig. 1 **a** SDS-PAGE of different steps in purification of recombinant EhPGAM. Lane M, molecular weight marker; lane 1, crude extract; lane 2, washed; lane 3, a unique band corresponding to EhPGAM eluted with 300 mM imidazole. **b** Chromatogram obtained from size exclusion chromatography, the main peak corresponds to a MW of 57 kDa



inhibition increased slightly. However, if a methyl group replaces the hydrogen at position 1, the potency is affected considerably (Compound 1 vs. Compound 5). The same

phenomenon is observed if a larger group replaces the carboxylate group at position 5 (Compound 2 vs. Compound 7). Other noteworthy structural combinations

XP 654182.1-E.h..	1	-----ME--GLKPNTKLPQPRQGPVVVCIIDGFGIDKEGPGNCVTLA	39
3NVL-T.brucei	1	MGSSHHHHHSSGLVPRGSHMALPLAAHKT--LPRRKLVLVVLGGVIGPRDEYDAVHVA	58
3IGZ-L.mexicana	1	-----MSALLLKPDK--LPRRTVLIVVMDGLGIGPEDDYDAVHMA	39
1EJJ-B.stearoth..	1	-----MSKPKVALIILDGFALRDETYGNAVAQA	28
2IFY-B.anthacis	1	-----RKPTALIILDGFGIDREETYGNAVAQA	26
		: : : * * * : : : * * *	
XP 654182.1-E.h..	40	NPEYYNKLAEAKEQHLHTIKANGPYVGLTEADMGNSEVGHNALGAGQIYSOGTKLVE	99
3NVL-T.brucei	59	KTEPLMDALFNDPK---HFRSICAHGTAVGLETDADMGNSEVGHNALGAGRVLVGGASLVD	115
3IGZ-L.mexicana	40	STFFMDAHRDRNR---HFCRVRAHGTAVGLETDADMGNSEVGHNALGAGRVALVGGASLVD	96
1EJJ-B.stearoth..	29	NKENFDRYWNEYF---HTTLKACGEAVGLE-GOMGNSEVGHNLNIGAGRIVYQSLTRIN	83
2IFY-B.anthacis	27	KKPNFDGYWNKFP---HTTLTACGEAVGLE-GOMGNSEVGHNLNIGAGRIVYQSLTRVN	81
		. * : . : * * * * * : * * * * * : * * * * * : * . . : :	
XP 654182.1-E.h..	100	ESIESGKFFETENWKNVGAAVKEGKTVHFIIGLLSDGNVHSNTQLEFQMDGVKCGGKK	159
3NVL-T.brucei	116	DALESGEIFTSEGYRYLHGAFSQPGRTHLHIGLLSDGGVHSRDNQVYQILKHAGANGAKR	175
3IGZ-L.mexicana	97	DAIKSGEITYTSEGYRYLHGAFSKEGSTLHHLIGLLSDGGVHSRDNQIYSIEHAVKDGAKR	156
1EJJ-B.stearoth..	84	IAIREGEFDRNETFLAAMNHVKQHGTSLHFLGLLSDGGVHSIHHLIYALLRLAAKEGVKR	143
2IFY-B.anthacis	82	VAIREGEFDKNETFQSAIKSVKEKGTALHLFGLLSDGGVHS#MNHMFALLRLAAKEGVEK	141
		: : . * * : : * : : * : : * * * * * * * * * : : : : : * : :	
XP 654182.1-E.h..	160	IRVHPLLDGRDVPDPSGLMYIDKLEKLAQLQAAGIDAKIASGGGRMHMTMDRYEADWSM	219
3NVL-T.brucei	176	IRVHALYDGRDVPDKTSFKETDELEEVLAKLREGGCDARIASGGGRMFVTMDRYEADWSI	235
3IGZ-L.mexicana	157	IRVHALYDGRDVPDGSSFRFETDELEAVLAKVRQNGCDAIASGGGRMFVTMDRYDADWSI	216
1EJJ-B.stearoth..	144	VYIHGFLDGRDVGFPQTAPOYIKELQEKIKEYGVGE---IATLSGRY-YSMDR-DKRWR	197
2IFY-B.anthacis	142	VYIHAFLDGRDVGPKTAQSYIDATNEVIKETGVGQ---FATISGRY-YSMDR-DKRWR	195
		: : * : * * * * * : : . : . : : : : : : : * : * * * * * : * .	
XP 654182.1-E.h..	220	VERGWKAHVRGIVPEGDITPEYTYGYSAKEAVELARKLFPEKLDQFNPAFVIVDQEGKE	279
3NVL-T.brucei	236	VERGWRAQVLGEG-----RAFKSAREALTKFREEDANISDQYYPFVIVAGDDGEP	285
3IGZ-L.mexicana	217	VERGWRAQVLGDA-----RHFSAKEAITTFREEDPKVTDQYYPFVIVVDEQDKE	266
1EJJ-B.stearoth..	198	VEKAYRAMVYGEFP-----TYRDPLECIEDS--YKHGIYDEFVLPSPVIVREDGEP	245
2IFY-B.anthacis	196	VEKCYRAMVNGEFP-----TYKSAEECVEDS--YANGIYDEEVLPSPVIVNEDNTE	243
		** : : * * * * : : . : * : : * : : * * * : : : : : * : :	
XP 654182.1-E.h..	280	IGKMPVDGDAVINFNFRGDRATEISKAFYQGEFKAEDRVYT-PKLRV-AGLLEYDSDNHV	337
3NVL-T.brucei	286	IGTIEDGDAVLCFNFRGDRVIEMSRAF-EEEEFDKENRVRL-EKVRV-AGMMRYDGDGLG	342
3IGZ-L.mexicana	267	LGTIEDGDAVLCVNFNRGDRVIESTRAF-EDEDENKEDRVRV-EKVRV-AGMMRYDGDGLG	323
1EJJ-B.stearoth..	246	VATIQNDAAIFYNFRPDRATQISNTE-TNEDEFEREDRGPKHPKHLFFVCLTHESE--TV	302
2IFY-B.anthacis	244	VATINDDAVIFYNFRPDRATQIARVE-TNGDEFEREDRGEKVEHIPEFVCMTHESE--TV	300
		: : . : * * * * : : * * * * * * * * * : : * * * * * : * : : : : :	
XP 654182.1-E.h..	338	PPQYLCAFPDIKGVSSSEYLVKSGVKCFIAIETHKYGHVITYEWNKNSGYFDDKLEKYEQI	397
3NVL-T.brucei	343	PNNFLVPEPKLTRTSEEYLGSGCNIFALSETQKEGHVITYEWNKNSGKLSSEERETFCEI	402
3IGZ-L.mexicana	324	PNNFLVPEPKLTRVSEYLYCGSGLNIFACSETQKEGHVITYEWNKNSGKIDKHETTFKEV	383
1EJJ-B.stearoth..	303	AGYVAFKFTNLDNTIGEVLSQHGLRQLRIAETEKYPHVTFFEMSGGREEFPGEDRIL--I	360
2IFY-B.anthacis	301	DGYVAFKEMNLDNTLGEVVAQAGLQRLRIAETEKYPHVTFFFSGGREAEFPGEERIL--I	358
		* : : . : * : : * : : * : : * * * * * * * * * : : * : : : : : :	
XP 654182.1-E.h..	398	KSLPNDLTESHPEMKAKEVCDRLIEVLESKEYKYLRVNFANPDMVGHGTGNIQSGVKAVLT	457
3NVL-T.brucei	403	PSDRVQF-NQKPLMKSKEITDAAVDAIKSGKYDMIRINYPNGDMVGHGTGDLKATITSLEA	461
3IGZ-L.mexicana	384	PSDRVQF-NEKPRMQSAATEAAEALKSGMYNVVRINFPNGDMVGHGTGDLKATITGVEA	442
1EJJ-B.stearoth..	361	NSPKVPTYDLKPEMSAYEVTDALKEIEADKYDAIILNYANPDMVGHSGKLEPTIKAVEA	420
2IFY-B.anthacis	359	NSPKVATYDLKPEMSIYEVTDALVNEIENDKHVILNLYANPDMVGHSGMMEPTIKAVEA	418
		* : : * : : * : : : : : : : : : : : : * * * * * * * * * : : : : : : :	
XP 654182.1-E.h..	458	CDECLKRLDEEVRKQKQKILVLTADHGNVETMLDK--LQK-----PMTSHTCNFPVN	505
3NVL-T.brucei	462	VDQSLQRLKEAVDSVNGVFLITADHGNSSDDMVQRDKKGPVVRDAEGNLMPLTSHTLAPVP	521
3IGZ-L.mexicana	443	VDESLAKLKDAVDSVNGVYIVTADHGNSSDDMAQRDKKGPMPKDGNGVNLPLTSHTLSPVP	502
1EJJ-B.stearoth..	421	VDECLGKVVDAI LAKGGIAI I TADHGNADEVLTTPD--GK-----PQTAHTTNPVP	468
2IFY-B.anthacis	419	TDECLGKVVDAI LAKDGVVALI TADHGNADELTSE--GE-----PMTAHTTNPVP	466
		* : * : : : : * : : * * * * * * : * : : * * * * * * * * * : * * * * * *	
XP 654182.1-E.h..	506	LFIRDYDYKGEYVIDESVEHPGLANVTATYINLLGFQPSFYKPSLIKFI-----	555
3NVL-T.brucei	522	VFIGGAGLDPRVQMRDTPRAGLANVTATFINLMGFAPSDYEPSLIEVA-----	571
3IGZ-L.mexicana	503	VFIGGAGLDPRVAMRDTLPAAGLANVTATFINLLGFAPEDYEPSLIYVEKLEHHHHHH	561
1EJJ-B.stearoth..	469	VIVTKKGIKLRD-----GGILGDLAPMLDGLLGPQKEMTGKSLIVK-----	511
2IFY-B.anthacis	467	FIVTKNDVELRE-----DGILGDLAPMLTLLGFQPSFYKPSLIKFI-----	508
		: : : . : . : * : : * : * * * * * * * * * : : : : : : :	

◀ **Fig. 2** Multiple sequence alignment of iPGAMs. The EhPGAM sequence (XP_654182.1) was aligned with homologous proteins from different species with a crystallographic structure reported in the PDB; identical (conserved) amino acids in different sequences are marked with a dark gray shadow; amino acids involved in the phosphatase domain are indicated with a diamond (◆); the serine residue directly implicated in enzyme catalysis is shown with a triangle (▲) and amino acids that participate in the transferase domain are marked with a circle (●). The alignment was performed in UNIPROT (<http://www.uniprot.org/>)

included a 4-nitrophenyl group at position 2 and a carboxylate at position 7 (Compound **3** and Compound **4**).

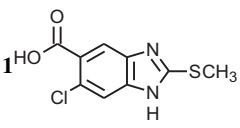
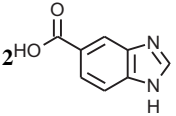
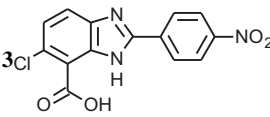
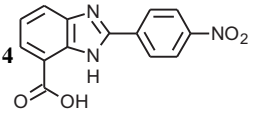
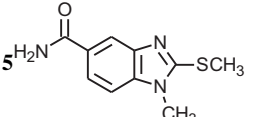
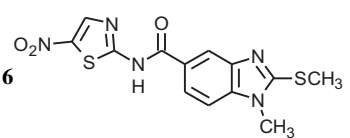
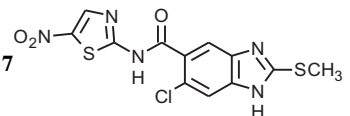
With the purpose of gaining more information about the EhPGAM-inhibitor complex, a detailed structural analysis of this interaction through the molecular docking and dynamics simulations was carried out.

Homology modeling and molecular dynamics

Because of the nonexistence of a crystallographic structure for EhPGAM, it was necessary to generate a 3D model of the enzyme. After evaluation of the four different models constructed, the one obtained with PRIME was selected as the best (Table 2). According to the Ramachandran plot, 86.2% of the residues were in the most favorable zones, 11% in allowed regions, 1.7% in generously allowed regions and 1.1% in disallowed regions. Furthermore, the model obtained a Z-score value of -0.59 (values closer to 0 are preferred), and a Qmean score of 0.71 (values closer to 1 are preferred) and RMSD of 0.129 between the model obtained and the protein used as template.

A structural analysis of the EhPGAM model showed the general characteristics of iPGAMs (Jedrzejewski 2000), such as

Table 1 ADME-Tox properties of active benzimidazoles and EhPGAM inhibition

Compound	MW < 500 ^a	logP < 5 ^a	HB Donors < 5 ^a	HB Acceptors < 10 ^a	Rotatable bonds < 10 ^a	tPSA ≤ 140 Å ² ^a	Toxicophores ^a	Drug likeness score ^b	% Inh. 100 μM
	242.68	2.49	2	4	2	94.11	Acc.	-0.56	73
	162.15	1.01	2	4	1	68.81	Acc.	-0.98	69
	317.68	3.13	2	7	3	113.51	Int.	-0.30	59
	283.24	2.5	2	7	3	113.51	Int.	-0.27	56
	221.28	1.81	1	4	2	83.25	Acc.	-0.64	54
	349.39	2.65	1	8	4	160.88	Int.	0.45	47
	369.81	3.32	2	8	4	171.74	Int.	0.45	47

^aADME-Tox properties obtained from the Fafdrugs4 server (<http://fafdrugs4.mti.univ-paris-diderot.fr/>)

^bDrug likeness score was obtained from Molsoft Ilc (<http://www.molsoft.com/>)

tPSA Topological Polar Surface Area, values less than 140 Å² represent a good probability of cell membranes permeation

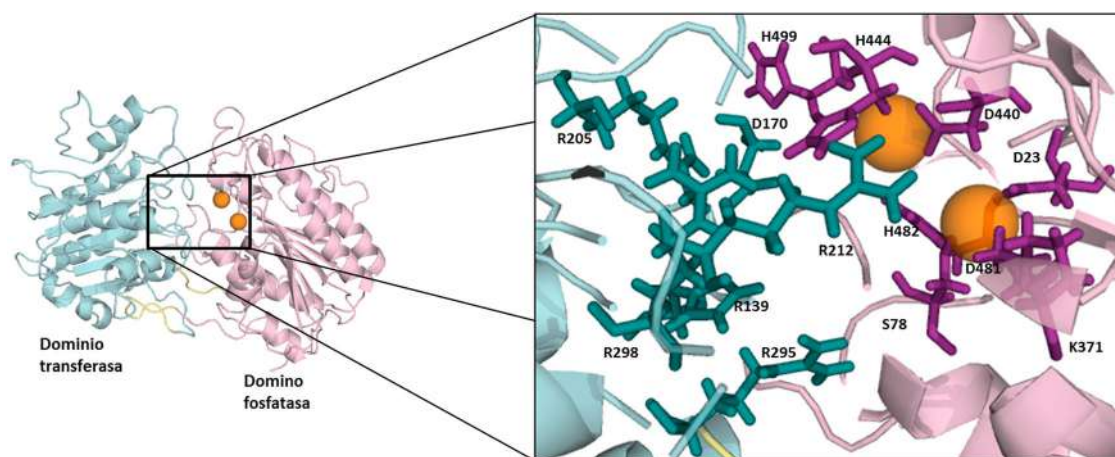


Fig. 3 EhPGAM 3D model. Transferase and phosphatase domains are depicted in cyan and violet, respectively. Amino acids involved in the catalytic center are highlighted and yellow spheres represent manganese ions

Table 2 EhPGAM models constructed through homology modeling

Program	RMSD	Q-mean	Z-score	Ramachandran plot (%)			
				F	P	G	NP
Swiss model	0.171	0.68	−0.90	84.1	12.5	2.3	1.1
ESyPrep3D	0.330	0.70	−0.53	90.8	7.9	0.6	0.6
PRIME	0.129	0.71	−0.59	86.2	11	1.7	1.1

Note: Ramachandran plot regions: (F) residues in most favored regions, (P) Residues in additional allowed regions, (G) residues in generously allowed regions, (NP) Residues in disallowed regions

Table 3 Binding energies and cluster sizes of EhPGAM inhibitors

Compound ^a	ΔG_{bind} (kcal/mol)	Cluster size	Compound ^a	ΔG_{bind} (kcal/mol)	Cluster size
1_A	−6.62	13	4_B	−6.22	16
1_B	−6.65	18	5	−6.01	14
2_A	−7.13	16	6	−4.88	8
2_B	−7.46	16	7_A	−5.49	19
3_A	−7.04	19	7_B	−4.71	12
3_B	−6.79	19			
4_A	−6.86	19			

^aThe letters A or B at the end of the compound, indicate the isomerism of the benzimidazole nucleus

the presence of the phosphatase and transferase domains, formed by an arrangement of beta sheets flanked by a series of alpha helices, and two handles that serve as inter-domain connectors (Fig. 3).

Once the model was generated, inhibitors were docked into the EhPGAM as described in the experimental section. The binding energies obtained showed that Compound 1 and Compound 2 had the highest values (Table 3), in agreement with the kinetic data since they were the best inhibitors (Table 1).

Structural analysis of the EhPGAM-Compound 1 complex showed the formation of hydrogen bonds between the compound and the side chains of His 482 and Asp 170, as

well as with manganese ions (Fig. 4a). The EhPGAM-Compound 2 complex showed a hydrogen bond between the N–H from the benzimidazole nucleus with Gly 443 and a possible interaction with the carboxylate group of the compound and the manganese ions (Fig. 4b). Compounds 3 and 4 formed a hydrogen bond with Arg 298, while Compound 5 formed this type of bond with Tyr 482 (Fig. 4c–e, respectively). Finally, Compound 6 interacted through a hydrogen bond with Asp 170, Lys 371 and Compound 7 with Arg 169, Asp 170, and Arg 298 (Fig. 4f–g, respectively).

To analyze the behavior of each inhibitor binding to the active site of EhPGAM, the complexes of the seven inhibitors were subjected to molecular dynamics studies.

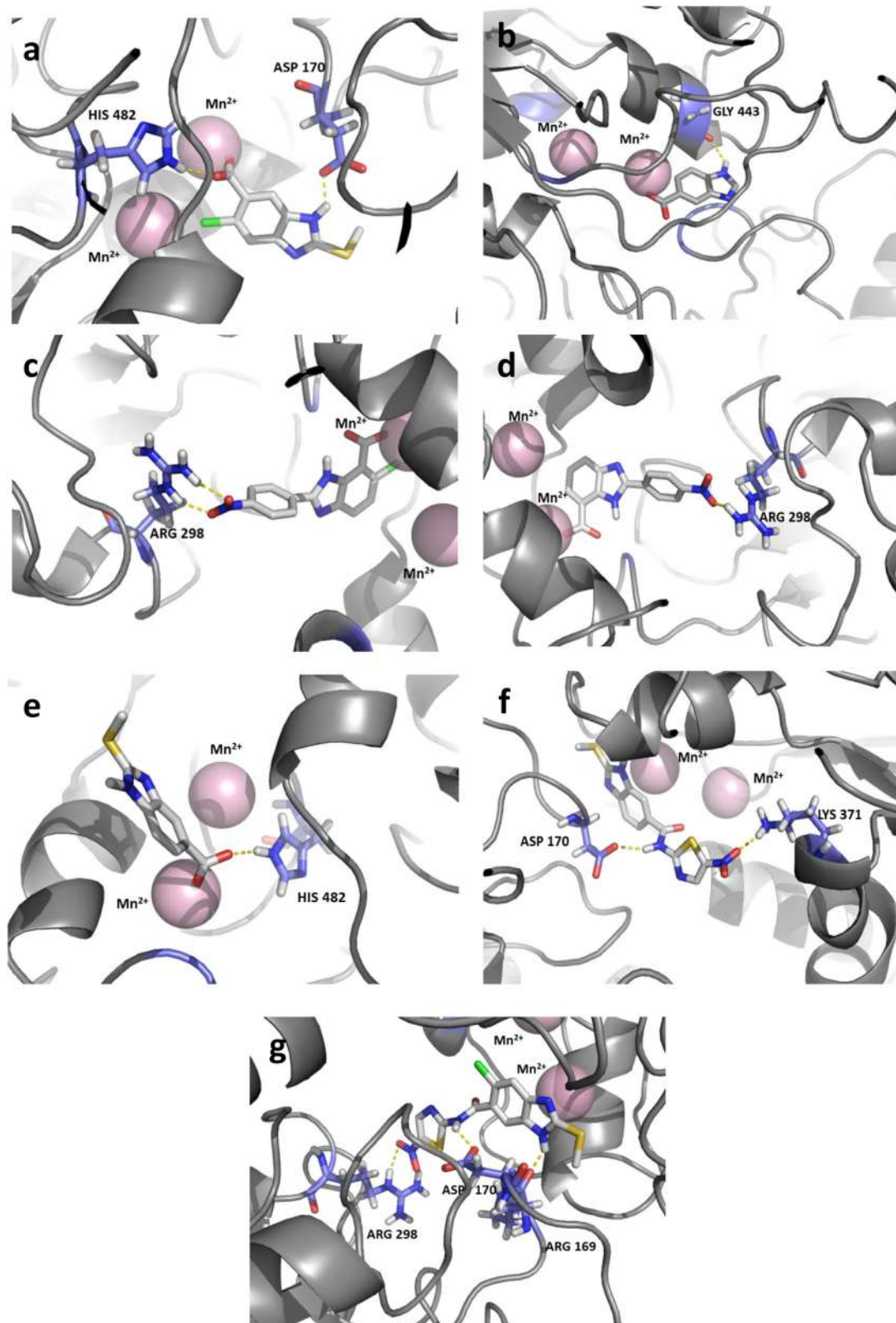


Fig. 4 Predicted binding modes of EhPGAM inhibitors. **a** Compound 1, **b** Compound 2, **c** Compound 3, **d** Compound 4, **e** Compound 5, **f** Compound 6, and **g** Compound 7. Hydrogen bonds are depicted as yellow dashed lines

According to the RMSD value, compounds **1** and **2** formed the most stable complexes with the enzyme, that is, the original position of these compounds into the enzyme almost do not suffered variations, to the contrary, in less active compounds, their binding mode was changing during molecular dynamics simulation time. The average value of the RMSD of these compounds was 0.3 nm, while for some of the less active compounds, their position moved above 0.4 nm (Fig. 5).

The analysis of the binding energies by the LIE method showed that Compound **1** and Compound **2** presented the most negative values, suggesting a more favorable binding. On the other hand, compounds with less than 50% of inhibition (Compound **6** and Compound **7**) presented positive energies. The key-finding being that the two better inhibitors meet three features: negative values in the total energy, at least one hydrogen bond during the molecular dynamics and strong values for the coulomb energy with Manganese atom. These features can lead to further computational analysis in order to find new EhPGAM inhibitors (Table 4).

The dynamics of the complex EhPGAM–Compound **1** confirmed the formation of a hydrogen bond with Asp 170, an amino acid located in the active site of the phosphatase

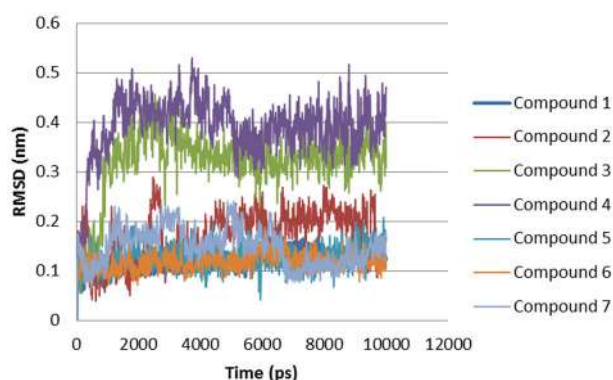


Fig. 5 Ligand positional RMSD in EhPGAM-inhibitor complex

domain (Jedrzejewski et al. 2000a, 2000b), but not bond with His 482, prediction made by docking. In the case of Compound **2**, unlike the interactions observed in docking simulations, no interactions were detected between this compound and the target during the entire course of molecular dynamics simulation; however, an interaction with Manganese ions could be expected, supporting the idea that an interaction with Manganese atom is important for biological activity.

The search for new antiamebic agents is a field that involves enzymatic and parasite assays. Regarding the study of enzymes as targets, several reports that treat different sections of *E. histolytica* metabolism exist (Azam et al. 2015; Debnath et al. 2014; Nagpal et al. 2012; Saucedo-Mendiola et al. 2014; Stephen et al. 2008). The inhibitors reported along with those described here show an inhibition in the μM range, although in some cases, only a computational approach was used to propose potential inhibitors. In the case of studies in parasites, there are several molecules, including benzimidazole derivatives, reported with amoebicidal activity (Debnath et al. 2014; Flores-Carrillo et al. 2017; Mori et al. 2015; Lopez-Vallejo et al. 2011; Soria-Arteche et al. 2013). However, for all except for one (Mori et al. 2015), the target of these compounds is unknown, and their potency lies within the μM range. With respect to other pathogens, literature is quite limited; there are only three works that study iPGAMs in nematodes, one of them reporting two inhibitors with an $\text{IC}_{50} > 10 \mu\text{M}$ for *Brugia malayi* iPGAM (Crowther et al. 2014). In another work, a computational study was performed to propose a set of potential inhibitors of *Wuchereria bancrofti* iPGAM (Sharma et al. 2013). Recently, another study with various iPGAMs from nematodes reported macrocyclic peptides as potent and selective inhibitors of these enzymes (Yu et al. 2017). Therefore, iPGAM inhibition remains an incipient research area where the compounds and structural data reported here looks to contribute to design new and more potent inhibitors.

Table 4 Binding free energies and hydrogen bonds of the protein-ligand complexes

Ligand	Energy (kJ/mol)						ΔG kcal/mol	Hydrogen bonds		
	$(V_{LJ})_{\text{bound Protein-Lig}}$	$(V_{LJ})_{\text{bound Mn-Lig}}$	$(V_{LJ})_{\text{free}}$	$(V_{CL})_{\text{bound Protein-Lig}}$	$(V_{CL})_{\text{bound Mn-Lig}}$	$(V_{CL})_{\text{free}}$		ΔG binding	Range	Average
1	-97.82	57.44	-49.54	102.95	-734.11	-336.34	-145.75	-34.83	0–3	3
2	-102.25	45.44	-20.29	41.02	-576.53	-379.98	-84.34	-20.15	0–2	1
3	-142.20	46.71	-80.83	89.712	-574.25	-342.51	-73.65	-17.60	0–2	0
4	-105.76	48.39	-69.79	89.18	-582.07	-355.66	-66.37	-15.86	0–3	0
5	-102.37	50.31	-45.13	99.84	-588.05	-351.98	-69.36	-16.57	0	0
6	-197.49	-1.65	-175.25	-31.64	0.04	-125.82	42.81	10.23	0–1	0
7	-186.83	-1.14	-123.11	-90.17	-5.98	-175.14	27.81	6.64	0–4	2

Note: The binding free energies were calculated using the LIE method

Conclusion

To the best of our knowledge, this represents the first report of EhPGAM inhibitors. According to the capacity for enzyme inhibition and with the physicochemical properties of the compounds studied in this work, make these molecules good candidates in the search of new drugs against amoebiasis.

Acknowledgements The authors acknowledge DGESCA for the use of supercomputer Miztli. ATV and CAD acknowledge CONACyT for grants No. 257848 and No. 258694, respectively. CONACyT is also acknowledged by ALC (fellowship No. 231153) and EESC (fellowship No. 283595).

Compliance with ethical standards

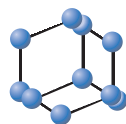
Conflict of interest The authors declare that they have no conflict of interest.

References

- Aguayo-Ortiz R, Mendez-Lucio O, Medina-Franco JL, Castillo R, Yopez-Mulia L, Hernandez-Luis F, Hernandez-Campos A (2013) Towards the identification of the binding site of benzimidazoles to beta-tubulin of *Trichinella spiralis*: insights from computational and experimental data. *J Mol Graph Model* 41:12–19
- Alam F, Salam MA, Hassan P, Mahmood I, Kabir M, Haque R (2014) Amebic liver abscess in northern region of Bangladesh: socio-demographic determinants and clinical outcomes. *BMC Res Notes* 7:625
- Ali V, Nozaki T (2007) Current therapeutics, their problems, and sulfur-containing-amino-acid metabolism as a novel target against infections by “amitochondriate” protozoan parasites. *Clin Microbiol Rev* 20(1):164–187
- Aqvist J, Medina C, Samuelsson JE (1994) A new method for predicting binding affinity in computer-aided drug design. *Protein Eng* 7(3):385–391
- Arnold K, Bordoli L, Kopp J, Schwede T (2006) The SWISS-MODEL workspace: a web-based environment for protein structure homology modelling. *Bioinformatics* 22(2):195–201
- Azam A, Peerzada MN, Ahmad K (2015) Parasitic diarrheal disease: drug development and targets. *Front Microbiol* 6:1183
- Baxt LA, Singh U (2008) New insights into *Entamoeba histolytica* pathogenesis. *Curr Opin Infect Dis* 21(5):489–494
- Bendsky A, Menendez D, Ostrosky-Wegman P (2002) Is metronidazole carcinogenic? *Mutat Res* 511(2):133–144
- Benkert P, Biasini M, Schwede T (2011) Toward the estimation of the absolute quality of individual protein structure models. *Bioinformatics* 27(3):343–350
- Best RB, Hummer G (2009) Optimized molecular dynamics force fields applied to the helix-coil transition of polypeptides. *J Phys Chem B* 113(26):9004–9015
- Biasini M, Bienert S, Waterhouse A, Arnold K, Studer G, Schmidt T, Kiefer F, Gallo Cassarina T, Bertoni M, Bordoli M, Schwede T (2014) SWISS-MODEL: modelling protein tertiary and quaternary structure using evolutionary information. *Nucleic Acids Res* 42:252–258
- Bruckner DA (1992) Amebiasis. *Clin Microbiol Rev* 5(4):356–369
- Crowther GJ, Booker ML, He M, Li T, Raverdy S, Novelli JF, He P, Dale NR, Fife AM, Barker Jr RH, Kramer ML, Van Voorhis WC, Carlow CK, Wang MW (2014) Cofactor-independent phosphoglycerate mutase from nematodes has limited druggability, as revealed by two high-throughput screens. *PLoS Negl Trop Dis* 8(1):e2628
- Cudmore SL, Delgaty KL, Hayward-McClelland SF, Petrin DP, Garber GE (2004) Treatment of infections caused by metronidazole-resistant *Trichomonas vaginalis*. *Clin Microbiol Rev* 17(4):783–793
- Chevalier N, Rigden DJ, Van Roy J, Opperdoes FR, Michels PA (2000) *Trypanosoma brucei* contains a 2,3-bisphosphoglycerate independent phosphoglycerate mutase. *Eur J Biochem* 267(5):1464–1472
- Debnath A, Shahinas D, Bryant C, Hirata K, Miyamoto Y, Hwang G, Gut J, Renslo AR, Pillai DR, Eckmann L, Reed SL, McKerrow JH (2014) Hsp90 inhibitors as new leads to target parasitic diarrheal diseases. *Antimicrob Agents Chemother* 58(7):4138–4144
- Egan WJ, KMJr Merz, Baldwin JJ (2000) Prediction of drug absorption using multivariate statistics. *J Med Chem* 43(21):3867–3877
- Espinosa-Cantellano M, Martinez-Palomo A (2000) Pathogenesis of intestinal amebiasis: from molecules to disease. *Clin Microbiol Rev* 13(2):318–331
- Flores-Carrillo P, Velazquez-Lopez JM, Aguayo-Ortiz R, Hernandez-Campos A, Trejo-Soto PJ, Yopez-Mulia L, Castillo R (2017) Synthesis, antiprotozoal activity, and chemoinformatic analysis of 2-(methylthio)-1H-benzimidazole-5-carboxamide derivatives: Identification of new selective giardicidal and trichomonocidal compounds. *Eur J Med Chem* 137:211–220
- Guerra DG, Vertommen D, Fothergill-Gilmore LA, Opperdoes FR, Michels PA (2004) Characterization of the cofactor-independent phosphoglycerate mutase from *Leishmania mexicana mexicana*. Histidines that coordinate the two metal ions in the active site show different susceptibilities to irreversible chemical modification. *Eur J Biochem* 271(9):1798–1810
- Haque R, Huston CD, Hughes M, Houpt E, Petri Jr WA (2003) Amebiasis. *N Engl J Med* 348(16):1565–1573
- Hehre WJ (2003) A guide to molecular mechanics and quantum chemical calculations. Wavefunction, Inc, Irvine, CA
- Hornak V, Abel R, Okur A, Strockbine B, Roitberg A, Simmerling C (2006) Comparison of multiple Amber force fields and development of improved protein backbone parameters. *Proteins* 65(3):712–725
- Jacob A, Lancaster J, Buhler J, Harris B, Chamberlain RD (2008) Mercury BLASTP: Accelerating Protein Sequence Alignment. *ACM Trans Reconfigurable Technol Syst* 1(2):9
- Jacobson MP, Friesner RA, Xiang Z, Honig B (2002) On the role of the crystal environment in determining protein side-chain conformations. *J Mol Biol* 320(3):597–608
- Jacobson MP, Pincus DL, Rapp CS, Day TJ, Honig B, Shaw DE, Friesner RA (2004) A hierarchical approach to all-atom protein loop prediction. *Proteins* 55(2):351–367
- Jedrzejewski MJ (2000) Structure, function, and evolution of phosphoglycerate mutases: comparison with fructose-2,6-bisphosphatase, acid phosphatase, and alkaline phosphatase. *Prog Biophys Mol Biol* 73(2-4):263–287
- Jedrzejewski MJ, Chander M, Setlow P, Krishnasamy G (2000a) Mechanism of catalysis of the cofactor-independent phosphoglycerate mutase from *Bacillus stearothermophilus*. Crystal structure of the complex with 2-phosphoglycerate. *J Biol Chem* 275(30):23146–23153
- Jedrzejewski MJ, Chander M, Setlow P, Krishnasamy G (2000b) Structure and mechanism of action of a novel phosphoglycerate mutase from *Bacillus stearothermophilus*. *EMBO J* 19(7):1419–1431
- Jorgensen WL, Chandrasekhar J, Madura JD, Impey RW, Klein ML (1983) Comparison of simple potential functions for simulating liquid water. *J Chem Phys* 79(2):926–935

- Lambert C, Leonard N, De Bolle X, Depiereux E (2002) ESyPred3D: Prediction of proteins 3D structures. *Bioinformatics* 18 (9):1250–1256
- Laskowski RA, MacArthur MW, Moss DS, Thornton JM (1993) PROCHECK: a program to check the stereochemical quality of protein structures. *J Appl Crystallogr* 26(2):283–291
- Lindorff-Larsen K, Piana S, Palmo K, Maragakis P, Klepeis JL, Dror RO, Shaw DE (2010) Improved side-chain torsion potentials for the Amber ff99SB protein force field. *Proteins* 78(8):1950–1958
- Lipinski CA, Lombardo F, Dominy BW, Feeney PJ (2001) Experimental and computational approaches to estimate solubility and permeability in drug discovery and development settings. *Adv Drug Deliv Rev* 46(1-3):3–26
- Lofmark S, Edlund C, Nord CE (2010) Metronidazole is still the drug of choice for treatment of anaerobic infections. *Clin Infect Dis* 50 (1):16–23
- Lopez-Vallejo F, Castillo R, Yopez-Mulia L, Medina-Franco JL (2011) Benzotriazoles and indazoles are scaffolds with biological activity against *Entamoeba histolytica*. *J Biomol Screen* 16 (8):862–868
- Moreno-Sanchez R, Encalada R, Marin-Hernandez A, Saavedra E (2008) Experimental validation of metabolic pathway modeling. *FEBS J* 275(13):3454–3469
- Mori M, Jeelani G, Masuda Y, Sakai K, Tsukui K, Waluyo D, Tarwadi, Watanabe Y, Nonaka K, Matsumoto A, Omura S, Nozaki T, Shiomi K (2015) Identification of natural inhibitors of *Entamoeba histolytica* cysteine synthase from microbial secondary metabolites. *Front Microbiol* 6:962
- Morris GM, Huey R, Lindstrom W, Sanner MF, Belew RK, Goodsell DS, Olson AJ (2009) AutoDock4 and AutoDockTools4: Automated docking with selective receptor flexibility. *J Comput Chem* 30(16):2785–2791
- Nagpal I, Raj I, Subbarao N, Gourinath S (2012) Virtual screening, identification and in vitro testing of novel inhibitors of O-acetyl-L-serine sulfhydrylase of *Entamoeba histolytica*. *PLoS One* 7(2): e30305
- Nowicki MW, Kuaprasert B, McNae IW, Morgan HP, Harding MM, Michels PAM, Fothergill-Gilmore LA, Walkinshaw MD (2009) Crystal Structures of *Leishmania mexicana* Phosphoglycerate Mutase Suggest a One-Metal Mechanism and a New Enzyme Subclass. *J Mol Biol* 394(3):535–543
- Punkvang A, Saparpakorn P, Hannongbua S, Wolschann P, Beyer A, Pungpo P (2010) Investigating the structural basis of arylamides to improve potency against *M. tuberculosis* strain through molecular dynamics simulations. *Eur J Med Chem* 45 (12):5585–5593
- Ramos F, Moran P, Gonzalez E, Garcia G, Ramiro M, Gomez A, Leon DE, Melendro EI, Valadez A, Ximenez C (2005) High prevalence rate of *Entamoeba histolytica* asymptomatic infection in a rural Mexican community. *Am J Trop Med Hyg* 73(1):87–91
- Roe FJ (1983) Toxicologic evaluation of metronidazole with particular reference to carcinogenic, mutagenic, and teratogenic potential. *Surgery* 93:158–164
- Saavedra E, Encalada R, Pineda E, Jasso-Chavez R, Moreno-Sanchez R (2005) Glycolysis in *Entamoeba histolytica*. Biochemical characterization of recombinant glycolytic enzymes and flux control analysis. *FEBS J* 272(7):1767–1783
- Saavedra E, Marin-Hernandez A, Encalada R, Olivos A, Mendoza-Hernandez G, Moreno-Sanchez R (2007) Kinetic modeling can describe in vivo glycolysis in *Entamoeba histolytica*. *FEBS J* 274 (18):4922–4940
- Saucedo-Mendiola ML, Salas-Pacheco JM, Aguirre-López B, Téllez-Valencia A (2012) Advances in the search of new drugs against amebiasis. In: Tellez-Valencia A (Ed.) Current topics of drug design in parasitic and bacterial diseases. Transworld Research Networks, Kerala, India, pp 67–81
- Saucedo-Mendiola ML, Salas-Pacheco JM, Najera H, Rojo-Dominguez A, Yopez-Mulia L, Avitia-Dominguez C, Tellez-Valencia A (2014) Discovery of *Entamoeba histolytica* hexokinase 1 inhibitors through homology modeling and virtual screening. *J Enzym Inhib Med Chem* 29(3):325–332
- Sharma OP, Vadlamudi Y, Liao Q, Strodel B, Suresh Kumar M (2013) Molecular modeling, dynamics, and an insight into the structural inhibition of cofactor independent phosphoglycerate mutase isoform 1 from *Wuchereria bancrofti* using cheminformatics and mutational studies. *J Biomol Struct Dyn* 31(7):765–778
- Soria-Arteche O, Hernández-Campos A, Yépez-Mulia L, Trejo-Soto PJ, Hernández-Luis F, Gres-Molina J, Maldonado LA, Castillo R (2013) Synthesis and antiprotozoal activity of nitazoxanide-N-methylbenzimidazole hybrids. *Bioorg Med Chem Lett* 23 (24):6838–6841
- Sousa da Silva AW, Vranken WF (2012) ACPYPE-AnteChamber PYthon Parser interfacE. *BMC Res Notes* 5:367
- Stephen P, Vijayan R, Bhat A, Subbarao N, Bamezai RN (2008) Molecular modeling on pyruvate phosphate dikinase of *Entamoeba histolytica* and in silico virtual screening for novel inhibitors. *J Comput Aided Mol Des* 22(9):647–660
- Theel ES, Pritt BS (2016) Parasites. *Microbiol Spectr* 4(4) <https://doi.org/10.1128/microbiolspec.DMIH2-0013-2015>
- Tovar J, Fischer A, Clark CG (1999) The mitosome, a novel organelle related to mitochondria in the amitochondrial parasite *Entamoeba histolytica*. *Mol Microbiol* 32(5):1013–1021
- Van Der Spoel D, Lindahl E, Hess B, Groenhof G, Mark AE, Berendsen HJ (2005) GROMACS: fast, flexible, and free. *J Comput Chem* 26(16):1701–1718
- Veber DF, Johnson SR, Cheng HY, Smith BR, Ward KW, Kopple KD (2002) Molecular properties that influence the oral bioavailability of drug candidates. *J Med Chem* 45(12):2615–2623
- Velázquez-López JM, Hernández-Campos A, Yépez-Mulia L, Téllez-Valencia A, Flores-Carrillo P, Nieto-Meneses R, Castillo R (2016) Synthesis and trypanocidal activity of novel benzimidazole derivatives. *Bioorg Med Chem Lett* 26(17):4377–4381
- Wang J, Wang W, Kollman PA, Case DA (2006) Automatic atom type and bond type perception in molecular mechanical calculations. *J Mol Graph Model* 25(2):247–260
- Wang J, Wolf RM, Caldwell JW, Kollman PA, Case DA (2004) Development and testing of a general amber force field. *J Comput Chem* 25(9):157–1174
- Wang Y, Wei Z, Liu L, Cheng Z, Lin Y, Ji F, Gong W (2005) Crystal structure of human B-type phosphoglycerate mutase bound with citrate. *Biochem Biophys Res Commun* 331(4):1207–1215
- Wiechelmann KJ, Braun RD, Fitzpatrick JD (1988) Investigation of the bicinchoninic acid protein assay: identification of the groups responsible for color formation. *Anal Biochem* 175(1):231–237
- Ximenez C, Moran P, Rojas L, Valadez A, Gomez A (2009) Reassessment of the epidemiology of amebiasis: state of the art. *Infect Genet Evol* 9(6):1023–1032
- Yu H, Dranchak P, Li Z, MacArthur R, Munson MS, Mehzabeen N, Baird NJ, Battalio KP, Ross D, Lovell S, Carlow CK, Suga H, Ingles J (2017) Macrocyclic peptides delineate locked-open inhibition mechanism for microorganism phosphoglycerate mutases. *Nat Commun* 3(8):14932

RESEARCH ARTICLE

BENTHAM
SCIENCE

Virtual Screening, Molecular Dynamics and ADME-Tox Tools for Finding Potential Inhibitors of Phosphoglycerate Mutase 1 from *Plasmodium falciparum*



Lluvia Ríos-Soto¹, Claudia Avitia-Domínguez¹, Erick Sierra-Campos², Mónica Valdez-Solana², Jorge Cisneros-Martínez¹, Marcelo Gómez Palacio-Gastellum³ and Alfredo Téllez-Valencia^{1,*}

¹Facultad de Medicina y Nutrición, Universidad Juárez del Estado de Durango, Av. Universidad y Fanny Anitua S/N, Durango, Dgo, C.P. 34000, México; ²Facultad de Ciencias Químicas, Universidad Juárez del Estado de Durango, Av. Artículo 123 S/N Fracc. Filadelfia, Gómez Palacio, Durango, CP. 35010, México; ³Facultad de Odontología, Universidad Juárez del Estado de Durango, Predio Canoas S/N, Colonia Los Angeles, Durango, Dgo, C.P. 34000, México

Abstract: Background: Nowadays, malaria is still one of the most important and lethal diseases worldwide, causing 445,000 deaths in a year. Due to the actual treatment resistance, there is an emergency to find new drugs.

Objective: The aim of this work was to find potential inhibitors of phosphoglycerate mutase 1 from *P. falciparum*.

Results: Through virtual screening of a chemical library of 15,123 small molecules, analyzed by two programs, four potential inhibitors of phosphoglycerate mutase 1 from *P. falciparum* were found: ZINC64219552, ZINC39095354, ZINC04593310, and ZINC04343691; their binding energies in SP mode were -7.3, -7.41, -7.4, and -7.18 kcal/mol respectively. Molecular dynamic analysis revealed that these molecules interact with residues important for enzyme catalysis and molecule ZINC04343691 provoked the highest structural changes. Physicochemical and toxicological profiles evaluation of these inhibitors with ADME-Tox method suggested that they can be considered as potential drugs. Furthermore, analysis of human PGAM-B suggested that these molecules could be selective for the parasitic enzyme.

Conclusion: The compounds reported here are the first selective potential inhibitors of phosphoglycerate mutase 1 from *P. falciparum*, and can serve as a starting point in the search of a new chemotherapy against malaria.

Keywords: Malaria, *Plasmodium falciparum*, Phosphoglycerate mutase 1, Virtual screening, Molecular dynamics, ADME-Tox.

1. INTRODUCTION

Malaria is a parasite caused disease by the infection with *P. falciparum*, *P. vivax*, *P. malariae*, *P. ovale*, and *P. knowlesi*, of which *P. falciparum* is responsible for the most severe and lethal cases [1]. Malaria has a devastating impact on human health; it is estimated that every year people in around 91 countries are at risk. In 2016 alone, a number of 211 million cases were reported, with a mortality rate of 445 000 deaths per year, mostly among children [1]. This disease is transmitted through the bite of a previously infected female *Anopheles* mosquito and can cause acute symptoms which can result in complications that can lead to death [2]. During the last few decades, different types of drugs have been used for its treatment such as Pyrimethamine, Quinine,

Lumefantrine, Amodiaquine, Piperaquine, Mefloquine, Chloroquine, Atovaquone, Pyronaridine, Sulfadoxine, Proguanil, and Primaquine [3]. Nowadays, first line treatments involve artemisinin and its derivatives Artesunate, Dihydroartemisinin, Artemether, or their combination with another drug [3]. However, due to reports of resistance in the last years [4], there is a growing necessity to develop new drugs for the treatment of this disease.

In this context, different strategies have been implemented to develop new treatments, one of them is the design of new drugs targeting important metabolic routes in the parasite, at its erythrocytic stage *P. falciparum* depends entirely on the glycolysis energy for cellular work [5]. Additionally, there are structural and biochemical differences between parasite and human glycolytic enzymes, which can be exploited to design selective inhibitors [6-12], for an excellent review about this see Alam *et al.* [13]. Therefore, enzymes in this pathway provide excellent targets for the development of new treatments against this disease.

*Address correspondence to this author at the Facultad de Medicina y Nutrición, Universidad Juárez del Estado de Durango, Av. Universidad y Fanny Anitua S/N, Durango, Dgo, C.P. 34000, México; Tel./Fax: (+52)6188121687; E-mail: atellez@ujed.mx

Phosphoglycerate mutase (PGAM) participates in the eight-step of glycolysis, catalyzing the reversible interconversion between 3-phosphoglycerate and 2-phosphoglycerate [14]. Regarding their requirement of 2,3-biphosphoglycerate for catalysis, PGAMs are classified as cofactor-dependent (dPGAMs) or independent (iPGAMs) [14]. Structurally, most dPGAMs are dimers formed by subunits of around 250 amino acids, instead, iPGAMs are monomers of around 500 amino acids [14]. It has been reported that dPGAMs support three catalytic activities, the principal as a mutase, catalyzing the reaction described above, the second as phosphatase, dephosphorylating 2,3-biphosphoglycerate into 3-phosphoglycerate or 2-phosphoglycerate, the last activity is as synthetase, where 1,3 biphosphoglycerate is transformed into 2,3-biphosphoglycerate [15].

P. falciparum possesses 2 types of PGAMs, the genes encoding for these two proteins are PF11_0208 and PFD0660w, which encodes for phosphoglycerate mutase type 1 (PfPGAM1) and the phosphoglycerate mutase type 2 (PfPGAM2), respectively [16]. PfPGAM2 is the only enzyme that has been characterized, reporting that it functions as a phosphatase instead of a mutase [17]. With respect to PfPGAM1, it is a true mutase [17], but there have been no kinetic or biochemical studies conducted, only its crystal structure has been reported as part of the consortium Structural Genomics of Pathogenic Protozoa [18]. This enzyme is a homodimer of 250 amino acids in each subunit and is classified as a dPGAM [17]. Here it is important to mention that human possesses two isoforms of dPGAM, HsPGAM-M and HsPGAM-B, which are tissue-specific, being type B that is present in erythrocytes [19, 20]. Furthermore, HsPGAM-B shares a 56 % identity with PfPGAM1, which means that even both are dPGAMs, it is possible to find potential selective inhibitors.

Keeping this in mind, in the present study a computer-assisted drug design strategy was applied through virtual screening and molecular dynamics studies to find potential inhibitors of PfPGAM1. Moreover, an *in silico* complete characterization was realized, as well as their possible selectivity against HsPGAM-B was evaluated.

2. MATERIALS AND METHODS

2.1. Selection and Preparation of Target Protein

The 3-D structure of PfPGAM1 and HsPGAM-B at a resolution of 2.6 Å and 2.8 Å, respectively, was retrieved from the Protein Data Bank (access code 1XQ9 [18] and 1YJX [21]). Both enzymes were prepared by eliminating water molecules and ligands present in the crystal structure.

2.2. Selection and Preparation of Ligands

Ligands were obtained from the ZINC Database [22] using the Drug-like subset that contains around 15 million small molecules which accomplish the Lipinski's Rule of five [23]. The subset was further processed applying a Tanimoto coefficient of 4 to reduce the structural redundancy and encourage the chemical diversity. After this action, the database was reduced to 15,123 compounds. The molecules were prepared according to the requirements of the two programs used for virtual screening as described below.

2.3. Virtual Screening

Virtual screening studies were performed using two programs, each one providing a different approach to calculate the potential binding energies.

2.3.1. Glide

Glide from Maestro suite (www.schrodinger.com) employs a hierarchical function that filters data and selects the most favorable interactions between a protein docking site and a ligand. The software was applied in the first stage using the Standard Precision (SP) mode followed by an Extra Precision (XP) mode [24-26] which performs an advanced scoring, which in turn, results in an enriched calculation that minimizes false positives. The equation used to calculate the binding energy in the XP mode was:

$$\text{XP Glide Score} = E_{\text{coul}} + E_{\text{vdw}} + E_{\text{bind}} + E_{\text{penalty}}$$

where E_{coul} and E_{vdw} represent van der Waals and electrostatic terms, respectively. E_{bind} and E_{penalty} make reference to contributions that favor binding or penalization of interactions that influence binding of a ligand.

The target proteins were refined and prepared through the Protein Preparation Wizard, for both PfPGAM1 and HsPGAM-B; only chain A was preserved. Elimination of co-crystallized waters and ligand was also carried out, bond orders were assigned along with the addition of hydrogen atoms, and OPLS_2005 forcefield was employed for formal charges. Ligands were prepared with the Ligprep utility at default values and the OPLS_2005 forcefield for energy minimization. The docking grid was created with default parameters selecting as center His11 with a grid box of 14 X 14 X 14 Å. The SP mode was used as an initial study and the best scores were later redocked with the XP docking mode. The output obtained was set so that only a maximum of 5 poses for each ligand was retained.

2.3.2. Autodock Vina

Autodock vina [27] uses a genetic algorithm that permits to search the best binding poses with favorable energies in a previously specified binding site. It calculates the interaction in a protein-ligand complex by taking into account electrostatic terms, van der Waals forces and the formation of hydrogen bonds. Additionally, it possesses a gradient optimization method that allows to speed up optimization; the binding energy is obtained by the next equation:

$$c = \sum_i < j f_{ij} (r^{ij})$$

where i and j are a pair of atoms that can move relative to each other, but separated by at least 3 consecutive covalent bonds.

The input data were prepared using Autodock Tools 1.5.6 [28], and as in Glide, only chain A from both enzymes was preserved. Ligands and co-crystallized waters present were eliminated, hydrogen atoms and partial charges were added with Gasteiger-Marsili algorithm [29]. The coordinates of the structures as well as ligands were later saved as a pdbqt file. The site for docking was determined with the Autogrid function and grid size was established in 14 x 14 x 14 Å

around its chosen center His11. Exhaustiveness was set on 10; this parameter permits to determine how much computational effort is allowed to perform, where a higher value indicates an improved result.

2.4. Molecular Dynamics Simulation

The protein-ligand complex structures used for molecular dynamics (MD) studies were those obtained in Glide and Autodock Vina with the best binding energy (two compounds in each case). The topology ligand parameters were obtained from the Dundee PRODRG server [30] with GROMOS [31]. MD simulations were made in GROMACS v 5.1.4 [32], and calculations were performed using the GROMOS9654a7 forcefield [33]. The enzyme-ligand complex was placed in a cubic box with a dimension of 1 nm; the explicit solvent-simple point charge model (SPC) was employed to recreate the aqueous environment. Sodium and chlorine ions were added to reach a concentration of 0.15 M to neutralize the system. The steepest descent energy minimization of 2000 steps was done followed by a canonical, isothermal-isobaric ensemble of 50000 and 250000 steps, respectively. Once the system was equilibrated relative to pressure and temperature, a full 20 ns molecular dynamics simulation at 300 K° of temperature was performed.

Analysis of the MD data involved Root Mean Square Deviation (RMSD), Root Mean Square Fluctuation (RMSF) and Energy of the system as well as calculation of binding free energy.

2.5. ADME Properties and Toxicity Prediction

Analysis of ADME properties of the selected molecules was carried out through the PreADMET (<https://preadmet.bmdrc.kr/adme/>) server. Toxicity studies were obtained through the Data warrior software [34], which predicts toxicity assessing molecule structure localizing fragments that can potentially cause toxic effects, which include mutagenicity, irritancy, reproductive effects, and tumorigenicity. The best-scored compounds were assessed along with a drug-likeness calculation that may indicate if the selected hits possess qualities to become new drugs.

3. RESULTS AND DISCUSSION

3.1. Virtual Screening

The general strategy followed to select the potential inhibitors of PfPGAM1 is shown in Fig. (1). After filtration of the original DrugLike database from ZINC [22], ligand preparation with Ligprep generated 100456 conformers to be docked. To this end, and with the aim to realize a detailed study of the small molecules database, it was analyzed through two different programs, Glide [24-26] and Autodock Vina [27]. From each, the four molecules with the highest binding energy were selected and were docked into HsPGAM-B to determine their potential selectivity.

The structures of the molecules selected are shown in (Fig. 2), and as can be seen, compounds with negative charge occupied the first places. This has certain logic because of the positive general charge of the PfGAM1 active site [35]. With respect to inhibitors reported to other cofactor-dependent PGAMs, there are only two for human PGAM trying to find a new lead for cancer treatment, one of

them was an indole derivative and the other an anthraquinone derivative [36, 37]; therefore their structures are totally different from the compounds reported here.

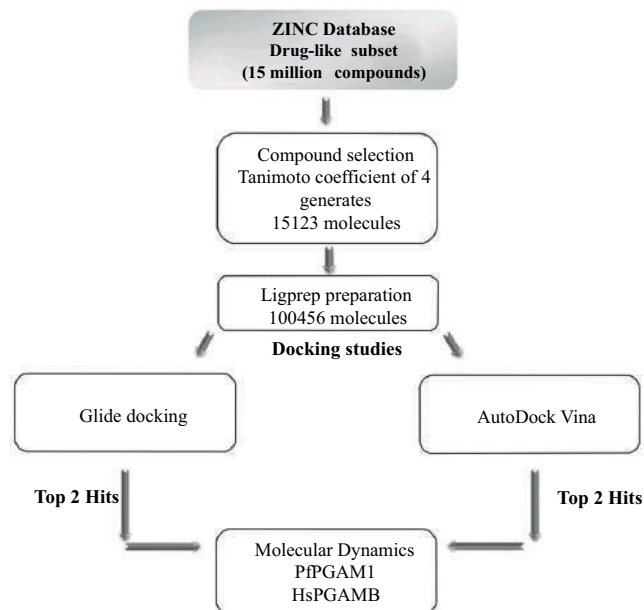


Fig. (1). Flowchart used to select the potential inhibitors of PpPGAM1.

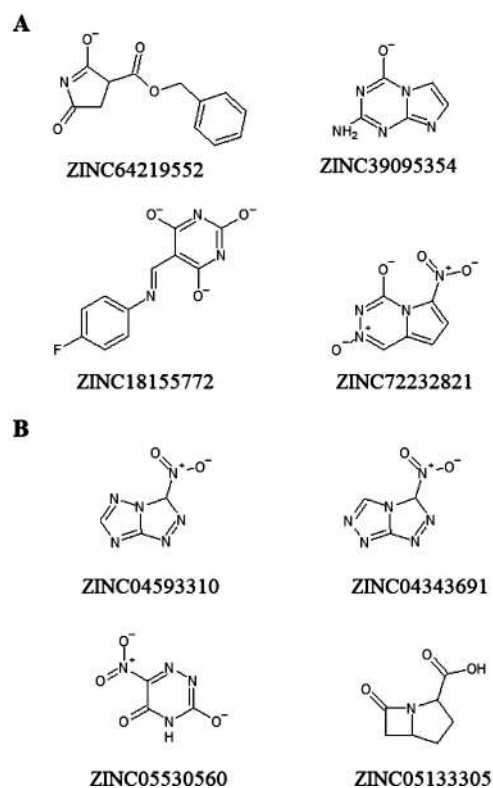


Fig. (2). Molecules selected after virtual screening with A) Glide and B) AutoDock Vina.

The binding energies for compounds in PpPGAM1 obtained after XP mode docking varied from a range of -6.1 to -2.8 Kcal/mol (Table 1). In principle, a huge difference could

appear between the first four molecules, but XP mode is more restrictive, in fact, binding energies in SP mode were -7.3, -7.41, -7.4, and -7.18 Kcal/mol for **ZINC64219552**, **ZINC39095354**, **ZINC18155772**, and **ZINC72232821**, respectively. The same phenomenon was observed in HsPGAM-B with energies ranging from -6.74 to -5.17 Kcal/mol in the SP mode. In both programs (Glide and AutoDock), the compounds obtained a higher binding energy with respect to PfPGAM1 (Table 1), and made more interactions (hydrogen bonds) with different residues, including those important for enzyme catalysis [35], suggesting the potential selectivity of these molecules for parasitic enzyme (Table 1).

3.2. Molecular Dynamics

With the aim to understand in detail the interaction of these molecules with PfPGAM1 and HsPGAM-B, the two compounds with the highest binding energy in each program (compounds **ZINC64219552**, **ZINC39095354**, **ZINC04593310**, and **ZINC04343691**) were selected for molecular dynamics studies. The complexes were submitted to 20ns of simulation as described in the methodology. Analysis of the stability in each system by means of the Root Mean Square Deviation (RMSD) showed that after 10ns, all the complexes become stable (Fig. 3). Comparing the trajectories of Apo-PfPGAM1 or Apo-HsPGAM-B with the complexes, it can be seen that compound **ZINC04343691** provokes the highest structural changes, and it was the complex that takes more time to reach stability (Fig. 3A, B and F). On the other hand, when trajectories between complexes in both enzymes are compared, the data showed that the four compounds followed different trajectories that alter the structure of both enzymes in a distinct manner (Fig. 3C, D, E and F).

Thereafter, protein flexibility was studied looking for changes in protein regions, to this end, Root Mean Square Fluctuations (RMSF) between Apo-protein and each com-

plex were determined (Fig. 4). The results indicated that the four molecules modify several regions in both enzymes (Fig. 4A vs. 4C-F, and 4B vs. 4C-F). In particular, compounds **ZINC64219552** and **ZINC39095354** in complex with PfPGAM1 showed differences in mobility in the region formed by residues 200-240 (Fig. 4C) and 130-150 (Fig. 4D), respectively. Complexes with **ZINC04593310** and **ZINC04343691** presented similar patterns of mobility with both enzymes, in particular residues 100-150 (Fig. 4E and F).

Furthermore, Linear Interaction Energy (LIE) analysis showed that in both enzymes, the binding of compounds **1**, **5**, and **6** was dominated by electrostatic interaction energy, whilst for compound **2**, it was governed by van der Waals component (Table 2).

3.3. ADME-Tox Studies

Determination of ADME properties such as, drug likeness score (which determines if the selected hits satisfy the essential characteristics to become a drug), along with toxicity descriptors was performed in the PreADMET server and Data Warrior software. The results obtained showed that according to the values obtained, all of the compounds possess the potential to become new drugs, however among the selected compounds, compounds **5** and **6** showed medium risk of mutagenic and tumorigenic effects (Table 3).

Taking together all the data, the bases for further studies is established that include cloning, expression, and characterization of PfPGAM1, as well as the *in vitro* activity assays of these compounds against PfPGAM1 and HsPGAM-B.

The analysis of ADME properties indicated that all the compounds, in general, obtained values among the middle and the best range permitted (Table 3). However, compounds **1**, **2**, **5**, **6**, and **8** passed all the evaluations (Table 4).

Table 1. Binding energies and interactions of the top scoring hits for PfPGAM1.

Program	Compound ID	Binding Energy (kcal/mol)		Binding Site Interactions (Hydrogen Bonds)	
		PfPGAM1	HsPGAM-B	PfPGAM1	HsPGAM-B
Glide XP	ZINC64219552 (1)	-6.113	-5.018	Arg10 , Tyr92, Arg116, Asn188	Asn17 , Ser23, Gly24, Lys100
	ZINC39095354 (2)	-4.191	-4.016	Arg10 , His11 , Glu89	Arg10 , Ser23
	ZINC18155772 (3)	-4.104	-4.070	Asn17 , Arg116	Asn17 , Ser23
	ZINC72232821 (4)	-2.872	-2.645	Ser14, Asn17 , Lys100, Arg116	Ser 23, Gly24
Autodock Vina	ZINC04593310 (5)	-6.0	-4.7	Ser14, Asn17 , Arg62	Arg10 , Lys100
	ZINC04343691 (6)	-5.7	-5.1	Ser14, Arg62	Arg10 , Lys100
	ZINC05530560 (7)	-5.5	-5.5	Arg10 , Arg62	Ser22, Gly187
	ZINC05133305 (8)	-4.8	-4.1	Ser14, Arg62	Arg10

Note. Residues corresponding to the catalytic site are highlighted in bold. In parenthesis are indicated the number to identify the compounds in other tables.

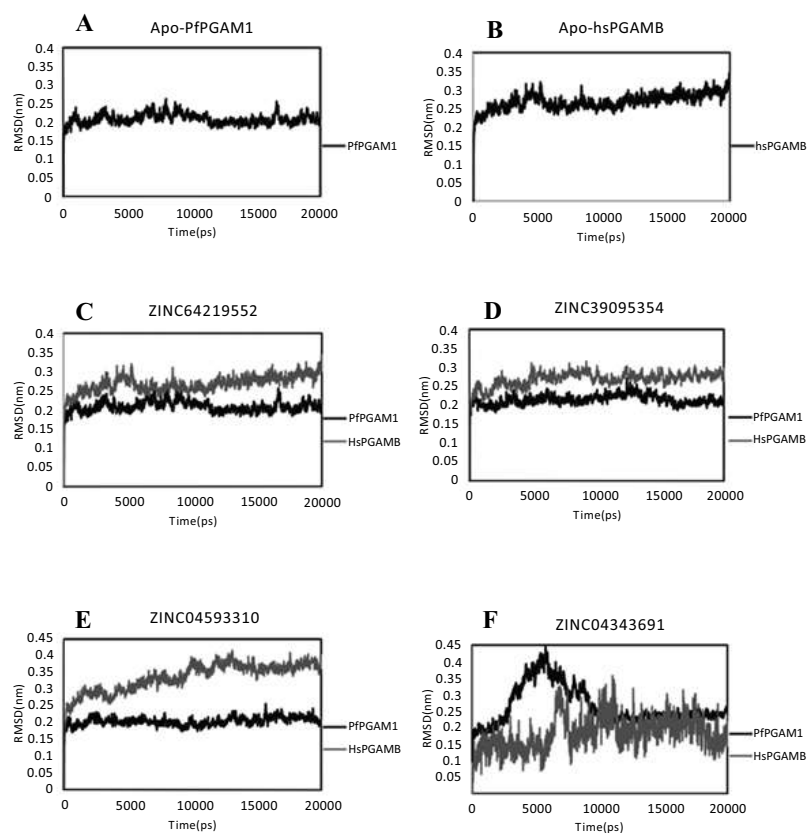


Fig. (3). RMSD of PfPGAM1 and HsPGAM-B in their free forms (Apo) and in complex with the four molecules selected by virtual screening.

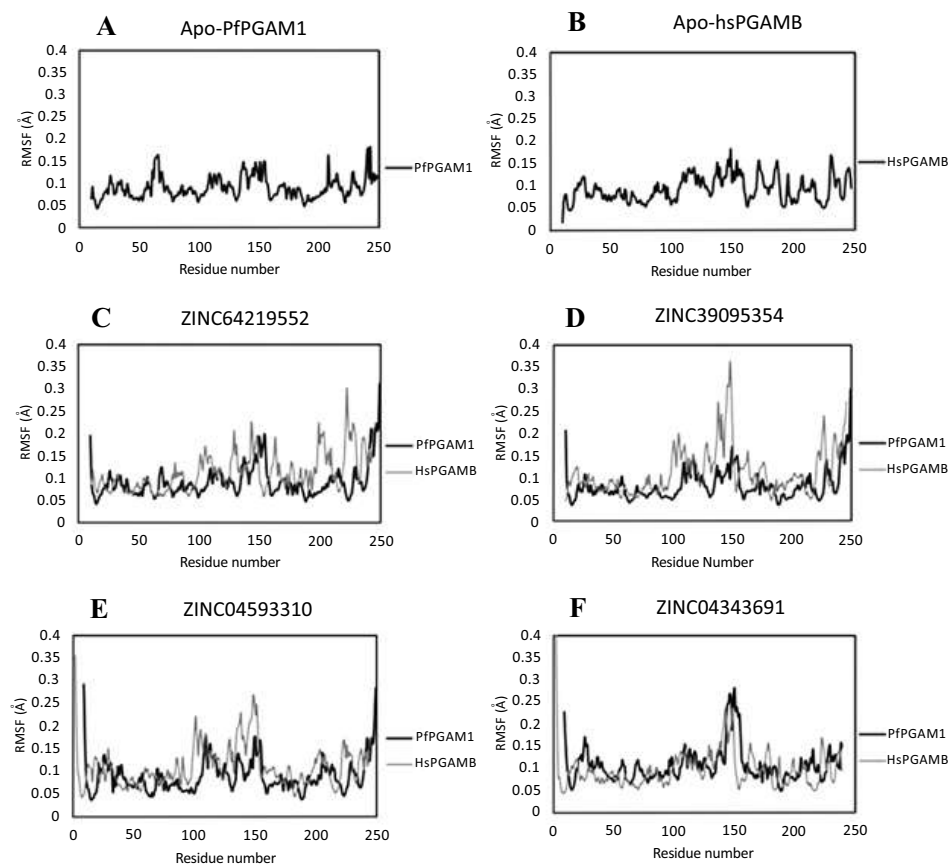


Fig. (4). RMSF plots of PfPGAM1 and HsPGAM-B in their free forms (Apo) and in complex with the four molecules selected by virtual screening.

Table 2. Binding free energies calculated by the LIE method for each complex in MD simulation.

Complex	Energy (kcal/mol)					Hydrogen Bond
	$(V_{LJ})_{bound}$	$(V_{LJ})_{free}$	$(V_{CL})_{bound}$	$(V_{CL})_{free}$	ΔG_{bind}	Range
PfPGAM1- 1	-1.03	-7.03	-34.87	-12.98	-13.70	0-7
HsPGAMB-1	-11.71	-4.06	-34.05	-4.06	-18.52	0-6
PfPGAM1-2	-13.93	-4.69	-6.89	-11.80	0.7	0-5
HsPGAMB-2	-15.87	-3.47	-6.74	-8.58	-1.30	0-4
PfPGAM1-5	-11.91	-2.54	-25.50	-13.39	-7.73	0-5
HsPGAMB-5	-13.21	-1.64	-30.92	-16.41	-9.33	0-6
PfPGAM1-6	-9.24	-1.52	-48.92	-13.78	-17.77	0-8
HsPGAMB-6	-9.48	-3.9	-49.49	-5.68	-22.90	0-7

The calculation of the binding free energy was based on the equation $\Delta G_{bind} = \alpha[(V_{LJ})_{bound} - (V_{LJ})_{free}] + \beta[(V_{CL})_{bound} - (V_{CL})_{free}] + \gamma$, where $(V_{LJ})_{bound}$ is the average Lennard-Jones energy for ligand-protein interaction; $(V_{LJ})_{free}$ is the average Lennard-Jones energy for ligand-water interaction; $(V_{CL})_{bound}$ is the average electrostatic energy for ligand-protein interaction; $(V_{CL})_{free}$ is the average electrostatic energy for ligand-water interaction; α , β , and γ are the LIE coefficients. For small drug-like ligands $\alpha = 0.18$, $\beta = 0.50$ and $\gamma = 0.00$ [38-40].

Table 3. Drug likeness and Toxicity parameters for the selected hits.

Compound ID	Drug likeness	ClogP	Mutagenic	Tumorigenic	Irritant	Reproductive Effect
1	-0.84	0.74	NONE	NONE	NONE	NONE
2	-0.70	0.34	NONE	NONE	NONE	NONE
3	-0.51	1.94	NONE	NONE	NONE	NONE
4	-0.26	0.30	NONE	NONE	NONE	NONE
5	-0.49	0.04	MEDIUM RISK	MEDIUM RISK	NONE	NONE
6	-0.49	0.04	MEDIUM RISK	MEDIUM RISK	NONE	NONE
7	-1.09	-0.69	NONE	NONE	NONE	NONE
8	-0.83	0.48	NONE	NONE	NONE	NONE

Table 4. ADME properties analysis for de selected hits.

	Compound ID							
	1	2	3	4	5	6	7	8
HIA (%)	91.49**	74.54**	77.99**	49.23*	39.62*	39.62*	15.25	85.92*
CaCo-2 (nm/sec)	18.24*	20.87*	1.50	19.23*	15.92*	17.78*	4.69*	20.64*
MDCK (nm/sec)	4.65*	13.51*	40.31*	1.55	339.04**	63.69*	0.7973	5.17*
PPB (%)	47.67**	2.74**	80.25**	0.4780**	69.29**	59.221**	33.42**	15.42**
BBBP	0.1703*	0.1169*	0.0526**	0.1046*	0.4602*	0.3327*	0.06734**	0.1714*

Abbreviations: HIA, Human Intestinal Absorption (20-70% moderately absorbed compounds; 70-100% well absorbed compounds); CaCo-2, *in vitro* CaCo-2 cell permeability (4-70 nm/sec, middle permeability; more than 70 high permeability); MDCK, *in vitro* MDCK cell permeability (4-70 nm/sec, middle permeability); PPB, *in vivo* Plasma Protein Binding (less than 90%, chemicals weakly bound); BBBP, *in vivo* Blood-Brain Barrier Penetration (less than 0.1, low absorption to Central Nervous System; 0.1-2, medium absorption).** means the value obtained is the best range; * means the value obtained is the middle range.

CONCLUSION

In the present work, a database of 15,123 small molecules was studied through a virtual screening protocol to find potential inhibitors of PfPGAM1. From this procedure, four compounds were selected showing a better binding energy for parasite enzyme than for human homologous. Molecular dynamics results suggested that compounds provoke structural changes in both enzymes following different trajectories. Their ADME-Tox parameters indicated that two compounds showed medium risk for mutagenic and tumorigenic effects, however, the rest of the properties evaluated were within the permitted ranges in the four molecules. Nowadays, there is no inhibitor reported for PfPGAM1, according to the detailed evaluation realized in this work, compounds reported here are potential inhibitors of this enzyme and, at least by the *in silico* data, they could be selective in comparison with HsPGAM-B. Therefore, these molecules serve as a starting point to design the first inhibitors of PfPGAM and future candidates for a new antimalarial chemotherapy.

ETHICS APPROVAL AND CONSENT TO PARTICIPATE

Not applicable.

HUMAN AND ANIMAL RIGHTS

No Animals/Humans were used for studies that are basis of this research.

CONSENT FOR PUBLICATION

Not applicable.

CONFLICT OF INTEREST

The authors declare no conflict of interest, financial or otherwise.

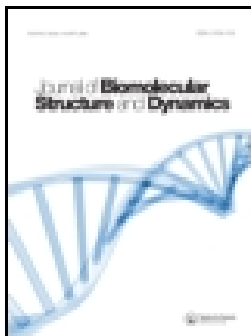
ACKNOWLEDGEMENTS

ATV and CAD acknowledge CONACyT for grants No. 257848 and 258694, respectively. CONACyT is also acknowledged for the fellowship granted to LIRS (No. 326361).

REFERENCES

- [1] World Malaria Report 2017. Geneva: World Health Organization, 2017.
- [2] Miller, L.H.; Ackerman, H.C.; Su, X.Z.; Wellems, T.E. Malaria biology and disease pathogenesis: Insights for new treatments. *Nat. Med.*, **2013**, *19*(2), 156-167.
- [3] Kumar, S.; Kumari, R.; Pandey, R. New insight-guided approaches to detect, cure, prevent and eliminate malaria. *Protoplasma*, **2015**, *252*(3), 717-753.
- [4] Miotto, O.; Almagro-Garcia, J.; Manske, M.; Macinnis, B.; Campino, S.; Rockett, K.A.; Amaratunga, C.; Lim, P.; Suon, S.; Sreng, S.; Anderson, J.M.; Duong, S.; Nguon, C.; Chuor, C.M.; Saunders, D.; Se, Y.; Lon, C.; Fukuda, M.M.; Amenga-Etego, L.; Hodgson, A.V.; Asoala, V.; Imwong, M.; Takala-Harrison, S.; Nosten, F.; Su, X.Z.; Ringwald, P.; Ariey, F.; Dolecek, C.; Hien, T.T.; Boni, M.F.; Thai, C.Q.; Amambua-Ngwa, A.; Conway, D.J.; Djimde, A.A.; Doumbo, O.K.; Zongo, I.; Ouedraogo, J.B.; Alcock, D.; Drury, E.; Auburn, S.; Koch, O.; Sanders, M.; Hubbard, C.; Maslen, G.; Ruano-Rubio, V.; Jyothi, D.; Miles, A.; O'Brien, J.; Gamble, C.; Oyola, S.O.; Rayner, J.C.; Newbold, C.I.; Berriman, M.; Spencer, C.C.; McVean, G.; Day, N.P.; White, N.J.; Bethell, D.; Dondorp, A.M.; Plowe, C.V.; Fairhurst, R.M.; Kwiatkowski, D.P. Multiple populations of artemisinin-resistant *Plasmodium falciparum* in Cambodia. *Nat. Genetics*, **2013**, *45*(6), 648-655.
- [5] Sherman, I.W. Carbohydrate metabolism of asexual stages, in *Malaria: Parasite biology, pathogenesis, and protection*. ASM Press: Washington, DC, **1998**.
- [6] Wanidworanun, C.; Nagel, R.L.; Shear, H.L. Antisense oligonucleotides targeting malarial aldolase inhibit the asexual erythrocytic stages of *Plasmodium falciparum*. *Mol. Biochem. Parasitol.*, **1999**, *102*(1), 91-101.
- [7] Dobeli, H.; Trzeciak, A.; Gillessen, D.; Matile, H.; Srivastava, I.K.; Perrin, L.H.; Jakob, P.E.; Certa, U. Expression, purification, biochemical characterization and inhibition of recombinant *Plasmodium falciparum* aldolase. *Mol. Biochem. Parasitol.*, **1990**, *41*(2), 259-268.
- [8] Kim, H.; Certa, U.; Dobeli, H.; Jakob, P.; Hol, W.G. Crystal structure of fructose-1,6-bisphosphate aldolase from the human malaria parasite *Plasmodium falciparum*. *Biochemistry*, **1998**, *37*(13), 4388-4396.
- [9] Dunn, C.R.; Banfield, M.J.; Barker, J.J.; Higham, C.W.; Moreton, K.M.; Turgut-Balik, D.; Brady, R.L.; Holbrook, J.J. The structure of lactate dehydrogenase from *Plasmodium falciparum* reveals a new target for anti-malarial design. *Nat. Struct. Biol.*, **1996**, *3*(11), 912-915.
- [10] Read, M.; Hicks, K.E.; Sims, P.F.; Hyde, J.E. Molecular characterisation of the enolase gene from the human malaria parasite *Plasmodium falciparum*. Evidence for ancestry within a photosynthetic lineage. *Eur. J. Biochem.*, **1994**, *220*(2), 513-520.
- [11] Velanker, S.S.; Ray, S.S.; Gokhale, R.S.; Suma, S.; Balaram, H.; Balaram, P.; Murthy, M.R. Triosephosphate isomerase from *Plasmodium falciparum*: The crystal structure provides insights into antimalarial drug design. *Structure*, **1997**, *5*(6), 751-761.
- [12] Robien, M.A.; Bosch, J.; Buckner, F.S.; Van Voorhis, W.C.; Worthey, E.A.; Myler, P.; Mehlin, C.; Boni, E.E.; Kalyuzhnyi, O.; Anderson, L.; Lauricella, A.; Gulde, S.; Luft, J.R.; DeTitta, G.; Caruthers, J.M.; Hodgson, K.O.; Soltis, M.; Zucker, F.; Verlinde, C.L.; Merritt, E.A.; Schoenfeld, L.W.; Hol, W.G. Crystal structure of glyceraldehyde-3-phosphate dehydrogenase from *Plasmodium falciparum* at 2.25 Å resolution reveals intriguing extra electron density in the active site. *Proteins*, **2006**, *62*(3), 570-577.
- [13] Alam, A.; Neyaz, M.K.; Ikramul Hasan, S. Exploiting unique structural and functional properties of malarial glycolytic enzymes for antimalarial drug development. *Mal. Res. Treat.*, **2014**, *2014*, 1-13.
- [14] Jedrzejewski, M.J. Structure, function, and evolution of phosphoglycerate mutases: Comparison with fructose-2,6-bisphosphatase, acid phosphatase, and alkaline phosphatase. *Prog. Biophys. Mol. Biol.*, **2000**, *73*(2-4), 263-287.
- [15] Bond, C.S.; White, M.F.; Hunter, W.N. High resolution structure of the phosphohistidine-activated form of *Escherichia coli* cofactor-dependent phosphoglycerate mutase. *J. Biol. Chem.*, **2001**, *276*(5), 3247-3253.
- [16] Aurecochea, C.; Brestelli, J.; Brunk, B.P.; Dommer, J.; Fischer, S.; Gajria, B.; Gao, X.; Gingle, A.; Grant, G.; Harb, O.S.; Heiges, M.; Innamorato, F.; Iodice, J.; Kissinger, J.C.; Kraemer, E.; Li, W.; Miller, J.A.; Nayak, V.; Pennington, C.; Pinney, D.F.; Roos, D.S.; Ross, C.; Stoeckert, C.J., Jr.; Treatman, C.; Wang, H. PlasmoDB: A functional genomic database for malaria parasites. *Nucleic Acids Res.*, **2009**, *37*, 539-543.
- [17] Hills, T.; Srivastava, A.; Ayi, K.; Wernimont, A.K.; Kain, K.; Waters, A.P.; Hui, R.; Pizarro, J.C. Characterization of a new phosphatase from plasmodium. *Mol. Biochem. Parasitol.*, **2011**, *179*(2), 69-79.
- [18] Fan, E.; Baker, D.; Fields, S.; Gelb, M.H.; Buckner, F.S.; Van Voorhis, W.C.; Phizicky, E.; Dumont, M.; Mehlin, C.; Grayhack, E.; Sullivan, M.; Verlinde, C.; DeTitta, G.; Meldrum, D.R.; Merritt, E.A.; Earnest, T.; Soltis, M.; Zucker, F.; Myler, P.J.; Schoenfeld, L.; Kim, D.; Worthey, L.; Lacount, D.; Vignali, M.; Li, J.; Mondal, S.; Massey, A.; Carroll, B.; Gulde, S.; Luft, J.; Desoto, L.; Holl, M.; Caruthers, J.; Bosch, J.; Robien, M.; Arakaki, T.; Holmes, M.; Le Trong, I.; Hol, W.G. Structural genomics of pathogenic protozoa: an overview. *Meth. Mol. Biol.*, **2008**, *426*, 497-513.
- [19] Prehu, M.O.; Calvin, M.C.; Prehu, C.; Rosa, R. Biochemical and immunological arguments for homology between red cell and liver

- phosphoglyceromutase isozymes. *Biochim. Biophys. Acta.*, **1984**, 787(3), 270-274.
- [20] Chen, S.H.; Anderson, J.E.; Giblett, E.R. Human red cell 2,3-diphosphoglycerate mutase and monophosphoglycerate mutase: Genetic evidence for two separate loci. *Am. J. Hum. Genet.*, **1977**, 29(4), 405-407.
- [21] Wang, Y.; Wei, Z.; Liu, L.; Cheng, Z.; Lin, Y.; Ji, F.; Gong, W. Crystal structure of human B-type phosphoglycerate mutase bound with citrate. *Biochem. Biophys. Res. Commun.*, **2005**, 331(4), 1207-1215.
- [22] Irwin, J.J.; Shoichet, B.K. ZINC a free database of commercially available compounds for virtual screening. *J. Chem. Inf. Model.*, **2005**, 45(1), 177-182.
- [23] Lipinski, C.A.; Lombardo, F.; Dominy, B.W.; Feeney, P.J. Experimental and computational approaches to estimate solubility and permeability in drug discovery and development settings. *Adv. Drug Deliv. Rev.*, **2001**, 46(1-3), 3-26.
- [24] Friesner, R.A.; Banks, J.L.; Murphy, R.B.; Halgren, T.A.; Klicic, J.J.; Mainz, D.T.; Repasky, M.P.; Knoll, E.H.; Shelley, M.; Perry, J.K.; Shaw, D.E.; Francis, P.; Shenkin, P.S. Glide: A new approach for rapid, accurate docking and scoring. 1. Method and assessment of docking accuracy. *J. Med. Chem.*, **2004**, 47(7), 1739-1749.
- [25] Halgren, T.A.; Murphy, R.B.; Friesner, R.A.; Beard, H.S.; Frye, L.L.; Pollard, W.T.; Banks, J.L. Glide: A new approach for rapid, accurate docking and scoring. 2. Enrichment factors in database screening. *J. Med. Chem.*, **2004**, 47(7), 1750-1759.
- [26] Friesner, R.A.; Murphy, R.B.; Repasky, M.P.; Frye, L.L.; Greenwood, J.R.; Halgren, T.A.; Sanschagrin, P.C.; Mainz, D.T. Extra precision glide: Docking and scoring incorporating a model of hydrophobic enclosure for protein-ligand complexes. *J. Med. Chem.*, **2006**, 49(21), 6177-6196.
- [27] Trott, O.; Olson, A.J. AutoDock Vina: Improving the speed and accuracy of docking with a new scoring function, efficient optimization and multithreading. *J. Comput. Chem.*, **2010**, 31(2), 455-461.
- [28] Morris, G.M.; Huey, R.; Lindstrom, W.; Sanner, M.F.; Belew, R.K.; Goodsell, D.S.; Olson, A.J. AutoDock4 and AutoDockTools4: Automated docking with selective receptor flexibility. *J. Comput. Chem.*, **2009**, 30(16), 2785-2791.
- [29] Gasteiger, J.; Marsili, M. Iterative partial equalization of orbital electronegativity - a rapid access to atomic charges. *Tetrahedron*, **1980**, 36(22), 3219-3228.
- [30] Schuttelkopf, A.W.; van Aalten, D.M. PRODRG: A tool for high-throughput crystallography of protein-ligand complexes. *Acta Crystallogr. D. Biol. Crystallogr.*, **2004**, 60(8), 1355-1363.
- [31] Scott, W.R.P.; Hünenberger, P.H.; Tironi, I.G.; Mark, A.E.; Billeter, S.R.; Fennel, J.; Torda, A.E.; Huber, T.; Krüger, P.; van Gunsteren, W.F. The GROMOS bio molecular simulation program package. *J. Phys. Chem. A*, **1999**, 103(19), 3596-3607.
- [32] Van Der Spoel, D.; Lindahl, E.; Hess, B.; Groenhof, G.; Mark, A.E.; Berendsen, H.J. GROMACS: Fast, flexible, and free. *J. Comput. Chem.*, **2005**, 26(16), 1701-1718.
- [33] Schmid, N.; Eichenberger, A.P.; Choutko, A.; Riniker, S.; Winger, M.; Mark, A.E.; van Gunsteren, W.F. Definition and testing of the GROMOS force-field versions 54A7 and 54B7. *Euro. Biophys. J.*, **2011**, 40(7), 843-856.
- [34] Sander, T.; Freyss, J.; von Korff, M.; Rufener, C. DataWarrior: An open-source program for chemistry aware data visualization and analysis. *J. Chem. Inf. Model.*, **2015**, 55(2), 460-473.
- [35] Fothergill-Gilmore, L.A.; Watson, H.C. The phosphoglycerate mutases. *Adv. Enzymol. Relat. Areas Mol. Biol.*, **1989**, 62, 227-313.
- [36] Evans, M.J.; Saghatelian, A.; Sorensen, E.J.; Cravatt, B.F. Target discovery in small-molecule cell-based screens by *in situ* proteome reactivity profiling. *Biotechnol.*, **2005**, 23(10), 1303-1307.
- [37] Hitosugi, T.; Zhou, L.; Elf, S.; Fan, J.; Kang, H.B.; Seo, J.H.; Shan, C.; Dai, Q.; Zhang, L.; Xie, J.; Gu, T.-L.; Jin, P.; Aleckovic, M.; LeRoy, G.; Kang, Y.; Sudderth, J.A.; DeBerardinis, R.J.; Luan, C.-H.; Chen, G.Z.; Muller, S.; Shin, D.M.; Owonikoko, T.K.; Lonial, S.; Arellano, M.L.; Khoury, H.J.; Khuri, F.R.; Lee, B.H.; Ye, K.; Boggon, T.J.; Kang, S.; He, C.; Chen, J. Phosphoglycerate mutase 1 coordinates glycolysis and biosynthesis to promote tumor growth. *Cancer Cell*, **2012**, 22(5), 585-600.
- [38] Åqvist, J.; Medina, C.; Samuelsson, J.E. A new method for predicting binding affinity in computer-aided drug design. *Protein Eng.*, **1994**, 7(3), 385-391.
- [39] Punkvang, A.; Saparpakorn, P.; Hannongbua, S.; Wolschann, P.; Beyer, A.; Pungpo, P. Investigating the structural basis of arylamides to improve potency against *M. tuberculosis* strain through molecular dynamics simulations. *Eur. J. Med. Chem.*, **2010**, 45(12), 5585-5593.
- [40] Aguayo-Ortiz, R.; Méndez-Lucio, O.; Medina-Franco, J.L.; Castillo, R.; Yépez-Mulia, L.; Hernández-Luis, F.; Hernández-Campos, A. Towards the identification of the binding site of benzimidazoles to β -tubulin of *Trichinella spiralis*: Insights from computational and experimental data. *J. Mol. Graph. Model.*, **2013**, 41, 12-19.



In silico hit optimization toward AKT inhibition: fragment-based approach, molecular docking and molecular dynamics study

Elkin Eduardo Sanabria-Chanaga, Irene Betancourt-Conde, Alicia Hernández-Campos, Alfredo Téllez-Valencia & Rafael Castillo

To cite this article: Elkin Eduardo Sanabria-Chanaga, Irene Betancourt-Conde, Alicia Hernández-Campos, Alfredo Téllez-Valencia & Rafael Castillo (2018): *In silico* hit optimization toward AKT inhibition: fragment-based approach, molecular docking and molecular dynamics study, Journal of Biomolecular Structure and Dynamics, DOI: [10.1080/07391102.2018.1546618](https://doi.org/10.1080/07391102.2018.1546618)

To link to this article: <https://doi.org/10.1080/07391102.2018.1546618>

 View supplementary material 

 Accepted author version posted online: 26 Nov 2018.
Published online: 29 Jan 2019.

 Submit your article to this journal 

 Article views: 30

 View Crossmark data 



In silico hit optimization toward AKT inhibition: fragment-based approach, molecular docking and molecular dynamics study

Elkin Eduardo Sanabria-Chanaga^a, Irene Betancourt-Conde^b, Alicia Hernández-Campos^a, Alfredo Téllez-Valencia^b and Rafael Castillo^a 

^aFacultad de Química, Departamento de Farmacia, Universidad Nacional Autónoma de México, Ciudad de México, Mexico; ^bDurango, Facultad de Medicina y Nutrición Universidad Juárez del Estado de Durango Av. Universidad y Fanny Anitúa S/N, Durango, Mexico

Communicated by Ramaswamy H. Sarma

ABSTRACT

Protein kinase B also known as AKT is a cardinal node in different signaling pathways that regulates diverse cell processes. AKT has three isoforms that share high homology. Hyperactivation of each isoform is related with different types of cancer. This work describes the computational search for new inhibitors using a hit optimization process of the previously reported AKT pan inhibitor, a 2,4,6-trisubstituted pyridine. A database of new molecules was proposed using a variant of fragment-based docking methodology and previous reported considerations. Molecular docking followed by molecular dynamics studies were performed to select the best compounds and analyze their behavior. Protein–ligand complexes energy was calculated using molecular mechanics Poisson–Boltzmann surface area protocol. Further, proposed molecules were compared with the ChEMBL database of compounds assayed against AKT. Data analysis leads to determine the structural requirements necessary for a favorable interaction of the proposed ligands with the AKT pocket. Molecular dynamics data suggested that the pK_a of the ligands is important for the stability in the AKT pocket. Molecular similarity analysis shows that proposed ligands have not been previously reported. Thus, ligands with high docking scores and favorable behavior on molecular dynamics simulations are proposed as potential AKT inhibitors.

Abbreviations: ATP: Adenosine triphosphate; BLAST: Basic local alignment search; MD: Molecular dynamics; MMPBSA: Molecular mechanics Poisson–Boltzmann surface area; AKT/PKB: Protein kinase B; RMSD: Root-mean-square deviation; RMSF: Root-mean-square fluctuation; SQM: Semi-empirical quantum chemistry program; WHO: The World Health Organization

ARTICLE HISTORY

Received 29 June 2018
Accepted 30 October 2018

KEYWORDS

AKT inhibitors; cancer; fragment-based docking; 2,4,6-trisubstituted pyridine; serine–threonine kinase B

1. Introduction

Cancer is a generic term for a large group of diseases characterized by the abnormal growth of cells beyond their usual boundaries, which can invade adjoining parts of the body and spread to other organs. According to World Health Organization (WHO), cancer is responsible for an estimated 9.6 million deaths in 2018, which is nearly one in six of all global deaths (<http://www.who.int/en/news-room/fact-sheets/detail/cancer>, 2018). Despite the effort of different research groups in finding new treatments, cancer remains as one of the main health issues worldwide. In the search for new alternatives of treatment, several research groups have focused their work in identifying molecular targets implicated in aberrant cell functions; one of the molecular targets recently identified as a druggable target is protein kinase B, also known as AKT (Huck & Mochalkin, 2017).

AKT is a serine–threonine kinase implicated in several signaling downstream that regulates different processes

associated with cell metabolism, growth, differentiation, division, apoptosis and proliferation (Manning & Cantley, 2007; Testa & Tsichlis, 2005). There are three subtypes of protein kinase B: AKT-1/PKB α , AKT-2/PKB β and AKT-3/PKB γ (Hennesy, Smith, Ram, Lu, & Mills, 2005). Each one has been associated with different types of cancer, such as colon, stomach, breast, ovarian tumors, hormone-insensitive breast and prostate cancers (Liby et al., 2012; Liu, Chen, Ward, Pegram, & Shen, 2016; Liu & Dong, 2014; Ma et al., 2018; Testa & Tsichlis, 2005; Zhu et al., 2014). PI3K/AKT pathway is the most commonly disrupted pathway in human cancers (Millis, Ikeda, Reddy, Gatalica, & Kurzrock, 2016).

Competitive ATP inhibitors against AKT have shown promising properties as alternative cancer therapies; however, existing inhibitors display high toxicity and are not used in current therapy (Huck & Mochalkin, 2017). Therefore, more efforts must be done to find better inhibitors. In this aspect, our research group previously reported a 2,4,6-trisubstituted pyridine as a new scaffold with an IC_{50} : 2.6, 1.5 and 4.0

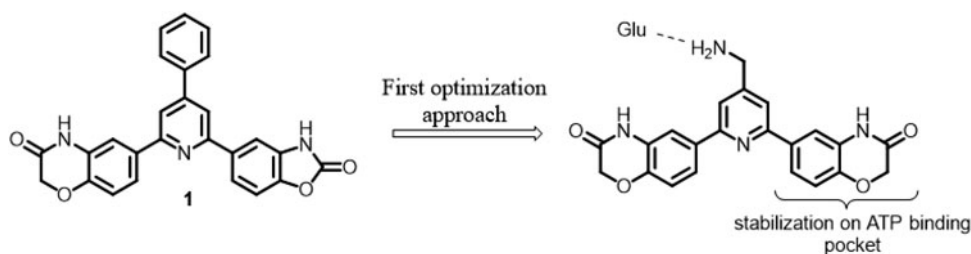


Figure 1. New pan inhibitor found **1** and the first optimization approach.

micromolar for AKT1/AKT2/AKT3, respectively (Medina-Franco et al., 2009).

Further studies proposed the replacement of the phenyl group at position four by an amino group, because this change improves the binding energy in the active site by hydrogen bonding with glutamate 236 in AKT2. Moreover, benzo[d]oxazol-2(3H)-one substituent was replaced for a 2H-benzo[b][1,4]oxazin-3(4H)-one system in order to improve interaction with the ATP loop region (Figure 1) (Hernández-Campos et al., 2010).

2,4,6-Trisubstituted pyridine scaffold has become a starting point to discover new compounds with potential biological activity on AKT. In the present research, a hit optimization process was made by combining contributions of the previous works and modification of fragment-based docking to propose new molecules with better AKT interaction profiles. Thus, to begin with, a new series of compounds derived from pyridine were proposed conserving the 2H-benzo[b][1,4]oxazin-3(4H)-one system at position two to interact with the ATP loop. Also, aniline derivatives were chosen as substituent at position four; the amino group was linked directly to the pyridine to increase the acidity of the hydrogens to form stronger hydrogen bonds with glutamate. Modification at position six in the new series of compounds was determined by a fragment-based docking. For this, fragments with satisfactory score and favorable overlapping on **1** were selected, and a new series of 2,4,6-trisubstituted pyridines were proposed and subjected to an *in silico* study. Results indicate that ligands with the best score values in molecular docking studies and the best behavior in molecular dynamics (MD) simulation represent new potential AKT inhibitors.

2. Materials and methods

2.1. AKT3 homology modeling

Since the 3D model of AKT3 isoform is needed in this study and is not reported yet, we made a search for a suitable template. First, AKT3 isoform FASTA sequence was obtained from UniProtKB database (accession number: Q9Y243), then, using basic local alignment search (BLAST) in UniProt server, we found AKT1 (accession number: P31749) as the most accurate template (The UniProt Consortium, 2016). Finally, different models of AKT3 were built using the crystal structure of AKT1 (PDB ID: 4GV1) (Addie et al., 2013) with Prime (Schrödinger release 2015-4: Prime version 4.2.), Modeller (Šali & Blundell, 1993) and SwissModel server (Benkert,

Biasini, & Schwede, 2011; Biasini et al., 2014). Structure of AKT3 models was optimized with protein preparation wizard module (Schrödinger release 2015-4: Protein Preparation Wizard; Epik version 3.4.) present in Maestro (Schrödinger release 2015-4: Maestro version 10.4.), and the quality of the homology models was appraised in MolProbity server (Chen et al., 2010; Davis et al., 2007). The AKT3 model with the best MolProbity score and the best stereochemical quality in Ramachandran plot was selected and used in this study (see supplementary information).

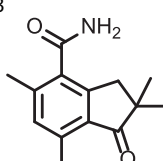
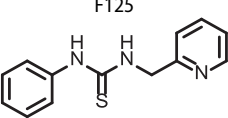
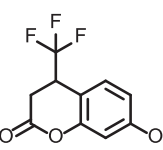
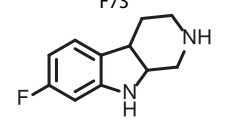
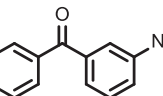
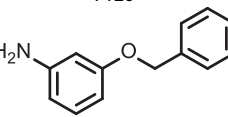
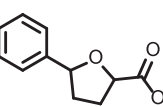
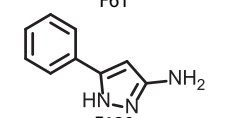
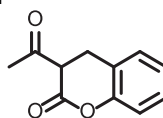
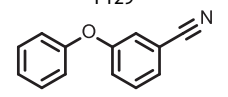
2.2. Structure-based design

To select the substituent at position six, we analyzed and depurated MayBridge fragment database. Then, docking studies of the selected fragments were carried out using Autodock 4.2 (Morris et al., 2009; Sanner, 1999) on AKT2 (PDB ID: 1O6L) (Yang et al., 2002). Ten fragments with the best score values were selected and overlapped on **1**; from this, six fragments showed good overlapping on the scaffold. These fragments were used to propose new substitution at position six of the 2,4,6-trisubstituted pyridine. Additionally, keeping the idea of H-donor group at position four, seven aniline derivatives with different substituents were proposed to modify this position, binding the amino group directly to the pyridine scaffold, conserving the 2H-benzo[b][1,4]oxazin-3(4H)-one system at position two.

2.3. Molecular docking

The 3D models for AKT1 and AKT2 were obtained from the protein data bank PDB ID: 4GV1 (Addie et al., 2013) and 1O6L (Yang et al., 2002), respectively; then water molecules, ions and ligands present in the protein crystallographic structures were removed. Finally, energy minimization was carried out with Protein Preparation Wizard using OPLS_2005 force field. All proposed ligands and reference inhibitor GSK690693 were built and submitted to a geometry optimization in Spartan' 10 (Wavefunction Inc., Spartan version 10, 2010), using the semi-empirical method PM6. 2,4,6-Trisubstituted pyridines were docked in isoforms AKT1, AKT2 crystal structures and AKT3 model using Glide (Schrödinger release 2015-4: Glide version 6.9.) and Autodock 4.2 (Morris et al., 2009; Sanner, 1999). In both programs, grid box was centered at x : -19.687, y : 5.811, z : 16.166 for AKT1 and AKT3; and x : 42.679, y : 30.329, z : 109.603 for AKT2. For Glide, dimensions of the grid box were $25 \times 25 \times 25$ Å; standard precision and extra precision modes were performed with flexible ligand

Table 1. Best 10 structures found through fragment-based docking.

Fragment	Score (kcal/mol)	Fragment	Score (kcal/mol)
F113	-7.9	F125	-7.1
			
F56	-7.6	F73	-6.9
			
F16	-7.5	F126	-6.9
			
F40	-7.2	F61	-6.8
			
F111	-7.2	F129	-6.8
			

adding penalization states of the Epik software in the docking score. For Autodock 4.2, MGLtools 1.5.6 was used to merge non-polar hydrogens and assign Gasteiger atomic charges to each atom in the proteins and ligands; the dimensions of the grid map were selected as $60 \times 60 \times 60$ points with a grid point spacing of 0.375 Å, and the conformational search of the ligand was carried out using a Lamarckian genetic algorithm with 20 GA runs, 25,000,000 of evaluations and 27,000 generations. The best binding mode of each molecule was selected based on the cluster size and lowest free binding energy. In order to select the best candidates, a normalization of docking score values was made using the GSK690693 score value as reference. Consensus score was calculated as average of the result of the normalization process on the two programs used.

2.4. MD simulation

The lowest binding free energy conformation of each selected complex was considered as the initial conformation for MD studies. Parameters and molecular topologies for the ligands were generated using the semi-empirical quantum chemistry program SQM of ACPYPE (Fogh et al., 2005; Nilges et al., 2008; Rieping et al., 2007; Sousa Da Silva & Vranken, 2012; Vranken et al., 2005; Wang et al., 2004; Wang, Wang, Kollman, & Case, 2006). All MD simulations of protein–ligand complexes were performed using GROMACS 4.6.7. Complexes were described using the all-atom Amber99-ILDN force field (Best & Hummer, 2009; Hornak et al., 2006; Lindorff-Larsen et al., 2010); protein–ligand complexes were solvated with water in a cubic box with 1.0 nm of water in all sides using a three-point model for water (TIP3P)

(Jorgensen, Chandrasekhar, Madura, Impey, & Klein, 1983); additionally, simulated NaCl solution of 0.15 M was added randomly.

First, an energy minimization of the system was carried out using the steepest-descent algorithm; in addition, the system was equilibrated by two 100 ps MD using the NVT with Berendsen thermostat (Berendsen, Postma, Van-Gunsteren, DiNola, & Haak, 1984) and NPT with the Parrinello–Rahman barostat (Parrinello & Rahman, 1980); finally, 10 ns MD simulations were performed on the protein–ligand complexes using 1000 frames and a canonical ensemble.

The root-mean-square deviation (RMSD) and root-mean-square fluctuation (RMSF) were analyzed during the complete MD simulation, and binding free energy of the complexes was calculated based on the molecular mechanics/Poisson–Boltzmann surface area (MMPBSA) (Homeyer & Gohlke, 2012) using g_mmpbsa package (Kumari, Kumar, Open Source Drug Discovery Consortium, & Lynn, 2014) installed in GROMACS during the last 3 ns. The value of dielectric constant for the solute used in the energy calculations was $\epsilon_{in} = 1$.

2.5. Molecular similarity analysis

To find the molecular similarity between the proposed molecules and the reported compounds with biological activity on AKT, it was necessary to download from ChEMBL server (Bento et al., 2014) the database of molecules assayed on AKT. The comparison between proposed molecules in this work and ChEMBL database was carried out with DataWarrior (Sander et al., 2015) using FragFp and PathFp.

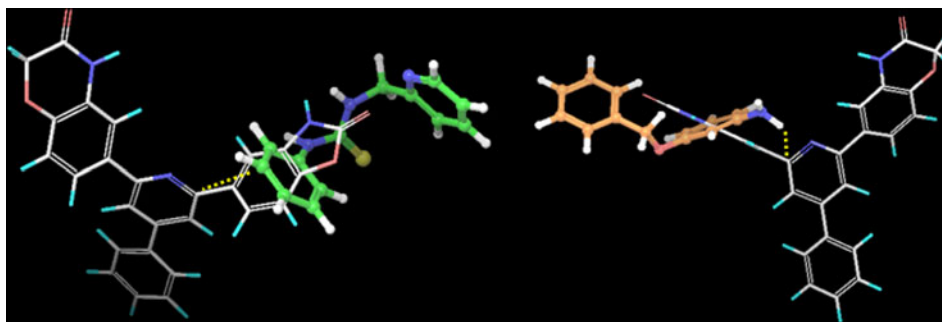


Figure 2. F125 (green) and F126 (orange) overlapped on 1.

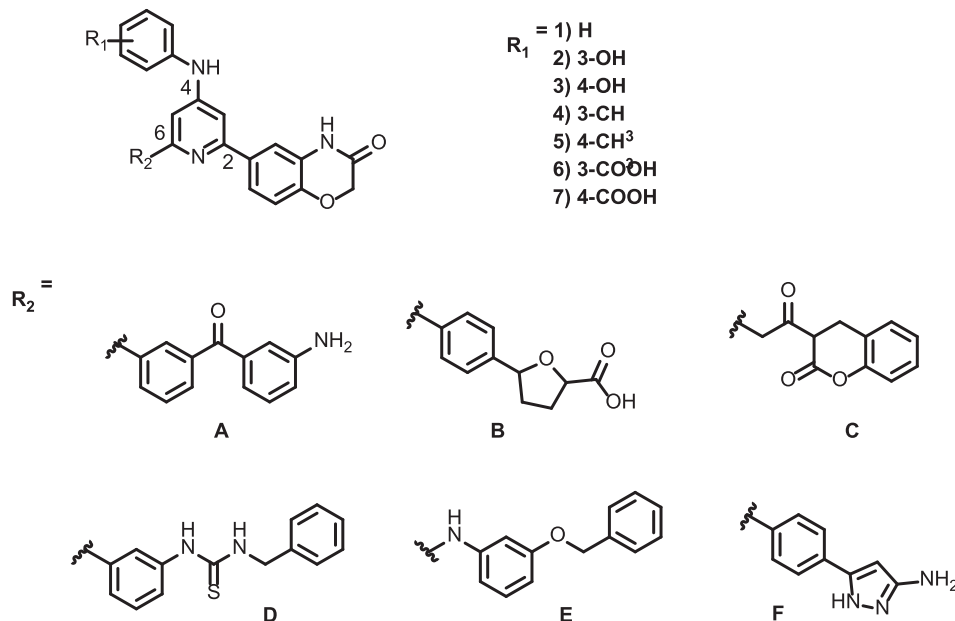


Figure 3. Positions of the pyridine substituents and proposed series obtained through fragment-based docking.

Tanimoto coefficient was used as molecular similarity parameter.

3. Results and discussion

3.1. Structure-based design

In this research, we propose a variant of fragment-based docking that can be helpful for an *in silico* hit optimization; the main idea is to find new fragments with good score values in molecular docking and good overlapping on the pyridine scaffold and propose new substitutions. The first step in our structure-based design was to analyze the MayBridge database and remove the fragments with groups that can provide an unacceptable toxicity (e.g. nitrile, epoxide or halogen groups) and fragments with a molecular weight greater than 250 g/mol; the purpose of this analysis was to substitute a 2*H*-benzo[*b*][1,4]oxazin-3(4*H*)-one system, and big fragments are no suitable for this aim. As a result, 141 fragments were selected. We carried out a fragment docking and selected the best 10 fragments for proposing new modifications at position six of compound 1. The best 10 fragments are listed in Table 1; the selection was made considering the score value in the docking study.

We overlapped each fragment on compound 1 in ATP binding site as shown in Figure 2. In cases where fragments have good overlapping, we proposed new links from position six of the pyridine to the closest atom of the fragment. F16, F40, F111, F125, F126 and F61 showed favorable overlapping on pyridine scaffold. These results led us to propose six new series (A–F) of pyridines 2,4,6-trisubstituted.

Additionally, with the aim of keeping the amine group at position four and to determine what kind of chemical group promotes a better interaction in the ATP binding site of the AKT, we proposed a series of anilines 3- or 4-substituted with a hydrogen donor group (–OH), hydrogen acceptor group (–COOH) and hydrophobic group (–CH₃). Finally, mixing proposed substitution, we create a database of 42 compounds to evaluate on AKT; the complete series subjected to this study is shown in Figure 3.

Fragments C and E, with electron-releasing capacity, increase the p*K*_a of the pyridine ring and thus protonate the nitrogen atom; especially, in those cases where *R*¹ is an electron-releasing group. Protonated and non-protonated pyridines can be possible in molecules with electron-withdrawing groups (*R*¹ in 6 and 7 is COOH). In this way, we evaluated the influence of the protonated pyridines in the stability and binding energy on AKT.

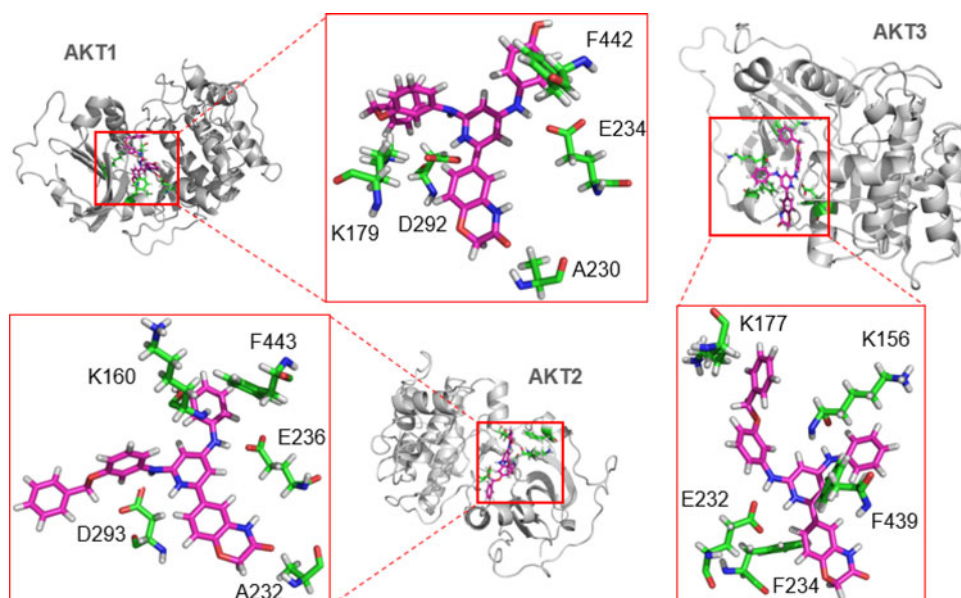


Figure 4. Structure of some compounds of series E docked in AKT1/AKT2/AKT3.

3.2. Molecular docking

After proposing a new database, we carried out molecular docking using Glide XP and Autodock 4.2. The reason to use two programs is the differences in the searching algorithm for each one; Glide uses a hierarchical filter where ligands are submitted a series of steps before to be evaluated in the searching site, and this feature avoids a stochastic method of conformational search (Friesner et al., 2004), while Autodock 4.2. starts with stochastic conformations, and using a genetic algorithm, the energy of each conformation is evaluated in the searching site. The main idea is that if two programs with different scoring functions find the same ligands as the most promising, it is possible to suggest those ligands as good candidates for further studies. The analysis of the molecular docking results for each AKT isoform revealed that the series with fragment 3-(benzyloxy)aniline (E) displays the best docking score value in all isoforms. This is due to protonated pyridine interacts with the anionic residues as Asp292/293 in AKT1/AKT2 and Glu232 in AKT3 binding pocket. Moreover, the amino group at position four aids the interaction with anionic residues as Glu234/236 in AKT1/AKT2 and backbone of Lys156 in AKT3; besides, π - π staking interactions are detected with Phe442/443/439 (Figure 4).

Additionally, molecules with fragment (3-aminophenyl)(-phenyl)methanone (A), especially with a methyl group in R^1 , showed good score values in AKT1. Derivatives with fragment A interact with crucial amino acid residues in ATP binding pocket such as Glu234, Asp274, Ala230, Lys179 and Phe442. While compounds constructed π - π stacking interaction with Phe442, hydrogen-bonding interactions appear with Glu234, Asp274, Ala230 and Lys179. With respect to AKT2, derivatives with fragment 1-phenyl-3-(pyridin-2-ylmethyl)thiourea (D) show satisfactory score values; nevertheless, these compounds just display π - π stacking interactions with Phe163 and Phe238. Additionally, molecules with fragment 3-acetylchroman-2-one (C) exhibit favorable score values on AKT3 isoform; these compounds present hydrogen-bonding

interactions with Glu232, constructed cation- π interaction with Lys177, Lys233 and Phe234 and establish π - π stacking interaction with Phe234. On the other hand, using the consensus score analysis, we found that the series with fragments B and F shows the worst score values in all studies; this finding led us to discard these series for MD simulations. Furthermore, compounds **6A**, **6D**, **7A** and **7D** display unfavorable score values in three AKT isoforms due to unfavorable interaction between carboxylate group on substituent at position four and Phe442/443/439; hence, these compounds were also discarded.

Finally, 24 compounds displayed a consensus score value higher than one with at least two AKT isoforms. For this reason, we selected these compounds for MD simulations with each AKT isoform to analyze their behavior in binding site, calculate the binding free energy of the complexes and evaluate selectivity toward one isoform. In the cases of compounds **6C**, **6E**, **7C** and **7E**, where protonated and non-protonated pyridines were possible, we chose the state with the best docking score value for MD study. Table 2 shows results of molecular docking studies, and compounds selected for MD simulations are highlighted in gray.

3.3. MD simulations

Stability of molecular docking complexes was verified by 10 ns of MD simulations of each compound in the three AKT isoforms. The dynamic stability of each protein-ligand complex was evaluated using RMSD values. For a clear visualization, we separated the ligands in protonated pyridines and non-protonated pyridines series (Figure 5). In the case of AKT1, compounds **1A**, **1D**, **1E**, **2C**, **2D**, **2E**, **5C** and **6E** show satisfactory behavior, since these molecules maintain their deviation below 0.3 nm, while ligands **1C**, **2A**, **3A**, **3C**, **4E** and **5E** have fluctuations above 0.4 nm, especially compounds **2A**, **4E** and **5E**. For AKT2, compounds exhibit the lowest values (0.05–0.7 nm); however, compounds **1D**, **1E**,

Table 2. Docking score values: consensus score is the average of ligand score values of each program divided by the GSK690693 score of each program.

Ligands	AKT1					AKT2					AKT3				
	Score AD 4.2	Score AD 4.2/GSK690693	Score Glide XP	Score Glide/GSK690693	Consensus score	Score AD 4.2	Score AD 4.2/GSK690693	Score Glide XP	Score Glide/GSK690693	Consensus score	Score AD 4.2	Score AD 4.2/GSK690693	Score Glide XP	Score Glide/GSK690693	Consensus score
1A	-8.51	1.05	-6.17	1.53	1.29	-9.06	1.20	-6.82	1.13	1.17	-5.8	0.81	-3.9	0.80	0.80
1B	-9.08	1.12	-3.8	0.94	1.03	-8.04	1.07	-5.35	0.89	0.98	-6.75	0.95	-2.5	0.51	0.73
1C	-10.67	1.31	-5.04	1.25	1.28	-8.56	1.14	-6.12	1.02	1.08	-8.26	1.16	-4.38	0.89	1.03
1D	-10.19	1.25	-6.08	1.50	1.38	-11.51	1.53	-6.36	1.06	1.29	-8.42	1.18	-4.19	0.86	1.02
1E	-10.68	1.31	-7.22	1.79	1.55	-9.77	1.30	-8.1	1.35	1.29	-9.17	1.29	-3.92	0.80	1.04
1F	-9.35	1.15	-3.69	0.91	1.03	-8.22	1.09	-4.38	0.73	0.91	-6.92	0.97	-3.48	0.71	0.84
2A	-6.95	0.85	-6.52	1.61	1.23	-8.72	1.16	-7.51	1.25	1.20	-7	0.98	-4.69	0.96	0.97
2B	-9.02	1.11	-3.01	0.75	0.93	-8.4	1.12	-5.67	0.94	1.03	-5.97	0.84	-4.54	0.93	0.88
2C	-8.78	1.08	-6.45	1.60	1.34	-9.66	1.28	-7.12	1.18	1.23	-7.45	1.04	-5.04	1.03	1.04
2D	-7.76	0.95	-6.14	1.52	1.24	-10.16	1.35	-7.18	1.19	1.27	-7.23	1.01	-4.78	0.98	0.99
2E	-7.93	0.98	-7.82	1.94	1.46	-9.7	1.29	-8.65	1.44	1.36	-6.3	0.88	-4.22	0.86	0.87
2F	-9.12	1.12	-3.33	0.82	0.97	-7.75	1.03	-4.75	0.79	0.91	-5.91	0.83	-4.5	0.92	0.87
3A	-8.59	1.06	-7.13	1.76	1.41	-9.06	1.20	-6.91	1.15	1.18	-6.96	0.98	-4.24	0.87	0.92
3B	-8.27	1.02	-4.77	1.18	1.10	-8.28	1.10	-4.22	0.70	0.90	-7.1	1.00	-3.64	0.74	0.87
3C	-9.37	1.15	-5.92	1.47	1.31	-8.95	1.19	-5.55	0.92	1.06	-6.69	0.94	-5.71	1.17	1.05
3D	-8.65	1.06	-5.29	1.31	1.19	-10.12	1.35	-6.47	1.08	1.21	-6.2	0.87	-4.96	1.01	0.94
3E	-8.43	1.04	-8.05	1.99	1.51	-9.31	1.24	-5.87	0.98	1.11	-8.76	1.23	-5.03	1.03	1.13
3F	-8.7	1.07	-5.12	1.27	1.17	-8.26	1.10	-5.37	0.89	1.00	-5.99	0.84	-4.37	0.89	0.87
4A	-9.19	1.13	-7.42	1.84	1.48	-9.66	1.28	-7.23	1.20	1.24	-6.86	0.96	-4.12	0.84	0.90
4B	-9.43	1.16	-3.86	0.96	1.06	-7.33	0.97	-4.4	0.73	0.85	-7.05	0.99	-3.7	0.76	0.87
4C	-10.62	1.31	-6.49	1.61	1.46	-10.23	1.36	-6.65	1.11	1.23	-6.94	0.97	-4.41	0.90	0.94
4D	-9.28	1.14	-5.95	1.47	1.31	-10.67	1.42	-6.98	1.16	1.29	-7.02	0.98	-4.55	0.93	0.96
4E	-10.59	1.30	-6.68	1.65	1.48	-10.95	1.46	-8.81	1.47	1.46	-8.74	1.23	-4.76	0.97	1.10
4F	-9.6	1.18	-3.88	0.96	1.07	-8.95	1.19	-4.8	0.80	0.99	-6.4	0.90	-3.68	0.75	0.82
5A	-9.51	1.17	-7.3	1.81	1.49	-9.02	1.20	-7.07	1.18	1.19	-7.66	1.07	-4.36	0.89	0.98
5B	-9.16	1.13	-4.46	1.10	1.12	-7.62	1.01	-3.91	0.65	0.83	-7.18	1.01	-3.09	0.63	0.82
5C	-8.54	1.05	-5.12	1.27	1.16	-8.87	1.18	-6	1.00	1.09	-7.14	1.00	-4.14	0.84	0.92
5D	-8.01	0.99	-5.35	1.32	1.15	-11.57	1.54	-6.95	1.16	1.35	-7.17	1.01	-4.95	1.01	1.01
5E	-10.54	1.30	-5.24	1.30	1.30	-9.68	1.29	-7.58	1.26	1.27	-7.51	1.05	-4.37	0.89	0.97
5F	-8.95	1.10	-3.27	0.81	0.96	-8.18	1.09	-4.55	0.76	0.92	-6.13	0.86	-3.38	0.69	0.77
6A	-8.44	1.04	-4.72	1.17	1.10	-8.45	1.12	-5.59	0.93	1.03	-6	0.84	-3.51	0.72	0.78
6B	-7.77	0.96	-1.26	0.31	0.63	-7.39	0.98	-3.12	0.52	0.75	-6.58	0.92	-3.01	0.61	0.77
6C	-7.56	0.93	-6.29	1.56	1.24	-8.4	1.12	-6.1	1.01	1.07	-6.57	0.92	-5.51	1.12	1.02
6D	-8.7	1.07	0.08	-0.02	0.53	-10.03	1.33	-6.29	1.05	1.19	-6.41	0.90	-4.47	0.91	0.91
6E	-8.52	1.05	-7.76	1.92	1.48	-8.98	1.19	-7.07	1.18	1.19	-7.13	1.00	-5.92	1.21	1.10
6F	-8.61	1.06	-4.28	1.06	1.06	-7.36	0.98	-4.94	0.82	0.90	-6.03	0.85	-3.75	0.77	0.81
7A	-7.24	0.89	-5.98	1.48	1.19	-8.12	1.08	-5.31	1.02	1.05	-6.11	0.87	-4.11	0.84	0.79
7B	-7.3	0.90	-5.67	1.40	1.15	-6.86	0.91	-5.91	0.98	0.95	-6.17	0.87	-3.97	0.81	0.84
7C	-9.4	1.16	-6.71	1.66	1.41	-6.29	0.84	-6.13	1.02	0.93	-6.27	0.88	-5.68	1.16	1.02
7D	-8	0.98	-4.87	1.21	1.09	-9.31	1.24	-7.38	1.23	1.23	-5.6	0.79	-4.93	1.01	0.90
7E	-8.12	1.00	-6.73	1.67	1.33	-8.67	1.15	-8.38	1.39	1.27	-8.65	1.21	-4.25	0.87	1.04
7F	-6.51	0.80	-3.73	0.92	0.86	-6.53	0.87	-5.02	0.84	0.85	-5.3	0.74	-3.25	0.66	0.70
GSK-690693	-8.13	1.00	-4.04	1.00	1.00	-7.52	1.00	-6.01	1.00	1.00	-7.13	1.00	-4.9	1.00	1.00

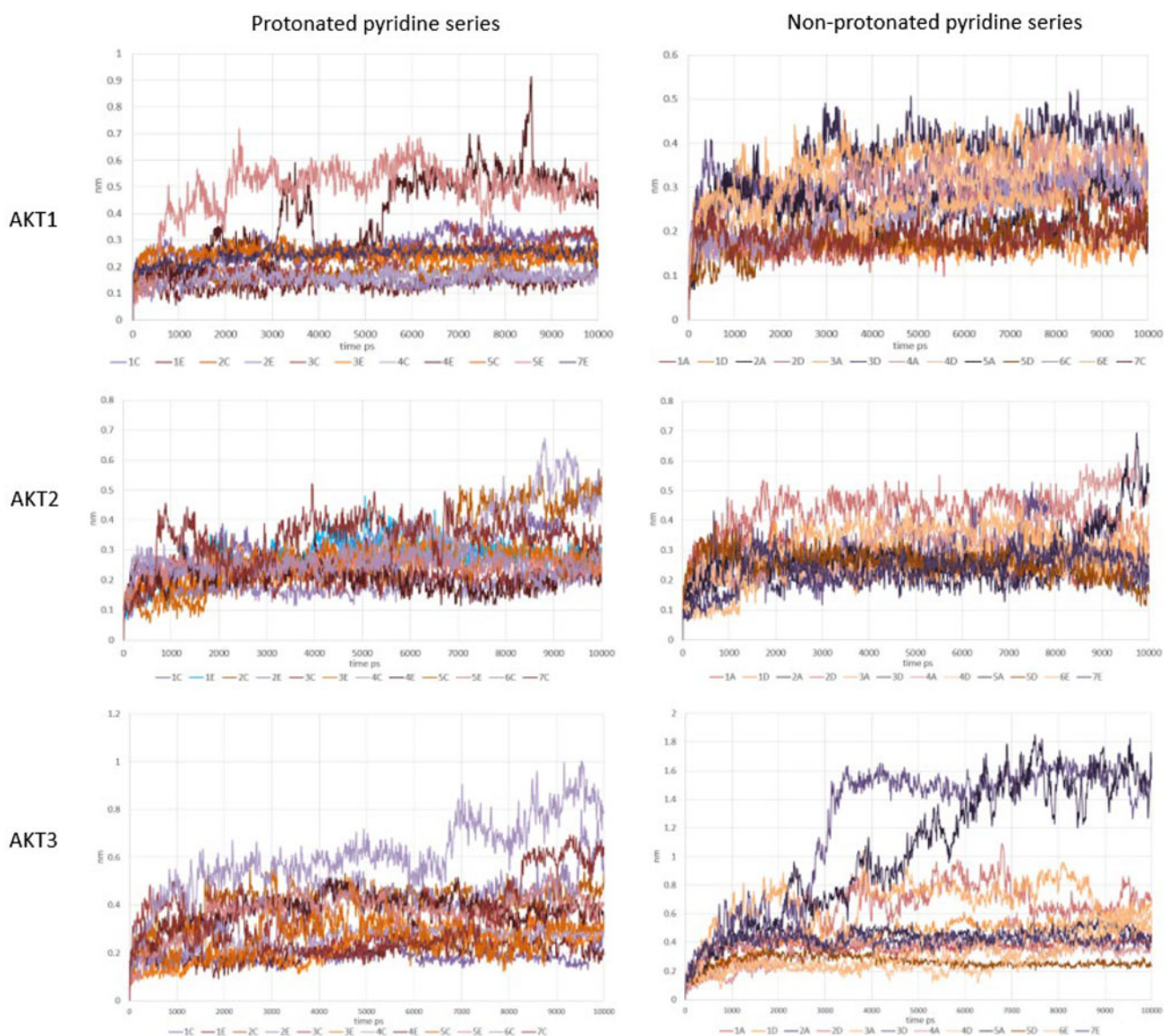


Figure 5. RMSD behavior of protonated and non-protonated pyridine series on each AKT isoform.

2A, 2E, 3C, 4D, 4E, 5C, 5D and **5E** display the best values of the series. Finally, AKT3–ligand complexes show the highest deviations, particularly, compounds **3D, 5A** and **6C**, because they reach a value of 1 nm or higher; nevertheless, ligands **1A, 1E, 3C, 4A, 5C** and **5D** exhibit favorable behavior with values of 0.3 nm or lower.

In general, compounds of series E show the most promising behavior in the three AKT isoforms. Stability of series E can be explained by the strong H-bond interaction between protonated pyridine scaffold and Asp292/293/289 for AKT1/AKT2/AKT3; moreover, the amino group at position six intensifies this interaction. The aromatic fragment at position four contributed to the stabilization of this series by interacting with Phe442/443/439. Additionally, the amine group at position four interacts with Glu234/236 AKT1/AKT2; in AKT3 case, this interaction is possible with Glu232 and Glu275, depending on the derivative; however, during MD simulations, interaction with Glu275 in AKT3 is the most conserved (for details of distance between H-donor and H-acceptor, see

supplementary information). Furthermore, fragment 3-(benzyloxy)aniline occupies the P-loop region and stabilizes these compounds due to interaction with Phe161/163/159. Compounds **6E** and **7E** show disadvantageous performance due to unfavorable interactions of the carboxylate group at position four in the ATP binding site. Series A exhibits positive behavior in AKT1; H-bond interactions with Asp292 and Lys179 are the key of the stability in the pocket. In addition, series A exhibits interactions among fragment (3-aminophenyl)(phenyl)methanone with Phe163 and Thr162 in AKT2, and Glu275 and Phe 234 in AKT3; however, these interactions cause loss of the interactions with Glu236/232 for AKT2/AKT3, generating instability on the pocket in these isoforms. Series C and D exhibit good interactions in AKT2. In series C, the main interactions are with Asp293, and these interactions are with the amine group at position four (compounds **2C** and **3C**) and protonated pyridine with compounds **1C, 4C** and **5C**. Compounds **2C** and **3C** occupy the hydrophobic zone with the 3-acetylchroman-2-one fragment,

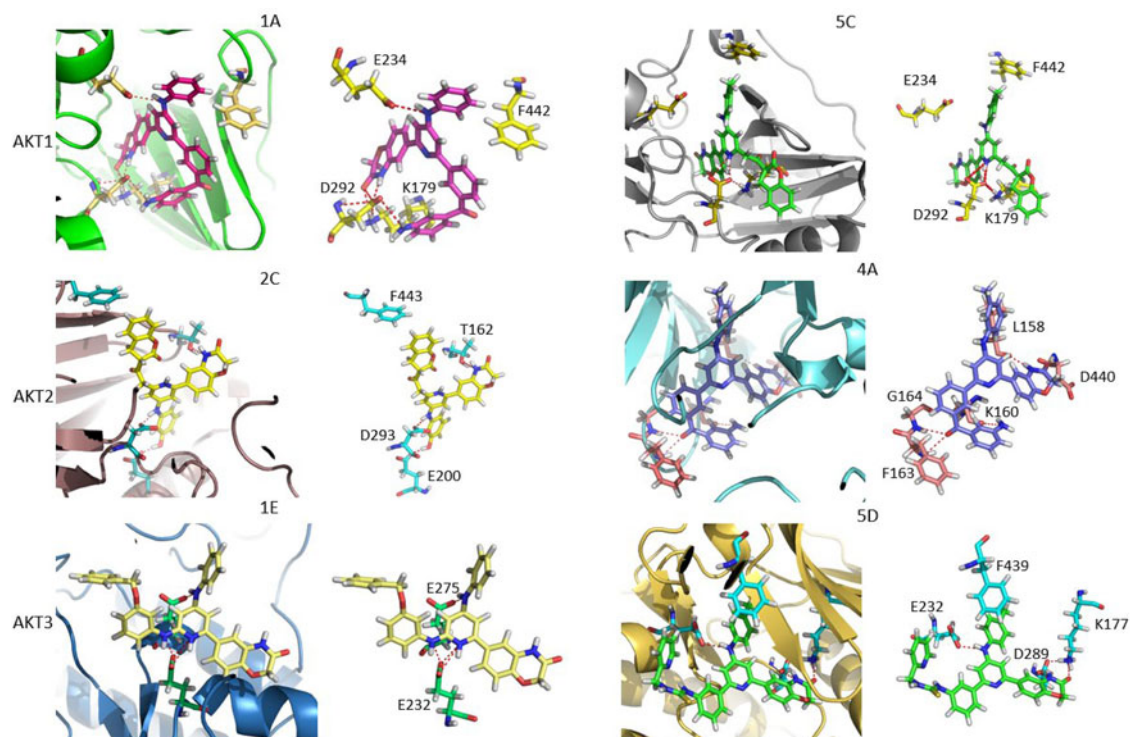


Figure 6. Interactions of selected ligands in the pocket of the three AKT isoforms.

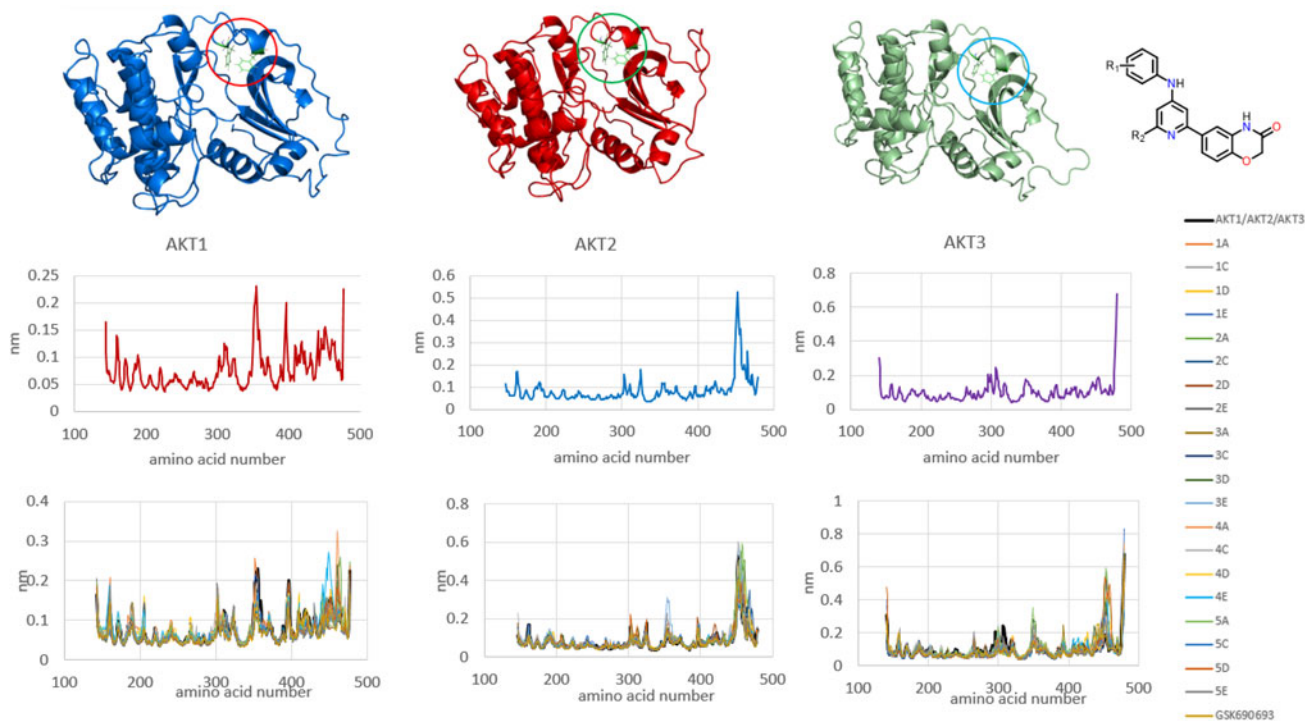


Figure 7. RMSF results of proteins and protein-ligand complexes: zone 1 is highlighted with a circle.

while compounds **1C**, **4C** and **5C** interact in this zone with substituent at position four. Besides, compound **2C** interacts with Glu200 through $-OH$ in AKT2; this interaction is not observed with other compounds. Series D displays good behavior in AKT2 because the fragment 1-phenyl-3-(pyridin-2-ylmethyl)thiourea occupies the P-loop region in AKT2. In AKT3, series C and E display favorable behavior in MD simulations; the main reason for the stability of these series is the

strong interaction between protonated pyridine and Glu232 or Asp289. In addition, series D exhibits unfavorable behaviors with this isoform, since fragment 1-phenyl-3-(pyridin-2-ylmethyl)thiourea unstabilizes the proposed ligands. However, compound **5D** shows an excellent behavior in AKT3 mainly due to interaction between Glu232 and NH of aniline moiety. Figure 6 shows some protonated and non-protonated ligands in ATP binding site.

Table 3. Binding free energy values for protein–ligand complexes.

Protonated compounds*			Non-protonated compounds*				
Ligand	AKT1	AKT2	AKT3	Ligand	AKT1	AKT2	AKT3
1C	-68.2	-111.9	-66.2	1A	-25.5	-12.8	-28.0
1E	-63.3	-120.8	-72.7	1D	-20.8	-23.8	-14.4
2C	-59.7	-125.9	-58.3	2A	-7.2	-26.6	-15.8
2E	-49.4	-109.4	-66.0	2D	-14.3	-20.0	-16.4
3C	-63.7	-119.8	-57.2	3A	-22.7	-25.2	-15.8
3E	-71.9	-108.4	-56.0	3D	-13.3	-14.7	-18.2
4C	-69.1	-112.8	-55.8	4A	-24.8	-29.3	-16.9
4E	-63.8	-121.8	-62.0	4D	-25.4	-25.7	-18.1
5C	-69.4	-120.2	-73.5	5A	-22.5	-27.3	-10.8
5E	-64.0	-122.7	-65.1	5D	-22.4	-27.2	-21.4
6C	-	-33.1	-18.0	6C	25.4	-	-
7C	-	-21.5	-9.4	6E	37.1	70.9	42.7
7E	-18.5	-	-	7C	26.0	-	-
GSK690693	-61.5	-107.8	-75.3	7E	-	62.3	26.4

*Energy values are expressed in kcal/mol.

RMSF analysis shows the highest fluctuations with external residues for AKT1 and AKT3; however, AKT1 displays high fluctuations with Glu355 and Ser396 too, because these amino acids are in contact with the solvent. AKT2 exhibits the highest fluctuations with residues Pro453, Tyr456 and Glu465, since these amino acids are in a coil with high mobility. On the other hand, RMSF analysis of the AKT1–ligand complexes shows that compounds **1A**, **2A**, **2C**, **4A**, **5A**, **5C** and **5E** decrease the fluctuation on zone 1 (see Figure 7). This zone is hydrophobic and has favorable interactions with R^1 of compounds **1A**, **4A**, **5A**, **5C** and **5E**. Compounds **2A** and **2C** interact through H-bond between –OH of R^1 and Asp439, interaction that makes possible the stabilization. Besides, compounds **2C** and **5C** decrease the movement of P-loop through interaction between the backbone of Thr160 and the carbonyl group of 3-acetylchroman-2-one. In the case of AKT2, ligands **1A**, **1C**, **2A**, **2C**, **2D**, **3C**, **3D**, **4C**, **4D**, **4E**, **5C**, **5D** and **5E** reduce the fluctuation of P-loop, but just **1E**, **3A**, **4E**, **5C**, **5D** and **5E** decrease the dynamic of hydrophobic zone 1. The reason for the reduction of the fluctuation is the hydrophobic features of the R^1 group. For AKT3, the lowest values of P-loop fluctuation are found in molecules **1A**, **1E**, **2A**, **4C**, **5C** and **5D**; however, only protonated pyridines with hydrophobic substituents **1E** and **5C** decrease the fluctuations of zone 1 of AKT3.

MMPBSA calculations were implemented for calculating complexes binding free energy (Table 3). Since we used a $\epsilon_i = 1$, it is possible that calculated energy for protonated ligands could have an overestimated value (Hou, Wang, Li, & Wang, 2011); however, our reference (GSK690693) is protonated too, which means that our comparison between protonated pyridines and reference was made with the same conditions; then, it is possible to compare energy results among pyridines and GSK690693. Taking into account that MMPBSA method is accurate with similar structures in similar systems (Homeyer & Gohlke, 2012), we divided the series in protonated and non-protonated compounds.

To begin with, compounds where $R^1 = \text{H}$, 3- CH_3 and 4- CH_3 exhibit good energy values with protonated and non-protonated series. The reason is that these substituents interact with a hydrophobic region rich in phenylalanine residues. Thus, hydrophobic substituents display the best interaction

in this region. Taking as reference the inhibitor GSK690693, compounds **1C**, **3E**, **4C** and **5C** display the best energy values in AKT1, showing at least 7 kcal/mol less than the reference. Talking about AKT2, all protonated pyridines show lower energy values than the reference, but compounds **1E**, **2C**, **4E**, **5C** and **5E** stand out because they have energy values lower than GSK690693 with 12 kcal/mol, or even more. In the case of AKT3, none of the compounds exceeded the energy value of the reference inhibitor; nevertheless, molecules **1E** and **5C** have close energy values with just about 2 kcal/mol of difference. Moreover, compounds **1C** and **2E** display good energy values. It is important to note that molecule **5C** displays good energy values with three AKT isoforms, while compound **2C** exposes selectivity toward AKT2. In general, series C presents preference for AKT1 with exception of **2C**, and series E discloses tendency toward AKT2; in case of AKT3, protonated series do not display a clear preference. For non-protonated series, compound **1A**, **4A** and **4D** exhibit good values for AKT1, while molecules **2A**, **4A**, **5A** and **5D** feature the best values with AKT2, besides compounds **1A** and **5D** present important energy values for AKT3. Energy analysis reinforces the idea that compounds where $R^1 = \text{H}$, 3- CH_3 and 4- CH_3 exhibit the best behavior in AKT pocket because they display favorable interactions between substituent at position four and the zone rich in phenylalanine. Nevertheless, compounds **2C** and **2A** show interesting profiles in AKT2; this finding leads to propose that a substituent H-donor on R^1 could display selectivity against AKT2. Additionally, compounds **6C**, **6E**, **7C** and **7E** exhibit the worst binding energy values with both protonated and non-protonated series. We can conclude that $R^1 = \text{carboxylate}$ group displays instability and unfavorable free binding energy in the ATP pocket. In Figure 8, we can see that carboxylate group is out of hydrophobic zone due to the repulsion interaction between them.

Gathering the analysis of RMSD, RMSF and energy values, compounds **4A** and **4C** show a promising profile as AKT1 inhibitors. On the other hand, compounds **4E** and **5E** show meaningful values in AKT2; this finding reinforces the idea that series E exhibits an interesting preference on AKT2; however, compound **2C** shows an attractive profile against AKT2, especially for its high free binding energy value and its different conformation and interactions in the binding site. In addition, compound **1A** shows an attractive selectivity toward AKT1 and AKT3, while compounds **1E** and **5D** show good values on AKT2 and AKT3; it is necessarily highlighted that compound **5D** is the only one that is able to conserve the main interactions discussed in the present work in the AKT3 pocket. Finally, compound **5C** displays a pan-inhibitor profile since it exhibits good values in the three isoforms.

In summary, compounds with hydrophobic substituents in R^1 and protonated pyridines display the best behavior due to favorable stabilization on the AKT pocket; moreover, ligands with –OH at position three of the aniline moiety show better interactions and less fluctuation than –OH at position four, especially in AKT2, so that H-bond donor in R^1 could display selectivity toward AKT2. In spite of the favorable energy values of series A in the three isoforms, the loss

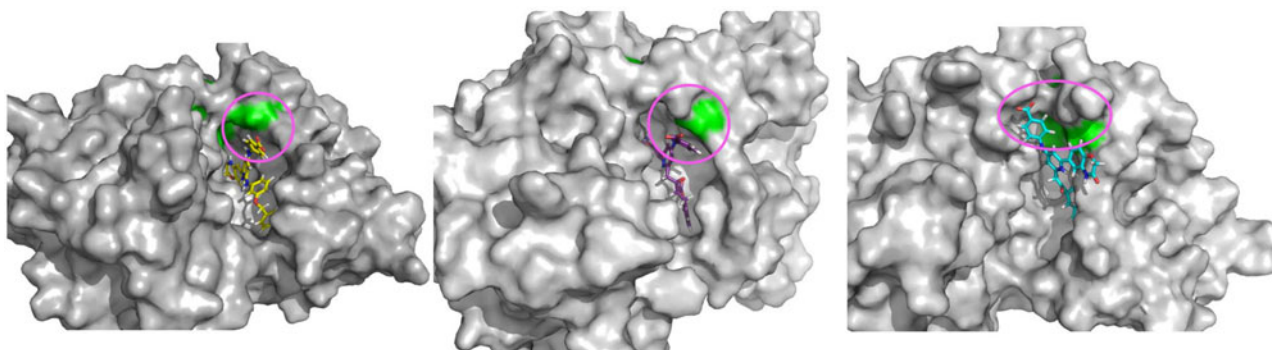


Figure 8. Compounds 7E, 6C and 7C in binding pocket of AKT1/AKT2/AKT3, respectively: we can see that carboxylate group is out of the hydrophobic zone highlighted in green.

of the stability in AKT2 and AKT3 leads us to propose that compounds with fragment (3-aminophenyl)(phenyl)methanone at position six of the pyridine could remain for more time in the AKT1 pocket and exhibit selectivity toward this isoform, with exception of **1A**. Additionally, ligands with fragment 3-(benzyloxy)aniline (series E) expose a clear tendency toward AKT2, mainly where R^1 is a methyl group.

3.4. Molecular similarity analysis

Database of compounds assayed against AKT from ChEMBL server includes >6000 compounds. Using DataWarrior, we compared the proposed compounds with ChEMBL database using FragFP and Pathfp descriptors included in the program. Analysis of molecular similarity was made using Tanimoto coefficient. In this sense, first, we carried out the similarity search using a Tanimoto coefficient of 0.9, because this value is considered good for structural similarity (<http://www.openmolecules.org/help/chemistry.html>, 2018); however, in this research, we did not find similarity between proposed molecules and assayed compounds. Then, we decreased the similarity value to a Tanimoto coefficient of 0.6 and found that about 4% of the database have similarity with our proposed compounds. Additionally, we compared our database against the ChEMBL compounds with $IC_{50} < 1 \mu\text{M}$ (about 2000 molecules) using the same Tanimoto coefficient (0.6). Analysis of the similarity between proposed molecules and reported compounds with a good value of activity showed that about 1% of the active compounds have similarity with our database. These findings and *in silico* results indicate that our proposed compounds are different from the previously reported inhibitors and could be of interest as new inhibitors of AKT (for molecular similarity details, see [supplementary information](#)).

4. Conclusion

The variant of fragment-based docking used in a hit optimization processes is a useful methodology to find new substitutions with high structural diversity. Such as at the present work, combining this methodology with modifications reported in previous works, it was possible to design a database of 42 compounds. As a result of the *in silico* analysis, we identified structural requirements to improve the affinity of the 2,4,6-trisubstituted pyridine scaffold in the ATP pocket of PKB/AKT. Among these,

we must highlight the importance of a system with a pK_a value able to be protonated at physiological pH and make favorable interactions with residues as glutamate or aspartate in ATP binding site. Besides, the hydrophobic substituents at position four that could interact with the hinge rich in phenylalanine are important. In addition, the reported idea about an H-bond donor adequate to interact with Glu234/236/232 and make an additional favorable interaction was supported. Finally, we identified a group of compounds not previously reported with high structural diversity and high selectivity profiles toward AKT1 and AKT2, as well as compounds with selectivity for two of the three isoforms. Results of this study can be useful for the design and development of new AKT inhibitors.

Acknowledgements

The authors acknowledge DGESCA for the use of the supercomputer Miztli in project LANCAD-UNAM-DGTIC-285. The authors thank Dr. Antonio Romo-Mancillas for his valuable contributions to this work.

Disclosure statement

No potential conflict of interest was reported by the authors.

Funding

The authors thank CONACyT for the financial support granted to the project [CB-251807]. EESC and IBC are grateful to CONACyT for the fellowships granted [Nos. 273595 and 521238], respectively.

ORCID

Rafael Castillo  <http://orcid.org/0000-0003-4466-2340>

References

- Addie, M., Ballard, P., Buttar, D., Crafter, C., Currie, G., Davies, B. R., ... Ruston, L. (2013). Discovery of 4-amino-N-[(1S)-1-(4-chlorophenyl)-3-hydroxypropyl]-1-(7H-pyrrolo[2,3-d]pyrimidin-4-yl)piperidine-4-carboxamide (AZD5363), an orally bioavailable, potent inhibitor of Akt kinases. *Journal of Medicinal Chemistry*, 56(5), 2059–2073.
- Benkert, P., Biasini, M., & Schwede, T. (2011). Toward the estimation of the absolute quality of individual protein structure models. *Bioinformatics*, 27(3), 343–350.

- Bento, A. P., Gaulton, A., Hersey, A., Bellis, L. J., Chambers, J., Davies, M., ... Overington, J. P. (2014). The ChEMBL bioactivity database: An update. *Nucleic Acids Research*, 42(D1), 1083–1090.
- Berendsen, H., Postma, J., Van-Gunsteren, W., DiNola, A., & Haak, J. (1984). Molecular dynamics with coupling to an external bath. *Journal of Chemical Physics*, 81(8), 3684–3690.
- Best, R., & Hummer, G. (2009). Optimized molecular dynamics force fields applied to the helix–coil transition of polypeptides. *Journal of Physical Chemistry B*, 113(26), 9004–9015.
- Biasini, M., Bienert, S., Waterhouse, A., Arnold, K., Studer, G., Schmidt, T., ... Schwede, T. (2014). SWISS-MODEL: Modelling protein tertiary and quaternary structure using evolutionary information. *Nucleic Acids Research*, 42(W1), W252–W258.
- Chen, V. B., Arendall 3rd, W. B., Headd, J. J., Keedy, D. A., Immormino, R. M., Kapral, G. J., ... Richardson, D. C. (2010). MolProbity: All-atom structure validation for macromolecular crystallography. *Acta Crystallographica Section D Biological Crystallography*, D66(1), 12–21.
- DataWarrior User Manual. (2018). Retrieved May 5, 2018, from <http://www.openmolecules.org/help/chemistry.html>
- Davis, I. W., Leaver-Fay, A., Chen, V. B., Block, J. N., Kapral, G. J., Wang, X., ... Richardson, D. C. (2007). MolProbity: All-atom contacts and structure validation for proteins and nucleic acids. *Nucleic Acids Research*, 35(Web Server), W375–W383.
- Fogh, R. H., Boucher, W., Vranken, W. F., Pajon, A., Stevens, T. J., Bhat, T. N., ... Laue, E. D. (2005). A framework for scientific data modeling and automated software development. *Bioinformatics*, 21(8), 1678–1684.
- Friesner, R. A., Banks, J. L., Murphy, R. B., Halgren, T. A., Klicic, J. J., Mainz, D. T., ... Shenkin, P. S. (2004). Glide: A new approach for rapid, accurate docking and scoring. 1. Method and assessment of docking accuracy. *Journal of Medicinal Chemistry*, 47(7), 1739–1749.
- Hennessy, B. T., Smith, D. L., Ram, P. T., Lu, Y., & Mills, G. B. (2005). Exploiting the PI3K/AKT pathway for cancer drug discovery. *Nature Reviews. Drug Discovery*, 4(12), 988–1004.
- Hernández-Campos, A., Velázquez-Martínez, I., Castillo, R., López-Vallejo, F., Jia, P., Yu, Y., ... Medina-Franco, J. (2010). Docking of protein kinase B inhibitors: Implications in the structure-based optimization of a novel scaffold. *Chemical Biology & Drug Design*, 76(3), 269–276.
- Homeyer, N., & Gohlke, H. (2012). Free energy calculations by the molecular mechanics Poisson–Boltzmann surface area method. *Molecular Informatics*, 31(2), 114–122.
- Hornak, V., Abel, R., Okur, A., Strockbine, B., Roitberg, A., & Simmerling, C. (2006). Comparison of multiple Amber force fields and development of improved protein backbone parameters. *PROTEINS: Structure, Function, and Bioinformatics*, 65(3), 712–725.
- Hou, T., Wang, J., Li, Y., & Wang, W. (2011). Assessing the performance of the MM/PBSA and MM/GBSA methods: I. The accuracy of binding free energy calculations based on molecular dynamics simulations. *Journal of Chemical Information and Modeling*, 51(1), 69–82.
- Huck, B., & Mochalkin, I. (2017). Recent progress towards clinically relevant ATP-competitive Akt inhibitors. *Bioorganic & Medicinal Chemistry Letters*, 27(13), 2838–2848.
- Jorgensen, W. L., Chandrasekhar, J., Madura, J. D., Impey, R. W., & Klein, M. L. (1983). Comparison of simple potential functions for simulating liquid water. *Journal of Chemical Physics*, 79(2), 926–935.
- Kumari, R., Kumar, R., Open Source Drug Discovery Consortium., & Lynn, A. (2014). *g_mmpbsa* – A GROMACS tool for high-throughput MM-PBSA calculations. *Journal of Chemical Information and Modeling*, 54(7), 1951–1962.
- Liby, T. A., Spyropoulos, P., Buff Lindner, H., Eldridge, J., Beeson, C., Hsu, T., & Muise-Helmericks, R. C. (2012). Akt3 controls vascular endothelial growth factor secretion and angiogenesis in ovarian cancer cells. *International Journal of Cancer*, 130(3), 532–543.
- Lindorff-Larsen, K., Piana, S., Palmo, K., Maragakis, P., Klepeis, J. L., Dror, R. O., & Shaw, D. E. (2010). Improved side-chain torsion potentials for the Amber ff99SB protein force field. *PROTEINS: Structure, Function, and Bioinformatics*, 78(8), 1950–1958.
- Liu, J., Chen, X., Ward, T., Pegram, M., & Shen, K. (2016). Combined niclosamide with cisplatin inhibits epithelial-mesenchymal transition and tumor growth in cisplatin-resistant triple-negative breast cancer. *Tumor Biology*, 37(7), 9825–9835.
- Liu, L., & Dong, X. (2014). Complex impacts of PI3K/AKT inhibitors to androgen receptor gene expression in prostate cancer cells. *PLoS One*, 9(10), e108780.
- Ma, L., Fu, Q., Xu, B., Zhou, H., Gao, J., Shao, X., ... Lyu, J. (2018). Breast cancer-associated mitochondrial DNA haplogroup promotes neoplastic growth via ROS-mediated AKT activation. *International Journal of Cancer*, 142(9), 1786–1796.
- Manning, B., & Cantley, L. (2007). AKT/PKB signaling: Navigating downstream. *Cell*, 129(7), 1262–1274.
- Medina-Franco, J., Giulianotti, M. A., Yu, Y., Shen, L., Yao, L., & Singh, N. (2009). Discovery of a novel protein kinase B inhibitor by structure-based virtual screening. *Bioorganic & Medicinal Chemistry Letters*, 19(16), 4634–4638.
- Millis, S. Z., Ikeda, S., Reddy, S., Gatalica, Z., & Kurzrock, R. (2016). Landscape of phosphatidylinositol-3-kinase pathway alterations across 19 784 diverse solid tumors. *JAMA Oncology*, 2(12), 1565–1573.
- Morris, G. M., Huey, R., Lindstrom, W., Sanner, M. F., Belew, R. K., Goodsell, D. S., & Olson, A. J. (2009). AutoDock4 and AutoDockTools4: Automated docking with selective receptor flexibility. *Journal of Computational Chemistry*, 30(16), 2785–2791.
- Nilges, M., Bernard, A., Bardiaux, B., Malliavin, T., Habeck, M., & Rieping, W. (2008). Accurate NMR structures through minimization of an extended hybrid energy. *Structure*, 16(9), 1305–1312.
- Parrinello, M., & Rahman, A. (1980). Crystal structure and pair potentials: A molecular-dynamics study. *Physical Review Letters*, 45(14), 1196–1199.
- Rieping, W., Habeck, M., Bardiaux, B., Bernard, A., Malliavin, T. E., & Nilges, M. (2007). ARIA2: Automated NOE assignment and data integration in NMR structure calculation. *Bioinformatics*, 23(3), 381–382.
- Šali, A., & Blundell, T. L. (1993). Comparative protein modelling by satisfaction of spatial restraints. *Journal of Molecular Biology*, 234(3), 779–815.
- Sander, T., Freyss, J., von Korff, M., & Rufener, C. (2015). DataWarrior: An open-source program for chemistry aware data visualization and analysis. *Journal of Chemical Information and Modeling*, 55(2), 460–473.
- Sanner, M. F. (1999). Python: A programming language for software integration and development. *Journal of Molecular Graphics & Modelling*, 17(1), 57–61.
- Schrödinger release 2015-4. (2015). *Glide version 6.9*. New York, NY: Schrödinger, LLC.
- Schrödinger release 2015-4. (2015). *Maestro version 10.4*. New York, NY: Schrödinger, LLC.
- Schrödinger release 2015-4. (2015). *Prime version 4.2*. New York, NY: Schrödinger, LLC.
- Schrödinger release 2015-4. (2015). *Protein Preparation Wizard; Epik version 3.4*. New York, NY: Schrödinger, LLC.
- Sousa Da Silva, A., & Vranken, W. F. (2012). ACPYPE – AnteChamber Python Parser interface. *BMC Research Notes*, 5(1), 367.
- Testa, J. R., & Tschlis, P. N. (2005). AKT signaling in normal and malignant cells. *Oncogene*, 24(50), 7391–7393.
- The UniProt Consortium. (2016). UniProt: The universal protein knowledgebase. *Nucleic Acids Research*, 45(D1), D158–D169.
- Vranken, W. F., Boucher, W., Stevens, T. J., Fogh, R. H., Pajon, A., Llinas, M., ... Laue, E. D. (2005). The CCPN data model for NMR spectroscopy: Development of a software pipeline. *PROTEINS: Structure, Function, and Bioinformatics*, 59(4), 687–696.
- Wang, J., Wolf, R. M., Caldwell, J. W., Kollman, P. A., & Case, D. A. (2004). Development and testing of a general amber force field. *Journal of Computational Chemistry*, 25(9), 1157–1174.
- Wang, J., Wang, W., Kollman, P. A., & Case, D. A. (2006). Automatic atom type and bond type perception in molecular mechanical calculations. *Journal of Molecular Graphics & Modelling*, 25(2), 247–260.
- Wavefunction Inc. (2010). *Spartan version 10*. Irvine, CA: Wavefunction Inc.
- WHO – Cancer. (2018). Retrieved October 2, 2018, from <http://www.who.int/en/news-room/fact-sheets/detail/cancer>
- Yang, J., Cron, P., Good, V. M., Thompson, V., Hemmings, B. A., & Barford, D. (2002). Crystal structure of an activated Akt/protein kinase B ternary complex with GSK3-peptide and AMP-PNP. *Nature Structural & Molecular Biology*, 9, 940–944.
- Zhu, L., Derijard, B., Chakrabandhu, K., Wang, B. S., Chen, H. Z., & Hueber, A. O. (2014). Synergism of PI3K/Akt inhibition and Fas activation on colon cancer cell death. *Cancer Letters*, 354(2), 355–364.

Article

Utility of Milk Coagulant Enzyme of *Moringa oleifera* Seed in Cheese Production from Soy and Skim Milks

María Alejandra Sánchez-Muñoz ¹, Mónica Andrea Valdez-Solana ¹, Claudia Avitia-Domínguez ², Patricia Ramírez-Baca ¹, María Guadalupe Candelas-Cadillo ¹, Miguel Aguilera-Ortiz ¹, Jorge Armando Meza-Velázquez ¹, Alfredo Téllez-Valencia ² and Erick Sierra-Campos ^{1,*}

¹ Facultad de Ciencias Químicas, Universidad Juárez del Estado de Durango, Av. Artículo 123 S/N Fracc. Filadelfia, Gómez Palacio, Durango, CP 35010, Mexico; airama33@gmail.com (M.A.S.-M.); valdezandyval@gmail.com (M.A.V.-S.); ramirezbp2000@hotmail.com (P.R.-B.); candelascadillo@gmail.com (M.G.C.-C.); maguilerao@hotmail.com (M.A.-O.); jorgemezav68@gmail.com (J.A.M.-V.)

² Facultad de Medicina y Nutrición, Universidad Juárez del Estado de Durango, Av. Universidad y Fanny Anitua S/N Col. Centro, Durango, Dgo, CP 34000, Mexico; avitiaclaudia@gmail.com (C.A.-D.); tellezalfredo@gmail.com (A.T.-V.)

* Correspondence: ericksier@gmail.com; Tel./Fax: +52-871-715-8810

Received: 31 May 2017; Accepted: 2 August 2017; Published: 5 August 2017

Abstract: In this study, the potential use of *Moringa oleifera* as a clotting agent of different types of milk (whole, skim, and soy milk) was investigated. *M. oleifera* seed extract showed high milk-clotting activity followed by flower extract. Specific clotting activity of seed extract was 200 times higher than that of flower extract. Seed extract is composed by four main protein bands (43.6, 32.2, 19.4, and 16.3 kDa). Caseinolytic activity assessed by sodium dodecyl sulphate-polyacrylamide gel electrophoresis (SDS-PAGE) and tyrosine quantification, showed a high extent of casein degradation using *M. oleifera* seed extract. Milk soy cheese was soft and creamy, while skim milk cheese was hard and crumbly. According to these results, it is concluded that seed extract of *M. oleifera* generates suitable milk clotting activity for cheesemaking. To our knowledge, this study is the first to report comparative data of *M. oleifera* milk clotting activity between different types of soy milk.

Keywords: soy milk; milk-coagulant activity; *Moringa oleifera*; seeds

1. Introduction

Nowadays, foods are intended not only to satisfy hunger and provide necessary nutrients for humans, but to prevent nutrition-related diseases and improve consumers' physical and mental well-being [1]. Moreover, there is plenty of scientific literature that demonstrates the close connection between diet and health, particularly related to chronic diseases, which have encouraged the development of growing spectrum products such as nutraceuticals, medifoods, and vitafoods [2,3].

In México, data from three national surveys conducted in 1988, 1999, and 2006, using the International Obesity Task Force classification system, described the upward trends on overweight and obesity in school-age children and teenagers at a national level [4]. Besides, increased world population, and the continuous rise of morbid obesity and other nutritional diseases have led to the employment of protein from vegetal sources, along with the preference of low-fat dairy products in consumers from our country. Therefore, people are constantly pursuing better life quality by eating low-fat dairy products which may reduce the risk of stroke or coronary heart disease [5]. Also, the remarkable sales in soy-based products can be attributed to the beneficial health properties of soy-derived foods.

Cheese is a widely consumed product by the general population, it is highly-concentrated, rich in proteins and lipids, essential amino acids, and minerals such as calcium and phosphorus. The first

step in cheesemaking is the milk clotting process where κ -caseinolytic enzymes contribute to micelle aggregation, usually performed by animal rennet, which has been the traditional coagulant in cheese manufacture for centuries [6]. However, dairy products have recently come under fire from researchers showing the detrimental effects of high saturated fat and cholesterol concentrations to the body [7]. Since full-fat dairy products contain more calories, many experts assumed that avoiding them would lower the risk of diabetes. However, some studies have found that yogurt intake, but not milk, is consistently associated with lower incidence of diabetes mellitus. On the other hand, cheese intake, despite the higher calories, fat, and saturated fat content, is also associated with lower diabetes risk in several but not all studies [7–9]. These findings suggest that health effects of dairy products may depend on multiple complex characteristics and represent promising areas for further research [10]. Although the data are controversial, Mexican gastronomy is innovating products (lactose-free, high calcium, and weight-control foods) using vegetables harvested in large amounts in Mexican soil.

Nutritionists have mentioned that the incorporation of bioactive components in dairy products might confer several advantages [11]. For example, phenolic compounds have been extracted from a variety of plant sources and used as matrix food ingredients improving functional properties of dairy products such as storage and heat stability, as well as foaming properties [12,13]. Dairy product enrichment with phenolic compounds has been proposed for beverages [13], yogurt [14], milk powder [15], and processed cheese [16]. Given that polyphenols interact with proteins [17], their addition to milk may result in a high yield recovery in cheese, mainly attributed to hydrophobic and hydrophilic interactions [18] that depend on pH, molar ratio, and molecular properties of the polyphenols [15]. However, recent studies have shown that rennet-induced coagulation is altered by the addition of tea polyphenols to milk [19,20] but in spite of this limitation, cheddar type cheese has been produced from milk enriched with green tea extract [21]. In addition, plant extracts could increase the shelf life of dairy products by inhibiting oxidation of polyunsaturated fatty acids and the development of off-flavor aromas [22].

Yadav et al. [23] stated that soy milk is a well-known protein enriched bio-functional food, but its acceptability is reduced by the presence of complex sugars which give a bean-like flavor. However, it was shown that fermentation produces a reduction of such off-flavor compounds. Hence, soy by-products such as yogurt and cheese can be nutraceutical products with antioxidant potential.

It has been reported that commercial plant proteases, such as bromelain and papain, can clot the protein in soy milk forming a curd [24]. Unfortunately, unlike casein in bovine milk, enzymatic curdling of soy milk produces poor flavor and texture since proteolysis is more pronounced in cheese processed with vegetable coagulants which leads to a soft and buttery cheese texture and, partly, to liquefaction and loss of shape [25,26]. In addition, short peptides produced by its high proteolytic activity affect the flavor, which results in an excessively acidic and bitter cheese [27]. For this reason, the commercial use of bromelain, ficin, and papain to clot soy milk has not been successful [28–30]. However, a more recent study showed that *Saccharomyces bayanus* SCY003 protease produced a soy curd with elasticity that resembles milk-casein cheese [31]. Therefore, it is important to continue the search of proteases with the capability to coagulate soy milk and improve the acceptability of soy cheese.

Moringa oleifera is grown in rural regions of Mexico and its different parts, such as leaves, flowers, and seeds, are edible. It is a source of protein, calcium, iron, carotenoids, and phytochemicals, and it is employed for several applications in developing countries [32]. Previously, it has been reported that *M. oleifera* is an interesting source of milk clotting enzyme. Pontual et al. [33] reported the caseinolytic and milk-clotting activities of *M. oleifera* flowers using azocasein and skim milk as substrates, respectively. *M. oleifera* seed extract was also used as a milk-clotting agent, and the resulting curd was white and firm [34]. Despite the aforementioned studies on milk-clotting enzyme from *M. oleifera*, a deep evaluation of this potential source of a rennet substitute is still absent. In addition, there are no studies that evaluate the efficiency of *M. oleifera* proteases to clot soy milk proteins. Thus, the aim of this research was to determine the potential ability of different parts from *M. oleifera* to

coagulate whole, skim, and soy milks and to investigate the use of *M. oleifera* in the production of soft cheese.

2. Materials and Methods

2.1. Vegetal and Dairy Material

Moringa oleifera seeds, flowers, and leaves were obtained from Lombardia, Michoacán, located at 19°01'30" N and 102°05'39" W. All the samples were dried and crushed at room temperature and stored in closed containers at −20 °C. Commercial cow whole and skimmed milk (Lala® and Carnation®, Nestle®, respectively) and soy milk powders (Soyapac®, Colpac; AdeS®, and Soyalac®) were used to evaluate different parameters related to the milk coagulant enzyme (MCE).

2.2. Enzyme Extraction

Briefly, duplicate samples of 2 g of powder of the different parts of the plant were immersed in 10 mL of 50 mM phosphate buffer, pH 7.0 (1:10; *w/v*), the mixtures were macerated by two methods: traditional stirring for 4 h and ultrasonic bath (42 KHz) for 15 min at room temperature. The extracts were centrifuged at 3500 rpm for 10 min. Finally, the supernatants were stored at 4 °C until used.

2.3. Milk-Clotting Activity (MCA)

The milk-clotting activity was determined following the procedure described by Arima et al. [35] with some modifications. Briefly, a suspension of skim milk powder was used as a substrate with 10 mM CaCl₂, pH 6.5. The milk was previously incubated at 35 °C for 5 min, then MCE was added at a 10:1 ratio (*v/v*, skim milk to enzyme extract). One unit of milk-clotting activity (MCA) is defined as the amount of enzyme to clot 1 mL of a solution containing 0.1 g skim milk powder in 40 min at 35 °C.

The time between the addition and the appearance of clots was registered and the total MCA was calculated as follows:

$$MCA \left(\frac{SU}{mL} \right) = \frac{2400}{Coagulation\ time\ (s)} \times dilution\ factor \quad (1)$$

In order to compare the efficiency of the milk clotting enzyme, rennet from calf stomach (mixture of chymosin and pepsin) from Sigma-Aldrich (Toluca, Mexico) and 5% NaCl were used as the positive and negative controls, respectively. The specific activity was determined by dividing the MCA between protein concentrations of extracts [Soxhlet units (SU)/mg protein].

2.4. Caseinolytic Activity

Caseinolytic activity was measured by Sarath's method [36]. Suitably diluted seed extract solution was added to 2.5 mL of 1% casein dissolved in 50 mM NaH₂PO₄ (pH 6.5). The mixture was incubated at 37 °C for 30 min and then 2.5 mL of 5% trichloroacetic acid solution (TCA) was added. After precipitation, all mixtures were centrifuged at 10,000 rpm for 20 min and the absorbance of the supernatant at 280 nm was registered. The blank sample was prepared in the same way by adding TCA prior to the addition of the substrate. One unit of caseinolytic activity of enzyme was defined as the amount of enzyme that delivers 1 µg of tyrosine (Tyr) and causes a 0.01 increase in absorbance at 280 nm through 1 cm of cuvette path length. Rennet from calf stomach (mixture of chymosin and pepsin) from Sigma-Aldrich and 5% NaCl were used as positive and negative controls, respectively.

2.5. Protein Determination

The protein concentration was determined according to Lowry et al. [37]. A standard curve was generated using bovine serum albumin (10–500 µg/mL) as the standard. Alkaline copper sulphate reagent was added to the different dilutions and sample solutions, which were incubated at room temperature for 10 min. Then, Folin & Ciocalteu's reagent (commercially available, F9252 from

Sigma-Aldrich) was added to each tube and incubated for 30 min. The mixture absorbance was measured using a spectrophotometer (600 nm, Hach DR 5000, USA Hach, Loveland, CO, United States).

2.6. Sodium Dodecyl Sulphate-Polyacrylamide Gel Electrophoresis (SDS-PAGE)

The crude extract from *M. oleifera* seed was characterized by sodium dodecyl sulphate-polyacrylamide gel electrophoresis (SDS-PAGE) [38]. The crude extract was first boiled for 5 min in the presence of SDS and β -mercaptoethanol and 50 μ g/mL of protein concentration was loaded into the gel (5% of stacking gel and 12% of separating gel). SDS-PAGE was run at 120 volts (Miniproteam II cell, Bio-Rad, Hercules, CA, USA) until the bromophenol blue dye marker disappeared from the separating gel. Proteins were stained with Coomassie blue R250 and washed with methanol/acetic acid/water (40:50:10) solution to remove the dye excess. A low molecular weight marker was used in a range of 20 to 110 KDa as the standard (Bio-Rad).

2.7. Cheese Elaboration

Cheesemaking was carried out by preheating portions of 1000 mL of skim and soy milks at 60 °C. Then, 5 mL of CaCl_2 (2 M, pH 6.5) was added only to skim milk, and 50 mL of seed crude extract (10 g/100 mL of milk) or renin (0.14 mg/mL) were incorporated into the mixture. After, both milks were incubated for 60 min at 50 °C, the curd was cut and stirred at 150 rpm in an orbital shaker, and then the whey were drained. Finally, the curds were placed in round-bottomed containers and cheeses were stored in polyethylene bags at 4 °C.

2.8. Statistical Analysis

The data of three independent experiments were collected and statistically analyzed using one-way analysis of variance (one-way ANOVA), followed by Tukey's honestly significant difference (HSD). Probability $p < 0.05$ indicated statistically significant differences.

3. Results and Discussion

Plant enzymes are widely studied as potential coagulants in cheese production, for example, extracts of *Cynara scolymus* L. [39], *Albizia lebbek* [40], *Centaurea calcitrapa* [41], the latex of *Sideroxylon obtusifolium* [42], the flowers of *Silybum marianum* [43], *Cynara scolymus* [44], and *Jacaratia corumbensis* O. Kuntze [45]. Ginger rhizome has been used as a source of milk coagulating clotting cysteine protease [46]. However, *Cynara cardunculus* L. extract is particularly popular due to its traditional use in elaborating artisanal sheep milk cheese [25]. In contrast, Mexican plants with milk-clotting activity have been scarcely studied. It has been reported that *Solanum elaeagnifolium* berry extract can be suitable for soft cheese manufacturing, for example for cream cheeses [47]. Therefore, generating knowledge and expanding the field of Mexican natural coagulants is of great importance.

3.1. Initial Analysis of Coagulant Activity in Different Parts of the *M. oleifera*

Previous studies have described milk clotting activity in different *M. oleifera* tissues [33,34]. To gain a more complete picture of the tissue-level localization of milk clotting activity in *M. oleifera*, we prepared extracts from seeds, flowers, and leaves. As summarized in Figure 1, the coagulant activity of each extract was studied using whole cow's milk as the substrate. Commercial rennet (tube 1) and 5% of NaCl (tube 2) were used as positive and negative controls, respectively. Seed extract showed high clotting activity (tube 3), while milk clotting activity was only slightly detected for flower extract (tube 4) and was absent for leaf extract (tube 5). The total milk clotting activity of the seed extract was 3419 SU/mL, which corresponds to 50% of the total activity obtained with calf rennet, however, in terms of specific activity only represents a 30% decrease (Table 1). These data are consistent with those reported by Talajsir et al. [34] for seeds only, but were not similar for other tissue extracts (leaves and flowers). The activity with flower extract was 13.66 SU/mL, which agrees with the activity reported by

Pontual et al. [33]. It is noteworthy that milk clotting activity of seed extract does not seem to depend on the milk type (whole or skim milks) and along with a previous background where similar activity values were reported on skim milk, our *M. oleifera* seed extract has approximately 8 times more activity. Therefore, we chose seed extract for the following experiments.

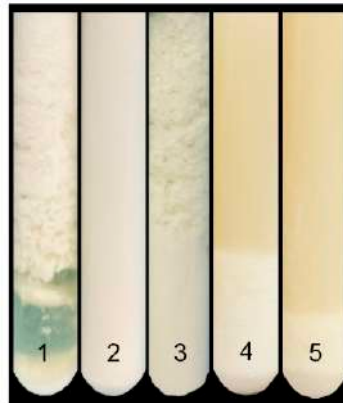


Figure 1. Test tubes of curd formation using *M. oleifera* crude extracts on whole milk. 1: Calf rennet (positive control); 2: NaCl 5% (negative control); 3: Seed extract; 4: Flower extract; 5: Leaf extract.

Table 1. Values of whole milk-clotting activity from the different parts of *M. oleifera*.

Crude Extract	Protein Concentration (mg/mL)	Total MCA (SU/mL)	Specific Activity (SU/mg Protein)
Seeds	10.30 ± 0.45	3419.26 ± 186.80	331.96
Flowers	10.62 ± 0.77	13.66 ± 1.12 **	0.77
Leaves	28.43 ± 3.04 *	ND	ND
Calf rennet	14.10 ± 0.95	6060.6 ± 0.71 *	429.82

The values are expressed as mean ± standard deviation. ND: None detected. MCA: milk-clotting activity. SU: Soxhlet unit. Asterisks represent statistical significance (three separate experiments) based on variance (one-way ANOVA), followed by Tukey's honestly significant difference (HSD) (* $p < 0.05$ vs. Seeds and Flowers; ** $p < 0.05$ vs. Seeds).

3.2. Electrophoretic Pattern of *Moringa oleifera* Extracts

Electrophoretic patterns of each extract were evaluated to determine the molecular weight of proteins with greater abundance that possibly participate in milk coagulation. The results of analysis by SDS-PAGE of *M. oleifera* extracts are shown in Figure 2. A comparison of protein content of different crude extracts shows the variable protein levels in leaves, flowers, and seeds. Both leaves' and flowers' protein patterns showed some discrete bands. On the other hand, predominant bands were found in seed crude extract. From molecular marker and sample protein, an electrophoretic mobility plot was made in order to determine the molecular weight of seed extract proteins. There were four main bands (a to d) and their apparent molecular mass were 43.6, 32.2, 19.4, and 16.3 kDa. Some bands observed in the extract had similar molecular weights as reported for calf rennet (mixture of chymosin and pepsin) and exhibited one prominent band of 48 kDa, suggesting that *M. oleifera* seeds may possess one or more enzymes with rennet-like activity. However, more studies on the structural characterization of these proteins are needed since lectin, an acid protein with 30 kDa, from *M. oleifera* seeds has coagulant properties which are mainly used to reduce water turbidity [48,49].

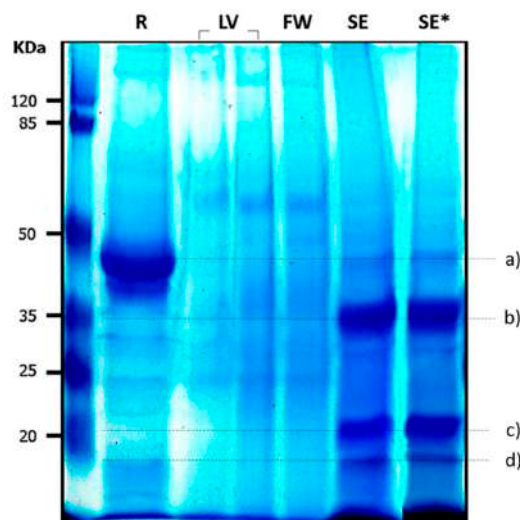


Figure 2. Electrophoretic pattern of *Moringa oleifera* crude extracts. R: Rennet, LV: Leaves, FW: flowers, SE: Seed extract, SE*: Seed extract macerated with ultrasonic bath. (a–d): Proteins of interest. Data are representative of three experiments.

3.3. Effect of Substrate and Enzyme Concentration on Skim Milk Clotting Activity

Measuring enzyme and substrate concentration, in terms of observed activity, is a key task to determine the quality of the milk coagulation process. It is well known that milk sources and enzyme types significantly affect the cheese yield and curd formation time [50]. Therefore, it is necessary to explore the effect of these parameters to control the hydrolysis of casein by *M. oleifera* seed extract.

In order to evaluate the effect of substrate concentration on milk-clotting activity, skim milk varied from 10 to 90 g/L. The use of this range of substrate concentrations allowed an accurate determination of time at the onset of lump formation. However, it is important to mention that it was almost impossible to measure the time required for coagulation when a low concentration of substrate was used (<10 g/L) because the concentration of 20 mg/mL of enzyme (seed extract) caused an instant coagulation; on the other hand, when a higher concentration of substrate was used, there was a marked increase in milk coagulation time. This is probably due to the increase in the viscosity of the reaction mixture. As shown in Figure 3, the milk-clotting activity decreased as substrate concentration was increased in a directly proportional manner until the concentration of substrate reached about 90 g/L. In addition, according to the clotting time present in these experiments, it was observed that 10 g/L of substrate, coagulated at 35 °C and pH 6.5 with CaCl₂, presented a clotting time of 5.47 ± 0.33 s. The reaction mixture with 90 g/L of substrate had a clotting time of 35.74 ± 10.04 s, which is 6.5-fold higher. Thus, our results revealed that the optimum substrate concentration was 10 g/L, suggesting that a high concentration of skim milk has an adverse effect over the catalytic efficiency. These results do not agree with those reported by Ahmed and Helmy [51] for *Aloe variegata* and *Bacillus licheniformis* 5A5 milk-clotting enzymes, who report that increasing skim milk concentration caused a significant increase in MCA up to 60 g/L for both enzymes. However, Wahba et al. [52] reported that substrate concentration over 60 to 210 g/L increased the clotting time. In addition, a study with *Mucor pusillus* pepsin showed a gradual decrease in milk clotting activity to 36.5% with skim milk concentration reaching the 200 g/L [53]. In any case, such retardation of milk-clotting by seed extract may be attributed to several factors. There is an insufficient amount of substrate (casein molecules) due to dilution which restricts the ability of the enzyme to act at its full capacity [54]. The increased viscosity of the solution at higher concentrations of milk diminishes the enzyme activity or it may be due to the smaller amount of hydrolyzed κ -casein when coagulation is initiated; both facts have been stated by Dagleish [55] and Low et al. [56].

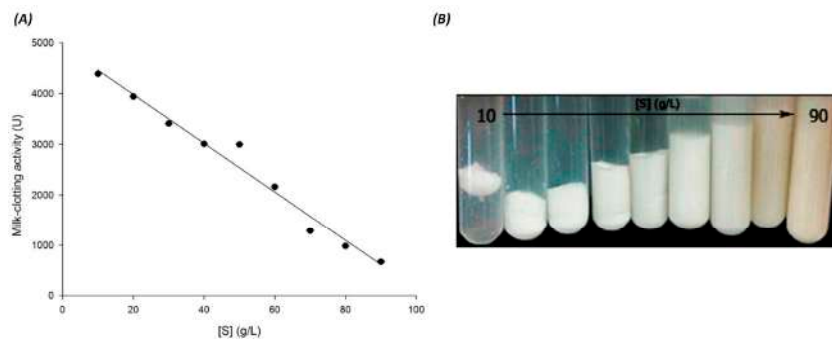


Figure 3. Substrate concentration effect on skimmed milk-clotting activity of seed extract. (A): Left plot was drawn using the data obtained from the milk-clotting activity assay. (B): Right image shows the curd formation in test tubes. One unit of milk-clotting activity (MCA) is defined as the amount of enzyme to clot 1 mL of a solution containing 0.1 g skim milk powder in 40 min at 35 °C. Substrate concentration is expressed as [S]. All experiments were performed in triplicate, and each data point represents the means of at least three determinations. The regression line equation is ($y = -48.03x + 4941.39$) with a correlation coefficient of $R = 0.99$.

The influence of enzyme concentration is an important parameter that affects cheese quality and yield. The effect of enzyme concentration on the milk coagulant activity of seed extract is shown in Figure 4. At a lower concentration of enzyme (<20 mg/mL) in 10 mL of the skim milk, the seed extract did not show any sign of coagulation for two or more hours at 35 °C. The relative activity increased linearly from 20 to 90 g/mL, suggesting that the maximum milk-clotting activity is reached when the enzyme concentration is up to 90 mg/mL. From the results, it can be deduced that a proportional relationship between the enzyme concentration and milk clotting activity exists. However, greatly diluted enzyme did not have enough activity to coagulate the skim milk. These results agree with those reported by other authors, who have mentioned that the clotting time decreased as the concentration of enzyme increased [51,57,58]. Lopez et al. [59] and Najera et al. [58] attributed this phenomena to a higher level of κ -casein proteolysis. On the other hand, at lower concentrations of enzyme, the activity decreased due to the insufficient amount of enzyme to clot the milk. It is noteworthy that milk coagulation by rennet combines an initial enzymatic hydrolysis reaction and a subsequent enzyme-independent protein aggregation reaction [60].

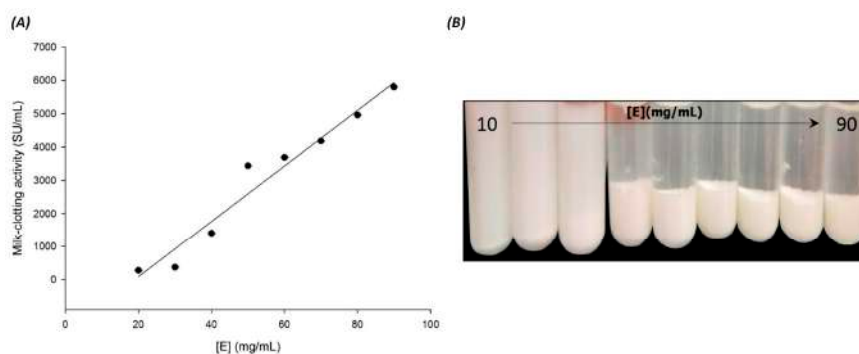


Figure 4. Enzyme concentration effect on skimmed milk-clotting activity of seed extract. (A): Left plot was drawn using the data obtained from the milk-clotting activity assay. (B): Right image shows the curd formation in test tubes. One unit of milk-clotting activity (MCA) is defined as the amount of enzyme to clot 1 mL of a solution containing 0.1 g skim milk powder in 40 min at 35 °C. Enzyme concentration is expressed as [E]. All experiments were performed in triplicate, and each data point represents the means of at least three determinations. The regression line equation is ($y = 83.55x + (-1582.85)$) with a correlation coefficient of $R = 0.98$.

3.4. Effect of Enzyme Concentration on Caseinolytic Activity

The dairy industry characterizes rennet enzyme using two parameters. The first is the milk-clotting activity (MCA) expressed in International Milk-clotting units, determined by a standard method [48] that describes the ability to aggregate micelles by cleaving the Phe105-Met106 bond or a nearby bond of κ -casein. The second property is the general proteolytic activity (PA), which is the ability to cleave any bond of casein [61]. The MCA/PA ratio captures the essential quality of a milk-clotting enzyme to cheese's elaboration.

Figure 5 shows the effect of seed extract concentration (enzyme) in the assays from 10 to 50 (mg/mL) on the rate of caseinolytic activity. The proteolytic activity was measured by the casein digestion method. It can be observed that the PA is dependent of the enzyme concentration. This result suggests that seed extract has an excellent catalytic property. In addition, the MCA/PA ratio (2995:1) for seed extract was observed, and it was much higher than that reported in most previous studies [33,34]. The high quality of the enzyme in *M. oleifera* seed extract seems to be a promising asset for industrial purposes.

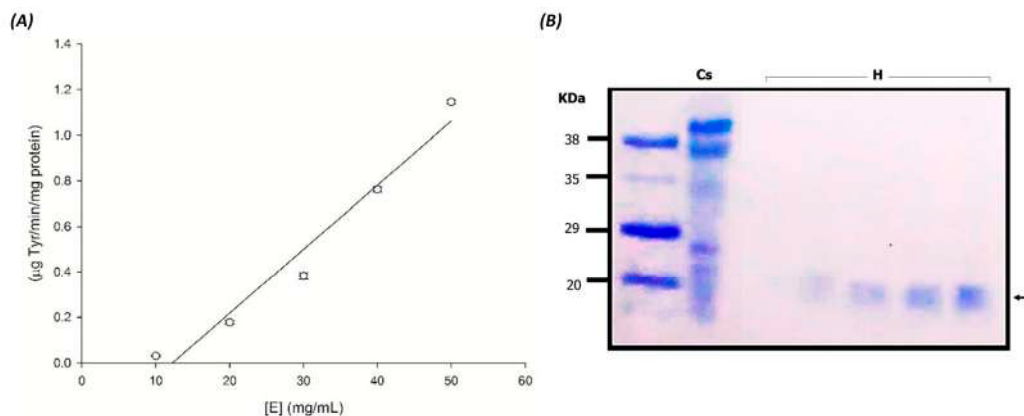


Figure 5. Effect of enzyme (seed extract) concentration on caseinolytic activity. (A): Left plot was drawn using the data obtained from the casein hydrolysates with different enzyme concentrations ([E]: 10, 20, 30, 40, and 50 mg/mL). (B): Right image shows SDS-PAGE of Cs: 1% Casein; and H: casein hydrolysates. All experiments were performed in triplicate.

3.5. Composition of Soy Milk

Many methods have been developed to measure the activity of milk clotting enzymes. Most are based on the time necessary to coagulate a casein-based substrate. These methods measure the enzymatic and non-enzymatic reactions in milk coagulation. The work of Zhao et al. [62], based on the Arima et al. [35] study, determined MCA, and the results were expressed in Soxhlet units. However, it is not clear if these methods are also regularly used to measure the coagulant activity of plant extracts with other types of milk such as soymilk. Therefore, we decided to assess if the constituents of different soy milks, such as protein and fat content, fiber, carbohydrates, and some minerals, may influence the milk clotting process and, consequently, the finished cheese.

Soy milk is a highly diverse fluid consisting of a vast number of substances, the main ones being soluble carbohydrates (sucrose, raffinose, stachyose, others), protein, fiber, minerals, and fat [63]. Soy milk has approximately 20% lipids but this concentration varies among regions. Soybeans harvested in the United States have more lipids than those from China. Thus, the actual composition of soy milk depends on many factors, including varieties, growing season, geographic location, environmental conditions, and methods of making soy milk (nama-shidori and kanetsu-shibori) [64].

Soy milk is an emulsion composed of soy protein, mainly glycinin and β -conglycinin which represent 60% of total soy milk protein, and lipids, mainly triacylglyceride composed of linoleic acid,

oleic acid, and phospholipids. In addition, phytic acid, minerals, and oligosaccharides are present in the soluble component of the emulsion and when some bivalent ions such as calcium and magnesium are added to soy milk in order to elaborate tofu, the ions combine with phytic acid [65]. As a result, the pH decreases and the protein immobilizes, forming a large body constructed with proteins, lipids, and minerals [66].

The chemical compositions of the different types of soy milk used in this study are presented in Table 2. From the results, all types of soy milk were mainly composed of protein and fat. However, a lower percentage of nutritional composition was found for Soyalac. To elaborate firm tofu, the average ratio of fat-protein is 0.55 to 1. The ratios for the different soy milks AdeS, Soyalac, and Soyapac were 0.72, 0.5, and 0.9, respectively due the protein content variations in commercial soy milk ranging from 2.0 to 6.6 g, while total fat content also varied from 1.0 to 4.5 g. These data suggest that Soyalac maintains the correct ratio to produce a cheese like firm tofu. However, the process of soy milk manufacturing might cause chemical changes, which leads to soy protein degradation. Therefore, it is known that the physicochemical properties of soy milk play an important role in tofu making. In addition, if the MCA of *M. oleifera* seed extract accepts different substrates, the question arises as to which soy milk should be used for the MCA assay. Thus, we decided to assess the effect of substrate concentration on the coagulant activity with different soy milks.

Table 2. Nutritional composition of different soymilk (per 1 cup).

Commercial Milk Type	Fat (g)	Fiber (g)	Protein (g)	CHO * (g)	Ratio †	Ca	Fe	P	Zn	Calories (Kcal)
[50]	4.67	3.18	6.73	4.43	0.69	9.8	1.4	120.05	NR	79
AdeS	4.5	3.0	6.2	10.8	0.72	mg	mg	mg	NR	109
Soyalac	1.0	2.0	2.0	10.0	0.50	27%	9%	NR	22%	60
Soyapac	6.0	0	6.6	9.1	0.90	19%	21%	NR	NR	117

* Carbohydrates; † the fat to protein ratio; NR, not reported. Nutritional facts were taken from the package labels of each type of milk.

3.6. Effect of Substrate (Soy Milk Types) on Milk Clotting Activity

Several factors affect the milk clotting activity, among them, different types of substrates and enzyme concentrations which modify the rate of an enzyme-catalyzed reaction. When the enzyme concentration is small, the enzyme can completely combine with the substrate, and the degree of hydrolysis is increased. When more enzyme is added, its amount is higher than that of the substrate, resulting in a relatively small substrate concentration. Then, some amount of enzyme cannot combine with its substrate, leading to a modification in the enzymatic activity.

Soy milk composition is variable, depending mainly of soybean varieties and processing methods [64]. Substrate specificity was determined using three different commercial soy milks (Figure 6). A high level of MCA was shown by substrate 1 (23,500 SU/mL) at 20 g/L and a moderated and poor MCA was revealed by substrates 2 and 3, respectively (Figure 6). Interestingly, seed extract activity is approximately 5 times higher using substrate 1 than using substrate 2. It is worth mentioning that when substrate 3 was used at low concentration (20 g/L), seed enzyme was not suitable to perform its activity. However, only at higher concentration (100 g/L of substrate 3), a good milk clotting activity of 6100 SU/mL was obtained, and it was even better than that obtained with skim milk at the same concentration (Figure 3). The differences between activities from all types of soy milk might be due to the difference in its physicochemical composition, mainly fats, proteins, and total solids in each kind of milk. Thus, seed extract possesses an exceptionally abundant and diverse specificity. Therefore, these results indicate that the milk clotting enzyme from *M. oleifera* seeds has a broad catalytic spectrum and suggests its usefulness for different applications in the dairy industry. Interestingly, our results indicated that Soyalac was the best substrate and hence it was selected for cheese production.

Numerous factors influence the primary and secondary coagulation phases as well as rheological properties to form gels. The most essential factors are protein (substrate) concentration, milk pH value,

milk clotting enzyme type and concentration, calcium concentration, and temperature [59,67]. Earlier reports indicated that bovine milk clotting time is affected by type and protein content of the coagulant. Mehaia [68], for instance, indicated that clotting time of bovine milk can be longer when the concentration ratio of the protein content of the coagulant enzyme is increased because of the increased effectiveness of collisions due to a decreasing aqueous phase. Bruno et al. [69] also reported that a higher dilution of hieronymus fruit extract prolonged bovine milk clotting time. In contrast, a significant decrease in bovine milk clotting time was observed with an increase in the amount of *Solanum macrocarpon* extract [70]. Moreover, it was reported that MCA is increased when crude extract concentration of ginger rhizome is diluted [71].

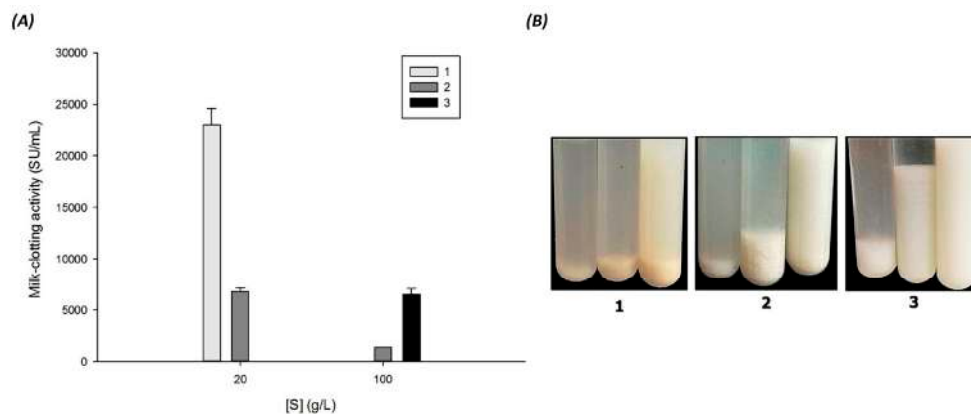


Figure 6. Milk-clotting activity from seed crude extract of *M. oleifera* on different types of commercial soy milk. (A): Left plot was drawn using the data obtained from the milk-clotting activity assay with different types of soy milk. (B): Right image shows the curd formation in test tubes. Substrate 1: AdeS; Substrate 2: Soyapac; Substrate 3: Soyalac. Asterisks represent statistical significance (three separate experiments) based on variance (one-way ANOVA), followed by HSD ($p < 0.05$ vs. Substrate 2: Soyapac).

3.7. Cheese Processing

Soy milk has been used as a cow milk alternative due to its high amounts of protein, iron, unsaturated fatty acids, and niacin but low amounts of fat, carbohydrates, and calcium compared with those of cow's milk [72]. Various soy cheeses are made in some countries and have attracted increasing attention and have been used as a soft cheese-like product [73–75].

To further confirm the suitability of the *M. oleifera* seed extract as a rennet substitute in cheesemaking, the potential of the milk-clotting enzyme from seed extract was proved. A soft-white cheese was obtained with soymilk (Soyalac) while the cheese made with skim milk was hard and crumbly (Figure 7). The results demonstrated no significant differences in the coagulation time using both types of milk, and cheeses of 3.6 to 6.8 g were obtained.

Liu and Chang [76] reported that tofu texture made from soy milk is affected by several factors including soybean composition, soy milk processing, type and amount of coagulant, and processing methods. Glycinin and β -conglycinin are the major storage proteins (globulins) in soy foods. Glycinin corresponds to the 11S protein, and β -conglycinin is the principal component of the 7S protein. Tezuka et al. [77] reported that higher amounts of coagulant are required for the 7S globulin-rich soy milk than 11S globulin-rich or normal soy milks. The gel hardness depended mainly on glycinin content, hence, if the 11S/7S ratio increases, the hardness of gel is enhanced [78]. In accordance with this background, we assumed that commercial soy milks used in this study presented a low glycinin fraction and an enriched 7S-globulin content. However, additional studies are needed to know the quality and composition of the main protein present in commercial soy milks.



Figure 7. Workflow employed in cheese making using seed crude extract. The upper photos show soy milk cheese's elaboration while the lower photos show skim milk cheese's elaboration, both processed with Moringa seed extract. All experiments were performed in triplicate.

4. Conclusions

Leaf and flower enzymes displayed a negligible value of milk-clotting activity, whereas the seed enzyme demonstrated a high milk-clotting activity on whole, skim, and soy milks. In addition, it would be interesting to consider if other components, such as phytochemicals found in *M. oleifera* seed extract, could have antioxidant effects, which may help to reduce the risk of cardiovascular diseases. With these results it can be inferred that Mexican *M. oleifera* seed extract can be successfully used for different types of cheese manufacture with nutritional benefits, as well as several industrial applications.

Acknowledgments: The authors would like to express their sincere gratitude to the Consejo Nacional de Ciencia y Tecnología (Conacyt, México) for financial support to ESC (grant 268184). The authors are also grateful to the Mexican Moringa producers (Akuanandi) for providing all samples for this study. María Alejandra Sánchez Muñoz is also grateful to Conacyt for the financial support for her Masters studies, grant 601630. Finally, special acknowledgement is given to Jaime de Lira Sánchez and Jorge Alejandro Sosa Gutiérrez for helpful discussions and critical reading of this paper and to Nancy Marissa Durán Arriaga for her technical assistance.

Author Contributions: M.A.S.-M., M.A.V.-S., and E.S.-C. planned and designed the experiments; M.A.S.-M. and C.A.-D. performed the experiments; E.S.-C., A.T.-V., and J.A.M.-V. analyzed the data; E.S.-C. wrote the manuscript, and P.R.-B., M.G.C.-C., M.A.-O., and E.S.-C. edited the manuscript.

Conflicts of Interest: The authors hereby declare that there are no competing interests in this work.

References

1. Roberfroid, M.B. Concepts and strategy of functional food science: The European perspective. *Am. J. Clin. Nutr.* **2000**, *71*, 1660s–1664s. [[PubMed](#)]
2. Massaro, M.; Scoditti, E.; Carluccio, M.A.; De Caterina, R. Nutraceuticals and prevention of atherosclerosis: Focus on ω -3 polyunsaturated fatty acids and mediterranean diet polyphenols. *Cardiovasc. Ther.* **2010**, *28*, e13–e19. [[CrossRef](#)] [[PubMed](#)]
3. Sofi, F.; Dinu, M.; Pagliai, G.; Marcucci, R.; Casini, A. Validation of a literature-based adherence score to mediterranean diet: The medi-lite score. *Int. J. Food Sci. Nutr.* **2017**, *68*, 757–762. [[CrossRef](#)] [[PubMed](#)]
4. Bonvecchio, A.; Safdie, M.; Monterrubio, E.A.; Gust, T.; Villalpando, S.; Rivera, J.A. Overweight and obesity trends in Mexican children 2 to 18 years of age from 1988 to 2006. *Salud Pública México* **2009**, *51*, S586–S594. [[CrossRef](#)]
5. Qin, L.-Q.; Xu, J.-Y.; Han, S.-F.; Zhang, Z.-L.; Zhao, Y.-Y.; Szeto, I.M. Dairy consumption and risk of cardiovascular disease: An updated meta-analysis of prospective cohort studies. *Asia Pac. J. Clin. Nutr.* **2015**, *24*, 90–100. [[PubMed](#)]
6. Ahmed, I.A.M.; Morishima, I.; Babiker, E.E.; Mori, N. Characterisation of partially purified milk-clotting enzyme from solanum dubium fresen seeds. *Food Chem.* **2009**, *116*, 395–400. [[CrossRef](#)]

7. Ohlsson, L. Dairy products and plasma cholesterol levels. *Food Nutr. Res.* **2010**, *54*, 5124. [[CrossRef](#)] [[PubMed](#)]
8. Gao, D.; Ning, N.; Wang, C.; Wang, Y.; Li, Q.; Meng, Z.; Liu, Y.; Li, Q. Dairy products consumption and risk of type 2 diabetes: Systematic review and dose-response meta-analysis. *PLoS ONE* **2013**, *8*, e73965. [[CrossRef](#)] [[PubMed](#)]
9. Chen, M.; Sun, Q.; Giovannucci, E.; Mozaffarian, D.; Manson, J.E.; Willett, W.C.; Hu, F.B. Dairy consumption and risk of type 2 diabetes: 3 cohorts of US adults and an updated meta-analysis. *BMC Med.* **2014**, *12*, 215. [[CrossRef](#)] [[PubMed](#)]
10. Mozaffarian, D. Dietary and policy priorities for cardiovascular disease, diabetes, and obesity. *Circulation* **2016**, *133*, 187–225. [[CrossRef](#)] [[PubMed](#)]
11. Abou-Zeid, N.A. Review of Egyptian cereal-based fermented product (Kishk). *Int. J. Agric. Innov. Res.* **2016**, *4*, 600–609.
12. O'connell, J.; Fox, P. Significance and applications of phenolic compounds in the production and quality of milk and dairy products: A review. *Int. Dairy J.* **2001**, *11*, 103–120. [[CrossRef](#)]
13. Boroski, M.; Giroux, H.J.; Sabik, H.; Petit, H.V.; Visentainer, J.V.; Matumoto-Pintro, P.T.; Britten, M. Use of oregano extract and oregano essential oil as antioxidants in functional dairy beverage formulations. *LWT-Food Sci. Technol.* **2012**, *47*, 167–174. [[CrossRef](#)]
14. Najgebauer-Lejko, D.; Sady, M.; Grega, T.; Walczycka, M. The impact of tea supplementation on microflora, pH and antioxidant capacity of yoghurt. *Int. Dairy J.* **2011**, *21*, 568–574. [[CrossRef](#)]
15. Gad, A.S.; El-Salam, M.H.A. The antioxidant properties of skim milk supplemented with rosemary and green tea extracts in response to pasteurisation, homogenisation and the addition of salts. *Int. J. Dairy Technol.* **2010**, *63*, 349–355. [[CrossRef](#)]
16. Chen, G.; Kocaoglu-Vurma, N.; Harper, W.J.; Rodriguez-Saona, L.E. Application of infrared microspectroscopy and multivariate analysis for monitoring the effect of adjunct cultures during Swiss cheese ripening. *J. Dairy Sci.* **2009**, *92*, 3575–3584. [[CrossRef](#)] [[PubMed](#)]
17. Frazier, R.A.; Deaville, E.R.; Green, R.J.; Stringano, E.; Willoughby, I.; Plant, J.; Mueller-Harvey, I. Interactions of tea tannins and condensed tannins with proteins. *J. Pharm. Biomed. Anal.* **2010**, *51*, 490–495. [[CrossRef](#)] [[PubMed](#)]
18. Hasni, I.; Bourassa, P.; Hamdani, S.; Samson, G.; Carpentier, R.; Tajmir-Riahi, H.-A. Interaction of milk α - and β -caseins with tea polyphenols. *Food Chem.* **2011**, *126*, 630–639. [[CrossRef](#)]
19. Kanakis, C.; Hasni, I.; Bourassa, P.; Tarantilis, P.; Polissiou, M.; Tajmir-Riahi, H.-A. Milk β -lactoglobulin complexes with tea polyphenols. *Food Chem.* **2011**, *127*, 1046–1055. [[CrossRef](#)] [[PubMed](#)]
20. Haratifar, S.; Corredig, M. Interactions between tea catechins and casein micelles and their impact on renneting functionality. *Food Chem.* **2014**, *143*, 27–32. [[CrossRef](#)] [[PubMed](#)]
21. Giroux, H.J.; De Grandpré, G.; Fustier, P.; Champagne, C.P.; St-Gelais, D.; Lacroix, M.; Britten, M. Production and characterization of cheddar-type cheese enriched with green tea extract. *Dairy Sci. Technol.* **2013**, *93*, 241–254. [[CrossRef](#)]
22. Gad, A.S.; Sayd, A.F. Antioxidant properties of rosemary and its potential uses as natural antioxidant in dairy products—A review. *Food Nutr. Sci.* **2015**, *6*, 179. [[CrossRef](#)]
23. Yadav, D.; Vij, S.; Hati, S.; Singh, B.P.; Dhanday, M.; Dahiya, M.; Vandna, V. Evaluation of total antioxidant activity of soy yoghurt. *Indian J. Dairy Sci.* **2012**, *65*, 220–224.
24. Murata, K.; Kusakabe, I.; Kobayashi, H.; Akaike, M.; Park, Y.W.; Murakami, K. Studies on the coagulation of soymilk-protein by commercial proteinases. *Agric. Biol. Chem.* **1987**, *51*, 385–389.
25. Galán, E.; Prados, F.; Pino, A.; Tejada, L.; Fernández-Salguero, J. Influence of different amounts of vegetable coagulant from cardoon *cynara cardunculus* and calf rennet on the proteolysis and sensory characteristics of cheeses made with sheep milk. *Int. Dairy J.* **2008**, *18*, 93–98. [[CrossRef](#)]
26. Pino, A.; Prados, F.; Galán, E.; McSweeney, P.L.; Fernández-Salguero, J. Proteolysis during the ripening of goats' milk cheese made with plant coagulant or calf rennet. *Food Res. Int.* **2009**, *42*, 324–330. [[CrossRef](#)]
27. Öner, M.; Akar, B. Separation of the proteolytic enzymes from fig tree latex and its utilization in gaziantep cheese production. *LWT-Food Sci. Technol.* **1993**, *26*, 318–321. [[CrossRef](#)]
28. Ilany, J.; Netzer, A. Milk-clotting activity of proteolytic enzymes. *J. Dairy Sci.* **1969**, *52*, 43–46. [[CrossRef](#)]
29. Xiu-ling, Z. Study on physical, chemical and biochemical characteristics of different milk-clotting enzymes during cheesemaking. *Resour. Dev. Mark.* **2009**, *2*, 002. [[CrossRef](#)]

30. Chye, S.J.; Ahmad, R.; Noor Aziah, A.A. Studies on the physicochemical and sensory characteristics of goat's milk dadih incorporated with tropical- fruit purees. *Int. Food Res. J.* **2012**, *19*, 1387–1392.
31. Hatanaka, S.; Maegawa, M.; Kanauchi, M.; Kasahara, S.; Shimoyamada, M.; Ishida, M. Characteristics and purification of soybean milk curdling enzyme-producing yeast *Saccharomyces bayanus* SCY003. *Food Sci. Technol. Res.* **2014**, *20*, 927–938. [[CrossRef](#)]
32. Idris, M.A.; Jami, M.S.; Hamed, A.M.; Jamal, P. *Moringa oleifera* seed extract: A review on its environmental applications. *Int. J. Appl. Environ. Sci.* **2016**, *11*, 1469–1486.
33. Pontual, E.V.; Carvalho, B.E.; Bezerra, R.S.; Coelho, L.C.; Napoleão, T.H.; Paiva, P.M. Caseinolytic and milk-clotting activities from *Moringa oleifera* flowers. *Food Chem.* **2012**, *135*, 1848–1854. [[CrossRef](#)] [[PubMed](#)]
34. Tajalsir, A.E.; Ebraheem, A.S.; Abdallah, A.M.; Khider, F.J.; Elsamani, M.O.; Ahmed, I.A.M. Partial purification of milk-clotting enzyme from the seeds of *Moringa oleifera*. *J. Microbiol. Biotechnol. Food Sci.* **2014**, *4*, 58. [[CrossRef](#)]
35. Arima, K.; Yu, J.; Iwasaki, S. Milk-clotting enzyme from *Mucor pusillus* var. *Lindt*. *Methods Enzymol.* **1970**, *19*, 446–459.
36. Sarath, G.; Motte, R.S.; Wagner, F.M. Protease assay methods. In *Proteolytic Enzyme—A Practical Approach*; Beynon, R.J., Bond, J.S., Eds.; IRL Press: Oxford, UK, 1989; pp. 25–55.
37. Lowry, O.H.; Rosebrough, N.J.; Farr, A.L.; Randall, R.J. Protein measurement with the folin phenol reagent. *J. Biol. Chem.* **1951**, *193*, 265–275. [[PubMed](#)]
38. Laemmli, V. Determination of protein molecular weight in polyacrylamide gels. *Nature* **1970**, *227*, 680–685. [[CrossRef](#)] [[PubMed](#)]
39. Chazarra, S.; Sidrach, L.; Lopez-Molina, D.; Rodríguez-López, J.N. Characterization of the milk-clotting properties of extracts from artichoke (*Cynara scolymus*, L.) flowers. *Int. Dairy J.* **2007**, *17*, 1393–1400. [[CrossRef](#)]
40. Egito, A.; Girardet, J.-M.; Laguna, L.; Poirson, C.; Mollé, D.; Miclo, L.; Humbert, G.; Gaillard, J.-L. Milk-clotting activity of enzyme extracts from sunflower and albizia seeds and specific hydrolysis of bovine κ -casein. *Int. Dairy J.* **2007**, *17*, 816–825. [[CrossRef](#)]
41. Raposo, S.; Domingos, A. Purification and characterization milk-clotting aspartic proteinases from *Centaurea calcitrapa* cell suspension cultures. *Process Biochem.* **2008**, *43*, 139–144. [[CrossRef](#)]
42. De Silva, A.C.; da Silva Nascimento, T.C.E.; da Silva, S.A.; Herculano, P.N.; Moreira, K.A. Potential of quixaba (*Sideroxylon obtusifolium*) latex as a milk-clotting agent. *Food Sci. Technol. (Camp.)* **2013**, *33*, 494–499. [[CrossRef](#)]
43. Cavalli, S.V.; Silva, S.V.; Cimino, C.; Malcata, F.X.; Priolo, N. Hydrolysis of caprine and ovine milk proteins, brought about by aspartic peptidases from *Silybum marianum* flowers. *Food Chem.* **2008**, *106*, 997–1003. [[CrossRef](#)]
44. Llorente, B.E.; Obregón, W.D.; Avilés, F.X.; Caffini, N.O.; Vairo-Cavalli, S. Use of artichoke (*Cynara scolymus*) flower extract as a substitute for bovine rennet in the manufacture of Gouda-type cheese: Characterization of aspartic proteases. *Food Chem.* **2014**, *159*, 55–63. [[CrossRef](#)] [[PubMed](#)]
45. Duarte, A.R.; Duarte, D.M.R.; Moreira, K.A.; Cavalcanti, M.T.H.; de Lima-Filho, J.L.; Porto, A.L.F. *Jacaratia corumbensis* O. Kuntze a new vegetable source for milk-clotting enzymes. *Braz. Arch. Biol. Technol.* **2009**, *52*, 1–9. [[CrossRef](#)]
46. Hashim, M.M.; Dong, M.; Iqbal, M.F.; Chen, X. Ginger rhizome as a potential source of milk coagulating cysteine protease. *Phytochemistry* **2011**, *72*, 458–464. [[CrossRef](#)] [[PubMed](#)]
47. Néstor, G.M.; Dely Rubí, C.G.; Héctor, J.C. Exploring the milk-clotting properties of a plant coagulant from the berries of *S. elaeagnifolium* var. *Cavanilles*. *J. Food Sci.* **2012**, *77*, C89–C94. [[CrossRef](#)] [[PubMed](#)]
48. Santos, A.F.; Luz, L.A.; Argolo, A.C.; Teixeira, J.A.; Paiva, P.M.; Coelho, L.C. Isolation of a seed coagulant *Moringa oleifera* lectin. *Process Biochem.* **2009**, *44*, 504–508. [[CrossRef](#)]
49. Ferreira, R.; Napoleão, T.H.; Santos, A.F.; Sá, R.; Carneiro-da-Cunha, M.; Morais, M.; Silva-Lucca, R.A.; Oliva, M.L.V.; Coelho, L.; Paiva, P.M. Coagulant and antibacterial activities of the water-soluble seed lectin from *Moringa oleifera*. *Lett. Appl. Microbiol.* **2011**, *53*, 186–192. [[CrossRef](#)] [[PubMed](#)]
50. Nasr, A.I.; Mohamed Ahmed, I.A.; Hamid, O.I. Characterization of partially purified milk-clotting enzyme from sunflower (*Helianthus annuus*) seeds. *Food Sci. Nutr.* **2016**, *4*, 733–741. [[CrossRef](#)] [[PubMed](#)]
51. Ahmed, S.; Helmy, W. Comparative evaluation of *Bacillus licheniformis* 5A5 and *Aloe variegata* milk-clotting enzymes. *Braz. J. Chem. Eng.* **2012**, *29*, 69–76. [[CrossRef](#)]

52. Wahba, A.; El-Abbassy, F.; El-Shafei, H.; Awad, S. Effect of some factors on the activity of milk clotting enzymes. *Egypt. J. Food Sci. (Egypt)* **1995**, *23*, 27–35.
53. Zhang, J.; Sun, Y.; Li, Z.; Luo, Q.; Li, T.; Wang, T. Structure-based design of mucor pusillus pepsin for the improved ratio of clotting activity / proteolytic activity in cheese manufacture. *Protein Pept. Lett.* **2015**, *22*, 660–667. [[CrossRef](#)] [[PubMed](#)]
54. Abdel-Fattah, A.; Mabrouk, S.S.; El-Hawwary, N.M. Production and some properties of rennin-like milk-clotting enzyme from *Penicillium citrinum*. *Microbiology* **1972**, *70*, 151–155. [[CrossRef](#)]
55. Dalgleish, D.G.; Brinkhuis, J.; Payens, T.A. The coagulation of differently sized casein micelles by rennet. *Eur. J. Biochem.* **1981**, *119*, 257–261. [[CrossRef](#)] [[PubMed](#)]
56. Low, Y.H.; Agboola, S.; Zhao, J.; Lim, M.Y. Clotting and proteolytic properties of plant coagulants in regular and ultrafiltered bovine skim milk. *Int. Dairy J.* **2006**, *16*, 335–343. [[CrossRef](#)]
57. Hashem, A.M. Optimization of milk-clotting enzyme productivity by *Penicillium oxalicum*. *Bioresour. Technol.* **1999**, *70*, 203–207. [[CrossRef](#)]
58. Nájera, A.; De Renobales, M.; Barron, L. Effects of pH, temperature, CaCl₂ and enzyme concentrations on the rennet-clotting properties of milk: A multifactorial study. *Food Chem.* **2003**, *80*, 345–352. [[CrossRef](#)]
59. López-Fandiño, R.; Olano, A. Effects of high pressures combined with moderate temperatures on the rennet coagulation properties of milk. *Int. Dairy J.* **1998**, *8*, 623–627. [[CrossRef](#)]
60. Van Hooydonk, A.; Walstra, P. Interpretation of the kinetics of the renneting reaction in milk. *Neth. Milk Dairy J.* **1987**, *41*, 19–48.
61. Kappeler, S.R.; Rahbek-Nielsen, H.; Farah, Z.; Puhan, Z.; Hansen, E.B.; Johansen, E. Characterization of recombinant camel chymosin reveals superior properties for the coagulation of bovine and camel milk. *Biochem. Biophys. Res. Commun.* **2006**, *342*, 647–654. [[CrossRef](#)] [[PubMed](#)]
62. Zhao, X.; Wang, J.; Zheng, Z.; Zhao, A.; Yang, Z. Production of a milk-clotting enzyme by glutinous rice fermentation and partial characterization of the enzyme. *J. Food Biochem.* **2015**, *39*, 70–79. [[CrossRef](#)]
63. Hajirostamloo, B. Comparison of nutritional and chemical parameters of soymilk and cow milk. *World Acad. Sci. Eng. Technol.* **2009**, *57*, 436–438.
64. Kanauchi, M.; Kanauchi, K. Diet quality and adherence to a healthy diet in Japanese male workers with untreated hypertension. *BMJ Open* **2015**, *5*, e008404. [[CrossRef](#)] [[PubMed](#)]
65. Ohno, A.; Ano, T.; Shoda, M. Use of soybean curd residue, okara, for the solid state substrate in the production of a lipopeptide antibiotic, iturin A, by *Bacillus subtilis* NB22. *Process Biochem.* **1996**, *31*, 801–806. [[CrossRef](#)]
66. Ono, T.; Katho, S.; Mothizuki, K. Influences of calcium and pH on protein solubility in soybean milk. *Biosci. Biotechnol. Biochem.* **1993**, *57*, 24–28. [[CrossRef](#)] [[PubMed](#)]
67. Guinee, T.P.; O’Callaghan, D.J.; Pudja, P.D.; O’Brien, N. Rennet coagulation properties of retentates obtained by ultrafiltration of skim milks heated to different temperatures. *Int. Dairy J.* **1996**, *6*, 581–596. [[CrossRef](#)]
68. Mehaia, M.A. Studies on rennet coagulation of skim camel milk concentrated by ultrafiltration. *J. King Saud Univ.* **1997**, *9*, 11–23.
69. Bruno, M.A.; Trejo, S.A.; Avilés, F.X.; Caffini, N.O.; López, L.M.I. Cloning, sequencing, and identification using proteomic tools of a protease from *Bromelia hieronymi* mez. *Appl. Biochem. Biotechnol.* **2011**, *165*, 583. [[CrossRef](#)] [[PubMed](#)]
70. Guiama, V.; Libouga, D.; Ngah, E.; Beka, R.; Ndi, K.; Maloga, B.; Bindzi, J.; Donn, P.; Mbofung, C. Milk-clotting potential of fruit extracts from *Solanum esculentum*, *Solanum macrocarpon* L. And *Solanum melongena*. *Afr. J. Biotechnol.* **2010**, *9*. [[CrossRef](#)]
71. Hailu, Y.; Seifu, E.; Yilma, Z. Physicochemical properties and consumer acceptability of soft unripened cheese made from camel milk using crude extract of ginger (*Zingiber officinale*) as coagulant. *Afr. J. Food Sci.* **2014**, *8*, 87–91.
72. Liu, K. Chemistry and nutritional value of soybean components. In *Soybeans*; Springer US, International Thomson Publishing Asia: Henderson Road, Singapore, 1997; pp. 25–113.
73. Liong, M.T.; Easa, A.M.; Lim, P.T.; Kang, J.Y. Survival, growth characteristics and bioactive potential of *Lactobacillus acidophilus* in a soy-based cream cheese. *J. Sci. Food Agric.* **2009**, *89*, 1382–1391. [[CrossRef](#)]
74. Rinaldoni, A.N.; Palatnik, D.R.; Zaritzky, N.; Campderrós, M.E. Soft cheese-like product development enriched with soy protein concentrates. *LWT-Food Sci. Technol.* **2014**, *55*, 139–147. [[CrossRef](#)]

75. Otieno, D.O.; Ashton, J.; Shah, N.E. Stability of β -glucosidase activity produced by *Bifidobacterium* and *Lactobacillus* spp. In fermented soymilk during processing and storage. *J. Food Sci.* **2005**, *70*, 236–241. [[CrossRef](#)]
76. Liu, Z.-S.; Chang, S.K.-C. Effect of soy milk characteristics and cooking conditions on coagulant requirements for making filled tofu. *J. Agric. Food Chem.* **2004**, *52*, 3405–3411. [[CrossRef](#)] [[PubMed](#)]
77. Tezuka, M.; Taira, H.; Igarashi, Y.; Yagasaki, K.; Ono, T. Properties of tofus and soy milks prepared from soybeans having different subunits of glycinin. *J. Agric. Food Chem.* **2000**, *48*, 1111–1117. [[CrossRef](#)] [[PubMed](#)]
78. Yagasaki, K.; Kousaka, F.; Kitamura, K. Potential improvement of soymilk gelation properties by using soybeans with modified protein subunit compositions. *Breed. Sci.* **2000**, *50*, 101–107. [[CrossRef](#)]



© 2017 by the authors. Licensee MDPI, Basel, Switzerland. This article is an open access article distributed under the terms and conditions of the Creative Commons Attribution (CC BY) license (<http://creativecommons.org/licenses/by/4.0/>).

Research Article

Streptozotocin-Induced Adaptive Modification of Mitochondrial Supercomplexes in Liver of Wistar Rats and the Protective Effect of *Moringa oleifera* Lam

María Alejandra Sánchez-Muñoz,¹ Mónica Andrea Valdez-Solana ¹,
Mara Ibeth Campos-Almazán ², Óscar Flores-Herrera,³ Mercedes Esparza-Perusquía,³
Sofía Olvera-Sánchez,³ Guadalupe García-Arenas,⁴ Claudia Avitia-Domínguez ²,
Alfredo Téllez-Valencia,² and Erick Sierra-Campos ¹

¹Facultad de Ciencias Químicas, Universidad Juárez del Estado de Durango Campus, Gómez Palacio, DGO, Mexico

²Facultad de Medicina y Nutrición, Universidad Juárez del Estado de Durango Campus, Durango, DGO, Mexico

³Departamento de Bioquímica, Facultad de Medicina, Universidad Nacional Autónoma de México, Mexico City, Mexico

⁴Facultad de Ciencias de la Salud, Universidad Juárez del Estado de Durango Campus, Gómez Palacio, DGO, Mexico

Correspondence should be addressed to Erick Sierra-Campos; ericksier@gmail.com

Received 15 November 2017; Accepted 28 December 2017; Published 1 March 2018

Academic Editor: Saad Tayyab

Copyright © 2018 María Alejandra Sánchez-Muñoz et al. This is an open access article distributed under the Creative Commons Attribution License, which permits unrestricted use, distribution, and reproduction in any medium, provided the original work is properly cited.

The increasing prevalence of diabetes continues to be a major health issue worldwide. Alteration of mitochondrial electron transport chain is a recognized hallmark of the diabetic-associated decline in liver bioenergetics; however, the molecular events involved are only poorly understood. *Moringa oleifera* is used for the treatment of diabetes. However, its role on mitochondrial functionality is not yet established. This study was aimed to evaluate the effect of *M. oleifera* extract on supercomplex formation, ATPase activity, ROS production, GSH levels, lipid peroxidation, and protein carbonylation. The levels of lipid peroxidation and protein carbonylation were increased in diabetic group. However, the levels were decreased in *Moringa*-treated diabetic rats. Analysis of in-gel activity showed an increase in all complex activities in the diabetic group, but spectrophotometric determinations of complex II and IV activities were unaffected in this treatment. However, we found an oxygen consumption abolition through complex I-III-IV pathway in the diabetic group treated with *Moringa*. While respiration with succinate feeding into complex II-III-IV was increased in the diabetic group. These findings suggest that hyperglycemia modifies oxygen consumption, supercomplexes formation, and increases ROS levels in mitochondria from the liver of STZ-diabetic rats, whereas *M. oleifera* may have a protective role against some alterations.

1. Introduction

Mitochondria, which are mainly composed by proteins and lipids, are considered the most complex and the most important organelles of eukaryotic cells. They not only play a leading role in the energy metabolism, but also closely involve in many cellular processes [1]. Moreover, mitochondria are highly dynamic organelles that continuously divide and fuse as well as move within the cell [2]. In addition, it is now well established that the individual respiratory complexes can be organized into supercomplexes,

but the composition and abundance of these may vary among organisms and tissues depending on the metabolic and physiological conditions [3–5] as well as on the lipid content of the mitochondrial inner membrane [6, 7]. However, mitochondria are a source of reactive oxygen species (ROS) which are involved in many pathological scenarios [8] and often play an essential role in physiological cell death mechanisms [9].

Mitochondrial dysfunction has recently been identified as a common metabolic defect associated with diabetes, obesity, and its metabolic complications [10, 11]. Previous

studies have demonstrated that chronic diabetes induced by streptozotocin (STZ) provoked significant alterations in hepatic mitochondrial function which were restored to normality with insulin treatment [12] or with mifepristone (RU 38486) treatment [13]. In addition, it has been postulated that STZ-induced cytotoxicity in HepG2 cells is mediated, at least in part, by the increase in ROS and reactive nitrogen species (RNS) production, oxidative stress, and mitochondrial dysfunction [14]. Moreover, diverse studies suggest that mitochondrial oxidative function was compromised in diabetic and prediabetic humans as evidenced by reduced levels of fatty acid oxidation, insulin-stimulated ATP synthesis, and expression of genes involved in oxidative phosphorylation (OXPHOS) [15–17]. With respect to OXPHOS, activity was suggested that mitochondrial diabetes may also affect the complex V [18], and it is interesting to mention that, in diabetic patients' muscle, blue native gel electrophoresis revealed a striking decrease in complex I, III, and IV containing supercomplexes [19]. In addition, impairment of pyruvate dehydrogenase complex on the citric acid cycle and glucokinase activity during diabetes has been reported [19, 20]. These findings can be associated with an increased in ROS production and a decrease in cellular reduced glutathione (GSH) content in STZ-induced diabetic rats [21] and diabetic patients [22].

Moringa oleifera is commonly used in folk medicine as an antidiabetic agent via its antioxidant property. Yet, its biological activity is not limited to the antioxidant capacity. In fact, other important biological activities such as hypolipidaemic, antiatherosclerotic, and anticarcinogenic activities of *M. oleifera* leaves and seeds have been reported [23–26]. However, phenolic compounds found in *M. oleifera*, especially flavonoids, possess both antioxidant and prooxidant properties depending on concentration used. The latter which is exhibited at higher concentrations of phenolic compounds such as quercetin, galangin, taxifolin, catechin, and prenylated flavonoid have been shown to affect mitochondrial energetic processes (see supplementary materials available here) [27, 28]. In addition, it has been shown that mitochondria are a plausible main target of flavonoids mediating preventive actions against stress and mitochondrial dysfunction-associated pathologies [29]. Recent evidence indicates that *M. oleifera* aqueous leaf extract presents anticancerous effect on A549 cancer cells by affecting mitochondrial membrane potential and ATP levels [30]. More recently, Khan et al. [31] showed that aqueous extract of *M. oleifera* leaf protects pancreas against ROS-mediated damage by enhancing cellular antioxidant defenses and minimizing hyperglycemia in STZ-induced diabetes, which might be due to the glucose uptake enhancement in skeletal muscle, insulin secretion stimulation, and alpha-amylase and alpha-glucosidase inhibition. Thus, the favorable roles of *M. oleifera* in glucose metabolism and antioxidant system led us to investigate the effects of *M. oleifera* on diabetes-induced mitochondrial changes in liver. The aim of this study was to investigate the protecting effect of *M. oleifera* extract upon STZ-induced mitochondrial dysfunction. To assess the degree of injury of the STZ, both respiratory and enzyme activity parameters were

evaluated and compared with the changes in the *M. oleifera*-treated group.

2. Materials and Methods

2.1. Preparation of the Extract. The extract was prepared using 23 g of dry-ground sample and 260 mL of 80% methanolic aqueous solution by successive maceration. The mixture was shaken in a magnetic grid at room temperature for 24 h and then filtered through Whatman filter paper number 1. The final extract was concentrated on a rotary evaporator, placed in a deep freezer for 24 h and lyophilized to obtain a powdered extract that was kept at -80°C .

2.2. Ethics Statement. All experiments were performed in compliance with the guideline for the welfare of experimental animals by the National Institutes of Health and in accordance with the guidelines of Institutional Animal Care. This study was approved by the Institutional Animal Ethics Committee at the Faculty of Health Science, UJED.

2.3. Diabetic Model and Treatment. Streptozotocin (STZ) was dissolved in a citrate buffer (0.1 M, pH 4.5) and intraperitoneally injected (55 mg/kg) to induce diabetes in rats. Rats injected only with citrate buffer served as control. Type 1 diabetes was confirmed evaluating fasting plasma glucose levels after 5 days of induction; the inclusion criteria to establish diabetes were 200 mg/dL of fasting plasma glucose. Rats were divided in control (C group), diabetic (D group), and *M. oleifera*-treated diabetic (M group) groups. M group was daily administered with a 200 mg/kg dose of extract by gavage during 3 weeks, and remaining groups were administered with water as vehicle.

2.4. Isolation and Purification of Mitochondria. The rat liver was collected immediately after euthanasia and homogenized in 100 mL of a buffer containing 20 mM Tris-HCl, 200 mM mannitol, 50 mM sucrose, 1 mM EDTA, 1 mM PMSF, 1 protease inhibitor tablet, and 0.1% bovine serum albumin (BSA) (pH 7.4; buffer A). Cellular and nuclear fractions were removed in the pellet by centrifuging at 3,500 rpm for 10 min at 4°C . Mitochondria were obtained by centrifuging the supernatant for 10 min at 11,000 rpm. Then, mitochondria were washed and resuspended in buffer A without BSA and centrifuged at 11,000 rpm for 10 min. Mitochondria were loaded on a Percoll gradient 15, 23, and 40% in buffer A without BSA and centrifuged for 35 min at 25,000 rpm at 4°C [32].

2.5. Oxygen Consumption. Oxygen uptake was estimated polarographically using a Clark-type electrode in a 1.5 ml water-jacketed chamber at 37°C . The mixture contained 250 mM sucrose, 20 mM HEPES, 50 mM K_2HPO_4 , 10 mM H_3PO_4 , 10 mM MgCl_2 , and 1 mM EGTA, 0.1% BSA (pH 7.4) [33]. Oxygen consumption was stimulated by the addition of 0.1 mM NADH or 10 mM succinate (in the presence of $2\ \mu\text{M}$ rotenone). Otherwise, artificial substrates such as

ascorbate/TMPD (10 mM and 100 μ M, respectively, in the presence of 2 μ M antimycin) were used for complex IV activity, and malonate and KCN were added to inhibit complex IV and complex II (10 mM and 5 mM, respectively).

2.6. NADH Dehydrogenase and Succinate Dehydrogenase Activities. Activities of complex I (NADH:DCPIP oxidoreductase) and complex II (succinate:DCPIP oxidoreductase) were determined spectrophotometrically at 600 nm by following the reduction of the artificial electron acceptor 2,6-dichlorophenol-indophenol (DCPIP; 50 μ M; $\epsilon_{\text{DCPIP}} = 21 \text{ mM}^{-1} \cdot \text{cm}^{-1}$). Mitochondria were permeabilized with 0.03% zwittergent and incubated in 10 mM KH_2PO_4 , 5 mM MgCl_2 , 1 mM EGTA, and 120 mM KCl (pH 7.4), either with 0.2 mM NADH (complex I) or 2 mM succinate (complex II), plus 0.2 mM methosulfate phenazine (PMS). Mitochondria protein concentration was 1 mg/ml, and the reaction was started by the addition of NADH or succinate [34].

2.7. ATP Synthase Assay. ATP hydrolysis of complex V was measured spectrophotometrically at 25°C using a coupled assay to the oxidation of NADH ($\epsilon_{340 \text{ nm}} = 6.22 \text{ mM}^{-1} \cdot \text{cm}^{-1}$). The assay contained 100 μ g mitochondrial protein, 10 mM HEPES (pH 8.0), 100 mM NaN_3 , 100 μ M NO_4Na , 90 mM KCl, 3 mM MgSO_4 ; the ATP regenerating system consisted of 5 mM phosphoenolpyruvate, 2 mM ATP, 0.03% zwittergent, 50 units/mL pyruvate kinase, and 30 units/mL lactate dehydrogenase. The ATPase reaction was started by the addition of 0.1 mM NADH. Oligomycin (6 μ g/mL) was added to inhibit ATPase activity and verify F1F0-ATP synthase integrity; mitochondria were incubated with oligomycin for 30 min [35].

2.8. Native Electrophoresis. Respiratory complexes and supercomplexes were resolved by native PAGE as reported previously [36]. Purified liver mitochondria (1 mg) were suspended in 50 mM Bis-Tris and 500 mM 6-aminocaproic acid (pH 7.0) and solubilized by adding digitonin (detergent : protein ratio of 1 : 5). The mixtures were incubated for 30 min at 4°C and centrifuged at 100,000 g for 30 min. The supernatants were recovered and immediately loaded on a linear gradient polyacrylamide gradient gels (4–10%) for Blue Native PAGE (BN-PAGE) or Clear Native PAGE high resolution (hrCN-PAGE).

For BN-PAGE, the anode buffer contained 50 mM Bis-Tris/HCl (pH 7.0); the cathode buffer contained 50 mM tricine and 15 mM Bis-Tris (pH 7.0), and Coomassie (0.02%). For the hrCN-PAGE, the anode buffer contained 25 mM imidazole/HCl (pH 7.0); while the cathode buffer contained 50 mM tricine, 7.5 mM imidazole, 0.01% β dodecyl D-maltoside, and 0.05% sodium deoxycholate (pH 7.0), supplemented with Ponceau S red [37]. Gels were run at 4°C and 35 V for 16 h. The molecular weights of the respiratory complexes or supercomplexes were estimated by using digitonin bovine heart mitochondrial complexes as standard: single complex: I = 1,000 kDa, V = 750 kDa, III₂ = 500 kDa,

IV = 230 kDa, II = 130 kDa; supercomplexes: I-III-IV₁₋₄ = 1500–2100 kDa, V₂ = 1500 kDa.

2.9. Complex and Supercomplexes In-Gel Activities. The in-gel activity assays were performed as Wittig and Schagger [38] for complex I activity (NADH:methylthiazolyl-diphenyl tetrazolium bromide reductase), complex II activity (succinate:methylthiazolyl-diphenyl tetrazolium bromide reductase), and complex IV activity (cytochrome *c*:diaminobenzidine reductase). In all cases, the assays were performed at 20–25°C and stopped with 50% methanol and 10% acetic acid, after 10–25 min.

The in-gel activity of complex V was performed in 50 mM glycine (adjusted to pH 8.0 with triethanolamine), 10 mM MgCl_2 , 0.15% $\text{Pb}(\text{ClO}_4)_2$, and 5 mM ATP. ATP hydrolysis was correlated with the development of white lead phosphate precipitates. The reaction was stopped using 50% methanol, and subsequently, the gel was transferred to water and scanned against a dark background as described previously [39].

2.10. SDS-Gel Electrophoresis and Western Blot Analysis. Liver mitochondrial proteins (20 μ g per well) were separated by SDS-PAGE according to Laemmli [40] in a 10% polyacrylamide gel under denaturing conditions. Proteins were then transferred from gel to PVDF membrane (Immobilon P; Millipore, Bedford, MA) in a semidry electroblotting system (Bio-Rad) at 25 V for 50 min. Membranes were blocked in 500 mM NaCl, 0.05% Tween-20, and 20 mM Tris-base (pH 7.5) (TTBS buffer), containing 5% blotting grade blocker nonfat dry milk. Then, membranes were incubated with antitotal OXPHOS antibody cocktail (at 1/500 dilution). Immunoreactive bands were visualized by enhanced chemiluminescence (Amersham Life Science, Inc.), according to the manufacturer's instructions, using horseradish peroxidase-conjugated antimouse IgG (at 1/10,000 dilution), and densitometric analyses were performed with the software Image Studio Lite version 5.2 (LI-COR Biosciences).

2.11. Protein Determination. The protein levels were estimated by the method described by Lowry et al. using BSA as standard [41].

2.12. Mitochondrial Glutathione Reductase Activity. Glutathione reductase enzymatic activity was recorded by NADPH consumption. Briefly, 50 μ g of purified mitochondria was placed in a phosphate buffer (50 mM, pH 7.0) containing 1 mM GSH and 0.1 M NADPH. NADPH reduction was measured at 340 nm ($\epsilon_{\text{NADPH}} = 6.22 \text{ M}^{-1} \cdot \text{cm}^{-1}$).

2.13. Measurement of Glutathione Concentration by HPLC-UV. To quantify GSH and GSSG concentrations, a standard curve of oxidized and reduced glutathione was used as described by Yilmaz et al. [42]. Mitochondrial samples were centrifuged at 500 rpm for 10 min and filtered to be injected

onto a Kromasil ETERNITY C18 column (4.6 × 150 mm). Mobile phase containing 10 mM of monobasic sodium phosphate and 2% methanol (pH 3.0) was used at a flow rate of 1 mL/min in isocratic run. GSH and GSSG eluted from the column were detected at 210 nm.

2.14. Lipid Peroxidation Assay. Mitochondrial lipid peroxidation was estimated by the thiobarbituric acid reactive substances (TBARS) method consisting of TBA-TCA-HCl reaction as described by Buege and Aust [43]. Samples were boiled at 95°C for 60 min, followed by a cooling and centrifugation steps at 12,000 rpm for 10 min at 4°C. The pink product absorbance (formed when the MDA reacts with TBA) was spectrophotometrically recorded at 532 nm ($\epsilon_{\text{MDA}} = 1.56 \times 10^5 \text{ M}^{-1} \cdot \text{cm}^{-1}$). MDA-TBA adduct peak was calibrated with tert-butyl hydroperoxide simultaneously processed as samples.

2.15. Mitochondrial H₂O₂ Measurement. H₂O₂ emission was determined by the fluorogenic indicator Amplex Red (Invitrogen) oxidation in presence of horseradish peroxidase as described by Starkov [44]. Fluorescence was recorded in a spectrofluorometer (LS 55 PerkinElmer Life Sciences) with excitation and emission wavelengths of 555 and 581, respectively. Briefly, 300 µg of purified mitochondria was added to 1 mL incubation buffer containing 125 mM KCl, 20 mM Hepes, 0.2 mM EGTA, 2 mM KH₂PO₄, 2% BSA, 1 µM Amplex Red, and 4 U horseradish peroxidase (pH 7.2). H₂O₂ production was initiated after addition of 5 mM pyruvate, 2.5 mM malate, and 10 mM succinate as substrates and 1 µM rotenone, 0.2 µM antimycin A, and 5 mM malonate as inhibitors.

2.16. Measurement of Protein Carbonylation. Determination of carbonyl content was followed as Levine et al. [45]. The oxidative damage to proteins was determined by carbonyl groups based on their reaction with 2,4-dinitrophenylhydrazine (DNPH) to form hydrazones. Briefly, 0.5 mg of mitochondria was incubated with 20 mM DNPH solution for 1 h; then proteins were precipitated with 20% (w/v) of trichloroacetic acid and redissolved in DNPH. In brief, the proteins were precipitated by the addition of 20% (w/v) of trichloroacetate; protein pellet was washed three times with ethanol : ethyl acetate (1:1) and resuspended in 1 mL of 6 M guanidine. The absorbance was recorded at 370 nm ($\epsilon_{\text{Hydrazone}} = 22 \times 10^3 \text{ M}^{-1} \cdot \text{cm}^{-1}$).

2.17. Measurement of HO-1 Activity. Fresh livers were placed in prechilled Dounce homogenizer, and cold homogenization buffer containing 100 mM potassium phosphate buffer (pH 7.4), 2 mM MgCl₂, 250 mM sucrose, and a protease inhibitor cocktail (10 µg/mL leupeptin, 10 µg/mL trypsin inhibitor, 2 µg/mL aprotinin, and 1 mM PMSF) was added. The homogenate was centrifuged at 10,000 g for 30 min at 4°C, followed by the supernatant centrifugation at 100,000 g for 60 min at 4°C, to obtain the microsomal fraction as a pellet. HO-1 activity was spectrophotometrically measured

as described previously [46]. The microsomal fraction (50 µL) was added to the reaction mixture (500 µL) containing 0.8 mM NADPH, 2 mM glucose-6-phosphate, 0.2 unit of glucose-6-phosphate dehydrogenase, 20 µM hemin, 100 mM potassium phosphate buffer (pH 7.4), and 2 mg of rat liver cytosol as a source of biliverdin reductase. The mixture was incubated at 37°C for 60 min in dark, and samples were left in an ice bath for at least 2 min to stop the reaction. Bilirubin product was determined by calculation from difference in optical density (OD) at 464 nm and 530 nm (OD₄₆₄ - OD₅₃₀ nm) of the sample. HO activity is expressed as pmol/min/mg protein.

2.18. Data Analysis. The obtained data are represented as mean ± standard deviation of three independent determinations, using the Sigma Plot software version 11.0. Differences between means were obtained by analysis of variance (ANOVA) and multiple comparison tests. *P* values < 0.05 were considered as significant.

3. Results and Discussion

The effectiveness of *M. oleifera* extract in alleviating diabetes was assessed in the STZ-induced diabetic model in Wistar rats. In response to STZ, rats showed increased water uptake, increased urine production, increased blood glucose levels, and reduced weight gain (D group = 229 ± 9.05 mg/dL and 156 ± 12 g), which were unaltered in the control group (C group = 78 ± 5.5 mg/dL and 187 ± 18 g), while M group significantly alleviated all parameters of diabetes (86 ± 4.2 mg/dl and 194 ± 8 g). These results suggest that *M. oleifera* leaf may be a potential agent in the treatment of type 1 diabetes and are agreed with the observations that suggest the beneficial effects of *Moringa oleifera* supplementation on diabetes [47, 48]. Hence, these results led us to investigate the valuable effects of the leaf extract on STZ-induced mitochondrial changes, in liver, evaluating STZ injury on both, respiratory and enzyme activities from respiratory chain and some of the antioxidant system comparing them with those from *M. oleifera* treatment.

3.1. *M. oleifera* Attenuates Oxidant Stress and the Decrease in the Glutathione System in Liver Mitochondria. Diabetic cells and tissues have the capacity to invoke adaptive mechanisms that evolved to defend against oxidative stress [49]. One putative mechanism is a defense system that would protect against ROS into mitochondria. These include the superoxide conversion to hydrogen peroxide (H₂O₂) by manganese superoxide dismutase (SOD) and scavenging H₂O₂ by catalase, glutathione peroxidase (GPx), or peroxiredoxin III [50]. Reduced glutathione (GSH) scavenges H₂O₂ via GPx, ubiquitously expressed both in the mitochondria matrix and intermembrane space [51]. In turn, the reduction of oxidized glutathione (GSSG) to GSH is catalyzed by glutathione reductase (GR), which requires NADPH. Thus, increased ROS removal results in increased NADPH turnover. Also, GSH can also be used in conjugation reactions to protect mitochondria enzymes from various toxins, for

TABLE 1: GSH and GSSG levels by HPLC-DAD and GR enzymatic activity in liver mitochondria from different groups.

Group	GSH ($\mu\text{mol}/\text{mg}$ protein)	GSSG ($\mu\text{mol}/\text{mg}$ protein)	GSH/GSSG ratio	Total GSH ($\mu\text{mol}/\text{mg}$ protein)	GR (U/min)
C	174.1 \pm 35.1	4.8 \pm 3.4	36.2 \pm 0.19	178.8 \pm 5.7	267.2 \pm 11.7
D	50.4 \pm 1*	49.8 \pm 1.1*	1 \pm 0.08*	100.2 \pm 1.3*	236 \pm 14.5
M	169 \pm 1.2**	54.7 \pm 2.2**	3 \pm 0.05**	223.7 \pm 2.9**	366.7 \pm 23.8**

C = control; D = diabetic; M = diabetic plus *Moringa*. *Significant difference versus control ($P < 0.05$). **Significant difference versus control and diabetic ($P < 0.05$).

TABLE 2: Levels of MDA and carbonyl groups in liver mitochondria from different treatments.

Group	MDA (nmol/mg prot)	Carbonyl groups (nmol/mg)	HO-1 (pmol/min/mg)
C	0.4317 \pm 0.009	3.7232 \pm 0.57	40.9 \pm 4.9
D	0.5028 \pm 0.06	12.738 \pm 0.28 [#]	85.7 \pm 2.1*
M	0.3851 \pm 0.02*	4.2645 \pm 0.98	105.2 \pm 3.4* [#]

C = control; D = diabetic; M = diabetic plus *Moringa*. *Significant difference versus diabetic ($P < 0.05$). [#]Significant difference versus control ($P < 0.05$).

example, by-products in lipid peroxidation such as 4-hydroxynonenal (HNE) [52].

To assess the influence of STZ injection on redox state, mitochondrial GSH levels and GR of liver were examined. A single dose of STZ caused a significant decrease in GSH and total GSH contents of diabetic rats (Table 1). Basal levels of total GSH were 178.8 \pm 5.7 $\mu\text{mol}/\text{mg}$ of protein in control mitochondria, whereas total GSH levels in isolated mitochondria from STZ-treated rats (D group) were significantly decreased by 70% compared with control (100.2 \pm 1.3 $\mu\text{mol}/\text{mg}$ of protein). In contrast, *M. oleifera* treatment prevented a STZ-mediated decrease in GSH levels (M group = 223.7 \pm 2.9 $\mu\text{mol}/\text{mg}$ of protein), which correspond to an increase of 25% compared with C group. It is worth to mention that M group rats showed a significant increase in values of GSH, total GSH (2 times), and GSH/GSSG ratio ($P < 0.05$) compared with D group. However, the M group ratio was 12 times reduced with respect to C group (Table 1). One possible explanation for this phenomenon may be the inactivation of mitochondrial GR activity. However, as observed in Table 1, STZ administration did not alter the GR activity in liver mitochondria when compared with control rats. However, M group samples significantly increased GR activity when compared with values of D and C groups (Table 1). Hence, these results show that GR inactivation is not the main mechanism of GSSG accumulation into the mitochondria.

The oxidative stress implications in diabetes pathogenesis are suggested to be produced not only by ROS generation but also by a nonenzymatic protein glycation, autooxidation of glucose, impairment of antioxidant enzymes, and peroxides formation. Therefore, GSH level decline is associated with oxidative damage to macromolecules, such as lipids and proteins. ROS-mediated lipid peroxidation is a crucial factor in the development of diabetic liver complications. In addition, GSH depletion induces heme oxygenase-1 (HO-1), a key microsomal enzyme in heme degradation to carbon monoxide (CO), iron (Fe^{2+}), and biliverdin; this latter being converted into bilirubin by the cytosolic biliverdin reductase [53, 54]. Moreover, some observations suggest the cytoprotective mechanism of HO-1 against oxidative stress

involving an increase in mitochondrial carrier levels and antiapoptotic proteins as well as in cytochrome *c* oxidase activity [55].

In order to evaluate this possibility, we measure carbonyls concentration, lipoperoxidation, and HO-1 activity. As observed in Table 2, C group showed the lowest levels of carbonylation and MDA. In contrast, STZ treatment increased lipid peroxidation and protein carbonyl content (Table 2). Besides, M group showed a significant decrease in lipoperoxidation in liver mitochondria ($P < 0.05$) when compared with D group. The carbonylation level in mitochondria of M group was significantly lower and showed significant difference when compared with D group (Table 2). In contrast, *M. oleifera* extract administration did not prevent the HO-1 induction provoked by STZ, where its enzymatic activity remained significantly higher. Our results clearly demonstrated that *M. oleifera* significantly suppressed both lipoperoxidation and protein carbonylation. However, *M. oleifera* did not lower the HO-1 activity, and little is known about the molecular mechanisms responsible for its activation, which requires further investigation.

It has been reported that *M. oleifera* exhibits bifunctional antioxidant properties related to its ability to react directly with ROS and to induce antioxidant enzymes expression such as superoxide dismutase, catalase, glutathione reductase, and glutathione peroxidase [56–58]. We confirmed previous data and showed that *Moringa* not only decreased lipoperoxidation and protein carbonylation levels in rat livers but also increased HO-1 activity, parameters associated with a cytoprotective mechanism against oxidative stress [59].

3.2. *Effects of STZ and M. oleifera on Oxygen Consumption.* Although many previous studies have reported pharmacological properties of *M. oleifera*, particularly as antioxidant and antidiabetic properties that may provide benefits for diabetic patients [25, 60, 61], there are no reports that show *M. oleifera* extract effect on mitochondria functionality. To determine the changes of mitochondria respiration in STZ-induced diabetic rats and *M. oleifera*

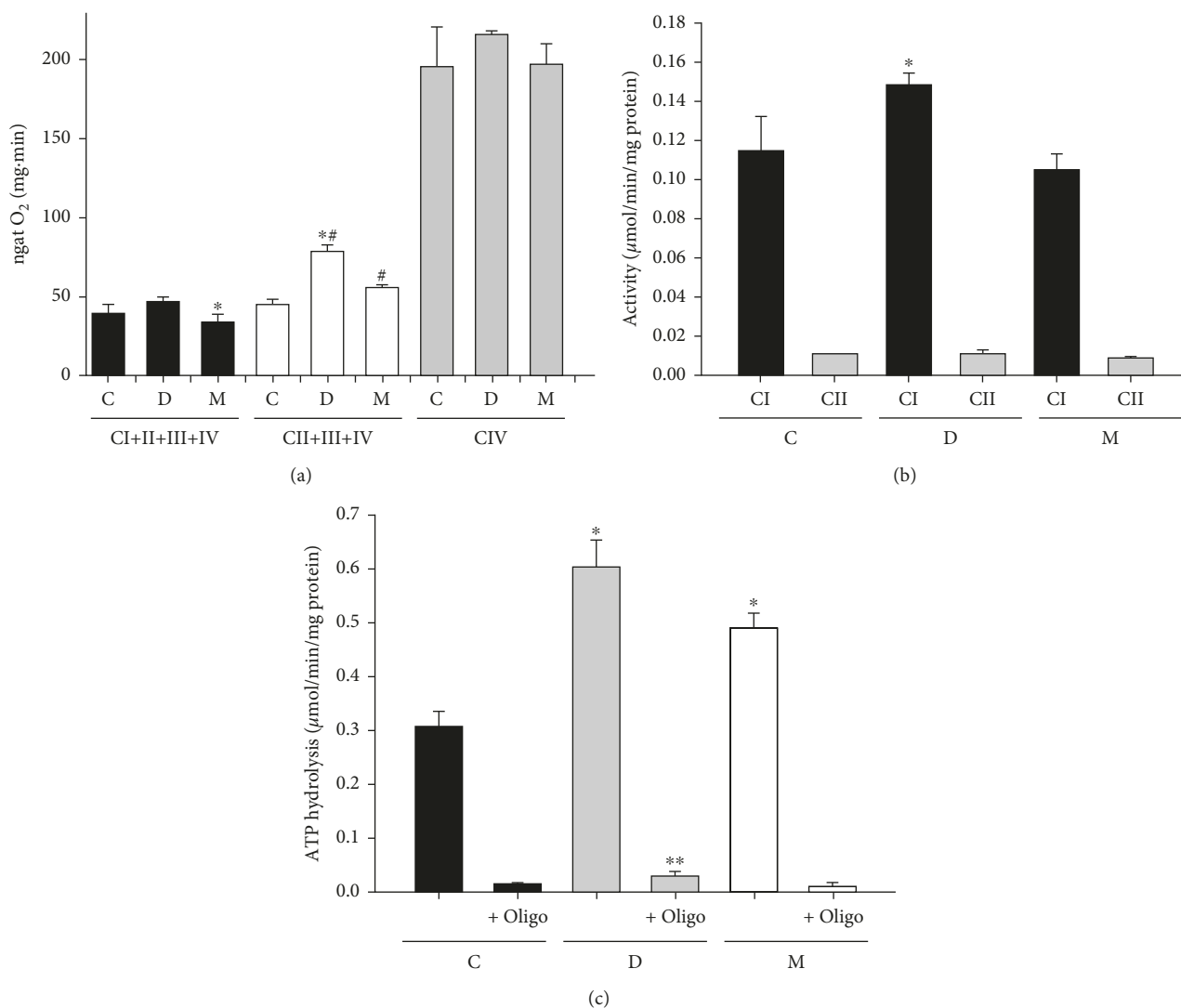


FIGURE 1: *Moringa oleifera* effect on mitochondrial respiratory chain. (a) Oxygen consumption (* $P < 0.05$ versus D; # $P < 0.05$ versus C); (b) enzymatic activity of complex I and II (* $P < 0.05$ versus C and M); (c) F₁/F₀ ATPase activity (* $P < 0.05$ versus C and M; ** $P < 0.05$ versus M + oligo) from liver mitochondria. C: control; D: diabetic; M: *Moringa*-treated diabetic groups.

protective effect, we measured the mitochondrial respiratory chain using Clark-type oxygen electrode and determined enzymatic activity of each complex by spectrophotometric methods.

Figure 1(a) shows the respiratory activity of all groups in presence of complex I, II, and IV substrates. The combination of pyruvate+malate indirectly investigates the monocarboxylate and dicarboxylate transporters and the pyruvate dehydrogenase activities. The substrate combination produces NADH which donates electrons to complex I. In D group, the state 4 respiration with pyruvate + malate was not affected. However, *Moringa* treatment resulted in 15% decrease in the state 4 respiration. By contrast, succinate donates electrons to FAD⁺ in complex II and yields significantly high respiration state 4 rates in both D and M groups compared with C group. Otherwise, in diabetic rats, state 4 respiration with succinate increased by 80% compared with control rats. The observed change in the diabetic

animals was rectified by *Moringa* treatment (Figure 1(a)). Additionally, functional analysis of complex IV (cytochrome *c* oxidase) maximal activity was assayed with ascorbate (Asc) and N,N,N',N'-tetramethyl-p-phenylenediamine (TMPD), which is an artificial redox mediator that assists the electron transfer from ascorbate to cytochrome *c*. Complex IV respiration was calculated as the portion sensitive to cyanide potassium (KCN), a specific inhibitor of cytochrome *c* oxidase (Figure 1(a)), revealing no differences among all experimental groups.

Additionally, we measured the specific activities of respiratory chain complexes in liver mitochondria. Spectrophotometric analysis showed a significant increase in complex I and ATPase activities in D group (Figure 1(c)), while *Moringa* treatment was effectively reversing this alteration nearly to control values. Complex II showed no significant change in mitochondrial fraction of D group (Figure 1(b)). These data show that individual activities of

mitochondrial electron transport chain (ETC) enzymes were not negatively modified in diabetic treatment. In addition, the respiratory properties of D and M groups have approximately 1.5–2 times succinate-respiratory rates compared with that of C group. Therefore, our results suggest that respiratory complex activities were not decreased in liver mitochondria in STZ-induced diabetic rats. These findings, which may appear, at first glance, contradictory, may be interpreted in terms of higher ETC efficiency, thus, avoiding energy losses by electron leakage in response to change in physiological functions and body energy requirements; ETC undergoes some modifications either during pathology development or disease [62]. In addition, several studies concerning STZ-treated rats have been performed with animals of different strains and different amounts of STZ [63, 64]. In addition, in isolated hepatocytes, increasing glucose concentration does not increase $\Delta\mu_{H^+}$, mitochondrial respiratory rate, or cytosolic NADH/NAD⁺ ratio; instead, most of glucose excess is converted to glycogen [65]. In fact, some authors have recently suggested that mitochondria overstimulation is a probable risk factor for insulin resistance, while moderate mitochondrial dysfunction may actually be protective under certain conditions, suggesting the mitochondrial modulation as a prospective therapy for metabolic diseases [66]. For this reason, it is important that future research clarifies the true energy functional state of isolated mitochondria from diabetic animals [67].

3.3. Modulation of Mitochondrial Complexes by STZ. As mitochondrial content can substantially impact on respiratory capacity, protein components of individual respiratory complexes were quantified. To test whether hyperglycemia and *M. oleifera* extract altered the composition of the ETC, we analyzed the expression level of nuclear-encoded mitochondrial complex I subunit NDUFB8, complex II subunit SDHB, complex III UQCRC2, complex IV MTCO1, and complex V ATP5A of each group. Interestingly, in diabetic rats, the NDUFB8 subunit resulted in an increase of complex I expression, while complex II and III were unaltered (Figure 2). These data which resulted in increased expression of NDUFB8 and MTCO1 support the suggestion that increased activity of mitochondrial respiratory chain could result from a proteome alteration leading to modulation of expression/activity of a range of mitochondrial components. More importantly, an upregulation of hepatic CI-NDUFB8 and CIV-MTCO1 was found in diabetic rats, consistent with changes in-gel activity of these complexes. Thus, it is plausible that increased NDUFB8 and MTCO1 contents observed in the STZ group, resulting from diabetes mellitus type 1, may account, in part, for the mitochondrial morphological changes observed, which could have downstream effects on mitochondrial functionality leading to hepatic dysfunction.

3.4. Loss of Redox State Does Not Destabilize Mitochondrial Supercomplexes. It is now widely accepted that mitochondrial respiratory chain is organized with stable and functional entities called supercomplexes (SC) [68]. SC consist of

various ratios of copies of individual complexes (I, III, IV, and V) to form stable, supramolecular structures; for instance, CI forms a supercomplex with CIII₂ and CIV (known as the respirasome), as well as with CIII₂ alone (SC I + III₂). CIII₂ forms a supercomplex with CIV (SC III₂ + IV), and CV forms dimers (CV₂). In addition, another recent advance is that the discovery of respiratory megacomplex (MC I₂III₂IV₂) represents the highest-order assembly of respiratory complexes [69], and it allows mitochondria to respond to energy requiring conditions and to minimize ROS generation during electron transfer reactions [70], as well as the sequestering of vulnerable sites of mitochondrial complexes from oxidative damage as a protective mechanism that prevents tight interactions between the individual complexes [71].

It is fairly well established in rectus abdominis muscle of diabetic obese patients. BN-PAGE revealed a striking decrease in complex I, III, and IV containing mitochondrial SC [72]. According to these results, Lenaz and Genova [71] suggest that oxidative stress acts primarily by disassembling supercomplex associations thereby establishing a vicious circle of oxidative stress and energy failure, ultimately leading to cell damage and disease.

It is interesting to mention that there are diverse specific regulatory proteins for the supramolecular organization of individual complexes that include CIV [73], respiratory SC factors 1 and 2 (Rcf1 and 2) [74], protein Cox interacting (Coi) [75], and COX7a2L [76]. These proteins down-regulation can impair the formation of SC; for instance, some studies show that diverse pathologies decrease CIV subunit levels affecting stoichiometry and assembly of SC [77, 78]. In addition, diabetes induces mitochondrial genome damage by an increased free radical production depleting antioxidant status [79]. Moreover, other structural components as cardiolipin have been shown to be crucial for functionality and SC formation and might be involved in the pathophysiology of diabetes [80]. Thus, the impact of complex IV failure and other enzymes may cause an energy crisis due to a lower ATP synthesis and an increased ROS production.

Figure 3(a) shows the Coomassie blue staining of the gels for all treatments and the colorimetric enzymatic staining of NADH, Succinate, COX, and ATPase complexes after detergent extraction and BN-PAGE or hrCN-PAGE (only for CV). Figure 3(b) clearly indicates that the major form of supercomplexes is present in all samples. In contrast, the amount of free complex I and IV were decreased in D group, and these values did not change in mitochondria isolated from M group. Otherwise, the in-gel activity of complex II was significantly lower in C group compared with those in the D and M groups. In addition, the brown bands indicate the presence of complex IV in all groups and its increase in D group (Figure 3(d)). On the other hand, in-gel ATP hydrolysis/lead phosphate precipitation assay revealed bands representing the F₁F₀ monomer and F₁F₀ dimer bands in Figures 3(e) and 3(f) showing the same functional patterns as the in-solution assays, indicating the level of intrinsic activity driven by complex V. In support, we have shown by comparing the in-gel enzyme activities that the ATPase

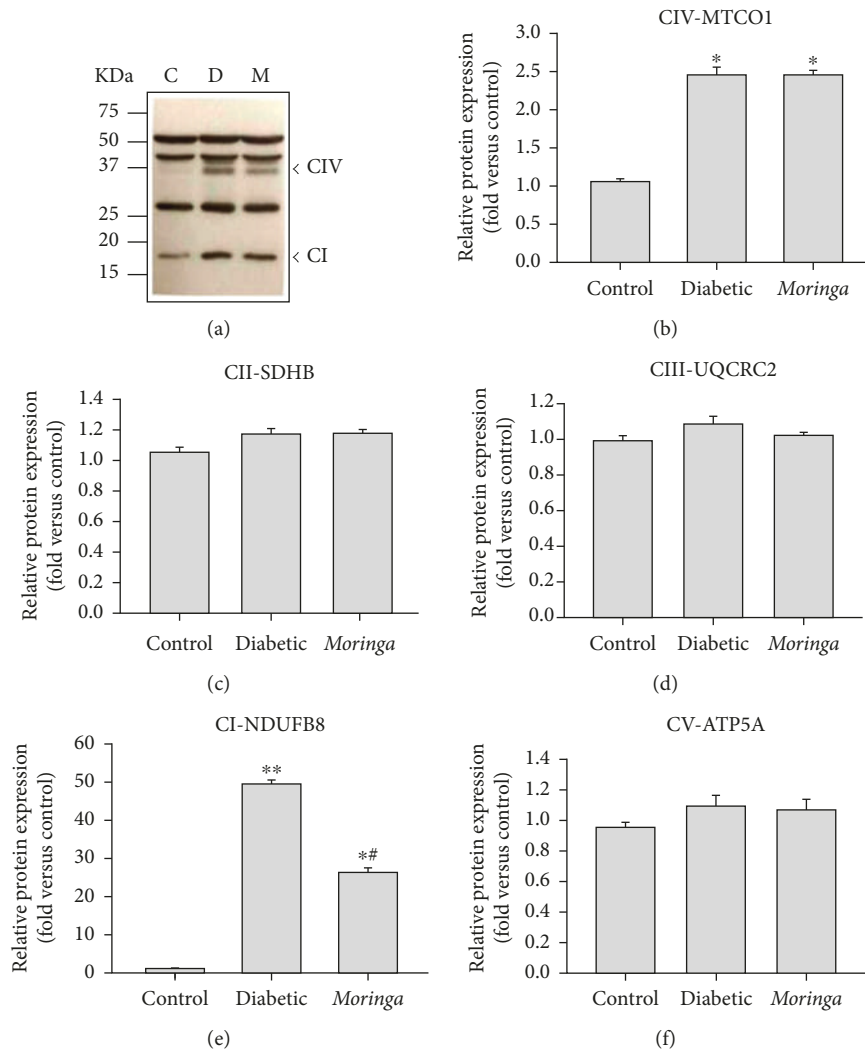


FIGURE 2: Characterization of OXPHOS proteins expressed in liver mitochondria during diabetes. (a) OXPHOS cocktail specificity demonstrated by a Western blot from liver-isolated mitochondria of diabetic rats and treated with *Moringa* extract. Relative expression of (b) MTC01 subunit of CIV, (c) SDHB subunit of CII, (d) UQCRC2 subunit of CIII, (e) NDUFB8 subunit of CI, and (f) ATP5A subunit of CV was performed by densitometric analysis from gel. Molecular mass standards are shown on the left panel of the gel. C: control; D: diabetic; M: *Moringa*-treated group. Data are shown as mean band density normalized relative to UQCRC2. Significant differences are represented by * $P < 0.05$ versus C; # $P < 0.05$ versus D.

activity of the F_1F_0 -ATP synthase is specifically and significantly increased in D group when compared with C group.

Our results are concerned with the changes in the amount of CIV subunits; for example, Cox6b1 is involved in the regulation of mitochondrial function by promoting SC formation, suggesting its antiaging effects of calorie restriction [81]. In addition, heart failure in dogs induced by coronary microembolism resulted in loss of complex IV containing SC of the electron transport chain [77, 78]. Similarly, in RAW 264.7 macrophages, knockdown of either subunit cytochrome *c* oxidase (CcO) Vb or CcO IV resulted in a significant decrease in CcO containing supercomplexes [78]. Liver mitochondria from ethanol-treated rat also showed a lower level of supercomplexes with a concomitant loss of CcO protein [82]. Therefore, complex IV has been

shown to be necessary for maintaining the stability of complex I in SC, as shown in mouse fibroblast cell lines, where a reduced expression of subunit IVi1 or nonsense mutation in subunit I not only resulted in lower CcO content but also caused significant reduction in complex I [83]. Structural defects in complex III also affected the amount of complex I, whereas chemical inhibition did not. Patients with defects in cytochrome *b* not only lose complex III but also show decreased amounts of complex I, while maintaining a normal enzymatic activity [84]. Conversely, the disruption of complex I function caused by nonsense mutations in NDUFS4, a subunit of this large multimeric complex, led to the partial loss of complex III activity in skin fibroblast cultures obtained from Leigh-like patients [85, 86]. However, defects in the complex I subunit ND5 did not cause a loss of complex III in the I-III supercomplex [87].

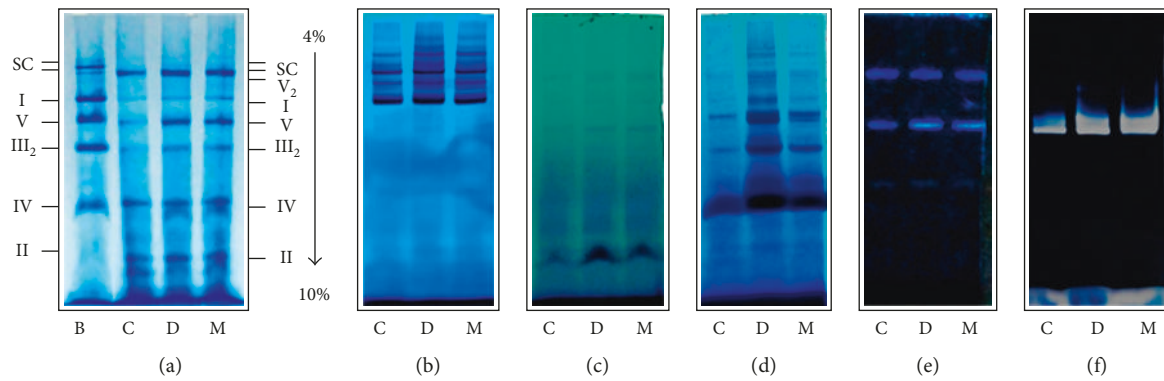


FIGURE 3: Electrophoretic representative pattern of liver mitochondrial solubilized of the different groups (5 g de digitonin/g protein). (a) Blue native polyacrylamide gel electrophoresis (BN-PAGE) stained with Coomassie blue; (b) complex I in-gel activity; (c) complex II in-gel activity; (d) complex IV in-gel activity; (e) complex IV in-gel activity; (f) high resolution clear native polyacrylamide gel electrophoresis (hrCN-PAGE) of complex V. B: bovine heart solubilized mitochondria (positive control); C: control; D: diabetic; M: *Moringa*-treated diabetic groups.

3.5. H_2O_2 Production by Liver Mitochondria Oxidizing Complex I and Complex II Substrates. Several studies have reported that ROS overproduction by mitochondrial ETC is responsible for hyperglycemia-induced oxidative stress and the pathogenesis of diabetic complications [88, 89]; however, it is not clear whether mitochondria of diabetic origin really generate ROS independently of the surrounding diabetic milieu. Herlein et al. [90] showed that the gastrocnemius, heart, and liver mitochondria of STZ-diabetic rats were not irrevocably altered to produce superoxide excess either by complex I or complex III. Moreover, gastrocnemius and heart mitochondria demonstrated an increased respiratory coupling, instead of a decrement. In addition, mitochondria of insulin-deficient diabetic rats did show signs of ROS overproduction. Thus, the detailed molecular mechanism and sites of ROS generation during diabetes are controversial.

In isolated mitochondria, the rate of mitochondrial ROS generation is directly governed by membrane potential ($\Delta\Psi_m$) and pH gradient across the inner membrane, favored only by a state 4 condition [91]. Hence, H_2O_2 production rate was measured in liver mitochondria using fluorescent dye Amplex Red and pyruvate plus malate or succinate, as complex I-III and II-III linked substrates, respectively, and the results are shown in Figure 4. Data presented in Figure 4 (a) show that the major source of ROS is complex I for liver mitochondria of C group, using pyruvate plus malate as substrate, reflecting the generation of superoxide anion. In contrast, with M group-isolated mitochondria oxidizing succinate in state 4 produced 6 times more ROS compared with other treatments (C and D groups) (Figure 4(b)). Therefore, the mitochondrial ROS production rates varied dramatically among the three experimental groups in response to addition of respiratory inhibitors.

At the level of ROS formation, all groups have the same basal formation using malate plus pyruvate or succinate, but the addition of respiratory inhibitors had a varied effect on ROS production in the different groups. In case of the C group, the addition of rotenone and antimycin stimulated

ROS production by using pyruvate and malate (Figure 4(a)). However, in both D group and M group, the addition of rotenone has no effect, while antimycin caused only a slight increase in ROS formation (Figure 4(a)). Nevertheless, with succinate, inhibitors have a different pattern. In the C group, the addition of rotenone causes no effect on ROS production, and antimycin favors its increase; but in this case, malonate has no effect (Figure 4(b)). However, in the diabetic group, antimycin has a greater effect on ROS production than control, and malonate adversely affects ROS formation (Figure 4(b)).

Finally, M group sensitivity to individual training inhibitors was unaltered in case of rotenone and malonate, but adding antimycin in this treatment favored ROS production (Figure 4(b)). Thus, measurements of ROS with Amplex Red cannot be used for sites of ROS generation from liver mitochondria treated with STZ and/or *M. oleifera*. This situation could be attributable to experimental conditions because complex I (rotenone), complex II (malonate), and complex III (antimycin A) inhibitors have been commonly used. However, the final concentration being used is not stationary, causing experimental errors that are different from one method to other. In addition, it is necessary to use other respiratory inhibitors, as stigmatellin and myxothiazol. No obstant, this does not deny other possible explanations that can affect ROS production as differences in the stoichiometry-activity ratios of the respiratory complexes [92], the susceptibility to proton pump slip at complex IV [93], or other mechanisms.

Damage to complex I, the most vulnerable ETC complex, increases ROS production, leading to a vicious circle of further mitochondrial dysfunction. It is important to note that complex I injury has a stronger impact on mitochondrial function compared with the damage to other complexes because mitochondria possess smaller amounts of complex I than other ETC complexes [94]. Superoxide production by complex I is much higher during reverse electron transport from succinate to NAD^+ [95]. In addition, it was found that defective complex I produces more ROS

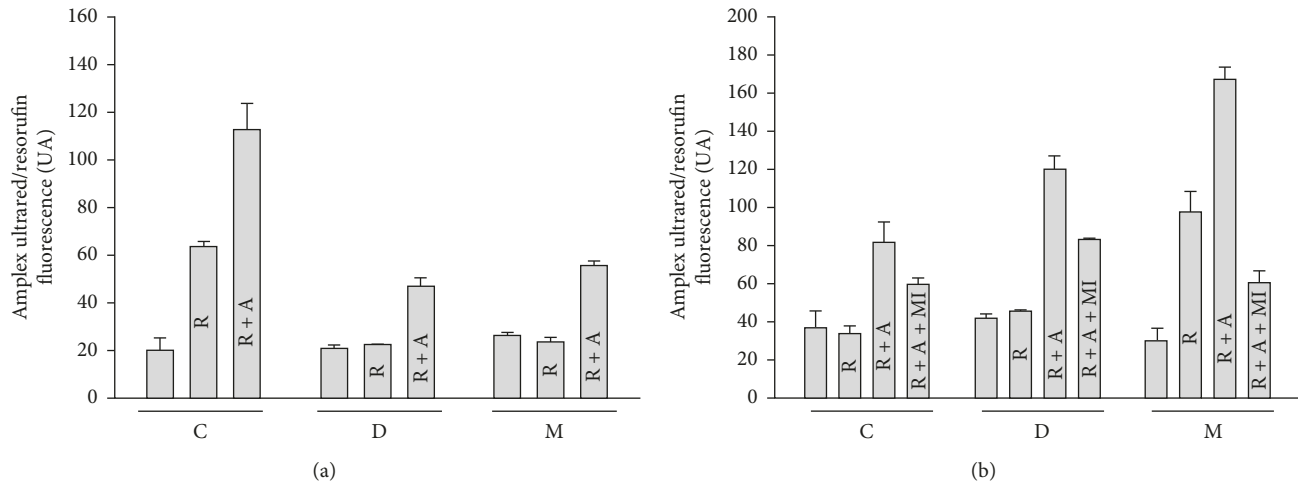


FIGURE 4: H_2O_2 production by mitochondrial respiratory chain measured by Amplex Red (UA) in liver mitochondria from different treatments (C: control; D: diabetic; M: *Moringa*-treated diabetic groups) oxidizing (a) pyruvate plus malate or (b) succinate as substrates and the effects of respiratory chain inhibitors (R: rotenone; A: antimycin A; MI: malonate). Mitochondria were studied during state 4 respiration. To correct for the increase in background fluorescence of the Amplex Red/HRP detection system overtime, fluorescence was monitored for a period of ten minutes. This background was subtracted from resorufin trace. Data are means \pm SEM ($n = 5$).

[96], suggesting that structural modifications of the enzyme may play a crucial role in ROS production process. Recently, it was reported that pancreatic mitochondrial complex I showed aberrant hyperactivity in type 1 and 2 STZ-diabetic mice and rat and in cultured β cells [97]. Further experiments focusing on STZ-induced diabetes in rats revealed that complex I's hyperactivity could be attenuated by metformin. Interestingly, in this study, no changes were reported in complex I activity in brain, liver, and heart by BN-PAGE [97]. However, the reason why complex I activity did not exhibit detectable increases in these tissues is unknown.

Our results in Figure 1(b) show that complex I activity was significantly higher in diabetes than in healthy individuals. This increased activity was apparently contributed by an increased NDUFB8 subunit protein content as shown in Figure 2(e). Moreover, the complex I hyperactivity also imposed pressure in complex IV (Figures 2(b) and 3(d)). These findings suggest that these elevated activities could be attributed for ROS production, given that higher ETC activity can also increase mitochondrial ROS generation [98, 99]. However, our results on specific sites of ROS generation along with ETC are controversial (Figure 4). This may explain why in some tissues seem that inhibition of electron transfer at complex I (by rotenone) may generate an increase in radical formation, whereas, in others, rotenone will reduce radical generation by preventing passage of electron further into the distal part of the chain. However, the basis for such a difference is obscure and presumed to be related to $\Delta\Psi_m$ changes and radicals leakage across the membranes [100].

Polyphenols have been traditionally viewed as antioxidants; however, increasing evidence has emerged supporting the ability of certain polyphenols to exert numerous ROS-scavenging independent actions. Then all these natural compounds modulate mitochondrial functions by inhibiting

organelle enzymes or metabolic pathways, by altering the production of ROS and modulating the activity of transcription factors which regulate the expression of mitochondrial proteins [101]. Thus, some particular polyphenols are now recognized as molecules capable of modulate pathways that define mitochondrial biogenesis (i.e., inducing sirtuins), mitochondrial membrane potential (i.e., mitochondrial permeability transition pore opening and uncoupling effects), mitochondrial electron transport chain and ATP synthesis (i.e., modulating complex I to V activity), intramitochondrial oxidative status (i.e., inhibiting/inducing ROS formation/removal enzymes), and ultimately mitochondrial-triggered cell death (modulating intrinsic apoptosis) (review in [102]). Thus, some studies have indicated that mitochondria may be the target organelle of phenolic compounds [103, 104]. Recently, it was reported that galangin (natural flavonoid) could maintain liver mitochondrial function in diabetic rats through oxidative stress reduction and both antioxidant enzymes and respiratory complexes activities enhancement [79]. Therefore, the likely role of mitochondrial ROS in diabetes has led to efforts for developing effective antioxidant compounds targeted to mitochondria.

This study was designed to investigate the protective effect of *M. oleifera* on liver bioenergetics and to elucidate its potential mechanism. *M. oleifera* resulted in a well-preserved mitochondrial redox potential, significantly by elevating heme oxygenase-1 and decreasing ROS formation and lipoperoxidation. These observations indicated that STZ-induced mitochondrial oxidative damage was remarkably attenuated. Thus, to our knowledge, we have shown for the first time that *M. oleifera* extract modulates mitochondrial respiratory activity, an effect that may account for some of the protective properties of phytochemicals. These effects may be of physiological significance since it seems that some phytochemicals are concentrated into mitochondria. The

results also support a pharmacological use of *M. oleifera* extract in drug to reduce mitochondrial damage in vivo. However, the details about mechanism of action require further investigation.

4. Conclusions

We provide experimental evidence indicating that *M. oleifera* extract targeting mitochondria can be used therapeutically to alleviate diabetes. Therefore, it will be important to identify regulatory proteins involved in the adjustment of respiratory chain complex organization/activity in response to altered redox state. In liver, the alteration of mitochondrial enzymatic activities and oxidative stress induced by STZ suggested of a compensatory response. In addition, *M. oleifera* extract upregulated mitochondrial genes linked with respiratory chain. Our data show an increased mitochondrial function and activity/expression of respiratory complexes in liver of STZ-diabetic rats, which can be normalized by *M. oleifera* at levels that do not markedly alter the consequences of hyperglycemia.

Conflicts of Interest

The authors declare no conflicts of interest.

Authors' Contributions

Erick Sierra-Campos, Mónica Andrea Valdez-Solana, and Óscar Flores-Herrera contributed to conceptualization, literature review, and writing the original draft. María Alejandra Sánchez-Muñoz, Mara Ibeth Campos-Almazán, and Guadalupe García-Arenas conducted the animal studies and performed the experiments. Erick Sierra-Campos, María Alejandra Sánchez-Muñoz, Mercedes Esparza-Perusquía, Sofía Olvera-Sánchez, and Óscar Flores-Herrera analyzed the data. Óscar Flores-Herrera, Alfredo Téllez-Valencia, Claudia Avitia-Domínguez, and Mónica Andrea Valdez-Solana contributed reagents/material/analysis tools. María Alejandra Sánchez-Muñoz and Erick Sierra-Campos wrote the paper. All authors read and approved the final manuscript.

Acknowledgments

The authors would like to express their sincere gratitude to the Consejo Nacional de Ciencia y Tecnología (Conacyt, México) for financial support to Erick Sierra-Campos (Grant 268184). The authors thank Héctor Vázquez-Meza for providing technical assistance. María Alejandra Sánchez Muñoz is also grateful to Conacyt, México, for the financial support for her Masters studies (Grant 601630). The authors are also grateful to the Mexican *Moringa oleifera* producers (Akuanandi) for providing all samples for this study.

Supplementary Materials

Figure S1: Possible mitochondrial processes that are modulated by *Moringa oleifera* extract. It is now well established that the individual mitochondrial respiratory complexes can

be organized into supercomplexes, but the composition and abundance of these may vary among organisms and tissues depending on the metabolic and physiological conditions. Alteration of mitochondrial electron transport chain is a recognized hallmark of the diabetic-associated decline in liver bioenergetics; however, the molecular events involved are only poorly understood. *Moringa oleifera* is used for the treatment of diabetes. However, its role on mitochondrial functionality is not yet established. This study was aimed to evaluate the effect of *M. oleifera* extract on supercomplex formation, ATPase activity, ROS production, GSH levels, lipid peroxidation, and protein carbonylation. The levels of lipid peroxidation and protein carbonylation were increased in the diabetic group. However, the levels were decreased in *M. oleifera*-treated diabetic rats. Analysis of in-gel activity showed an increase in all complexes activities in the diabetic group, but spectrophotometric determinations of complex II and IV activities were unaffected in this treatment. However, we found an oxygen consumption abolition through complex I-III-IV pathway in the diabetic group treated with *Moringa*. Respiration with succinate feeding into complex II-III-IV was increased in the diabetic group. We have shown for the first time that *M. oleifera* extract modulates mitochondrial respiratory activity, an effect that may account for some of the protective properties of phytochemicals. These effects may be of physiological significance since it seems that some phytochemicals are concentrated into mitochondria. The results also support a pharmacological use of *M. oleifera* extract in drug to reduce mitochondrial damage in vivo. (*Supplementary Materials*)

References

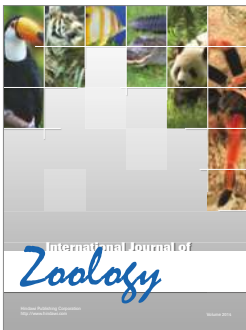
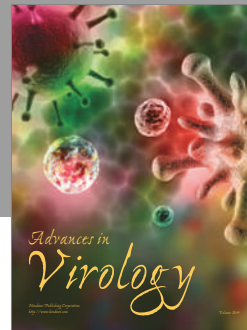
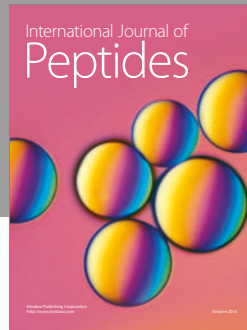
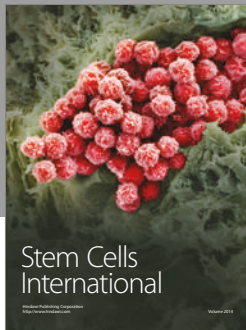
- [1] L. D. Osellame, T. S. Blacker, and M. R. Duchon, "Cellular and molecular mechanisms of mitochondrial function," *Best Practice & Research Clinical Endocrinology & Metabolism*, vol. 26, no. 6, pp. 711-723, 2012.
- [2] D. C. Chan, "Mitochondria: dynamic organelles in disease, aging, and development," *Cell*, vol. 125, no. 7, pp. 1241-1252, 2006.
- [3] C. Greggio, P. Jha, S. S. Kulkarni et al., "Enhanced respiratory chain supercomplex formation in response to exercise in human skeletal muscle," *Cell Metabolism*, vol. 25, no. 2, pp. 301-311, 2017.
- [4] S. J. Ramírez-Aguilar, M. Keuthe, M. Rocha et al., "The composition of plant mitochondrial supercomplexes changes with oxygen availability," *Journal of Biological Chemistry*, vol. 286, no. 50, pp. 43045-43053, 2011.
- [5] A. O. Helbig, M. J. L. de Groot, R. A. van Gestel et al., "A three-way proteomics strategy allows differential analysis of yeast mitochondrial membrane protein complexes under anaerobic and aerobic conditions," *Proteomics*, vol. 9, no. 20, pp. 4787-4798, 2009.
- [6] L. Böttinger, S. E. Horvath, T. Kleinschroth et al., "Phosphatidylethanolamine and cardiolipin differentially affect the stability of mitochondrial respiratory chain supercomplexes," *Journal of Molecular Biology*, vol. 423, no. 5, pp. 677-686, 2012.
- [7] J. E. Vance and G. Tasseva, "Formation and function of phosphatidylserine and phosphatidylethanolamine in mammalian cells," *Biochimica et Biophysica Acta (BBA)*-

- Molecular and Cell Biology of Lipids*, vol. 1831, no. 3, pp. 543–554, 2013.
- [8] A. Görlach, E. Y. Dimova, A. Petry et al., “Reactive oxygen species, nutrition, hypoxia and diseases: problems solved?,” *Redox Biology*, vol. 6, pp. 372–385, 2015.
- [9] M. P. Murphy and R. A. J. Smith, “Targeting antioxidants to mitochondria by conjugation to lipophilic cations,” *Annual Review of Pharmacology and Toxicology*, vol. 47, pp. 629–656, 2007.
- [10] B. B. Lowell and G. I. Shulman, “Mitochondrial dysfunction and type 2 diabetes,” *Science*, vol. 307, no. 5708, pp. 384–387, 2005.
- [11] K. Morino, K. F. Petersen, and G. I. Shulman, “Molecular mechanisms of insulin resistance in humans and their potential links with mitochondrial dysfunction,” *Diabetes*, vol. 55, no. 2, pp. S9–S15, 2006.
- [12] J. A. Brignone, C. M. C. de Brignone, R. R. Rodriguez, B. N. Badano, and A. O. M. Stoppani, “Modified oscillation behavior and decreased D-3-hydroxybutyrate dehydrogenase activity in diabetic rat liver mitochondria,” *Archives of Biochemistry and Biophysics*, vol. 214, no. 2, pp. 581–588, 1982.
- [13] J. A. Brignone, C. M. C. de Brignone, C. R. Ricci, I. R. de Mignone, M. C. Susemihl, and R. R. Rodríguez, “Favourable, significant effect of the dose-dependent treatment with RU 38486 (RU) on the alterations of the hepatic mitochondrial function of diabetic rats,” *Diabetes Research and Clinical Practice*, vol. 32, no. 3, pp. 141–148, 1996.
- [14] H. Raza and A. John, “Implications of altered glutathione metabolism in aspirin-induced oxidative stress and mitochondrial dysfunction in HepG2 cells,” *PLoS One*, vol. 7, no. 4, article e36325, 2012.
- [15] G. K. Bandyopadhyay, G. Y. Joseph, J. Ofrecio, and J. M. Olefsky, “Increased malonyl-CoA levels in muscle from obese and type 2 diabetic subjects lead to decreased fatty acid oxidation and increased lipogenesis; thiazolidinedione treatment reverses these defects,” *Diabetes*, vol. 55, no. 8, pp. 2277–2285, 2006.
- [16] J. G. Duncan, “Mitochondrial dysfunction in diabetic cardiomyopathy,” *Biochimica et Biophysica Acta (BBA)-Molecular Cell Research*, vol. 1813, no. 7, pp. 1351–1359, 2011.
- [17] L. Rato, A. I. Duarte, G. D. Tomás et al., “Pre-diabetes alters testicular PGC1- α /SIRT3 axis modulating mitochondrial bioenergetics and oxidative stress,” *Biochimica et Biophysica Acta (BBA)-Bioenergetics*, vol. 1837, no. 3, pp. 335–344, 2014.
- [18] W. C. Parks and R. L. Drake, “Insulin mediates the stimulation of pyruvate kinase by a dual mechanism,” *Biochemical Journal*, vol. 208, no. 2, pp. 333–337, 1982.
- [19] G. Antoun, F. McMurray, A. B. Thrush et al., “Erratum to: Impaired mitochondrial oxidative phosphorylation and supercomplex assembly in rectus abdominis muscle of diabetic obese individuals,” *Diabetologia*, vol. 59, no. 2, pp. 396–397, 2016.
- [20] C. D. Berdanier, H. B. Everts, C. Hermoyian, and C. E. Mathews, “Role of vitamin A in mitochondrial gene expression,” *Diabetes Research and Clinical Practice*, vol. 54, no. 2, pp. S11–S27, 2001.
- [21] D. Loven, H. Schedl, H. Wilson et al., “Effect of insulin and oral glutathione on glutathione levels and superoxide dismutase activities in organs of rats with streptozocin-induced diabetes,” *Diabetes*, vol. 35, no. 5, pp. 503–507, 1986.
- [22] P. S. Samiec, C. Drews-Botsch, E. W. Flagg et al., “Glutathione in human plasma: decline in association with aging, age-related macular degeneration, and diabetes,” *Free Radical Biology and Medicine*, vol. 24, no. 5, pp. 699–704, 1998.
- [23] A. Abd El Latif, B. E. S. El Bialy, H. D. Mahboub, and M. A. Abd Eldaim, “*Moringa oleifera* leaf extract ameliorates alloxan-induced diabetes in rats by regeneration of β cells and reduction of pyruvate carboxylase expression,” *Biochemistry and Cell Biology*, vol. 92, no. 5, pp. 413–419, 2014.
- [24] S. Sreelatha and P. R. Padma, “Antioxidant activity and total phenolic content of *Moringa oleifera* leaves in two stages of maturity,” *Plant Foods for Human Nutrition*, vol. 64, no. 4, pp. 303–311, 2009.
- [25] P. Chumark, P. Khunawat, Y. Sanvarinda et al., “The *in vitro* and *ex vivo* antioxidant properties, hypolipidaemic and antiatherosclerotic activities of water extract of *Moringa oleifera* Lam. leaves,” *Journal of Ethnopharmacology*, vol. 116, no. 3, pp. 439–446, 2008.
- [26] A. L. Al-Malki and H. A. El Rabey, “The antidiabetic effect of low doses of *Moringa oleifera* Lam. seeds on streptozotocin induced diabetes and diabetic nephropathy in male rats,” *BioMed Research International*, vol. 2015, Article ID 381040, 13 pages, 2015.
- [27] D. J. Dorta, A. A. Pigoso, F. E. Mingatto et al., “The interaction of flavonoids with mitochondria: effects on energetic processes,” *Chemico-Biological Interactions*, vol. 152, no. 2-3, pp. 67–78, 2005.
- [28] I. Elingold, M. P. Isollabella, M. B. Casanova et al., “Mitochondrial toxicity and antioxidant activity of a prenylated flavonoid isolated from *Dalea elegans*,” *Chemico-Biological Interactions*, vol. 171, no. 3, pp. 294–305, 2008.
- [29] R. Lagoa, I. Graziani, C. Lopez-Sanchez, V. Garcia-Martinez, and C. Gutierrez-Merino, “Complex I and cytochrome *c* are molecular targets of flavonoids that inhibit hydrogen peroxide production by mitochondria,” *Biochimica et Biophysica Acta (BBA)-Bioenergetics*, vol. 1807, no. 12, pp. 1562–1572, 2011.
- [30] N. Madi, M. Dany, S. Abdoun, and J. Usta, “*Moringa oleifera*’s nutritious aqueous leaf extract has anticancerous effects by compromising mitochondrial viability in an ROS-dependent manner,” *Journal of the American College of Nutrition*, vol. 35, no. 7, pp. 604–613, 2016.
- [31] W. Khan, R. Parveen, K. Chester, S. Parveen, and S. Ahmad, “Hypoglycemic potential of aqueous extract of *Moringa oleifera* leaf and *in vivo* GC-MS metabolomics,” *Frontiers in Pharmacology*, vol. 8, p. 577, 2017.
- [32] R. Hovius, H. Lambrechts, K. Nicolay, and B. de Kruijff, “Improved methods to isolate and subfractionate rat liver mitochondria. Lipid composition of the inner and outer membrane,” *Biochimica et Biophysica Acta (BBA)-Biomembranes*, vol. 1021, no. 2, pp. 217–226, 1990.
- [33] E. Sierra-Campos, I. Velazquez, D. Matuz-Mares, A. Villavicencio-Queijeiro, and J. P. Pardo, “Functional properties of the *Ustilago maydis* alternative oxidase under oxidative stress conditions,” *Mitochondrion*, vol. 9, no. 2, pp. 96–102, 2009.
- [34] D. D. L. R. Castillo, M. Zarco-Zavala, S. Olvera-Sanchez et al., “Atypical cristae morphology of human syncytiotrophoblast mitochondria role for complex V,” *Journal of Biological Chemistry*, vol. 286, no. 27, pp. 23911–23919, 2011.
- [35] M. Esparza-Perusquia, S. Olvera-Sánchez, J. P. Pardo, G. Mendoza-Hernández, F. Martínez, and O. Flores-Herrera, “Structural and kinetics characterization of the F₁F₀-ATP synthase dimer. New repercussion of monomer-monomer contact,” *Biochimica et Biophysica Acta (BBA)-Bioenergetics*, vol. 1858, no. 12, pp. 975–981, 2017.

- [36] H. Schagger and G. von Jagow, "Blue native electrophoresis for isolation of membrane protein complexes in enzymatically active form," *Analytical Biochemistry*, vol. 199, no. 2, pp. 223–231, 1991.
- [37] I. Wittig, M. Karas, and H. Schagger, "High resolution clear native electrophoresis for in-gel functional assays and fluorescence studies of membrane protein complexes," *Molecular & Cellular Proteomics*, vol. 6, no. 7, pp. 1215–1225, 2007.
- [38] I. Wittig and H. Schagger, "Electrophoretic methods to isolate protein complexes from mitochondria," *Methods in Cell Biology*, vol. 80, pp. 723–741, 2007.
- [39] S. J. Couoh-Cardel, S. Uribe-Carvajal, S. Wilkens, and J. J. García-Trejo, "Structure of dimeric F₁F₀-ATP synthase," *Journal of Biological Chemistry*, vol. 285, no. 47, pp. 36447–36455, 2010.
- [40] U. K. Laemmli, "Cleavage of structural proteins during the assembly of the head of bacteriophage T4," *Nature*, vol. 227, no. 5259, pp. 680–685, 1970.
- [41] O. H. Lowry, N. J. Rosebrough, A. L. Farr, and R. J. Randall, "Protein measurement with the Folin phenol reagent," *Journal of Biological Chemistry*, vol. 193, no. 1, pp. 265–275, 1951.
- [42] O. Yilmaz, S. Keser, M. Tuzcu et al., "A practical HPLC method to measure reduced (GSH) and oxidized (GSSG) glutathione concentrations in animal tissues," *Journal of Animal and Veterinary Advances*, vol. 8, no. 2, pp. 343–347, 2009.
- [43] J. A. Buege and S. D. Aust, "Microsomal lipid peroxidation," *Methods in Enzymology*, vol. 52, pp. 302–310, 1978.
- [44] A. A. Starkov, "Measurement of Mitochondrial ROS Production," in *Protein Misfolding and Cellular Stress in Disease and Aging. Methods in Molecular Biology (Methods and Protocols)*, P. Bross and N. Gregersen, Eds., vol. 648, pp. 245–255, Springer, New York, NY, USA, 2010.
- [45] R. L. Levine, D. Garland, C. N. Oliver et al., "Determination of carbonyl content in oxidatively modified proteins," *Methods in Enzymology*, vol. 186, pp. 464–478, 1990.
- [46] P. Naughton, R. Foresti, S. K. Bains, M. Hoque, C. J. Green, and R. Motterlini, "Induction of heme oxygenase 1 by nitrosative stress. A role for nitroxyl anion," *Journal of Biological Chemistry*, vol. 277, no. 43, pp. 40666–40674, 2002.
- [47] P. Kiranmayi and B. Babitha, "Effect of *Moringa oleifera* Leaf powder on blood glucose levels in type II diabetes mellitus patients," *Vegetos-An International Journal of Plant Research*, vol. 24, no. 2, pp. 114–116, 2011.
- [48] P. Anthanont, N. Lumlerdkij, P. Akarasereenont, S. Vannasaeng, and A. Sriwijitkamol, "*Moringa oleifera* leaf increases insulin secretion after single dose administration: a preliminary study in healthy subjects," *Journal of the Medical Association of Thailand*, vol. 99, no. 3, pp. 308–313, 2016.
- [49] A. C. Maritim, R. A. Sanders, and J. B. Watkins III, "Effects of α -lipoic acid on biomarkers of oxidative stress in streptozotocin-induced diabetic rats," *Journal of Nutritional Biochemistry*, vol. 14, no. 5, pp. 288–294, 2003.
- [50] A. C. Maritim, R. A. Sanders, and J. B. Watkins III, "Diabetes, oxidative stress, and antioxidants: a review," *Journal of Biochemical and Molecular Toxicology*, vol. 17, no. 1, pp. 24–38, 2003.
- [51] A. B. Egorova, Y. A. Uspenskaya, and V. P. Nefedov, "NAD and glutathione modulate sensitivity of bone marrow cells to oxidative stress," *Bulletin of Experimental Biology and Medicine*, vol. 132, no. 1, pp. 637–640, 2001.
- [52] W. Völkel, R. Alvarez-Sánchez, I. Weick, A. Mallya, W. Dekanta, and A. Pähler, "Glutathione conjugates of 4-hydroxy-2 (E)-nonenal as biomarkers of hepatic oxidative stress-induced lipid peroxidation in rats," *Free Radical Biology and Medicine*, vol. 38, no. 11, pp. 1526–1536, 2005.
- [53] R. Tenhunen, H. S. Marver, and R. Schmid, "The enzymatic conversion of heme to bilirubin by microsomal heme oxygenase," *Proceedings of the National Academy of Sciences*, vol. 61, no. 2, pp. 748–755, 1968.
- [54] R. K. Kutty and M. D. Maines, "Purification and characterization of biliverdin reductase from rat liver," *Journal of Biological Chemistry*, vol. 256, no. 8, pp. 3956–3962, 1981.
- [55] M. A. Di Noia, S. Van Driesche, F. Palmieri et al., "Heme oxygenase-1 enhances renal mitochondrial transport carriers and cytochrome c oxidase activity in experimental diabetes," *Journal of Biological Chemistry*, vol. 281, no. 23, pp. 15687–15693, 2006.
- [56] D. Jaiswal, P. K. Rai, S. Mehta et al., "Role of *Moringa oleifera* in regulation of diabetes-induced oxidative stress," *Asian Pacific Journal of Tropical Medicine*, vol. 6, no. 6, pp. 426–432, 2013.
- [57] R. Gupta, M. Mathur, V. K. Bajaj et al., "Evaluation of antidiabetic and antioxidant activity of *Moringa oleifera* in experimental diabetes," *Journal of Diabetes*, vol. 4, no. 2, pp. 164–171, 2012.
- [58] A. F. Santos, A. C. Argolo, P. M. Paiva, and L. C. Coelho, "Antioxidant activity of *Moringa oleifera* tissue extracts," *Phytotherapy Research*, vol. 26, no. 9, pp. 1366–1370, 2012.
- [59] C. S. T. Origassa and N. O. S. Câmara, "Cytoprotective role of heme oxygenase-1 and heme degradation derived end products in liver injury," *World Journal of Hepatology*, vol. 5, no. 10, p. 541, 2013.
- [60] D. Jaiswal, P. K. Rai, A. Kumar, S. Mehta, and G. Watal, "Effect of *Moringa oleifera* Lam. leaves aqueous extract therapy on hyperglycemic rats," *Journal of Ethnopharmacology*, vol. 123, no. 3, pp. 392–396, 2009.
- [61] S. Adisakwattana and B. Chanathong, "Alpha-glucosidase inhibitory activity and lipid-lowering mechanisms of *Moringa oleifera* leaf extract," *European Review for Medical and Pharmacological Sciences*, vol. 15, no. 7, pp. 803–808, 2011.
- [62] F. M. Ferreira, C. M. Palmeira, R. Seica, A. J. Moreno, and M. S. Santos, "Diabetes and mitochondrial bioenergetics: alterations with age," *Journal of Biochemical and Molecular Toxicology*, vol. 17, no. 4, pp. 214–222, 2003.
- [63] S. Ardestani, D. L. Deskins, and P. P. Young, "Membrane TNF-alpha-activated programmed necrosis is mediated by Ceramide-induced reactive oxygen species," *Journal of Molecular Signaling*, vol. 8, p. 12, 2013.
- [64] D.-D. Zhao, N. Yu, X.-K. Li et al., "Antidiabetic and anti-oxidative effect of Jiang Tang Xiao Ke granule in high-fat diet and low-dose streptozotocin induced diabetic rats," *Evidence-Based Complementary and Alternative Medicine*, vol. 2014, Article ID 475192, 8 pages, 2014.
- [65] E. K. Ainscow and M. D. Brand, "Top-down control analysis of ATP turnover, glycolysis and oxidative phosphorylation in rat hepatocytes," *FEBS Journal*, vol. 263, no. 3, pp. 671–685, 1999.
- [66] C. Desler, T. L. Hansen, J. B. Frederiksen, M. L. Marcker, K. K. Singh, and L. J. Rasmussen, "Is there a link between mitochondrial reserve respiratory capacity and aging?," *Journal of Aging Research*, vol. 2012, Article ID 192503, 9 pages, 2012.
- [67] D. A. Rendon, K. Kotedia, S. F. Afshar et al., "Mapping radiation injury and recovery in bone marrow using ¹⁸F-FLT

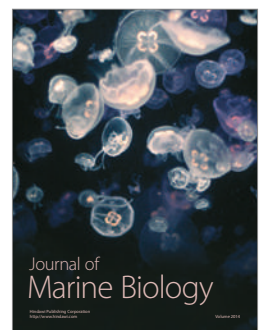
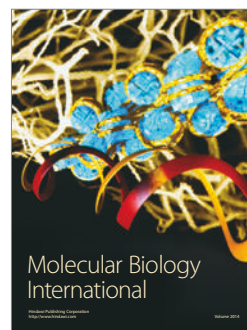
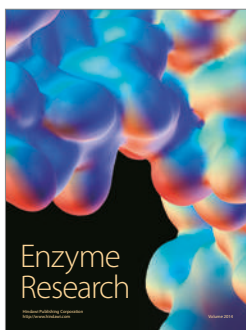
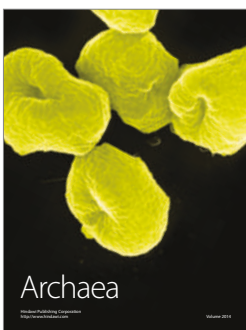
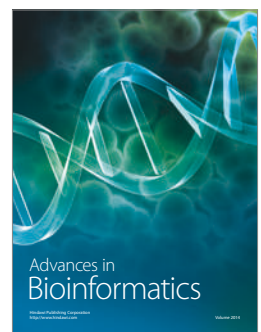
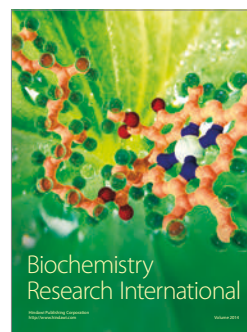
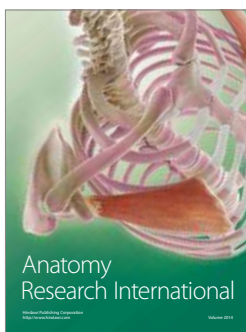
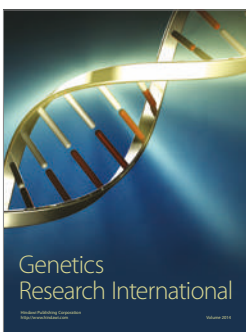
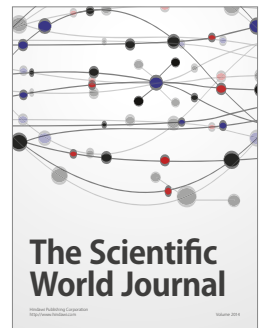
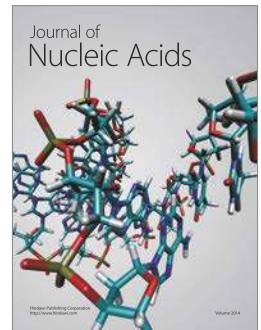
- PET/CT and USPIO MRI in a rat model,” *Journal of Nuclear Medicine*, vol. 57, no. 2, pp. 266–271, 2016.
- [68] T. Lobo-Jarne and C. Ugalde, “Respiratory chain super-complexes: structures, function and biogenesis,” *Seminars in Cell & Developmental Biology*, 2017, in press.
- [69] R. Guo, S. Zong, M. Wu, J. Gu, and M. Yang, “Architecture of human mitochondrial respiratory megacomplex I₂III₂IV₂,” *Cell*, vol. 170, no. 6, pp. 1247–1257, 2017.
- [70] D. R. Winge, “Sealing the mitochondrial respirasome,” *Molecular and Cellular Biology*, vol. 32, no. 14, pp. 2647–2652, 2012.
- [71] G. Lenaz and M. L. Genova, “Supramolecular organisation of the mitochondrial respiratory chain: a new challenge for the mechanism and control of oxidative phosphorylation,” *Advances in Experimental Medicine and Biology*, vol. 748, pp. 107–144, 2012.
- [72] G. Antoun, F. McMurray, A. B. Thrush et al., “Impaired mitochondrial oxidative phosphorylation and supercomplex assembly in rectus abdominis muscle of diabetic obese individuals,” *Diabetologia*, vol. 58, no. 12, pp. 2861–2866, 2015.
- [73] C. Oswald, U. Krause-Buchholz, and G. Rödel, “Knockdown of human COX17 affects assembly and supramolecular organization of cytochrome c oxidase,” *Journal of Molecular Biology*, vol. 389, no. 3, pp. 470–479, 2009.
- [74] C. R. Lundin, C. von Ballmoos, M. Ott, P. Ädelrotha, and P. Brzezinski, “Regulatory role of the respiratory super-complex factors in *Saccharomyces cerevisiae*,” *Proceedings of the National Academy of Sciences of the United States of America*, vol. 113, no. 31, pp. E4476–E4485, 2016.
- [75] R. K. Singhal, C. Kruse, J. Heidler et al., “Coil is a novel assembly factor of the yeast complex III–complex IV supercomplex,” *Molecular Biology of the Cell*, vol. 28, no. 20, pp. 2609–2622, 2017.
- [76] R. Pérez-Pérez, T. Lobo-Jarne, D. Milenkovic et al., “COX7A2L is a mitochondrial complex III binding protein that stabilizes the III₂ + IV supercomplex without affecting respirasome formation,” *Cell Reports*, vol. 16, no. 9, pp. 2387–2398, 2016.
- [77] M. G. Rosca, E. J. Vazquez, J. Kerner et al., “Cardiac mitochondria in heart failure: decrease in respirasomes and oxidative phosphorylation,” *Cardiovascular Research*, vol. 80, no. 1, pp. 30–39, 2008.
- [78] D. Galati, S. Srinivasan, H. Raza et al., “Role of nuclear-encoded subunit Vb in the assembly and stability of cytochrome c oxidase complex: implications in mitochondrial dysfunction and ROS production,” *Biochemical Journal*, vol. 420, no. 3, pp. 439–449, 2009.
- [79] A. A. Aloud, C. Veeramani, C. Govindasamy, M. A. Alsaif, A. S. El Newehy, and K. S. Al-Numair, “Galangin, a dietary flavonoid, improves antioxidant status and reduces hyperglycemia-mediated oxidative stress in streptozotocin-induced diabetic rats,” *Redox Report*, vol. 22, no. 6, pp. 290–300, 2017.
- [80] V. B. Ritov, E. V. Menshikova, K. Azuma et al., “Deficiency of electron transport chain in human skeletal muscle mitochondria in type 2 diabetes mellitus and obesity,” *American Journal of Physiology-Endocrinology and Metabolism*, vol. 298, no. 1, pp. E49–E58, 2010.
- [81] S.-E. Kim, R. Mori, T. Komatsu et al., “Upregulation of cytochrome c oxidase subunit 6b1 (Cox6b1) and formation of mitochondrial supercomplexes: implication of Cox6b1 in the effect of calorie restriction,” *Age*, vol. 37, no. 3, p. 45, 2015.
- [82] S. Bansal, M. Siddarth, D. Chawla, B. D. Banerjee, S. V. Madhu, and A. K. Tripathi, “Advanced glycation end products enhance reactive oxygen and nitrogen species generation in neutrophils in vitro,” *Molecular and Cellular Biochemistry*, vol. 361, no. 1-2, pp. 289–296, 2012.
- [83] Y. Li, J.-S. Park, J.-H. Deng, and Y. Bai, “Cytochrome c oxidase subunit IV is essential for assembly and respiratory function of the enzyme complex,” *Journal of Bioenergetics and Biomembranes*, vol. 38, no. 5-6, pp. 283–291, 2006.
- [84] H. Schägger, R. de Coo, M. F. Bauer, S. Hofmann, C. Godinot, and U. Brandt, “Significance of respirasomes for the assembly/stability of human respiratory chain complex I,” *Journal of Biological Chemistry*, vol. 279, no. 35, pp. 36349–36353, 2004.
- [85] S. Budde, L. van den Heuvel, R. Smeets et al., “Clinical heterogeneity in patients with mutations in the NDUFS4 gene of mitochondrial complex I,” *Journal of Inherited Metabolic Disease*, vol. 26, no. 8, pp. 813–815, 2003.
- [86] S. Scacco, V. Petruzzella, S. Budde et al., “Pathological mutations of the human NDUFS4 gene of the 18-kDa (AQDQ) subunit of complex I affect the expression of the protein and the assembly and function of the complex,” *Journal of Biological Chemistry*, vol. 278, no. 45, pp. 44161–44167, 2003.
- [87] P. Cardol, L. Boutaffala, S. Memmi, B. Devreese, R. F. Matagnea, and C. Remaclea, “In *Chlamydomonas*, the loss of ND5 subunit prevents the assembly of whole mitochondrial complex I and leads to the formation of a low abundant 700 kDa subcomplex,” *Biochimica et Biophysica Acta (BBA)-Bioenergetics*, vol. 1777, no. 4, pp. 388–396, 2008.
- [88] M. Brownlee, “The pathobiology of diabetic complications,” *Diabetes*, vol. 54, no. 6, pp. 1615–1625, 2005.
- [89] M. R. Duchon, “Roles of mitochondria in health and disease,” *Diabetes*, vol. 53, no. 1, pp. S96–S102, 2004.
- [90] J. A. Herlein, B. D. Fink, Y. O’Malley, and W. I. Sivitz, “Superoxide and respiratory coupling in mitochondria of insulin-deficient diabetic rats,” *Endocrinology*, vol. 150, no. 1, pp. 46–55, 2008.
- [91] M. D. Brand, C. Affourtit, T. C. Esteves et al., “Mitochondrial superoxide: production, biological effects, and activation of uncoupling proteins,” *Free Radical Biology and Medicine*, vol. 37, no. 6, pp. 755–767, 2004.
- [92] L. K. Kwong and R. S. Sohal, “Substrate and site specificity of hydrogen peroxide generation in mouse mitochondria,” *Archives of Biochemistry and Biophysics*, vol. 350, no. 1, pp. 118–126, 1998.
- [93] B. Kadenbach, “Intrinsic and extrinsic uncoupling of oxidative phosphorylation,” *Biochimica et Biophysica Acta (BBA)-Bioenergetics*, vol. 1604, no. 2, pp. 77–94, 2003.
- [94] A. Musatov and N. C. Robinson, “Susceptibility of mitochondrial electron-transport complexes to oxidative damage. Focus on cytochrome c oxidase,” *Free Radical Research*, vol. 46, no. 11, pp. 1313–1326, 2012.
- [95] A. J. Lambert and M. D. Brand, “Inhibitors of the quinone-binding site allow rapid superoxide production from mitochondrial NADH: ubiquinone oxidoreductase (complex I),” *Journal of Biological Chemistry*, vol. 279, no. 38, pp. 39414–39420, 2004.
- [96] S. Raha and B. H. Robinson, “Mitochondria, oxygen free radicals, disease and ageing,” *Trends in Biochemical Sciences*, vol. 25, no. 10, pp. 502–508, 2000.
- [97] J. Wu, X. Luo, N. Thangthaeng et al., “Pancreatic mitochondrial complex I exhibits aberrant hyperactivity in diabetes,” *Biochemistry and Biophysics Reports*, vol. 11, pp. 119–129, 2017.

- [98] H. Raza, S. K. Prabu, A. John, and N. G. Avadhani, "Impaired mitochondrial respiratory functions and oxidative stress in streptozotocin-induced diabetic rats," *International Journal of Molecular Sciences*, vol. 12, no. 5, pp. 3133–3147, 2011.
- [99] J. Škrha Jr., M. Kalousová, J. Švarcová et al., "Relationship of soluble RAGE and RAGE ligands HMGB1 and EN-RAGE to endothelial dysfunction in type 1 and type 2 diabetes mellitus," *Experimental and Clinical Endocrinology & Diabetes*, vol. 120, no. 5, pp. 277–281, 2012.
- [100] O. Demin, H. Westerhoff, and B. Kholodenko, "Mathematical modelling of superoxide generation with the bcl complex of mitochondria," *Biochemistry. Biokhimiia*, vol. 63, no. 6, pp. 634–649, 1998.
- [101] L. Gibellini, E. Bianchini, S. De Biasi, M. Nasi, A. Cossarizza, and M. Pinti, "Natural compounds modulating mitochondrial functions," *Evidence-Based Complementary and Alternative Medicine*, vol. 2015, Article ID 527209, 13 pages, 2015.
- [102] C. Sandoval-Acuña, J. Ferreira, and H. Speisky, "Polyphenols and mitochondria: an update on their increasingly emerging ROS-scavenging independent actions," *Archives of Biochemistry and Biophysics*, vol. 559, pp. 75–90, 2014.
- [103] L. Raudone, D. Burdulis, R. Raudonis et al., "Effect of Perilla Frutescens extracts and rosmarinic acid on rat heart mitochondrial functions," *Acta Poloniae Pharmaceutica*, vol. 73, no. 1, pp. 135–145, 2016.
- [104] G. B. Melo, R. L. Silva, V. A. Melo et al., "Effect of the aqueous extract of *Hyptis pectinata* on liver mitochondrial respiration," *Phytomedicine*, vol. 12, no. 5, pp. 359–362, 2005.



Hindawi

Submit your manuscripts at
<https://www.hindawi.com>



Article

Novel Mixed-Type Inhibitors of Protein Tyrosine Phosphatase 1B. Kinetic and Computational Studies

Marie Jazmín Sarabia-Sánchez ¹, Pedro Josué Trejo-Soto ², José Miguel Velázquez-López ², Carlos Carvente-García ², Rafael Castillo ², Alicia Hernández-Campos ², Claudia Avitia-Domínguez ¹, Daniel Enríquez-Mendiola ¹, Erick Sierra-Campos ³ , Mónica Valdez-Solana ³, José Manuel Salas-Pacheco ⁴ and Alfredo Téllez-Valencia ^{1,*}

¹ Facultad de Medicina y Nutrición, Universidad Juárez del Estado de Durango, Av. Universidad y Fanny Anitúa S/N, Durango, Durango C.P. 34000, Mexico; marie_sarabia@hotmail.com (M.J.S.-S.); avitiaclaudia@gmail.com (C.A.-D.); qfb.dan.enriquez@hotmail.com (D.E.-M.)

² Facultad de Química, Departamento de Farmacia, Universidad Nacional Autónoma de México, Ciudad de México C.P. 04510, Mexico; Piter_jo@comunidad.unam.mx (P.J.T.-S.); miguelzx42@hotmail.com (J.M.V.-L.); krbnt@hotmail.com (C.C.-G.); rafaelc@unam.mx (R.C.); hercam@unam.mx (A.H.-C.)

³ Facultad de Ciencias Químicas, Universidad Juárez del Estado de Durango, Av. Artículo 123 S/N Fracc. Filadelfia, Gómez Palacio, Durango C.P. 35010, Mexico; ericksier@gmail.com (E.S.-C.); valdezandyval@gmail.com (M.V.-S.)

⁴ Instituto de Investigación Científica, Universidad Juárez del Estado de Durango, Av. Universidad S/N, Durango, Durango C.P. 34000, Mexico; jsalas_pacheco@hotmail.com

* Correspondence: atellez@ujed.mx; Tel./Fax: +52-618-812-1687

Received: 21 November 2017; Accepted: 16 December 2017; Published: 20 December 2017

Abstract: The Atlas of Diabetes reports 415 million diabetics in the world, a number that has surpassed in half the expected time the twenty year projection. Type 2 diabetes is the most frequent form of the disease; it is characterized by a defect in the secretion of insulin and a resistance in its target organs. In the search for new antidiabetic drugs, one of the principal strategies consists in promoting the action of insulin. In this sense, attention has been centered in the protein tyrosine phosphatase 1B (PTP1B), a protein whose overexpression or increase of its activity has been related in many studies with insulin resistance. In the present work, a chemical library of 250 compounds was evaluated to determine their inhibition capability on the protein PTP1B. Ten molecules inhibited over the 50% of the activity of the PTP1B, the three most potent molecules were selected for its characterization, reporting K_i values of 5.2, 4.2 and 41.3 μM , for compounds **1**, **2**, and **3**, respectively. Docking and molecular dynamics studies revealed that the three inhibitors made interactions with residues at the secondary binding site to phosphate, exclusive for PTP1B. The data reported here support these compounds as hits for the design more potent and selective inhibitors against PTP1B in the search of new antidiabetic treatment.

Keywords: protein tyrosine phosphatase 1B; type 2 diabetes; benzimidazole derivatives; enzyme inhibition; docking; molecular dynamics

1. Introduction

In its sixth edition, the Atlas of Diabetes reported 415 million diabetics worldwide, surpassing in half the time the twenty year projection [1,2]. Type 2 diabetes is the most frequent type of the disease; it is characterized by a defect in the secretion of insulin and resistance in its target organs. For its treatment there are several hypoglycemic agents, these have different mechanisms of action such as an increase in insulin production, decrease of the hepatic glucose production, limiting the

absorption of postprandial glucose, and inhibiting gluconeogenesis [3]. Nevertheless, after 3 or 4 years of treatment the efficacy of these drugs is diminished, even with combinations among them, and insulin administration becomes necessary [4]. Therefore, there is an urgency for new drugs with other mechanisms of action that can provide different alternative treatments for type 2 diabetes.

To this end, one of the main strategies consists in promoting the action of insulin [5], and the attention has been focused in the protein tyrosine phosphatase 1B (PTP1B), a protein which overexpression and increase in its activity has been related in many studies with insulin resistance [6–8]. PTP1B works specifically by dephosphorylating residues of phosphotyrosine both from the insulin receptor (IR) and insulin receptor substrate (IRS) [9]. In a recent study, Munc18c was discovered as a substrate for the PTP1B, it is related to the regulation of glucose transporter GLUT4 in adipocytes, allowing or impeding, the insertion of the vesicle into the membrane [10]. These and other evidences [11–13] validate this enzyme as a potential therapeutic target against type 2 diabetes.

Since the establishment of the PTP1B as a biological target, there has been an effort to obtain inhibitors of its activity [14,15]. Different strategies such as diverse computational techniques, natural products research, and medicinal chemistry have been applied in the search for PTP1B inhibitors [16–20]. The first efforts to obtain inhibitors consisted in the search for phosphotyrosine (pTyr) mimetics such as difluoromethylene phosphate (DFMP) [21–24], carboxylic acids [25–28], 1,2,5-thiazolidin-3-one 1,1-dioxide (TZD), and the (*S*)-isomer of isothiazolidinone ((*S*)-IZD) [24,29], which achieve different degrees of inhibition of the enzyme. Furthermore, natural products and some derivatives have been reported too [30,31], as well as small molecules optimized from the previous ones [23,32]. Nevertheless, finding a potent, selective and with good oral availability molecule is still a challenge to be overcome.

The highly conserved catalytic site in the phosphatases family hinders the finding of a selective molecule, especially against its closest homologous T-cell protein tyrosine phosphatase (TCPTP) [33,34]. One strategy is to seek interactions with specific sites of the PTP1B [35–37]. In this sense, the enzyme has two aryl phosphate binding sites, a catalytic site with high affinity that contains the Cys215, and another one with low affinity that contains the Arg24 and Arg254. The former, denominated as site B, is specific for PTP1B. A few molecules based on this concept have reached clinical trials, among which ertiprotafib, ISIS 113715 and trodusquemine may be highlighted [38–40], however they did not continue to later stages.

In the present work, a chemical library composed by 250 compounds was evaluated to determine their inhibition capabilities on the PTP1B. The three most potent molecules were selected for further characterization, including their mechanism and inhibition constants. Structural studies of the PTP1B-inhibitor interaction were performed through docking and molecular dynamics simulations as well as an estimation of their drug-like and toxicological properties.

2. Results and Discussion

2.1. Compounds Screening

With the aim of finding new compounds capable of inhibiting PTP1B activity, a chemical library of 250 small molecules was evaluated at 200 μ M. From the total of compounds evaluated, 26 inhibited the enzyme activity by more than 60%, 26 of them between 31–59% (Table S1), and the rest below 30%. The characteristics of the ten most potent compounds are shown in Table 1, and their structures in Figure 1.

According to their structure, the three most potent PTP1B inhibitors (compounds 1, 2 and 3) all contain a benzimidazole nucleus. The analysis suggests that bulky substituents are required at positions 2 (1 vs. 9 and 10) and 5 (1 vs. 10) of the benzimidazole skeleton to increase their inhibition capability. The presence of the benzimidazole nucleus in the structure of the PTP1B inhibitors has been reported before, nevertheless, due to their substituents, they showed permeability and specificity problems with respect to other phosphatases [41–43].

Table 1. The ten most potent PTP1B inhibitors.

Molecule	MW ^a	HBD ^a	HBA ^a	LogP ^a	Drug Likeness ^b	Binding Energy (Kcal/mol)	% Inhibition (200 μ M)
1	567.27	2	7	6.68	1.07	−4.20	100
2	466.96	2	6	6.00	0.86	−4.99	99
3	424.59	2	5	5.53	0.66	−4.47	92
4	356.36	1	8	2.94	−0.49	−3.70	88
5	496.32	0	9	5.13	0.18	−4.02	85
6	498.47	2	8	4.26	−0.12	−5.24	84
7	499.94	1	7	4.95	0.41	−3.49	80
8	446.51	1	5	5.80	0.05	−3.98	74
9	384.64	1	5	4.36	0.76	−3.99	70
10	356.83	1	4	4.35	0.08	−4.01	65

^a Server FAFDrugs [44], filter Drug-like soft was used: MW 100–600; HBD \leq 5; HBA \leq 12; LogP −3 to 6. ^b Server Molsoft [45], Drug-Likeness score was determined, values between −1 to 2 are accepted.

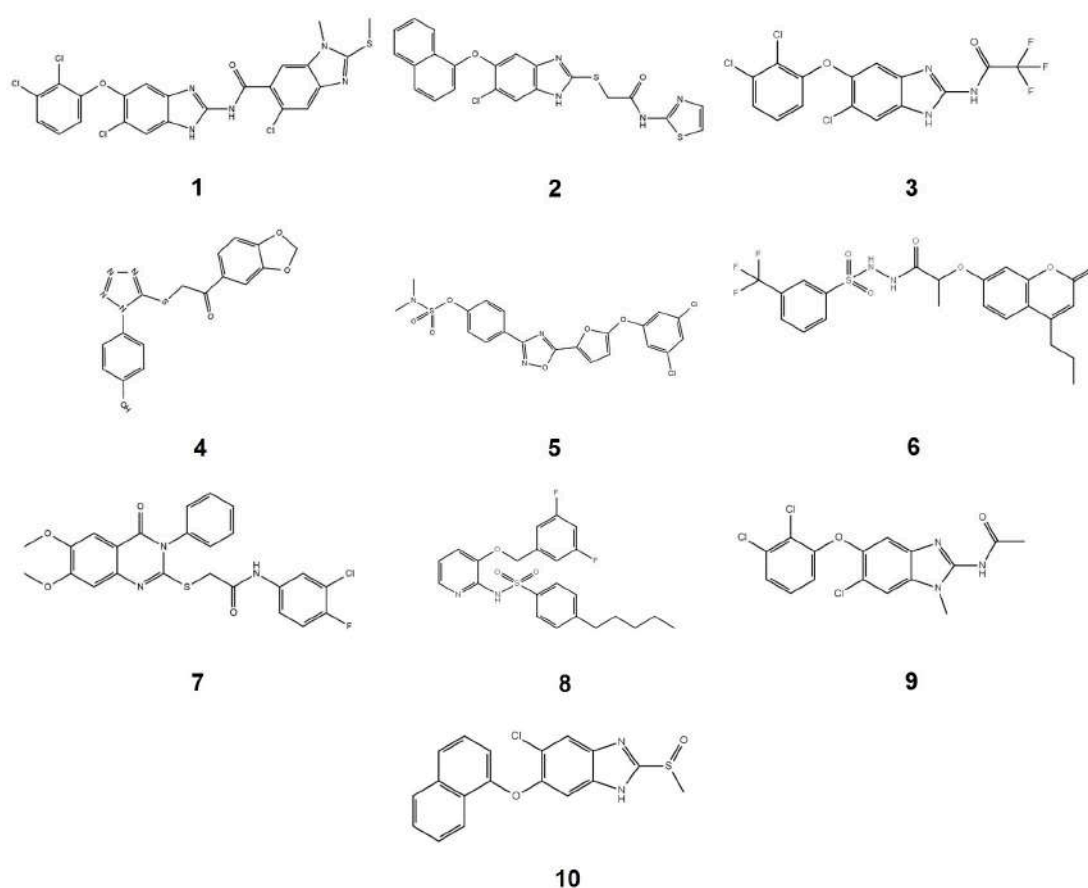


Figure 1. Chemical structures of the ten most potent PTP1B inhibitors. The number of each compound corresponds to that indicated in Table 1.

Regarding molecules 5, 6 and 8 they have in their structure substituents that have been reported before in PTP1B inhibitors [28]. Molecules 4 and 7 represent a new chemical nucleus, which extends the structural diversity of molecules that inhibit PTP1B reported to date. Finally, molecules 1, 2 and 3 were selected to characterize their inhibition mechanism by enzymatic kinetics, docking and molecular dynamics.

2.2. Kinetic Studies

Analysis of the plots at different substrate and fixed inhibitor concentrations indicated that the three compounds showed a mixed type inhibition mechanism (Figure 2a–c). This suggests that the three molecules are able to recognize both the free enzyme and the enzyme-substrate complex, generating the enzyme-substrate-inhibitor ternary complex, which is inactive [46] (Figure 2d). Something interesting to highlight is that compound 1 had an α value close to 1 suggesting that it recognizes, almost with the same affinity, both the free enzyme and the enzyme-substrate complex [46], whilst in compounds 2 and 3 this value was close to 3, suggesting a three times lower affinity with respect to the enzyme-substrate complex. These results suggest that the noncompetitive component of these inhibitors is stronger than the competitive component into inhibition mechanism, where the values of K_i and IC_{50} in our study were very similar [47]. The kinetic parameters were obtained from the adjustment of the data to the correspondent equation (Table 2).

The ChEMBL database from the Bioinformatics European Institute [48], reported 5854 compounds active against PTP1B. Of interest of this work, 30 of them show a reported mixed type inhibition mode, but only eight presented a K_i value lower than $5 \mu\text{M}$ [49–61]. Something important is that the chemical structures of these inhibitors are totally different from those reported here, and include DMFS derivatives [58], benzoic acid-based derivatives [57], insulin-mimetic selaginellins [59], pentacyclic acid triterpenoids [52], and oleanilic acid derivatives [61]. Also interesting is that α value reported was in the same range as for compounds 1, 2, and 3.

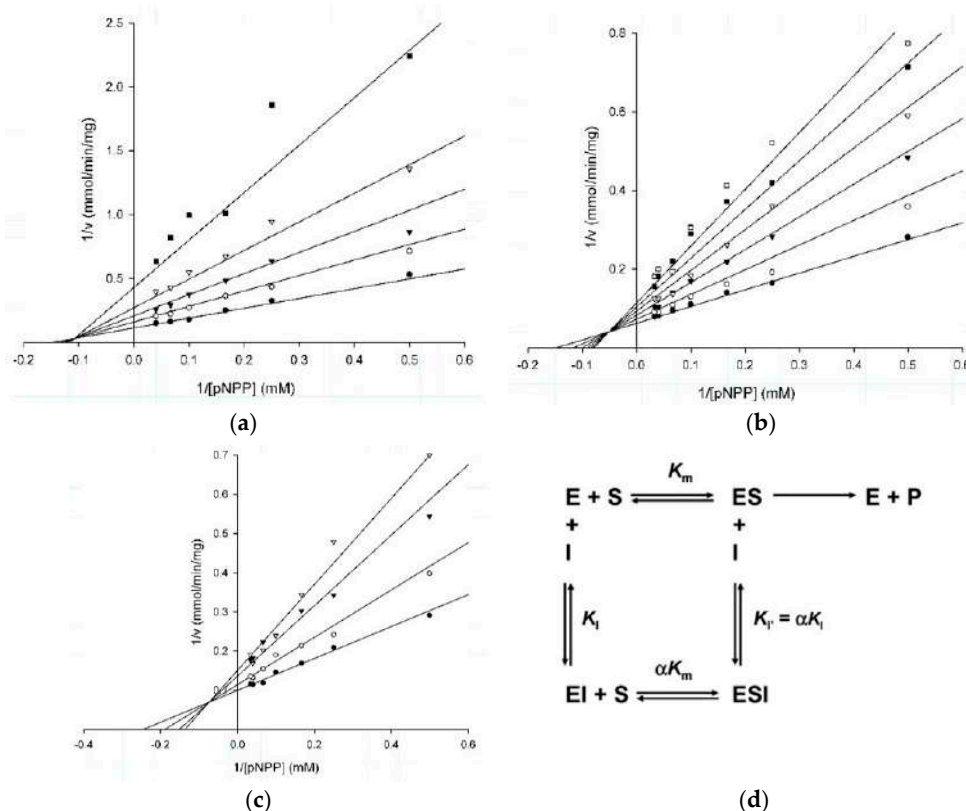


Figure 2. Lineweaver-Burk plots of (a) compound 1 at 0 (filled circles), 3 (open circle), 6 (filled triangle), 10 (open triangle), and $20 \mu\text{M}$ (filled squares); (b) compound 2 at 0 (filled circles), 2 (open circle), 4 (filled triangles), 6 (open triangles), 8 (filled squares), and $10 \mu\text{M}$ (open squares); and (c) compound 3 at 0 (filled circles), 20 (open circle), 50 (filled triangles), and $70 \mu\text{M}$ (open triangles); (d) kinetic model for mixed type inhibition. In the scheme, E corresponds to free enzyme; S is the substrate; ES is the enzyme-substrate complex; EI corresponds to the enzyme-inhibitor complex; ESI is the enzyme-substrate-inhibitor ternary complex; and P is the reaction product.

Table 2. Type of inhibition and kinetic parameters for PTP1B inhibitors.

Molecule	K _i (μM)	IC ₅₀ (μM)	α	V _{max} (μmol/min/mg)	K _m (mM)	Inhibition Type
1	5.2	7.5	1.4	8.8	6.7	Mixed
2	4.2	8.4	2.9	16	6.8	Mixed
3	41.3	31.3	3.3	10	4.1	Mixed

With respect to available drugs for the treatment of type 2 diabetes, classified in a general way as sulfonylureas, meglitidines, biguanides, thiazolidinediones, α -glucosidase inhibitors, glucagon-like peptide-1 receptor agonists, dipeptidyl peptidase-4 inhibitors, sodium glucose transporter-2 inhibitors, synthetic amylin analogues, and dopamine-2 agonists [62,63], none of them are benzimidazole derivatives, on the contrary, they are made up of different chemical groups such as sulfonylureas, guanidines, thiazolidinediones, disaccharides, glucose derivatives, peptidomimetics, among others [63]. The above makes the compounds **1**, **2** and **3** novel structural proposals.

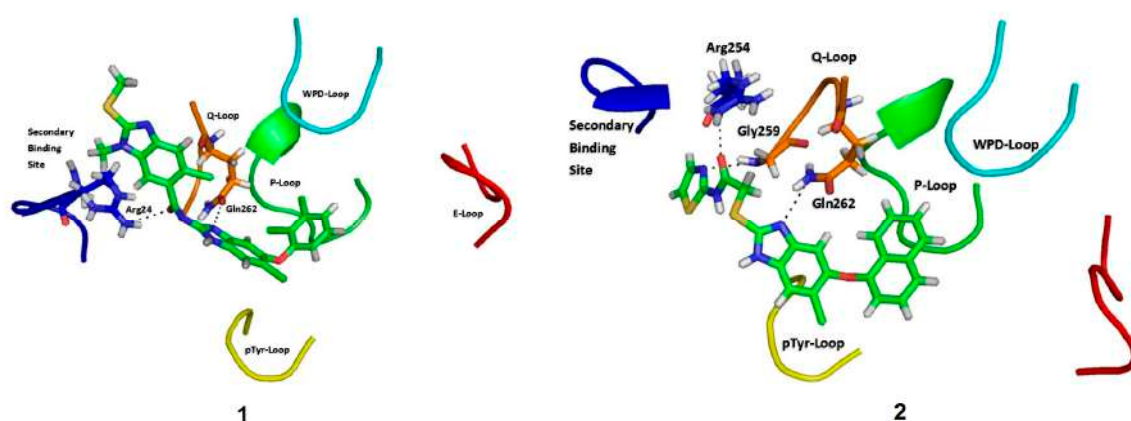
After kinetic studies, the binding mode and the type of interactions between the inhibitors and the PTP1B were analyzed by docking and molecular dynamics studies.

2.3. Molecular Docking

Before the molecular docking of the inhibitors, the protocol was validated through the binding mode of the inhibitor reported in the crystallographic structure used [64]. The RMSD value obtained from the modeling using Glide and the crystallographic complex was of 0.24 Å, which indicated that the docking protocol was done correctly (data not shown). After this, the three inhibitors were docked, obtaining binding energies of -4.2 , -5.0 and -4.5 Kcal/mol for compounds **1**, **2**, and **3**, respectively.

As for their binding modes, the three compounds formed interactions with residues from the secondary binding site to phosphate (Arg24, Arg254, Gly259, Gln262 and Asp48) [65]. In the three cases, the molecules block the cavity of the catalytic site without interacting with the signature residues of phosphatases.

The interaction with Asp48 has been reported before in different crystallographic structures of PTP1B in complex with other benzimidazole derivatives [41–43]. Additionally the interaction of the benzimidazole nucleus with the Gln262 found in the three inhibitors has been also reported [66,67], (Figure 3). A more detailed analysis of the interactions between these molecules and the enzyme were performed by molecular dynamic studies, the results are described below.

**Figure 3.** Cont.

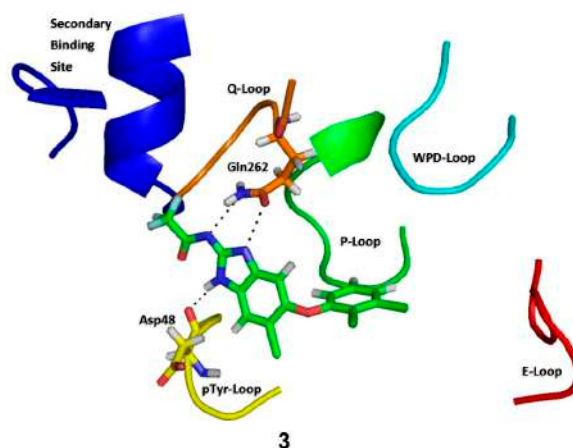


Figure 3. Binding mode of compounds 1, 2 and 3 in PTP1B. Loops are highlighted as follows: P loop (green), WPD loop (cyan), Q262 loop (orange), pTyr46 loop (yellow), and E loop (red). Secondary phosphate binding site is highlighted in blue.

2.4. Molecular Dynamics Simulations

The complexes obtained by molecular docking were submitted to a simulation of 10 ns. The total energy variation plots showed that the energy variation was around -12 Kcal/mol, which indicate that the average energy remains constant and there is structural stability of the complexes (Figure S1). The RMSD analysis showed that the three complexes had fluctuations in the first 3500 ps, achieving the stability from the 4000 ps up to the 10,000 ps without exceeding a 0.30 Å variation (Figure S2). It also was observed the influence of the inhibitors over the protein, with the variation of the RMSD in comparison with the protein alone.

The analysis of the binding energies showed that the compound 1 presented the best global binding energy, followed by compounds 2 and 3, which is in accordance with the inhibitory activity observed in the kinetic studies. The same situation was repeated in the individual values of the different components of the global energy, except in the electrostatic one, where compound 2 obtained the highest value (Table 3).

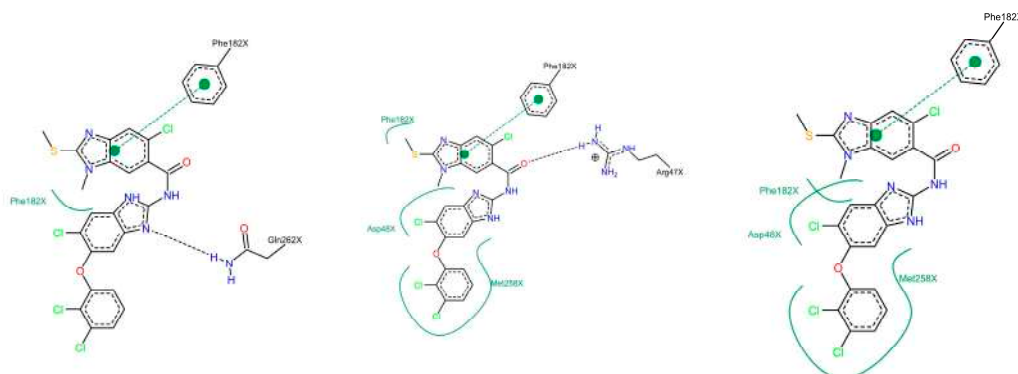
Table 3. Binding free energies determined by the MMPBSA method, and hydrogen bonds of the protein-ligand complexes.

Complex	Energy (kcal/mol)				Hydrogen Bonds		
	Van der Waals Energy	Electrostatic Energy	Polar Solvation Energy	SASA Energy	ΔG Binding	Range	Average
PTP1B-1	-47.56	-17.97	32.34	-4.17	-37.36	0-3	3
PTP1B-2	-35.46	-27.01	33.57	-3.54	-32.43	0-5	4
PTP1B-3	-29.50	-3.63	12.33	-2.93	-23.74	0-4	2

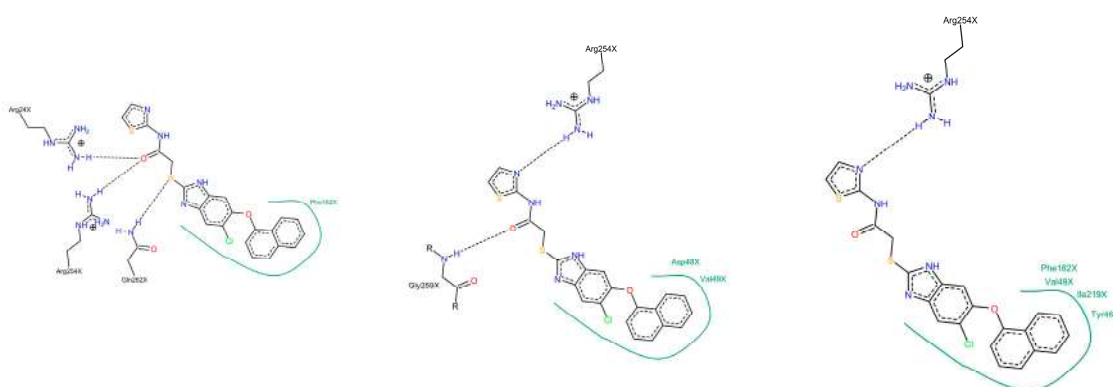
The structural analysis along the simulation time showed that the three molecules formed interactions, being the most important, the hydrophobic type interaction with the Asp48 and compound 1 (70% of occupancy), meanwhile compound 2 interacted with Phe182 (87% of occupancy). Compound 3 formed hydrogen bonds with Ala264, Gln262, and Arg24, as well as a hydrophobic interaction with Phe182, all of them with occupancy of 40% (Figure 4). Something interesting to highlight is that the interactions formed by the three inhibitors include important residues for the enzyme function like Gln262 and the Asp48, without having interactions with the denominated signature residues of the phosphatases (H/V)CXXGXXR(S/T) [34,68]. In this context, several studies have shown that selectivity against TCPTP can be achieved by interactions with residues such as Arg24, Arg47, Asp48, Arg254, Met258, and Gln262 [35,65]. Additionally, we investigated their binding mode

in TCTPT by molecular docking, finding that the three compounds made interactions with different residues of the enzyme (Figure S3). In conclusion, computational studies suggest that these inhibitors could be selective for PTP1B.

Complex PTP1B - 1



Complex PTP1B - 2



Complex PTP1B - 3

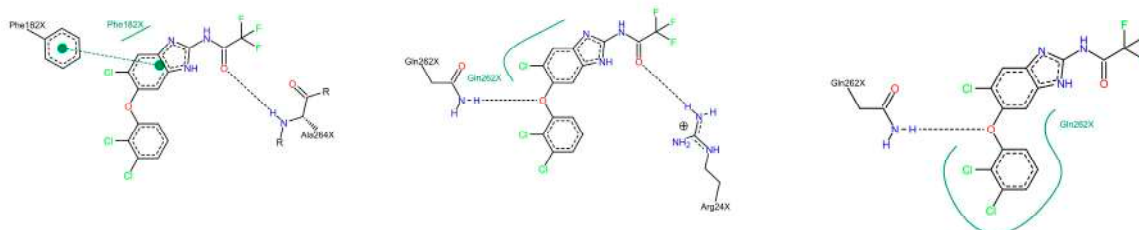


Figure 4. Two dimensional maps of interaction from the complexes PTP1B-1, PTP1B-2, and PTP1B-3. The image shows interactions at different times during entire dynamics: beginning, stabilized (4 ns), and final (10 ns). Hydrogen bonds between protein and ligand are drawn as dashed lines. Hydrophobic contacts are represented by means of spline sections highlighting the hydrophobic parts of the ligand and the name of the contacting amino acid. Maps were generated in Server Poseview (<http://proteinsplus.zbh.uni-hamburg.de/#poseview>).

2.5. Physicochemical and Drug-Like properties

The in silico evaluation of the physicochemical and drug-like parameters suggested that these molecules possess the necessary chemical features to potentially have an acceptable oral absorption [69–71] (Table 1 and Figure 5).

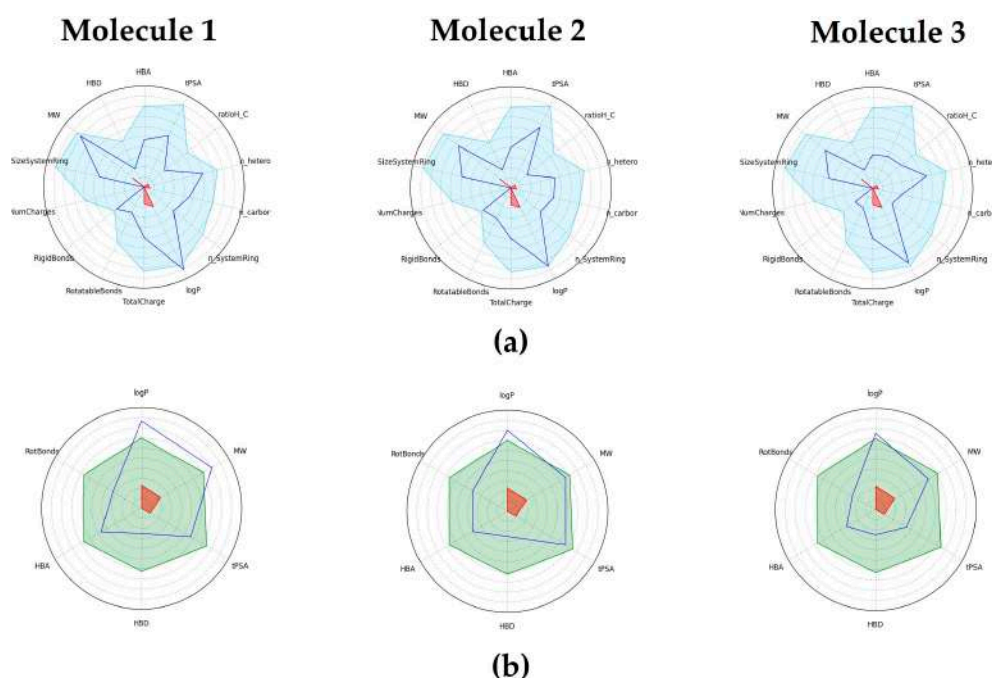


Figure 5. (a) Scheme of PhysChem Filter Positioning, compound values (blue line) should fall within the drug-like filter area (light blue); (b) Scheme of Oral Absorption Estimation, compound values (blue line) should fall within RO5 and Veber rules area (light green). The logarithm of the partition coefficient between n-octanol and water, logP; Molecular Weight, MW; Hydrogen Bond Donors, HBD; Hydrogen Bond Acceptors, HBA; topological Polar Surface Area, tPSA; het/carbon atoms ratio, ratioH/C; Number of Heteroatoms, n_hetero; Number of Carbon Atoms, n_carbor; Number of Smallest Set of Smallest Rings, n_SystemRing.

2.6. Toxicological Evaluation

An important point to analyze during the development of any new drug is the toxicological profile of the molecule. In this matter, using different softwares available online, a detailed study to predict the toxicological potential of these three inhibitors was performed. The estimation of the lethal dose 50 (LD₅₀) suggested that the three molecules are moderately toxic. Nevertheless, according to software evaluation, there are no toxic fragments reported in their structure, neither biological targets that can denote toxicity. With respect to their mutagenic, tumorigenic, irritability and reproductive effects, the only molecule that did not show any of these features was compound 2 (Table 4).

Taking into account all the data presented, compound 2 is the most viable option to continue with its optimization since it showed the best kinetic and predicted physicochemical and toxicological features. However, compounds 1 and 3 are still interesting structures that provide important information for the design of new inhibitors.

Table 4. Toxicological profile of PTP1B inhibitors.

Molecule	LD50 ^a (mg/kg)	Toxicity Class ^a	Toxic Frag. ^a	Toxicity Targets ^a	Mutagenic ^b	Tumorigenic ^b	Reprod. Effec. ^b	Irritant ^b	Drug Likeness ^c
1	1600	4	None	No Binding	Low	None	High	High	1.07
2	1000	4	None	No Binding	None	None	None	None	0.86
3	1600	4	None	No Binding	Low	None	High	High	0.66

^a Toxicity Class was determined in Server PROTOX [72], values ranged between 1 to 6, 1 is toxic and 6 is safe. Toxicity targets were determined for: Adenosine A2A receptor, Adrenergic beta 2 receptor, Androgen receptor, Amine oxidase, Dopamine D3 receptor, Estrogen receptor 1 and 2, Glucocorticoid receptor, Histamine H1 receptor, Nuclear receptor subfamily 1 group I member 2, Opioid receptor kappa, Opioid receptor mu, cAMP-specific 3',5'-cyclic phosphodiesterase 4D, Prostaglandin G/H synthase 1, Progesterone receptor. ^b Mutagenic, Tumorigenic, Reproductive effective and Irritant effects were determined using Data Warrior [73]. ^c Drug-Likeness score was determined with Server Molsoft [45], values between -1 to 2 are accepted.

3. Materials and Methods

3.1. General Information

The reagents used were purchased from Sigma-Aldrich (St. Luis, CA USA), kinetic analysis were performed in a diode array spectrophotometer model 8453 from Agilent (Santa Clara, CA, USA).

3.2. Compounds

The tested chemical library was composed of an in-house set of 100 compounds and 150 small molecules of the Fragment Library and HitFinderTM collection from Maybridge (Waltham, MA, USA). Compounds **4** to **8** belong to Maybridge with the identification codes HTS 01664 for '1-(1,3-benzodioxol-5-yl)-2-[[1-(4-hydroxyphenyl)-1*H*-1,2,3,4-tetraazol-5-yl]sulfanyl]-1-ethanone (**4**); SP 00892 for 4-[5-[5-(3,5-dichlorophenoxy)-2-furyl]-1,2,4-oxadiazol-3-yl]phenyl-*N,N*-dimethylsulfamate (**5**); RJF 01991 for 'N'1-{2-[(2-oxo-4-propyl-2*H*-chromen-7-yl)oxy]propanoyl}-3-(trifluoromethyl)benzene-1-sulfonohydrazide (**6**); HTS 02534 for 'N-(3-chloro-4-fluorophenyl)-2-[(6,7-dimethoxy-4-oxo-3-phenyl-3,4-dihydro-2-quinazolinyl)sulfanyl]acetamide (**7**); RH 02067 for 'N-[3-[(3,5-difluorobenzyl)oxy]pyridin-2-yl]-4-pentylbenzenesulfonamide (**8**). The general synthesis method for compounds **1**, **2**, **3**, **9** and **10** is outlined below.

Compounds **1–3** and **9** were prepared from the appropriate benzimidazole-2-amine and the adequate acid or anhydride under the guidelines of our synthetic procedure previously reported for similar benzimidazole derivatives [74,75]. Briefly, for compound **1**: the substituted benzimidazol-2-amine was reacted with 5-chloro-1-methyl-2-(methylthio)-6-carboxylic acid, previously treated with 1,1'-carbonyldiimidazole in DMF at room temperature for 2 h; then, the reaction mixture was heated at 140 °C under MW irradiation for 30 min. For compounds **3** and **9**: the substituted benzimidazol-2-amine was reacted with trifluoroacetic anhydride (compound **3**) or acetic anhydride (compound **9**) at 0 °C to r.t. in CH₂Cl₂ or CHCl₃; compound **2** was prepared from 6-chloro-5-(1-naphthyl)-1*H*-benzimidazole-2-thiol [76] and 2-chloro-*N*-(thiazol-2-yl)acetamide in acetone at 0 °C [77]. Compound **10** was obtained as previously reported [78].

5-Chloro-*N*-[6-chloro-5-(2,3-dichlorophenoxy)-1*H*-benzimidazol-2-yl]-1-methyl-2-(methylthio)-1*H*-benzimidazole-6-carboxamide (**1**). Recrystallized from DMF/MeOH white solid (89%); m.p. 269–270 °C. ¹H-NMR (DMSO-*d*₆; 400 MHz): δ 2.75 (s, 3H, S-CH₃); 3.72 (s, 3H, N-CH₃); 6.69 (dd, 1H, *J* = 8.2 Hz, 1.2 Hz, H-6 dichlorophenoxy); 7.27 (t, 1H, *J* = 8.2 Hz, H-5 dichlorophenoxy); 7.33 (s, 1H, H-4'); 7.37 (dd, 1H, *J* = 8.4 Hz, 1.2 Hz, H-4 dichlorophenoxy); 7.68 (s, 1H, H-7'); 7.71 (s, 1H, H-5); 7.91 (s, 1H, H-7); 12.40 (bs, 1H, NH, int. D₂O). ¹³C-NMR (DMSO-*d*₆; 100 MHz): δ 14.48 (S-CH₃); 30.56 (N-CH₃); 110.93 (C-7 benzimidazole); 115.64 (C-6 dichlorophenoxy); 118.45 (C-4 benzimidazole); 118.59 (C-7'a benzimidazole); 121.36 (C-2 dichlorophenoxy); 123.73 (C-5 benzimidazole); 124.69 (C-4 dichlorophenoxy); 127.79 C-6 benzimidazole); 129.11 (C-5 dichlorophenoxy); 133.23 (C-3 dichlorophenoxy); 135.63 (C-7a benzimidazole); 144.89 (C-3a benzimidazole); 145.04 (C-6' benzimidazole); 148.58 (C-2' benzimidazole); 155.10 (C-1 dichlorophenoxy); 157.27 (C-2

benzimidazole); 166.85 (C=O amide). EI-MS: m/z 565 (M^+); HRMS (FAB⁺): 565.9752 [$M + H$]⁺ (Calcd for $C_{23}H_{15}O_2N_5Cl_4SH^+$ 565.9773).

2-[6-Chloro-5-(1-naphthalylloxy)-1H-benzimidazol-2-yl]thio-N-(thiazol-2-yl)acetamide (2). Recrystallized from methanol to give a beige solid (20% yield); m.p. 155–157 °C. ¹H-NMR (400 MHz, DMSO): δ 4.37 (s, 2H, -CH₂-). 6.64 (d, $J = 7.6$ Hz, 1H, H-2 naphtyloxy), 7.23 (d, $J = 3.6$ Hz, 1H, H-5 thiazolyl), 7.27 (s, 1H, H-7), 7.37 (t, $J = 8.0$ Hz, 1H, H-3 naphtyloxy), 7.48 (d, $J = 3.6$ Hz, 1H, H-4 thiazolyl), 7.61–7.57 (m, 2H, H-6 y H-7 naphtyloxy), 7.64 (d, $J = 8.0$ Hz, 1H, H-4 naphtyloxy), 7.72 (s, 1H, H-4), 7.99–7.95 (m, 1H, H-5 naphtyloxy), 8.27–8.22 (m, 1H, H-8 naphtyloxy), δ 12.70 (s, 1H, CONH). ¹³C-NMR (DMSO-*d*₆; 100 MHz): δ 34.79 (SCH₂), 109.88 (C-2 naphtyloxy), 113.78 (C-3 naphtyloxy), 119.12 (C-5 thiazolyl), 121.36 (C-8 naphtyloxy), 122.45 (C-4 naphtyloxy), 124.86 (C-5 or C-6), 126.02 (C-6 or C-7 naphtyloxy), 126.13 (C-6 or C-7 naphtyloxy), 126.85 (C-4a or C-8a naphtyloxy), 127.77 (C-5 naphtyloxy), 134.45 (C-4a or C-8a naphtyloxy), 137.76 (C-4 thiazolyl), 146.06 (C-3a or C-7a), 151.96 (C-3a or C-7a), 153.37 (C-2), 157.81 (C-2 thiazolyl), 166.22 (CONH). MS (DART): m/z (%): 467 ([$M + H$]⁺, 15). HRMS (DART): Calcd for $C_{22}H_{15}ClN_4O_2S_2$ [$M + H$]⁺: 467.04032, found: 467.04177.

N-[6-Chloro-5-(2,3-dichlorophenoxy)-1H-benzimidazol-2-yl]-2,2,2-trifluoroacetamide (3). Purified by washing with cold water. Beige solid; m.p. > 200 °C (d). ¹H-NMR (400 MHz, DMSO) δ : 6.84 (dd, 1H, $J_1 = 8.3$, $J_2 = 1.3$ Hz, H-6'); 7.21 (s, 1H, H-4); 7.32 (t, 1H, $J = 8.2$ Hz, H-5'); 7.44 (dd, 1H, $J_1 = 8.1$ Hz, $J_2 = 1.3$ Hz, H-4'); 7.66 (s, 1H, H-7); 13.07 (bs, 1H, CO-NH). ¹³C-NMR (DMSO-*d*₆; 100 MHz): δ 105.22 (C-4), 114.10 (C-7), 116.97 (C-6'), 117.52 (q, $J_{F-C} = 287$ Hz, -CF₃), 120.37 (C-6), 122.15 (C-2'), 125.65 (C-4'), 127.03, 129.22, 129.36 (C-5'), 133.41 (C-3'), 147.07 (C-5), 153.98 (C-2), 154.17 (C-1'), 162.99 (q, $J_{F-C} = 35$ Hz, CO).

N-[6-Chloro-5-(2,3-dichlorophenoxy)-1-methyl-1H-benzimidazol-2-yl]acetamide (9). Recrystallized from ethanol, white crystals (84% yield); m.p. 237.5–238.9 °C. ¹H-NMR (400 MHz, DMSO) δ : 2.16 (s, 3H, CO-CH₃); 3.64 (s, 1H, N-CH₃); 6.65 (d, 1H, $J_1 = 8.2$ Hz, $J_2 = 0.9$ Hz, H-6'); 7.24 (t, 1H, $J = 8.2$ Hz, H-5'); 7.36 (dd, 1H, $J_1 = 8.1$ Hz, $J_2 = 1.3$ Hz, H-4'); 7.42 (s, 1H, H-4); 7.88 (s, 1H, H-7); 10.97 (bs, 1H, CO-NH). ¹³C-NMR (DMSO-*d*₆; 100 MHz): δ 23.43 (CO-CH₃), 30.97 (N-CH₃), 111.95 (C-4), 112.27 (C-7), 115.51 (C-6'), 119.52 (C-6), 121.28 (C-2'), 124.70 (C-4'), 129.16 (C-5'), 133.25, 140.41 (C-3'), 145.39 (C-4), 148.37 (C-2), 155.14 (C-1'), 170.57 (CO). EA. Calc.: C₁₆H₁₂Cl₃N₃O₂: C, 49.96; H, 3.14; N, 10.9. Found: C, 49.82; H, 2.57; N, 10.6. HMRS (ESI) Calcd for $C_{16}H_{12}Cl_3N_3O_2$ [$M + Na$]: 406.0073; found 406.

3.3. Expression and Purification of PTP1B

The region of the gene PTPN1 that encodes for PTP1B (residues 1–321) was synthesized by Integrated DNA Technologies and inserted in the pIDTSmart plasmid. Then, the gene was liberated by restriction reactions using NdeI and BamHI enzymes and inserted into the overexpression vector pET28A. Afterwards, *E. coli* BLR strains were transformed for the overexpression of the protein. With this purpose, 500 mL of LB liquid culture medium was grown supplemented with Kanamycin (50 μ g/mL) at 37 °C, once it reached an optical density of 0.9 at 600 nm, 1mM of IPTG was added to induce the overexpression, incubating four more hours. Right away, cells were cultured by centrifugation and lysed by sonication. The supernatant was passed through a Ni-agarose column and the enzyme was purified by an imidazole gradient. The fractions were analyzed by SDS-PAGE electrophoresis and those with the presence of the protein were pooled and concentrated with a Plus-70 centricon, immediately the enzyme was precipitated with ammonium sulfate (80% saturation).

3.4. Enzymatic Activity

The PTP1B activity was measured based on the Goldstein method [79]. The assay was performed with a final reaction volume of 500 μ L in HEPES buffer (50 mM HEPES, 1mM DTT, 2 mM EDTA and 150 mM NaCl, pH 7.0), DMSO (10%) and p-nitrophenol phosphate (pNPP) as substrate (50 mM), the reaction was started with the PTP1B (1.5 μ g/mL). After 30 min of incubation at 37 °C, the reaction

was stopped by the addition of 500 μL of NaOH 5N reading the absorbance at 405 nm. The number of hydrolyzed moles of pNPP was determined using the molar extinction coefficient of the product pNP ($18,500 \text{ M}^{-1} \text{ cm}^{-1}$).

3.5. Inhibition Assays

Inhibition assays were performed under the above described conditions, adding to the reaction each one of the molecules at a final concentration of 200 μM . The concentration that inhibits 50% (IC_{50}) of the PTP1B activity was determined through curves at different concentration of each compound, adjusting the data to the equation reported elsewhere [80]. The inhibition type and constant were obtained by the measurement of the initial velocities of hydrolysis varying the substrate concentration in a range of 2–30 μM , in absence or presence of fixed concentrations of each inhibitor. For compound 1 the concentrations used were 3, 6, 10 and 20 μM ; in the case of compound 2 were 2, 4, 6, 8, and 10 μM ; and for compound 3 were 20, 50, 70 and 90 μM . The experimental data were analyzed through the Lineweaver-Burk plot using the software Sigma Plot V12.3 (Systat Software, Inc., San Jose, CA, USA).

3.6. Molecular Docking

The molecules were built in Maestro 10.4 (www.schrodinger.com) and prepared in Ligprep 2.3 [81]. The crystallographic structure of the PTP1B protein was obtained from the RCSB Protein Data Bank with the code PDB ID 2F71 [64]. Hydrogen atoms were added to the structure, bond angles, and distances were corrected, and charges were assigned using Protein Preparation Wizard [82], all ions and the inhibitor present in the crystallographic structure were withdrawn. Water molecules were also withdrawn, with exception of those located in the WPD loop, since these are considered necessary to give better binding poses [83]. Energy minimization was performed with the OPLS_2005 force field with an RMSD of 0.3 Å. The molecular docking simulations in the active site of the PTP1B were performed using Glide [84,85]. The Van der Waals scale was of a factor of 0.80 and a cutting partial charge of 0.15. The files were limited to at least one pose for ligand, rejecting poses with energies smaller than 0.5 kcal/mol. Standard precision and Extra precision modes were used with flexible ligand adding penalization states of the Epik software [86] in the docking score.

3.7. Molecular Dynamic Simulations

The initial structures for the simulations were those with the lowest binding energy of each complex obtained by docking. The necessary topology files for each ligand (compounds 1, 2 and 3) were calculated and obtained using PRODRG [87]. The systems were solvated within a water box with 1.0 nm of distance from the proteins surface with the Single Point Charge (SPC) water model. Sodium and Chlorine ions were added to neutralize the systems charge until a 0.15 M concentration was reached. First, a descending steps energy minimization was done. Afterwards, a canonic assemble was performed, continuing by an isobaric-isothermal assemble, maintaining a constant temperature, volume and pressure. Finally, 10 ns simulations were performed for each complex and the free enzyme in GROMACS 5.1 software [88] using the Gromos 43a147 force field. All simulations were performed at 1 bar of pressure and 300 °K of temperature. The free binding energy was calculated based on the molecular mechanics of surface area of Poisson-Boltzmann (MM-PBSA) method [89].

3.8. Drug-Like and Toxicological Propierties

The FAF-Drugs4 server [42] and the Molsoft [45] program, available on the web were used. The Drug-like soft filter used in FAF-Drugs4 combines the physicochemical properties described in several articles and an analysis of the descriptor values of 916 oral medications of the FDA, allowing defining a filter threshold that comprises up to 90% of these drugs. The ranges of the permitted values used by the software are shown in Table 1. Regarding Molsoft, it uses the fingerprints technique with a set of 5000 commercialized drugs and 10,000 non-pharmacological compounds. After the process, it reports a score that places the molecules in a range between the parameters of the drugs

and the non-drugs, which allows defining their pharmacological potential; values between -1 to 2 are accepted.

With respect to toxicological parameters, PROTOX [72] server was used, as well the Data Warrior software [73] to determine mutagenesis, tumorigenic, reproductive effects and irritability. PROTOX uses the identification of fragments over-represented in toxic compounds and similarity analyses of compounds with known LD50 values. Furthermore, based on pharmacophores, it indicates possible toxicity targets. Data Warrior uses chemical descriptors to make several molecular similarity measures and predict properties such as mutagenicity, tumorigenicity, irritant and reproductive effects.

4. Conclusions

In the present work three new mixed type inhibitors for PTP1B are reported, which based on their inhibition capability and mechanism, potential selectivity against TCPTP, and predicted drug-like properties, could represent a good starting point for the development of more potent molecules that can guide the design of a new drug to treat type 2 diabetes.

Supplementary Materials: Supplementary materials are available online.

Acknowledgments: Access to the Maybridge Fragment Library collection kindly provided by Armando Gómez-Puyou is highly appreciated. ATV and CAD acknowledge CONACyT for grants No. 257848 and No. 258694, respectively. RC and AHC acknowledge to CONACyT for financial support of project No. 251726 and DGAPA-PAPIIT, UNAM for project No. IN221416. CONACyT is also acknowledged for the fellowship granted to MSS (No. 271541), PJTS (No. 409406/No. 258048), and JMV (No. 225078). We thank Rosa Isela del Villar Morales and Nayeli López Baliaux for the determination of NMR spectra.

Author Contributions: Performed the experiments: M.J.S.-S., P.J.T.-S., J.M.V.-L., and C.C.-G. Conceived and designed in-house compounds library: R.C. and A.H.-C. Conceived, designed the experiments and contributed reagents/materials/analysis tools: R.C., A.H.-C., C.A.-D., E.S.-C., J.M.S.-P., and A.T.-V. Analyzed the data and wrote the paper: M.S.-S., D.E.-M., C.A.-D., E.S.-C., M.V.-S., and A.T.-V.

Conflicts of Interest: The authors declare no conflict of interest.

References

1. International Diabetes Federation. *IDF Diabetes Atlas*, 2nd ed.; International Diabetes Federation: Brussels, Belgium, 2003.
2. International Diabetes Federation. *IDF Diabetes Atlas*, 6th ed.; International Diabetes Federation: Brussels, Belgium, 2014.
3. Bujaidar, E.M.; Juárez, N.G. Revisión de las características clínicas, metabólicas y genéticas de la diabetes mellitus. *Bioquímica* **2003**, *28*, 14–23.
4. Gershell, L. Type 2 diabetes market. *Nat. Rev. Drug Discov.* **2005**, *4*, 367–368. [[CrossRef](#)] [[PubMed](#)]
5. Shinde, R.N.; Sobhia, M.E. Binding and discerning interactions of PTP1B allosteric inhibitors: Novel insights from molecular dynamics simulations. *J. Mol. Graph. Model.* **2013**, *45*, 98–110. [[CrossRef](#)] [[PubMed](#)]
6. Di Paola, R.; Frittitta, L.; Miscio, G.; Bozzali, M.; Baratta, R.; Centra, M.; Spampinato, D.; Santagati, M.G.; Ercolino, T.; Cisternino, C.; et al. A variation in 3' UTR of hPTP1B increases specific gene expression and associates with insulin resistance. *Am. J. Hum. Genet.* **2002**, *70*, 806–812. [[CrossRef](#)] [[PubMed](#)]
7. Bento, J.L.; Palmer, N.D.; Mychaleckyj, J.C.; Lange, L.A.; Langefeld, C.D.; Rich, S.S.; Freedman, B.I.; Bowden, D.W. Association of protein tyrosine phosphatase 1B gene polymorphisms with type 2 diabetes. *Diabetes* **2004**, *53*, 3007–3012. [[CrossRef](#)] [[PubMed](#)]
8. Asante-Appiah, E.; Kennedy, B.P. Protein tyrosine phosphatases: the quest for negative regulators of insulin action. *Am. J. Physiol. Endocrinol. Metab.* **2003**, *284*, E663–E670. [[CrossRef](#)] [[PubMed](#)]
9. Cho, H. *Protein Tyrosine Phosphatase 1B (PTP1B) and Obesity*, 1st ed.; Elsevier Inc.: Amsterdam, The Netherlands, 2013; Volume 91.
10. Bakke, J.; Bettaieb, A.; Nagata, N.; Matsuo, K.; Haj, F.G. Regulation of the SNARE-interacting protein Munc18c tyrosine phosphorylation in adipocytes by protein-tyrosine phosphatase 1B. *Cell Commun. Signal.* **2013**, *11*, 57. [[CrossRef](#)] [[PubMed](#)]

11. Elchebly, M.; Payette, P.; Michaliszyn, E.; Cromlish, W.; Collins, S.; Loy, A.L.; Normandin, D.; Cheng, A.; Himms-Hagen, J.; Chan, C.C.; et al. Increased insulin sensitivity and obesity resistance in mice lacking the protein tyrosine phosphatase-1B gene. *Science* **1999**, *283*, 1544–1548. [[CrossRef](#)] [[PubMed](#)]
12. Klamann, L.D.; Boss, O.; Peroni, O.D.; Kim, J.K.; Martino, J.L.; Zabolotny, J.M.; Moghal, N.; Lubkin, M.; Kim, Y.B.; Sharpe, A.H.; et al. Increased energy expenditure, decreased adiposity, and tissue-specific insulin sensitivity in protein-tyrosine phosphatase 1B-deficient mice. *Mol. Cell. Biol.* **2000**, *20*, 5479–5489. [[CrossRef](#)] [[PubMed](#)]
13. Kushner, J.A.; Haj, F.G.; Klamann, L.D.; Dow, M.A.; Kahn, B.B.; Neel, B.G.; White, M.F. Islet-sparing effects of protein tyrosine phosphatase-1b deficiency delays onset of diabetes in IRS2 knockout mice. *Diabetes* **2004**, *53*, 61–66. [[CrossRef](#)] [[PubMed](#)]
14. He, R.; Zeng, L.F.; He, Y.; Zhang, S.; Zhang, Z.Y. Small molecule tools for functional interrogation of protein tyrosine phosphatases. *FEBS J.* **2013**, *280*, 731–750. [[CrossRef](#)] [[PubMed](#)]
15. Tamrakar, A.K.; Maurya, C.K.; Rai, A.K. PTP1B inhibitors for type 2 diabetes treatment: A patent review (2011–2014). *Expert Opin. Ther. Pat.* **2014**, *24*, 1101–1115. [[CrossRef](#)] [[PubMed](#)]
16. Zhou, Y.; Zhang, W.; Liu, X.; Yu, H.; Lu, X.; Jiao, B. Inhibitors of Protein Tyrosine Phosphatase 1B from Marine Natural Products. *Chem. Biodivers.* **2017**, *14*, e1600462. [[CrossRef](#)] [[PubMed](#)]
17. Jiang, C.-S.; Liang, L.; Guo, Y. Natural products possessing protein tyrosine phosphatase 1B (PTP1B) inhibitory activity found in the last decades. *Acta Pharmacol. Sin.* **2012**, *33*, 1217–1245. [[CrossRef](#)] [[PubMed](#)]
18. Bharatam, P.V.; Patel, D.S.; Adane, L.; Mittal, A.; Sundriyal, S. Modeling and informatics in designing anti-diabetic agents. *Curr. Pharm. Des.* **2007**, *13*, 3518–3530. [[CrossRef](#)] [[PubMed](#)]
19. Combs, A.P. Recent advances in the discovery of competitive protein tyrosine phosphatase 1B inhibitors for the treatment of diabetes, obesity, and cancer. *J. Med. Chem.* **2010**, *53*, 2333–2344. [[CrossRef](#)] [[PubMed](#)]
20. Popov, D. Novel protein tyrosine phosphatase 1B inhibitors: Interaction requirements for improved intracellular efficacy in type 2 diabetes mellitus and obesity control. *Biochem. Biophys. Res. Commun.* **2011**, *410*, 377–381. [[CrossRef](#)] [[PubMed](#)]
21. Adams, D.R.; Abraham, A.; Asano, J.; Breslin, C.; Dick, C.A.J.; Ixkes, U.; Johnston, B.F.; Johnston, D.; Kewnay, J.; Mackay, S.P.; et al. 2-Aryl-3,3,3-trifluoro-2-hydroxypropionic acids: A new class of protein tyrosine phosphatase 1B inhibitors. *Bioorg. Med. Chem. Lett.* **2007**, *17*, 6579–6583. [[CrossRef](#)] [[PubMed](#)]
22. Zhao, H.; Liu, G.; Xin, Z.; Serby, M.D.; Pei, Z.; Szczepankiewicz, B.G.; Hajduk, P.J.; Abad-Zapatero, C.; Hutchins, C.W.; Lubben, T.H.; et al. Isoxazole carboxylic acids as protein tyrosine phosphatase 1B (PTP1B) inhibitors. *Bioorg. Med. Chem. Lett.* **2004**, *14*, 5543–5546. [[CrossRef](#)] [[PubMed](#)]
23. Black, E.; Breed, J.; Breeze, A.L.; Embrey, K.; Garcia, R.; Gero, T.W.; Godfrey, L.; Kenny, P.W.; Morley, A.D.; Minshull, C.A.; et al. Structure-based design of protein tyrosine phosphatase-1B inhibitors. *Bioorg. Med. Chem. Lett.* **2005**, *15*, 2503–2507. [[CrossRef](#)] [[PubMed](#)]
24. Douty, B.; Wayland, B.; Ala, P.J.; Bower, M.J.; Pruitt, J.; Bostrom, L.; Wei, M.; Klabe, R.; Gonneville, L.; Wynn, R.; et al. Isothiazolidinone inhibitors of PTP1B containing imidazoles and imidazolines. *Bioorg. Med. Chem. Lett.* **2008**, *18*, 66–71. [[CrossRef](#)] [[PubMed](#)]
25. Shrestha, S.; Bhattarai, B.R.; Lee, K.H.; Cho, H. Mono- and disalicylic acid derivatives: PTP1B inhibitors as potential anti-obesity drugs. *Bioorg. Med. Chem.* **2007**, *15*, 6535–6548. [[CrossRef](#)] [[PubMed](#)]
26. Akamatsu, M.; Roller, P.P.; Chen, L.; Zhang, Z.Y.; Ye, B.; Burke, T.R. Potent inhibition of protein-tyrosine phosphatase by phosphotyrosine-mimic containing cyclic peptides. *Bioorg. Med. Chem.* **1997**, *5*, 157–163. [[CrossRef](#)]
27. Burke, T.R.; Yao, Z.J.; Zhao, H.; Milne, G.W.A.; Wu, L.; Zhang, Z.Y.; Voigt, J.H. Enantioselective synthesis of nonphosphorus-containing phosphotyrosyl mimetics and their use in the preparation of tyrosine phosphatase inhibitory peptides. *Tetrahedron* **1998**, *54*, 9981–9994. [[CrossRef](#)]
28. Wilson, D.P.; Wan, Z.K.; Xu, W.X.; Kirincich, S.J.; Follows, B.C.; Joseph-McCarthy, D.; Foreman, K.; Moretto, A.; Wu, J.; Zhu, M.; et al. Structure-based optimization of protein tyrosine phosphatase 1B inhibitors: From the active site to the second phosphotyrosine binding site. *J. Med. Chem.* **2007**, *50*, 4681–4698. [[CrossRef](#)] [[PubMed](#)]
29. Combs, A.P.; Yue, E.W.; Bower, M.; Ala, P.J.; Wayland, B.; Douty, B.; Takvorian, A.; Polam, P.; Wasserman, Z.; Zhu, W.; et al. Structure-based design and discovery of protein tyrosine phosphatase inhibitors incorporating novel isothiazolidinone heterocyclic phosphotyrosine mimetics. *J. Med. Chem.* **2005**, *48*, 6544–6548. [[CrossRef](#)] [[PubMed](#)]

30. Ye, D.; Zhang, Y.; Wang, F.; Zheng, M.; Zhang, X.; Luo, X.; Shen, X.; Jiang, H.; Liu, H. Novel thiophene derivatives as PTP1B inhibitors with selectivity and cellular activity. *Bioorg. Med. Chem.* **2010**, *18*, 1773–1782. [[CrossRef](#)] [[PubMed](#)]
31. Liu, Z.; Lee, W.; Kim, S.-N.; Yoon, G.; Cheon, S.H. Design, synthesis, and evaluation of bromo-retrochalcone derivatives as protein tyrosine phosphatase 1B inhibitors. *Bioorg. Med. Chem. Lett.* **2011**, *21*, 3755–3758. [[CrossRef](#)] [[PubMed](#)]
32. Seo, C.; Choi, Y.H.; Sohn, J.H.; Ahn, J.S.; Yim, J.H.; Lee, H.K.; Oh, H. Ohioensins F and G: Protein tyrosine phosphatase 1B inhibitory benzonaphthoxanthones from the Antarctic moss *polytrichastrum alpinum*. *Bioorg. Med. Chem. Lett.* **2008**, *18*, 772–775. [[CrossRef](#)] [[PubMed](#)]
33. Iversen, L.F.; Møller, K.B.; Pedersen, A.K.; Peters, G.H.; Petersen, A.S.; Andersen, H.S.; Branner, S.; Mortensen, S.B.; Møller, N.P.H. Structure determination of T cell protein-tyrosine phosphatase. *J. Biol. Chem.* **2002**, *277*, 19982–19990. [[CrossRef](#)] [[PubMed](#)]
34. Andersen, J.N.; Mortensen, O.H.; Peters, G.H.; Drake, P.G.; Iversen, L.F.; Olsen, O.H.; Peter, G.; Andersen, H.S.; Tonks, N.K.; Møller, P.H.; et al. Structural and Evolutionary Relationships among Protein Tyrosine Phosphatase Domains Structural and Evolutionary Relationships among Protein Tyrosine Phosphatase Domains. *Mol. Cell. Biol.* **2001**, *21*, 7117–7136. [[CrossRef](#)] [[PubMed](#)]
35. Li, X.Q.; Wang, L.J.; Shi, D.Y. The design strategy of selective PTP1B inhibitors over TCPTP. *Bioorg. Med. Chem.* **2016**, *24*, 3343–3352. [[CrossRef](#)] [[PubMed](#)]
36. Du, Y.; Ling, H.; Zhang, M.; Shen, J.; Li, Q. Discovery of novel, potent, selective and cellular active ADC type PTP1B inhibitors via fragment-docking-oriented de novel design. *Bioorg. Med. Chem.* **2015**, *23*, 4891–4898. [[CrossRef](#)] [[PubMed](#)]
37. Liu, P.; Du, Y.; Song, L.; Shen, J.; Li, Q. Novel, potent, selective and cellular active ABC type PTP1B inhibitors containing (methanesulfonyl-phenyl-amino)-acetic acid methyl ester phosphotyrosine mimetic. *Bioorg. Med. Chem.* **2015**, *23*, 7079–7088. [[CrossRef](#)] [[PubMed](#)]
38. Lantz, K.A.; Hart, S.G.E.; Planey, S.L.; Roitman, M.F.; Ruiz-White, I.A.; Wolfe, H.R.; McLane, M.P. Inhibition of PTP1B by trodusquemine (MSI-1436) causes fat-specific weight loss in diet-induced obese mice. *Obesity* **2010**, *18*, 1516–1523. [[CrossRef](#)] [[PubMed](#)]
39. Liu, J.Z.; Zhang, S.E.; Nie, F.; Yang, Y.; Tang, Y.B.; Yin, W.; Tian, J.Y.; Ye, F.; Xiao, Z. Discovery of novel PTP1B inhibitors via pharmacophore-oriented scaffold hopping from Ertiprotafib. *Bioorg. Med. Chem. Lett.* **2013**, *23*, 6217–6222. [[CrossRef](#)] [[PubMed](#)]
40. Swarbrick, M.M.; Havel, P.J.; Levin, A.A.; Bremer, A.A.; Stanhope, K.L.; Butler, M.; Booten, S.L.; Graham, J.L.; McKay, R.A.; Murray, S.F.; et al. Inhibition of protein tyrosine phosphatase-1B with antisense oligonucleotides improves insulin sensitivity and increases adiponectin concentrations in monkeys. *Endocrinology* **2009**, *150*, 1670–1679. [[CrossRef](#)] [[PubMed](#)]
41. Ala, P.J.; Gonneville, L.; Hillman, M.; Becker-Pasha, M.; Yue, E.W.; Douty, B.; Wayland, B.; Polam, P.; Crawley, M.L.; McLaughlin, E.; et al. Structural insights into the design of nonpeptidic isothiazolidinone-containing inhibitors of protein-tyrosine phosphatase 1B. *J. Biol. Chem.* **2006**, *281*, 38013–38021. [[CrossRef](#)] [[PubMed](#)]
42. Combs, A.P.; Zhu, W.; Crawley, M.L.; Glass, B.; Polam, P.; Sparks, R.B.; Modi, D.; Takvorian, A.; McLaughlin, E.; Yue, E.W.; et al. Potent benzimidazole sulfonamide protein tyrosine phosphatase 1B inhibitors containing the heterocyclic (S)-isothiazolidinone phosphotyrosine mimetic. *J. Med. Chem.* **2006**, *49*, 3774–3789. [[CrossRef](#)] [[PubMed](#)]
43. Sparks, R.B.; Polam, P.; Zhu, W.; Crawley, M.L.; Takvorian, A.; McLaughlin, E.; Wei, M.; Ala, P.J.; Gonneville, L.; Taylor, N.; et al. Benzothiazole benzimidazole (S)-isothiazolidinone derivatives as protein tyrosine phosphatase-1B inhibitors. *Bioorg. Med. Chem. Lett.* **2007**, *17*, 736–740. [[CrossRef](#)] [[PubMed](#)]
44. Lagorce, D.; Sperandio, O.; Galons, H.; Miteva, M.A.; Villoutreix, B.O. FAF-Drugs2: Free ADME/tox filtering tool to assist drug discovery and chemical biology projects. *BMC Bioinform.* **2008**, *9*, 396. [[CrossRef](#)] [[PubMed](#)]
45. Molsoft. Available online: <http://molsoft.com/mprop/> (accessed on 5 June 2017).
46. Segel, I.H. *Enzyme Kinetics: Behavior and Analysis of Rapid Equilibrium and Steady-State Enzyme Systems*; John Wiley Sons: New York, NY, USA, 1993.
47. Cheng, Y.; Prusoff, W.H. Relationship between the inhibition constant (K₁) and the concentration of inhibitor which causes 50 per cent inhibition (I₅₀) of an enzymatic reaction. *Biochem. Pharmacol.* **1973**, *22*, 3099–3108. [[PubMed](#)]

48. EMBL-EBI The European Bioinformatics Institute. Available online: <http://www.ebi.ac.uk/> (accessed on 7 December 2017).
49. Haftchenary, S.; Ball, D.P.; Aubry, I.; Landry, M.; Shahani, V.M.; Fletcher, S.; Page, B.D.G.; Jouk, A.O.; Tremblay, M.L.; Gunning, P.T. Identification of a potent salicylic acid-based inhibitor of tyrosine phosphatase PTP1B. *Med. Chem. Commun.* **2013**, *4*, 987–992. [[CrossRef](#)]
50. Raj, B.; Kafle, B.; Hwang, J.; Wook, S.; Lee, K.; Park, H.; Han, I.; Cho, H. Novel thiazolidinedione derivatives with anti-obesity effects: Dual action as PTP1B inhibitors and PPAR activators. *Bioorg. Med. Chem. Lett.* **2010**, *20*, 6758–6763. [[CrossRef](#)]
51. Cheung, A.W.; Banner, B.; Bose, J.; Kim, K.; Li, S.; Marcopulos, N.; Orzechowski, L.; Sergi, J.A.; Thakkar, K.C.; Wang, B.; et al. 7-Phenyl-pyrido[2,3-d]pyrimidine-2,4-diamines: Novel and highly selective protein tyrosine phosphatase 1B inhibitors. *Bioorg. Med. Chem. Lett.* **2012**, *22*, 7518–7522. [[CrossRef](#)] [[PubMed](#)]
52. Ramírez-Espinosa, J.J.; Rios, M.Y.; López-Martínez, S.; López-Vallejo, F.; Medina-Franco, J.L.; Paoli, P.; Camici, G.; Navarrete-Vázquez, G.; Ortiz-Andrade, R.; Estrada-Soto, S. Antidiabetic activity of some pentacyclic acid triterpenoids, role of PTP-1B: In vitro, in silico, and in vivo approaches. *Eur. J. Med. Chem.* **2011**, *46*, 2243–2251. [[CrossRef](#)] [[PubMed](#)]
53. Li, Y.; Yu, Y.; Jin, K.; Gao, L.; Luo, T.; Sheng, L.; Shao, X.; Li, J. Synthesis and biological evaluation of novel thiadiazole amides as potent Cdc25B and PTP1B inhibitors. *Bioorg. Med. Chem. Lett.* **2014**, *24*, 4125–4128. [[CrossRef](#)] [[PubMed](#)]
54. Li, W.; Li, S.; Higai, K.; Sasaki, T.; Asada, Y.; Ohshima, S.; Koike, K. Evaluation of licorice flavonoids as protein tyrosine phosphatase 1B inhibitors. *Bioorg. Med. Chem. Lett.* **2013**, *23*, 5836–5839. [[CrossRef](#)] [[PubMed](#)]
55. Navarrete-Vazquez, G.; Paoli, P.; León-Rivera, I.; Villalobos-Molina, R.; Medina-Franco, J.L.; Ortiz-Andrade, R.; Estrada-Soto, S.; Camici, G.; Diaz-Coutiño, D.; Gallardo-Ortiz, I.; et al. Synthesis, in vitro and computational studies of protein tyrosine phosphatase 1B inhibition of a small library of 2-arylsulfonylaminobenzothiazoles with antihyperglycemic activity. *Bioorg. Med. Chem.* **2009**, *17*, 3332–3341. [[CrossRef](#)] [[PubMed](#)]
56. Navarrete-Vazquez, G.; Ramírez-Martínez, M.; Estrada-Soto, S.; Nava-Zuazo, C.; Paoli, P.; Camici, G.; Escalante-García, J.; Medina-Franco, J.L.; López-Vallejo, F.; Ortiz-Andrade, R. Synthesis, in vitro and in silico screening of ethyl 2-(6-substituted benzo[d]thiazol-2-ylamino)-2-oxoacetates as protein-tyrosine phosphatase 1B inhibitors. *Eur. J. Med. Chem.* **2012**, *53*, 346–355. [[CrossRef](#)] [[PubMed](#)]
57. Ottanà, R.; Maccari, R.; Mortier, J.; Caselli, A.; Amuso, S.; Camici, G.; Rotondo, A.; Wolber, G.; Paoli, P. Synthesis, biological activity and structure–activity relationships of new benzoic acid-based protein tyrosine phosphatase inhibitors endowed with insulinomimetic effects in mouse C2C12 skeletal muscle cells. *Eur. J. Med. Chem.* **2014**, *71*, 112–127. [[CrossRef](#)] [[PubMed](#)]
58. Hussain, M.; Ahmed, V.; Hill, B.; Ahmed, Z.; Taylor, S.D. A re-examination of the difluoromethylenesulfonic acid group as a phosphotyrosine mimic for PTP1B inhibition. *Bioorg. Med. Chem.* **2008**, *16*, 6764–6777. [[CrossRef](#)] [[PubMed](#)]
59. Nguyen, P.H.; Zhao, B.T.; Ali, M.Y.; Choi, J.S.; Rhyu, D.Y.; Min, B.S.; Woo, M.H. Insulin-mimetic selaginellins from selaginella tamariscina with protein tyrosine phosphatase 1B (PTP1B) inhibitory activity. *J. Nat. Prod.* **2015**, *78*, 34–42. [[CrossRef](#)] [[PubMed](#)]
60. Nguyen, P.H.; Ji, D.J.; Han, Y.R.; Choi, J.S.; Rhyu, D.Y.; Min, B.S.; Woo, M.H. Selaginellin and biflavonoids as protein tyrosine phosphatase 1B inhibitors from Selaginella tamariscina and their glucose uptake stimulatory effects. *Bioorg. Med. Chem.* **2015**, *23*, 3730–3737. [[CrossRef](#)] [[PubMed](#)]
61. Ramírez-Espinosa, J.J.; Rios, M.Y.; Paoli, P.; Flores-Morales, V.; Camici, G.; Rosa-Lugo, V.D.L.; Hidalgo-Figueroa, S.; Navarrete-Vázquez, G.; Estrada-Soto, S. Synthesis of oleanolic acid derivatives: In vitro, in vivo and in silico studies for PTP-1B inhibition. *Eur. J. Med. Chem.* **2014**, *87*, 316–327. [[CrossRef](#)] [[PubMed](#)]
62. Thrasher, J. Pharmacologic Management of Type 2 Diabetes Mellitus: Available Therapies. *Am. J. Med.* **2017**, *130*, S4–S17. [[CrossRef](#)] [[PubMed](#)]
63. Safavi, M.; Foroumadi, A.; Abdollahi, M. The importance of synthetic drugs for type 2 diabetes drug discovery. *Expert Opin. Drug Discov.* **2013**, *8*, 1339–1363. [[CrossRef](#)] [[PubMed](#)]
64. Klopfenstein, S.R.; Evdokimov, A.G.; Colson, A.O.; Fairweather, N.T.; Neuman, J.J.; Maier, M.B.; Gray, J.L.; Gerwe, G.S.; Stake, G.E.; Howard, B.W.; et al. 1,2,3,4-Tetrahydroisoquinolinyll sulfamic acids as phosphatase PTP1B inhibitors. *Bioorg. Med. Chem. Lett.* **2006**, *16*, 1574–1578. [[CrossRef](#)] [[PubMed](#)]

65. Puius, Y.A.; Zhao, Y.; Sullivan, M.; Lawrence, D.S.; Almo, S.C.; Zhang, Z.Y. Identification of a second aryl phosphate-binding site in protein-tyrosine phosphatase 1B: A paradigm for inhibitor design. *Proc. Natl. Acad. Sci. USA* **1997**, *94*, 13420–13425. [[CrossRef](#)] [[PubMed](#)]
66. Joshi, P.; Deora, G.S.; Rathore, V.; Tanwar, O.; Rawat, A.K.; Srivastava, A.K.; Jain, D. Identification of ZINC02765569: A potent inhibitor of PTP1B by vHTS. *Med. Chem. Res.* **2013**, *22*, 28–34. [[CrossRef](#)]
67. Rakse, M.; Karthikeyan, C.; Deora, G.S.; Moorthy, N.S.H.N.; Rathore, V.; Rawat, A.K.; Srivastava, A.K.; Trivedi, P. Design, synthesis and molecular modelling studies of novel 3-acetamido-4-methyl benzoic acid derivatives as inhibitors of protein tyrosine phosphatase 1B. *Eur. J. Med. Chem.* **2013**, *70*, 469–476. [[CrossRef](#)] [[PubMed](#)]
68. Sarmiento, M.; Zhao, Y.; Gordon, S.; Zhang, Z. Molecular basis for substrate specificity of protein-tyrosine phosphatase 1B. *J. Biol. Chem.* **1998**, *273*, 26368. [[CrossRef](#)]
69. Lipinski, C.A.; Lombardo, F.; Dominy, B.W.; Feeney, P.J. Experimental and Computational Approaches to Estimate Solubility and Permeability in Drug Discovery and Development Settings. *Adv. Drug Deliv. Rev.* **1997**, *23*, 3–25. [[CrossRef](#)]
70. Veber, D.F.; Johnson, S.R.; Cheng, H.; Smith, B.R.; Ward, K.W.; Kopple, K.D. Molecular Properties That Influence the Oral Bioavailability of Drug Candidates. *J. Med. Chem.* **2002**, *45*, 2615–2623. [[CrossRef](#)] [[PubMed](#)]
71. Egan, W.J.; Merz, K.M.; Baldwin, J.J. Prediction of drug absorption using multivariate statistics. *J. Med. Chem.* **2000**, *43*, 3867–3877. [[CrossRef](#)] [[PubMed](#)]
72. Drwal, M.N.; Banerjee, P.; Dunkel, M.; Wettig, M.R.; Preissner, R. ProTox: A web server for the in silico prediction of rodent oral toxicity. *Nucleic Acids Res.* **2014**, *42*, 53–58. [[CrossRef](#)] [[PubMed](#)]
73. Sander, T.; Freyss, J.; Von Korff, M.; Rufener, C. DataWarrior: An open-source program for chemistry aware data visualization and analysis. *J. Chem. Inf. Model.* **2015**, *55*, 460–473. [[CrossRef](#)] [[PubMed](#)]
74. Valdez, J.; Cedillo, R.; Hernández-Campos, A.; Yépez, L.; Hernández-Luis, F.; Navarrete-Vázquez, G.; Tapia, A.; Cortés, R.; Hernández, M.; Castillo, R. Synthesis and antiparasitic activity of 1H-benzimidazole derivatives. *Bioorg. Med. Chem. Lett.* **2002**, *12*, 2221–2224. [[CrossRef](#)]
75. Flores-Carrillo, P.; Velázquez-López, J.M.; Aguayo-Ortiz, R.; Hernández-Campos, A.; Trejo-Soto, P.J.; Yépez-Mulia, L.; Castillo, R. Synthesis, antiprotozoal activity, and chemoinformatic analysis of 2-(methylthio)-1H-benzimidazole-5-carboxamide derivatives: Identification of new selective giardicidal and trichomonocidal compounds. *Eur. J. Med. Chem.* **2017**, *137*, 211–220. [[CrossRef](#)] [[PubMed](#)]
76. Hernández-Campos, A.; Ibarra-Velarde, F.; Vera-Montenegro, Y.; Rivera-Fernández, N.; Castillo, R. Synthesis and Fasciolicidal Activity of 5-Chloro-2-methylthio-6-(1-naphthyloxy)-1H-benzimidazole. *Chem. Pharm. Bull.* **2002**, *50*, 649–652. [[CrossRef](#)]
77. Velázquez-López, J.M.; Hernández-Campos, A.; Yépez-Mulia, L.; Téllez-Valencia, A.; Flores-Carrillo, P.; Nieto-Meneses, R.; Castillo, R. Synthesis and trypanocidal activity of novel benzimidazole derivatives. *Bioorg. Med. Chem. Lett.* **2016**, *26*, 4377–4381. [[CrossRef](#)] [[PubMed](#)]
78. Soria-Arteche, O.; Castillo, R.; Hernández-Campos, A.; Hurtado-de la Peña, M.; Gabriel Navarrete-Vázquez, G.; Medina-Franco, J.L.; Gómez-Flores, K. Studies on the Selective S-Oxidation of Albendazole, Fenbendazole, Triclabendazole, and other Benzimidazole Sulfides. *J. Mex. Chem. Soc.* **2005**, *49*, 353–358.
79. Goldstein, B.J.; Bittner-Kowalczyk, A.; White, M.F.; Harbeck, M. Tyrosine Dephosphorylation and Deactivation of Insulin Receptor Substrate-1 by Protein-tyrosine Phosphatase 1B. *J. Biol. Chem.* **2000**, *275*, 4283–4289. [[CrossRef](#)] [[PubMed](#)]
80. Téllez-Valencia, A.; Najera, H.; Sampedro, J.; Aguirre, B.; Olivares, V.R.A. Diseño de fármacos antiparasitarios. Inhibición especie específica de la triosafosfato isomerasa de Leishmania mexicana. *Boletín Inf. los Serv. Salud del Estado Hidalgo* **2006**, *29*, 2–3.
81. Schrödinger Release 2014-1: *LigPrep*, version 2.9; Schrödinger: New York, NY, USA, 2014.
82. Madhavi Sastry, G.; Adzhigirey, M.; Day, T.; Annabhimoju, R.; Sherman, W. Protein and ligand preparation: Parameters, protocols, and influence on virtual screening enrichments. *J. Comput.-Aided Mol. Des.* **2013**, *27*, 221–234. [[CrossRef](#)] [[PubMed](#)]
83. Ghattas, M.A.; Atatreh, N.; Bichenkova, E.V.; Bryce, R.A. Protein tyrosine phosphatases: Ligand interaction analysis and optimisation of virtual screening. *J. Mol. Graph. Model.* **2014**, *52C*, 114–123. [[CrossRef](#)] [[PubMed](#)]
84. Friesner, R.A.; Banks, J.L.; Murphy, R.B.; Halgren, T.A.; Klicic, J.J.; Mainz, D.T.; Repasky, M.P.; Knoll, E.H.; Shaw, D.E.; Shelley, M.; et al. Glide: A New Approach for Rapid, Accurate Docking and Scoring. 1. Method and Assessment of Docking Accuracy. *J. Med. Chem.* **2004**, *47*, 1739–1749. [[CrossRef](#)] [[PubMed](#)]

85. Friesner, R.A.; Murphy, R.B.; Repasky, M.P.; Frye, L.L.; Greenwood, J.R.; Halgren, T.A.; Sanschagrin, P.C.; Mainz, D.T. Extra Precision Glide: Docking and Scoring Incorporating a Model of Hydrophobic Enclosure for Protein-Ligand Complexes. *J. Med. Chem.* **2006**, *49*, 6177–6196. [[CrossRef](#)] [[PubMed](#)]
86. Shelley, J.C.; Cholleti, A.; Frye, L.L.; Greenwood, J.R.; Timlin, M.R.; Uchimaya, M. Epik: A software program for pKa prediction and protonation state generation for drug-like molecules. *J. Comput.-Aided Mol. Des.* **2007**, *21*, 681–691. [[CrossRef](#)] [[PubMed](#)]
87. Schüttelkopf, A.W.; Van Aalten, D.M.F. PRODRG—A tool for highthroughput crystallography of protein—Ligand complexes. *Acta Crystallogr.* **2004**, *60*, 1355–1363.
88. Van Der Spoel, D.; Lindahl, E.; Hess, B.; Groenhof, G.; Mark, A.E.; Berendsen, H.J.C. GROMACS: Fast, flexible, and free. *J. Comput. Chem.* **2005**, *26*, 1701–1718. [[CrossRef](#)] [[PubMed](#)]
89. Kumari, R.; Kumar, R.; Source, O.; Discovery, D.; Lynn, A. *g_mmpbsa*—A GROMACS Tool for High-Throughput MM-PBSA Calculations. *J. Chem. Inf. Model.* **2014**, *54*, 1951–1962. [[CrossRef](#)] [[PubMed](#)]

Sample Availability: Samples of the compounds are not available from the authors.



© 2017 by the authors. Licensee MDPI, Basel, Switzerland. This article is an open access article distributed under the terms and conditions of the Creative Commons Attribution (CC BY) license (<http://creativecommons.org/licenses/by/4.0/>).

Article

Effects of *Moringa oleifera* Leaves Extract on High Glucose-Induced Metabolic Changes in HepG2 Cells

Jorge A. Sosa-Gutiérrez¹, Mónica A. Valdéz-Solana¹, Tamara Y. Forbes-Hernández²,
Claudia I. Avitia-Domínguez³, Gonzalo G. Garcia-Vargas⁴, José M. Salas-Pacheco⁵,
Oscar Flores-Herrera⁶, Alfredo Téllez-Valencia³, Maurizio Battino²  and Erick Sierra-Campos^{1,*} 

¹ Facultad de Ciencias Químicas, Universidad Juárez del Estado de Durango Campus Gómez Palacio, Avenida Artículo 123 S/N, Fracc. Filadelfia, 35010 Gómez Palacio, Mexico; sosa_jasg@hotmail.com (J.A.S.-G.); valdezandyval@gmail.com (M.A.V.-S.)

² Dipartimento di Scienze Cliniche Specialistiche ed Odontostomatologiche (DISCO)-Sez. Biochimica, Facoltà di Medicina, Università Politecnica delle Marche, 60131 Ancona, Italy; tamaraforbe@gmail.com (T.Y.F.-H.); m.a.battino@univpm.it (M.B.)

³ Facultad de Medicina y Nutrición, Universidad Juárez del Estado de Durango Campus Durango, Avenida Universidad y Fanny Anitúa S/N, 34000 Durango, Mexico; avitiaclaudia@gmail.com (C.I.A.-D.); tellezalfredo@gmail.com (A.T.-V.)

⁴ Facultad de Ciencias de la Salud, Universidad Juárez del Estado de Durango Campus Gómez Palacio, Calzada Palmas 1, Colonia Revolución, 35050 Gómez Palacio, Mexico; ggarcia_vargas@hotmail.com

⁵ Instituto de Investigación Científica, Universidad Juárez del Estado de Durango, Avenida Universidad S/N, 34000 Durango, Mexico; jsalas_pacheco@hotmail.com

⁶ Departamento de Bioquímica, Facultad de Medicina, Universidad Nacional Autónoma de México, 04510 Ciudad de México, Mexico; oflores@bq.unam.mx

* Correspondence: ericksier@gmail.com; Tel.: +52-(871)-7158810; Fax: +52-(871)-7152964

Received: 14 May 2018; Accepted: 25 June 2018; Published: 26 June 2018



Abstract: Mitochondrial dysfunction is a hallmark of diabetes, but the metabolic alterations during early stages of the disease remain unknown. The ability of liver cells to rearrange their metabolism plays an important role in compensating the energy shortage and may provide cell survival. *Moringa oleifera* leaves have been studied for its health properties against diabetes, insulin resistance, and non-alcoholic liver disease. We postulated that *M. oleifera* executes a protective function on mitochondrial functionality in HepG2 treated with high glucose. We evaluated the effect of high glucose treatment on the mitochondrial function of HepG2 cells using a Seahorse extracellular flux analyzer (Agilent, Santa Clara, CA, USA), blue native polyacrylamide gel electrophoresis (BN-PAGE), and western blot analysis. For assessment of mitochondrial abnormalities, we measured the activity of mitochondrial Complex I and IV as well as uncoupling protein 2, and sirtuin 3 protein contents. Our results demonstrate that, under conditions mimicking the hyperglycemia, Complex I activity, UCP2, Complex III and IV subunits content, supercomplex formation, and acetylation levels are modified with respect to the control condition. However, basal oxygen consumption rate was not affected and mitochondrial reactive oxygen species production remained unchanged in all groups. Treatment of HepG2 cells with *M. oleifera* extract significantly increased both protein content and mitochondrial complexes activities. Nonetheless, control cells' respiratory control ratio (RCR) was 4.37 compared to high glucose treated cells' RCR of 15.3, and glucose plus *M. oleifera* treated cells' RCR of 5.2, this indicates high-quality mitochondria and efficient oxidative phosphorylation coupling. Additionally, the state app was not altered between different treatments, suggesting no alteration in respiratory fluxes. These findings enhance understanding of the actions of *M. oleifera* and suggest that the known antidiabetic property of this plant, at least in part, is mediated through modulating the mitochondrial respiratory chain.

Keywords: HepG2 cells; *Moringa oleifera*; mitochondria; UCP2; SIRT3

1. Introduction

A growing body of experimental and epidemiological evidence suggests that *Moringa oleifera* Lam have antidiabetic and antioxidant effects against the harmful damages of oxidative stress and diabetic complications [1–3]. The beneficial activities of *M. oleifera* on carbohydrate metabolism have been shown by different physiological processes, including preventing and restoring the integrity and function of pancreatic β -cells, increasing insulin action, improving glucose uptake and utilization [4]. Recent studies have demonstrated that phenolic compounds of *M. oleifera* significantly decreased total intracellular cholesterol, inhibited the activity of HMG CoA reductase (3-hydroxy-3-methyl-glutaryl-coenzyme A reductase), and enhanced low-Density Lipoprotein (LDL) receptor binding activity in HepG2 cells [5]. Furthermore, it was reported that the *M. oleifera* during adipogenesis improves adipocyte functionality and upregulates the expression of uncoupling protein 1 (UCP1), sirtuin 1 (SIRT-1), and peroxisome proliferator-activated receptor gamma coactivator 1-alpha (PGC-1 α) involved in thermogenesis modulating lipid metabolism [6]. In association with these results, it has been suggested that mitochondrial proton leak (UCP activity) might play a role in the pathophysiology of diabetic complications [7] and cardiovascular diseases [8]. We recently demonstrated changes in oxygen consumption, supercomplex formation, and increased lipoperoxidation levels in isolated mitochondria from liver of streptozotocin (STZ)-diabetic rats, where *M. oleifera* extract may have a protective role against some of these alteration [9]. These data suggested that *M. oleifera* works intracellularly via several metabolic pathways within mitochondria. Thereby, there are diverse promising candidates for suppressing mitochondrial dysfunction, two potential targets that caught our attention are sirtuins (SIRT) and uncoupling proteins (UCPs) which seem to be critically important in the pathogenesis of diabetes, cardiovascular disease, and obesity [10].

The SIRTs are a family of nicotinamide adenine dinucleotide (NAD⁺) dependent deacetylases and they play a critical role in restoring homeostasis during stress responses. They can influence multiple protein functions, including DNA—protein interactions, transcriptional activity, subcellular localization, protein stability, and enzymatic activity [11,12]. The crucial role played by SIRT in the regulation of metabolism has been extensively studied. For example, in liver and heart, SIRT1 regulates gluconeogenic activity by modulating cAMP responsive element binding protein, PGC-1 α a nuclear-encoded transcriptional coactivator that regulates the expression of nuclear-encoded mitochondrial proteins, including nuclear respiratory factors 1 and 2 (NRF1 and NRF2), estrogen-related receptor- α (ERR- α), and mitochondrial transcription factor A (TFAM) [13,14]. In addition, SIRT1 activators improve insulin sensitivity in liver and heart. SIRT3 is a member of the sirtuin family that is localized in mitochondria. It is decreased in skeletal muscle of diabetic models [15] and it has been shown that high fat feeding induces a shift in acetylation balance, causing protein hyperacetylation in liver [16], SIRT3 is also involved in the regulation of oxidative phosphorylation through the deacetylation of Complex I and succinate dehydrogenase subunits [17,18]. In diabetes, increases in mitochondrial uncoupling induce mild metabolic stress by dissipating the hydrogen ion gradient across the inner mitochondrial membrane. As a stress response, glucose uptake and NADH oxidation are stimulated with an increase in respiration, NAD⁺ levels, and the NAD⁺/NADH ratio in mitochondria. Thus NAD⁺ dependent SIRT1 is activated [19]. Therefore, SIRT1 and 3 regulation is a promising new therapeutic approach for treating diabetic complications [20] and some research groups are now focusing on the development of high affinity small molecule activators of SIRT1 [21,22].

In this context, it was demonstrated that resveratrol significantly increases SIRT1 activity through allosteric interaction, resulting in the increase of SIRT1 affinity for both NAD⁺ and the acetylated substrate, causing deacetylation of PGC1 α , forkhead box protein O1 (FOXO1), and the target of rapamycin kinase 2 (TORC2) which in turn leads to increased fatty acid oxidation and gluconeogenesis [23,24]. However, it is still unknown whether these mitochondrial defects result in change in others SIRTs.

On the other hand, UCPs are a family of carriers expressed in the mitochondrial inner membrane that uncouple oxygen consumption by the respiratory chain from ATP synthesis. UCP2 is expressed in

a wide range of tissues and acts in the protection against oxidative stress, in the negative regulation of insulin secretion by beta cells, and in fatty acid metabolism. Most of the studies about the role of UCP2 in diabetes have focused on the UCP2 functions in β -cells, and the results have shown a deleterious effect of UCP2 in diabetes [25]. As UCP2 is widely expressed in many tissues such as liver, its antioxidant activity makes it logical to search look for benefits on diabetes through counteracting the oxidative stress appeared in diabetes and its complications. Moreover, Korean red ginseng promoted the expression of insulin and downregulated the expression of UCP2 in spontaneously diabetic Goto-Kakizaki rats [26]. Due to the close correlation between these proteins (SIRT and UCP) and mitochondrial oxidative phosphorylation, we hypothesized that *M. oleifera* may exert a protective effect against the development of diabetes through regulatory effect of SIRT3 and UCP2.

Finally, HepG2 cells are a suitable and well characterized model of human liver, which has been widely used in biochemical and nutritional studies [27–29]. Numerous studies have used a high concentration of glucose (25 mM) as an in vitro model for investigation of hyperglycemia-induced toxicity which simulated in vivo condition of diabetic ketoacidosis observed in acute or untreated diabetes [30–32]. Therefore, we used this cell line to explore the effect of high glucose on modulating mitochondrial SIRT3 and UCP2 and the possible protective role of *M. oleifera* over these alterations to determine the molecular targets by which this plant exerts its beneficial properties in the treatment of diabetes.

2. Materials and Methods

2.1. Reagents

All the reagents used in this study were of reagent grade and were purchased from Sigma Aldrich (Toluca, Mexico); Gibco, Thermo Fisher Scientific (Waltham, MA, USA); Invitrogen Thermo Fisher Scientific (Waltham, MA, USA); and Abcam (Cambridge, MA, USA).

2.2. *Moringa oleifera* Extract Preparation

Extract preparation was carried out as previously described [33]. 100 g of crushed dried moringa leaves were macerated for 24 h in 1 L of 20:80 v/v methanol in constant stirring. Solution was then filtered and distilled in a rotary evaporator at 60 °C, the aqueous fraction was then frozen at –80 °C for 24 h prior freeze drying to yield the final powdered extract. The extract was stored at –80 °C until its use.

2.3. Cell Culture

HepG2 cells were grown in 75 cm² flasks in Dulbecco's modified Eagle's medium (DMEM) (5 mM glucose) supplemented with 10% fetal bovine serum (FBS) and penicillin/streptomycin and kept at 37 °C with 5% CO₂. Media was changed every third day until confluence was reached. Then, cells were divided into three groups: control (C); 25 mM glucose (G) and 25 mM glucose + 500 µg/mL of *M. oleifera* extract (GM). Cells were kept in high glucose media for 24 h. After incubation, cells were washed with fresh DMEM and kept in media supplemented with moringa extract for 2 h. Cells were detached with trypsin and resuspended in DMEM to inactivate trypsin, then centrifuged at 600 × g for 10 min to recover the cellular pellet.

2.4. Mitochondrial Isolation

Mitochondria from HepG2 cells were isolated with mitochondria isolation kit (MITOISO2 Sigma) following manufacturer indications.

2.5. Viability Assay

Ninety-six-well plates were seeded with 5000 cells per well to perform viability experiments. Cells were incubated with different concentrations of moringa extract (50–500 µg/mL), glucose (50 mM),

and the combination of both for 24 h at 37 °C with 5% CO₂. Cells were then incubated for 2 h with 30 µL of 3-(4,5-dimethylthiazol-2-yl)-2,5-diphenyltetrazolium bromide (MTT) solution per well. The media was discarded and 100 µL of dimethyl sulfoxide (DMSO) was used to dissolve the formazan crystals and to extract the blue color. Absorbance was read in a microplate reader at 595 nm.

2.6. Oxygen Consumption Rate

A measure of 30,000 cells/mL were seeded in 24-well seahorse XF-24 plates and let attach for 24 h. Cells were then incubated with glucose (25 mM) for 24 h, followed by moringa extract addition (500 µg/mL) for 2 h. After incubation, media was replaced with DMEM without FBS and placed at 37 °C without CO₂. The injection ports were loaded with sequence of oligomycin, carbonyl cyanide 4 (trifluoromethoxy) phenylhydrazone (FCCP), rotenone (Rot), and antimycin A (AA) for final assay concentrations of 2.5 µg/mL, 2.5 µM, 1 µM, and 10 µM, respectively. Flux pack was hydrated overnight and calibrated for 30 min prior oxygen consumption rate (OCR) analysis.

The cellular bioenergetic parameters determined were ATP linked respiration, proton leak, maximal OCR, and reserve capacity. ATP linked respiration was derived from the difference between OCR at baseline and respiration following oligomycin addition. The change in OCR between antimycin A and oligomycin represented the amount of oxygen consumed due to proton leak. Maximal OCR was determined by subtracting the OCR after antimycin A addition from the OCR induced by FCCP. Lastly, the reserve capacity was calculated by the difference between maximal (FCCP) and basal respiration.

The intermediate turnover state, known as State 3.5 (the state app) and respiratory flux control were derived as detailed in [34]. In these experiments, the assumption is made that State 3 respiration is equivalent to the rate measured after addition of FCCP (State 3_{FCCP} or State 3u) and State 4 is the rate measured after addition of oligomycin (State 4_{oligomycin} or State 4o). These assumptions allowed the calculation of the apparent respiratory state of the cells using the equation

$$\text{State}_{\text{apparent}} = 4 - [(\text{Basal} - \text{Oligo}) / (\text{FCCP} - \text{Oligo})]$$

where Basal represents the basal OCR, Oligo represents the oligomycin-insensitive OCR (proton leak), and FCCP represents the FCCP-stimulated OCR (maximal OCR). Using the same assumptions regarding the relative State 3 and State 4 respiration, the respiratory control ratio (RCR) was calculated as the State 3u rate divided by State 4o rate (maximal OCR/oligomycin insensitive OCR). Coupling efficiency is the proportion of the oxygen consumed to drive ATP synthesis compared with that driving proton leak and was calculated as the fraction of basal mitochondrial OCR used for ATP synthesis (ATP-linked OCR/basal OCR) [35]. Finally, the fraction of respiration that was used under routine conditions to produce ATP (phosphorylating respiration) was estimated as the ratio between ATP-linked OCR and maximal OCR (FCCP) (ATP linked OCR/maximal OCR) as described in [36].

2.7. Measurement of Reactive Oxygen Species Levels

Six-well plates were seeded with 150,000 cells per well and incubated with glucose (25 mM) for 24 h, followed by incubation with moringa extract (500 µg/mL) for 2 h at 37 °C with 5% CO₂. After incubation, cells were washed with PBS, detached with trypsin and resuspended in a final volume of 0.5 mL. Cell suspension was incubated with 1 µL of CellROX orange reagent for 30 min at 37 °C. The cell suspension was centrifuged at 600× g for 10 min and the pellet resuspended in 100 µL of PBS. Measures of 25 µL of the final suspension were used to quantify the fluorescence in a Tali image-based cytometer.

2.8. SDS-PAGE and Western Blot Analysis

Cellular pellet was resuspended in 0.1 mL of lysis buffer containing 20 mM Tris (tris(hydroxymethyl)aminomethane), pH 7.5, 150 mM KCl, 1 mM ethylenediaminetetraacetic acid (EDTA), and 1% Triton X-100 and protease inhibitor cocktail. Cells were rapidly frozen

and thawed three times with liquid nitrogen to ensure maximal cell lysis and centrifuged at $5000\times g$ for 15 min, supernatants were recovered and used for further analysis. 50 μg of protein (determined by bicinchoninic acid (BCA) analysis) were loaded into a 12% sodium dodecyl sulfate (SDS)-polyacrylamide gel and run at 120 V for 90 min. Proteins were then transferred to a polyvinylidene difluoride (PVDF) membrane previously activated with methanol. Membranes were incubated overnight with the primary antibody (anti UCP2—ab67241, anti SIRT3—ab189860, anti-acetyl lysine—ab80178, and anti OXPHOS—ab110413) at dilutions of 1:500, followed by 2 h incubation with the secondary antibody at dilutions of 1:1000. The intensity of bands was determined by Image Studio Lite v.5.2 software (LI-COR Biosciences, Lincoln, NE, USA).

2.9. BN-PAGE

Respiratory supercomplexes and complexes were solubilized using digitonin (a very-mild detergent) as described by [37] with minor modifications. Briefly, mitochondrial proteins isolated from HepG2 cells (10 mg/mL) were suspended in 3.5 mL of 50 mM Bis-Tris and 500 mM 6-aminocaproic acid, pH 7.0, and 140 μL digitonin (50% stock) were added to reach a detergent/protein ratio of 2:1 and incubated in this condition during 30 min. The mixture was centrifuged at $100,000\times g$ for 30 min at 4 °C and supernatant was recovered.

Supercomplexes and complexes were loaded on a linear polyacrylamide gradient gel (4–10%) for Blue Native PAGE (BN-PAGE). Anode buffer contained 50 mM Bis-Tris/HCl, pH 7.0 and cathode buffer 50 mM tricine, 15 mM Bis-Tris, pH 7.0 and Coomassie Brilliant Blue R-125 dye (0.02%). The voltage was set to 35 V for 10 h at 4 °C and the run was stopped when the sharp line of the dye approached the gel front. Molecular weight of the respiratory complexes and supercomplexes was determined by their electrophoretic mobility and in-gel catalytic activity, using the digitonin-solubilized bovine heart mitochondria as standard. The intensity of bands was determined by Image Studio Lite v.5.2 software.

2.10. In-Gel CI and CIV Activities

The in-gel assays were performed as described by [38] using gel loaded with isolated digitonine-solubilized supercomplexes. CI activity was assayed in a buffer containing 5 mg MTT and 3.75 mg NADH in 10 mL of 10 mM Tris/HCl, pH 7.4. Once activity-staining appeared (10–20 min) reaction was stopped with fixing solution (50% methanol, 10% acetic acid). To assay the activity of complex IV the gel was incubated in 10 mL of 50 mM K_2HPO_4 , pH 7.2, 10 mg of diaminobenzidine (DAB) and 2 mg of horse heart cytochrome c. After 30–40 min of incubation at 20–25 °C, the activity was observed as a brown precipitate and the reaction was stopped with the fixing solution. The intensity of bands was determined by Image Studio Lite v.5.2 software.

2.11. Statistical Analysis

Data were analyzed by one-way ANOVA using the SigmaPlot v.12.3 (Systat Software, Inc., San Jose, CA, USA). Differences among groups were considered significant when $p \leq 0.05$.

3. Results

3.1. Toxicity of the Extract and High Glucose

Previous studies have also shown that HepG2 cells are a better model than fresh human hepatocytes to define mitotoxicity [39] and it was reported that high glucose treatment at 25 mM for 72 h increased apoptosis in HepG2 cells through increase oxidative stress [40]. Recent reports demonstrated that the nano-micelle of *M. oleifera* seed oil remarkably induces mitochondrial apoptosis mediating cell death [41]. Moreover, *M. oleifera* aqueous leaf extract treatment resulted in a significant decrease in mitochondrial membrane potential (1 h) and ATP levels (3 h), followed by an increase in (6 h) ROS, caspase activation, proapoptotic proteins expression, and poly [ADP-ribose] polymerase 1 cleavage on different types of cells, including HepG2 [42]. Taken together, both high glucose and

M. oleifera extract could decrease cell viability by promoting mitochondrial dysfunction and oxidative stress. Therefore, we further investigated whether such experimental conditions affect our cell line.

In order to demonstrate that *M. oleifera* components and glucose do not have adverse effects on the overall viability of HepG2 cells, we performed an assay with different concentrations of the extract with or without high glucose. We did not find evidence of apoptosis in glucose treated cells. First, our MTT assay results showed that neither the extract nor glucose have negative effects over the viability of cells. Second, even at larger concentrations (500 $\mu\text{g}/\text{mL}$) *M. oleifera* extract did not showed any difference with respect to control group, in fact, the groups treated with glucose and the extract showed slightly higher viability than control cells (Figure 1). Hence, it is possible that *M. oleifera* extract can induce mitochondrial metabolic changes without affecting cell viability in early stages of treatment, supporting our previous results with an animal model. Although glucose had no negative effects on cells' viability, it influenced the mitochondrial respiration.

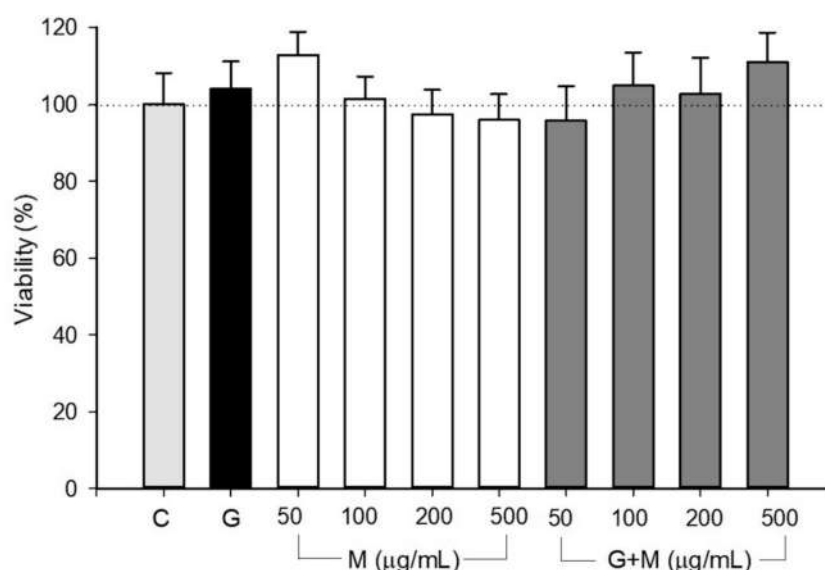


Figure 1. Viability of HepG2 cells treated with glucose and *M. oleifera* extract. Cells were incubated as described in material and methods section and incubated with 25 mM glucose (G) and different concentrations of *M. oleifera* extract (GM; 50–500 $\mu\text{g}/\text{mL}$). Data are expressed as the average \pm SD from $n = 4$.

3.2. Effect of Moringa Extract on Mitochondrial OCR

To assess the effect of high glucose and *M. oleifera* extract on oxygen consumption rate (OCR) we used the Seahorse XF-24 analyzer. All OCR readings in the three groups were normalized to total protein concentration and the parameters analyzed were; the basal respiration (State II) is controlled by proton leak and substrate oxidation. In the presence of oligomycin, respiration is highly dependent on proton leak. The injection of uncoupling agent FCCP reestablishes electron flux and gives rise to maximum capacity of ATP generation or oxygen consumption. Finally, the residual oxygen consumption can be measured by injection of respiratory inhibitors rotenone/antimycin A.

Initially, the basal respiration did not differ between control and other treatments. HepG2 cells treated with high glucose showed no difference in basal respiration but the results demonstrated that the ATP-linked respiration and respiratory capacity was significantly reduced in the high glucose treated cells in contrast to untreated cells. Oligomycin was added at 7 min to inhibit ATP synthesis, interestingly, we observed that the lack of sensitivity of glucose-treated cells (HG cells) to oligomycin is likely because under these conditions the cells can compensate for mitochondrial impairment by utilizing glycolysis for ATP generation. In contrast, cells grown in high glucose and incubated with *M. oleifera* extract (GM cells) rely mostly on OXPHOS to produce ATP because they are more

sensitive to oligomycin. *M. oleifera* treatment not only increased ATP-linked respiration in HG cells but also completely restored their capacity compared to non-treated control cells (Figure 2). The proton ionophore FCCP was added at 13 min to assess the maximum possible oxygen consumption, the FCCP stimulated OCR and demonstrated that uncoupling of OXPHOS provokes an increase in proton leak across the inner mitochondrial membrane and effectively depletes the mitochondrial membrane potential. Interestingly, the stimulation of respiration by FCCP after oligomycin was substantially lower in the presence of high glucose. Moreover, rotenone and antimycin A was added at 19 min to inhibit electron flow through Complex I and III, limiting mitochondrial function with a decrease in OCR. Respiratory control ratio (RCR) was similar between control and GM treatment cells. Control cells RCR was 4.37 compared to HG cells RCR of 15.3, and GM cells RCR of 5.2, these values indicates high-quality mitochondria and efficient oxidative phosphorylation coupling. However, coupling efficiency of control cells was 0.4, which was decreased to 0.1 by the high glucose and significantly suppressed by *M. oleifera* extract (0.31). In addition, phosphorylating respiration in HG cells was 0.065. This was significantly lower than the phosphorylating respiration exhibited by control cells, 0.23. As a comparison, coupling efficiency in control cells was higher than both HG cells and GM cells. Additionally, the state app was not altered between different treatments (Control, 3.56; HG, 3.36, and GM, 3.49), suggesting no alteration in respiratory fluxes which could alter the oxidative phosphorylation machinery.

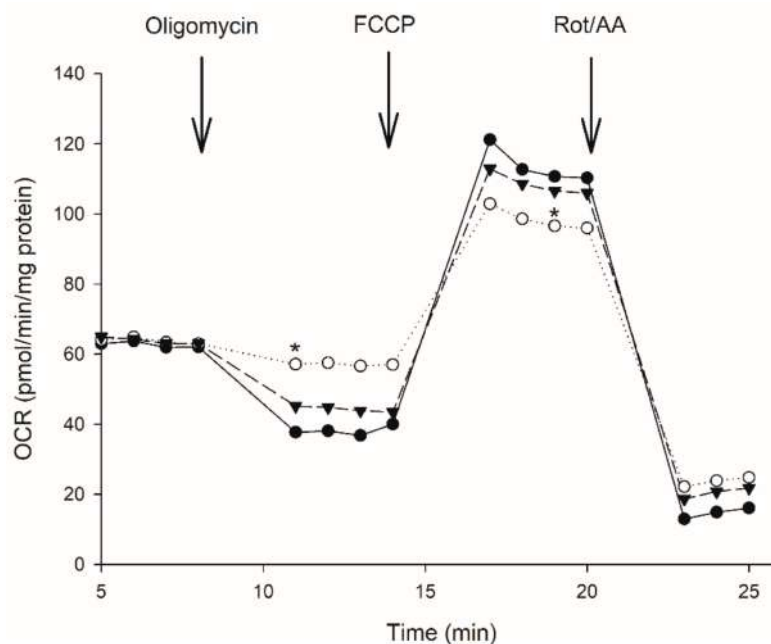


Figure 2. Absolute change in mitochondrial function in intact HepG2 cells treated with glucose 25 mM (white circle) and *M. oleifera* extract 500 $\mu\text{g}/\text{mL}$ (inverted gray triangle). The addition of oligomycin at 5 min inhibits ATP production resulting in a decrease in oxygen consumption rate (OCR). The OCR increases in all treatments following the addition of FCCP at 13 min (uncoupled state). Electron transport chain inhibitors mix (Rotenone and Antimycin A) decrease oxygen consumption rates to very low levels inhibiting total mitochondrial respiration at 18 min. * significant difference against control $p \leq 0.05$.

3.3. Uncoupling Protein Level (UCP2)

To assess whether the above respiration profile data were directly linked to some defect inside the respiratory chain or induce of alternative components, we reasoned that UCP2 activation is likely, at least partially, responsible for the reactive oxygen species inhibitory effect of high glucose in HepG2 cells. In addition, the presence of high glucose caused an increase close to 50% in proton

leak (uncoupling protein activity). In support of this hypothesis, we observed that the combined treatment of high glucose and *M. oleifera* extract enhances ATP production and maximal respiration (Figure 2). Our hyperglycemic model showed more than three-fold increase in UCP2 levels in those cells exposed to 24 h of high glucose (Figure 3). We can assume that UCP2 is highly upregulated during hyperglycemia in liver and its presence correlates with the adaptability of hepatic cells to high concentrations of extracellular glucose. Interestingly, after only 2 h of incubation with *M. oleifera* extract, UCP2 levels normalized (Figure 3). These results suggest that antioxidant properties of extract regulate the UCP2 expression in HepG2 and possibly the ROS production.

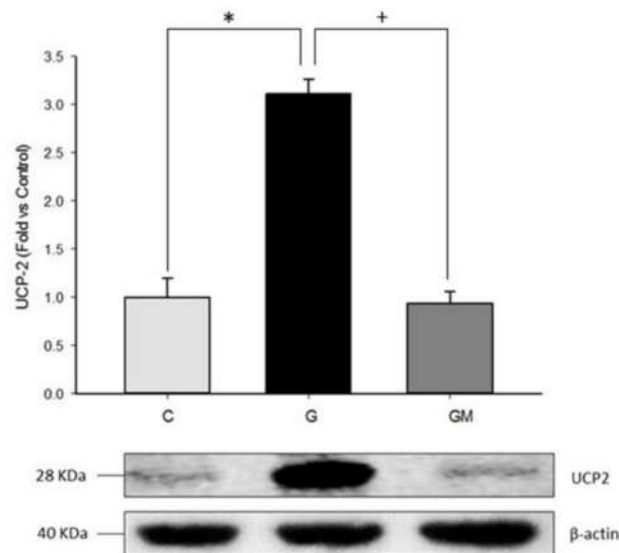


Figure 3. UCP2 protein levels in HepG2 cells treated with glucose 25 mM (G) and *M. oleifera* extract 500 µg/mL (GM). Cells without treatment represent control condition (C). * significant difference against control $p \leq 0.05$. + significant difference against G cells $p \leq 0.05$. Data normalized to control group using β -actin.

3.4. Reactive Oxygen Species Levels

Higher production of ROS is often stated as both cause and consequence of mitochondrial dysfunction [43]. There is evidence that supports the fact that under hyperglycemic conditions ROS production is significantly higher [44]. To identify the role of ROS in the context of hyperglycemia and mitochondrial dysfunction, we carried out fluorescence tests to HG cells and GM cells. However, after performing CellROX orange fluorescence test, data from the Tali cytometer showed no significant changes of ROS between control cells ($5 \pm 1.39\%$ of cells) and those treated with glucose ($4 \pm 1.42\%$), nor the combination glucose plus *M. oleifera* ($4 \pm 1.42\%$). Therefore, we performed repeated tests using Amplex Red ROS-specific probe, and all data were negative for high glucose induced ROS production (data not shown). Hence, the lack of ROS overproduction in our model suggests that diverse metabolic adjustments have occurred at the level of the OXPHOS proteins, which allows cells to adapt to the high glucose environment, and that some regulatory mechanisms could be playing an important role.

3.5. OXPHOS Activities

In order to evaluate this possibility, we measured both the specific activities and analyzed the expression level of individual respiratory complexes. Initially, we evaluated the activity of Complex I and IV to establish if respiration disruptions observed during hyperglycemia are consequence of protein activities. Interestingly, Complex I activity was significantly lower in those HG cells (Figure 4b), correlating with the disruptions observed in respiratory rates in the same samples (Figure 2). As for Complex IV, we found no significant differences among groups (Figure 4c). Despite the clear effect

of high glucose over Complex IV protein levels, this protein can modulate its activity to adapt and sustain cell viability. We were not able to measure Complex III activity, however, due to the lower levels of Complex III and the diminished activity of Complex I found in HG cells, we can assume that these two complexes are responsible for the respiratory alterations observed in our hyperglycemic model. As shown in Figure 4a, Complex III significantly decreases when the cells are treated with high glucose, interestingly this effect is reverted after only 2 h of incubation with 500 $\mu\text{g}/\text{mL}$ of *M. oleifera* extract. On the other hand, Complex IV (Figure 4a) is also decreased in those cells incubated with high glucose, but moringa extract can revert this negative effect. Although protein levels are not as high as control group, these are still significantly different from those found in HG cells. This finding is consistent with [45], who used mass spectrometry analysis to report a 46% decrease in Complex III levels alongside with 20–30% downregulation of subunits from Complex I–IV in cardiac and skeletal muscle mitochondria from diabetic rats. In other reports, proteomic analysis of obese and type 2 diabetic skeletal muscle mitochondria, found less presence of several mitochondrial proteins, including those in the electron transport chain in both human [46] and mice samples [47]. This suggests that tissues with high energy demand or involved in glucose homeostasis are the first ones to suffer from alterations in OXPHOS subunits under hyperglycemic conditions.

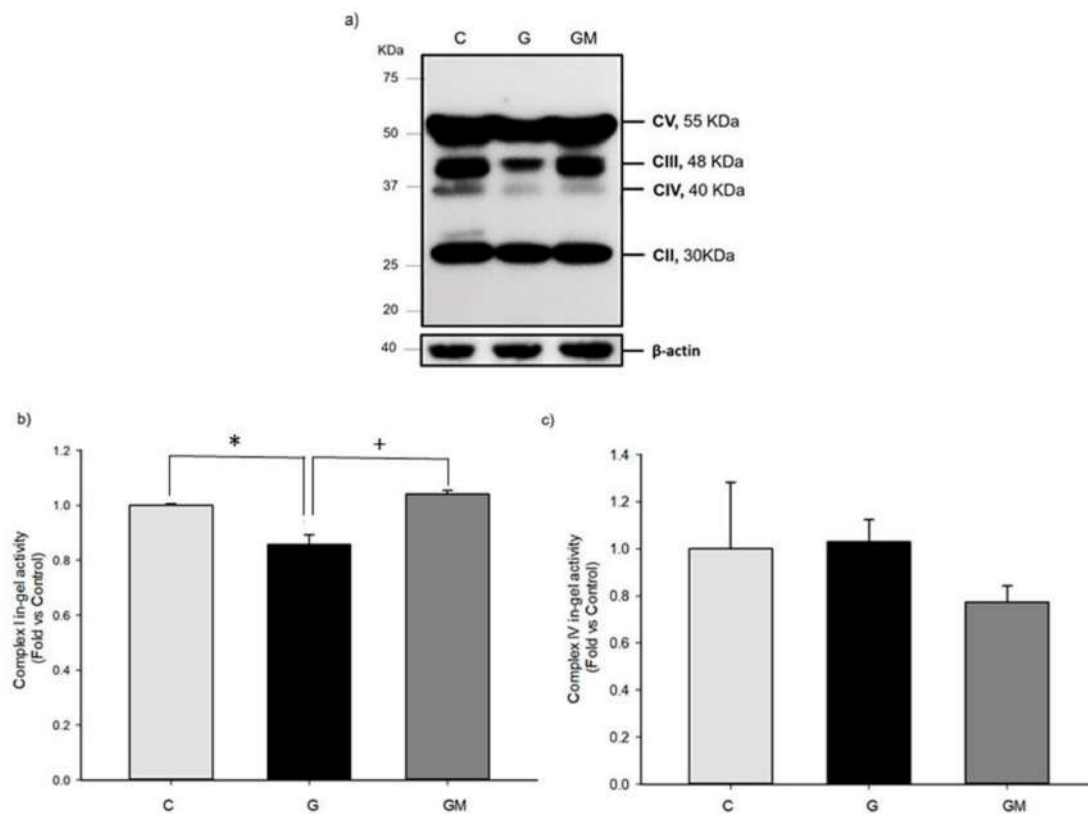


Figure 4. (a) Characterization of OXPHOS proteins expressed in HepG2 cells during high glucose with or without *M. oleifera* extract. OXPHOS cocktail specificity demonstrated by Western blot of MTC01 subunit of CIV, SDHB subunit of CII, UQCRC2 subunit of CIII, NDUFB8 subunit of CI, and ATP5A subunit of CV. BN-PAGE. Activity of CI (b) and CIV (c) in isolated mitochondria from HepG2 cells under normal (C), glucose 25 mM (G), and 500 $\mu\text{g}/\text{mL}$ *M. oleifera* extract (GM) conditions. * significant difference against control $p \leq 0.05$. + significant difference against G cells $p \leq 0.05$. Data normalized to control group using β -actin.

3.6. Mitochondrial Supercomplex Levels

Recent experimental evidence has replaced the random diffusion model of electron transfer with a model of supramolecular organization based upon specific interaction between individual respiratory complexes [48]. Supercomplexes (SC) is the term given to associations between different mitochondrial complexes [49]. Three of the electron-transfer complexes form SC and several functions have been attributed to SC in mitochondria, and although information regarding this matter is controversial, there are reports of SC modulating ROS formation and facilitate efficient energy generation [50,51].

Since we observed changes in protein levels from Complexes III and IV, which are important components of SC, we conducted experiments using BN-PAGE to assess the amount of SC in our model to establish if complex interaction is lost under hyperglycemic conditions. Same as in individual complexes, exposition to high glucose lowers the overall interaction between mitochondrial complexes. Again, the presence of *M. oleifera* extract reverted this effect (Figure 5) indicating that components in the extract are not only capable of preserving OXPHOS protein levels, but also preserving the interactions between them, ensuring a better mitochondrial metabolism.

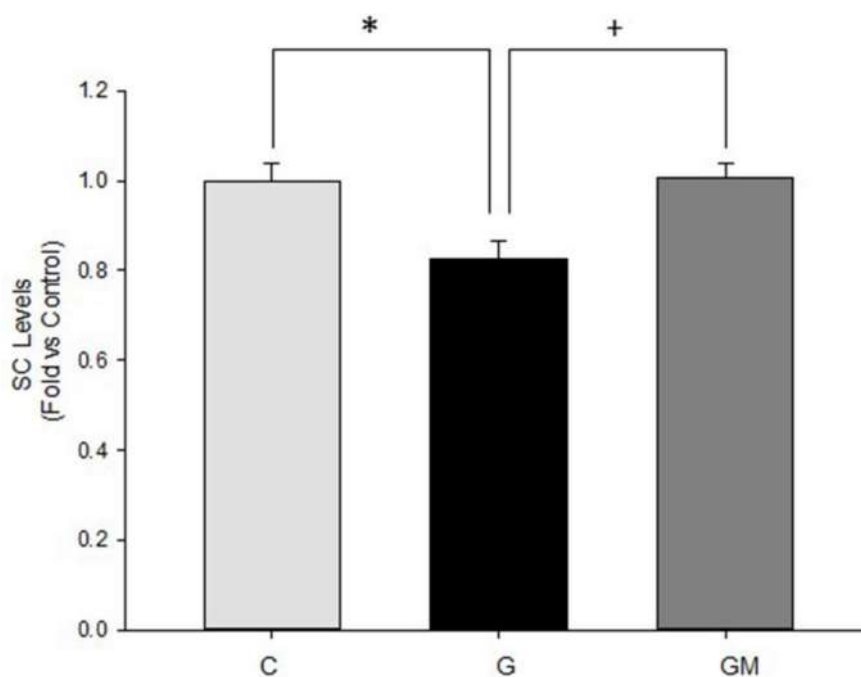


Figure 5. Interactions between mitochondrial complexes in HepG2 cells under normal (C), glucose 25 mM (G), and 500 µg/mL *M. oleifera* extract (GM) conditions. * significant difference against control $p \leq 0.05$. + significant difference against G cells $p \leq 0.05$.

3.7. Acetylation Levels by SIRT3

Protein post-translational modification is an important process for quickly and transiently modifying the structure of a protein by the covalent addition of functional groups, proteolytic cleavage of regulatory subunits, or degradation of entire proteins, which causes changes in enzyme activity as well as interfering or aiding protein-protein interactions. To date, no work has specifically analyzed the role of post-translational modification in SC assembly or function, but there is a large body of information on post-translational modification of individual respiratory complexes and other mitochondrial proteins [52].

Our results indicated that acetylation percentage is higher in those cells treated with high glucose, and after 2 h of exposure to *M. oleifera* extract, acetylation levels diminished significantly, even below control levels (Figure 6a). Our results regarding SIRT3, showed that there is no significant difference

among groups, however, levels in *M. oleifera* treated cells are slightly higher than those found in high glucose treated cells (Figure 6a), existing the possibility that lower acetylation levels in cells treated with the extract are due to higher amounts of SIRT3, and of course, other SIRTs. Our data is contrasting with previous findings where the content of SIRT3 was heavily decreased in diabetic pancreas and lung [53], possibly the alterations in SIRT3 in diabetes are likely tissue dependent [54]. Moreover, when total mitochondrial protein acetylation profile was assessed by anti-acetylation western blot analysis, an increased acetylation on numerous proteins could be detected in diabetes [55], which corresponds with our results (Figure 6b).

Although we were not able to identify the acetylated mitochondrial proteins, our results clearly show that the level of acetylation in the high glucose treated cells was increased by 40% with respect to the control group. In addition, the acetylation levels were decreased three times with respect to the group treated with high glucose plus *M. oleifera* (Figure 6b). It is difficult to determine which biochemical feature is affected by acetylation; enzyme activity, protein-protein interactions, protein-DNA interactions, stability, localization, allostery, and others.

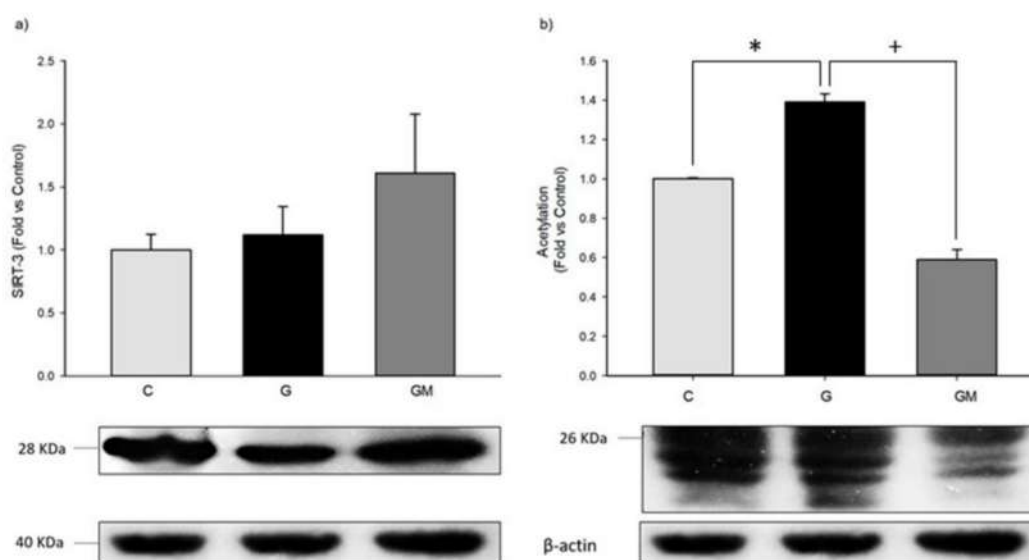


Figure 6. Sirt3 (a) and overall acetylation (b) protein levels in HepG2 cells under normal (C), 25 mM glucose (G) and 500 µg/mL *M. oleifera* extract (GM) conditions. * significant difference against control $p \leq 0.05$. + significant difference against G cells $p \leq 0.05$. Data normalized to control group using β -actin.

4. Discussion

There is significant evidence that energy production is impaired during diabetes; however, the molecular events involved are poorly understood. Many compounds isolated from *M. oleifera* have been reported to show antidiabetic and biological properties [56,57]. However, the molecular targets in which the phytochemicals of the *M. oleifera* extract act are unknown. In addition, a recent interest has been devoted to studying the effects on mitochondria of natural compounds as quercetin, resveratrol, and curcumin [58]. Many of these compounds turned out to exert their functions by affecting mitochondrial function, either directly, by inhibiting specific enzymes, or indirectly, by modulating signal from or to mitochondria [59–61].

Reports in C57BL/6 mice, showed that quercetin clearly reduced the expression levels of mitochondrial proteins that control mitochondrial dynamics. Interestingly, they found that quercetin reduced the activity only in monomeric Complex IV [62]. Our previous findings with liver isolated mitochondria of STZ-treated rats demonstrated changes in both amount and composition of SC [9],

which were replicated in HepG2 cells. Our results show that high glucose also reduced the levels of OXPHOS proteins subunits from respiratory complexes (Figure 4a). Specifically, UQCRC2 subunit of Complex III and MTC01 subunit of Complex IV were significantly reduced. While SDHB subunit of Complex II, and ATP5A subunit of Complex V were not decreased in high glucose treatment. Interestingly, we were not able to detect the representative band of the NDUF8 subunit of Complex I in either control cells or those treated with high glucose and/or *M. oleifera* extract. However, all groups present significant specific enzymatic activity of this complex. One possible explanation is that the antibody recognition region into the Complex I protein subunit is not available because this complex is always associated with other components of the respiratory chain. In addition, the inhibition of Complex I in high glucose treated cells would cause a decrease in energy supply that would in turn lead to a higher AMP/ATP ratio, and the concomitant activation of AMP-activated protein kinase, although an increase in UCP2 levels could also produce the same result [63]. These results support the idea of several groups who have proposed a stabilizing factor for respiratory supercomplex assembly, cytochrome c oxidase (COX) subunit 7a-related polypeptide (COX7RP) [64,65]. Recently, it has been shown that a metabolic phenotype of Cox7rp knockout mice exhibit lower blood glucose levels after insulin or pyruvate injection. Notably, ATP synthesis rate was reduced in Cox7rp knockout mice liver, in accordance with decreased percentages of Complex III subunit RISP and Complex COX1 involved in respirasome fraction [65]. This result suggests that COX7RP-mediated mitochondrial respiration plays crucial roles in the regulation of glucose homeostasis and its impairment will lead to the pathophysiology of metabolic states.

On the other hand, computational studies have shown that up to 20% of mitochondrial proteins can be acetylated on their lysine residues and are putatively regulated by SIRT3 [43]. Three NAD-dependent deacetylases; SIRT3–5; are localized to the mammalian mitochondria. SIRT3 has been implicated in regulating metabolism by deacetylating Complex I subunit NDUF9 and affect NADH-dependent respiration in mice, as well as α and OSCP subunits from F0F1ATPase and the SdhA subunit from Complex II, demonstrating the role of acetylation/deacetylation in the regulation of oxidative phosphorylation [17,18]. However, from the 700 acetylated mitochondrial proteins, only 26 proteins that display functional effects when acetylated [66]. Several acetylome proteomic studies have identified many lysine-acetylated mitochondrial proteins, including six tricarboxylic acid (TCA) cycle proteins, 26 proteins involved in oxidative phosphorylation, 27 β -oxidation, 8 associated with amino acid metabolism, 10 with carbohydrate metabolism, 3 with nucleotide metabolism, and 2 with the urea cycle [67,68]. With respect to mitochondrial dehydrogenases, 21 were lysine acetylated, among them, 9 subunits of NADH dehydrogenase (Complex I). In this study, Figure 6b shows also that mean value of acetylation of high-glucose treated cells was significantly (at $p < 0.05$) increased compared with control cells. Treating these high-glucose treated cells with *M. oleifera* extract significant (at $p < 0.05$) ameliorated with that high-glucose treated cells. In contrast, Figure 6a shows also that the mean value of SIRT3 was not significantly increased due to high glucose treated cells. Interestingly, treating these cells with *M. oleifera* extract no significantly reduced the SIRT3. These data suggest that other members of SIRT3 family may be participate into mitochondria as SIRT1 or 5. However, it is necessary more experimental evidence.

Increased oxidative stress has been hypothesized to activate uncoupling protein 2 (UCP2) which is a regulator of ROS production in the inner membrane of mitochondria. In addition, the liver is the largest metabolic organ in the human body, and mitochondrial proton leak accounts for 20–30% of the oxygen consumption of isolated resting hepatocytes [69]. In the liver, UCP2 has been localized to Kupffer cells, with very low or undetectable levels in hepatocytes. However, this expression pattern appears to be the opposite in fatty liver [70]. Accordingly, we found that the levels of UCP2 was increased in HG cells (Figure 3) and *M. oleifera* extract caused remarkable decrease in UCP2 expression, this last finding is probably due to a direct modulation of mitochondrial environment by components in the extract, where UCP2 is no longer needed in higher levels. This is supported by the fact that *M. oleifera* extract is also capable of restoring alterations in mitochondrial free fatty

acids accumulation, a known activator of UCP2 [71–74], and previous reports where UCP2 levels are regulated by quercetin [74], a component present in our extract [33]. These results suggest that HepG2 protection against high glucose injury is associated with the upregulation of UCP2. Thus, our results are in accordance with findings of non-alcoholic fatty liver disease (NAFLD) [75].

NAFLD is part of the metabolic syndrome with insulin resistance as a primary underlying derangement. Available evidence suggests that UCP2 may theoretically contribute to pathogenesis of NAFLD [76]. In addition, the expression of SIRT1 is significantly lowered and UCP2 increased in the liver of rats with diabetes and NAFLD. It was proposed that UCP2 regulates the activity of SIRT3 through sensing the energy levels and, in turn, maintaining the mitochondrial steady state, which demonstrates a cytoprotective effect on cerebral ischemia-reperfusion injury [77]. UCP2 induces mitochondrial proton leak and increases susceptibility of non-alcoholic steatohepatitis liver (NASH) to ischemia-reperfusion injury [78]. Moreover, cardiolipin a phospholipid located at inner mitochondrial membrane, plays an important role in several processes involved in mitochondrial bioenergetics and apoptosis. Cardiolipin peroxidation has been associated with the destabilization of mitochondrial respiratory supercomplexes could be another factor contributing to ROS generation and to mitochondrial bioenergetic decay in NAFLD [79].

On the other hand, metformin can increase the expression of SIRT1 and reduce the expression of UCP2, with negative correlation between the expression of SIRT1 and UCP2 [80]. Berberine can downregulate the expression level of UCP2 mRNA and UCP2 proteins of hepatic tissue from NAFLD rats [81]. Interestingly, dietary polyphenols have been identified to offer a potential therapy for NAFLD and its progression to nonalcoholic steatohepatitis [82]. Several polyphenols, such as kaempferol, have been reported to activate both SIRT1 and SIRT3 [83]. Polyphenols found in beverages, such as red wine and grape juice, could bear an effect on energy metabolism, being able to increase UCP2 expression, by increasing energy expenditure, even when administered in a high fat diet situation [84]. Thus, in line with our results, decreased expression of the mitochondrial biogenesis transcription factors PGC1 α and NRF1, and decreased expression of respiratory Complex I and V subunits NDUF58 and ATP5G1 in the HepG2 cell model of steatosis have been reported. The treatment with different polyphenols protected by more than 50% against the oleic acid induced increase in ROS and prevented the decrease of UCP2 [85].

Taken together, we proposed a model to explain our data. Under physiological conditions (Figure 7a), mitochondria play a key role in energy metabolism by generating most of the energy used by mammalian cells. The redox power from organic acids oxidation is provided to the respiratory chain by reduced donors (NADH + H⁺; FADH₂) or directly by specific dehydrogenases via electron-transfer complexes to the quinone pool before reducing final electron acceptor (molecular oxygen). Electron flow is conveyed along the mitochondrial respiratory chain and part of its energy is converted to an electrochemical force by pumping out protons across the inner mitochondrial membrane. This generates electrochemical gradient (also called the proton motive force, pmf) that can be used to synthesize ATP or exchange proteins or ions (Ca²⁺) across the inner mitochondrial membrane. The efficiency with which reduced equivalents are used to generate ATP by oxidative phosphorylation is dependent on mitochondrial coupling. Uncoupling the proton transport across the membrane participates in the regulation of energy homeostasis and defaults in electron transfer can enhance ROS production. Under conditions of excess in energy intake (high glucose) and tight mitochondrial coupling (Figure 7b), pmf can rise to a maximum. Thus, mitochondrial respiratory complexes are highly reduced and may release electrons directly to oxygen resulting in a higher ROS production that could alter oxidative phosphorylation system and lead to a drop of mitochondrial ATP levels. Thus, excessive ROS production would lead to induced uncoupling protein 2 (UCP2). UCP2 is thought to protect against oxidative stress although, alternatively, it could play an energy dissipation role. Consequently, in our study, the increase of UCP2 associated with the increase of proton leak (uncoupling state) may improve the mitochondrial NAD⁺/NADH ratio by suppressing the ATP synthesis and ROS production. SIRT3 is a key regulatory protein, which can sense the NAD⁺ levels. Therefore, it

might be possible that UCP2 increases the $NAD^+ / NADH$ ratio to activate SIRT6 in high glucose conditions. Furthermore, treatment of high glucose treated cells with *M. oleifera* extract (Figure 7c), increases the levels of acetylation and lowers the UCP2 protein. *M. oleifera* also increases the levels of supercomplexes to optimize the Complex I activity and coupling state. In accordance with these results, we also observed a recovery of the disturbed bioenergetics homeostasis (RCR, coupling efficiency and phosphorylating respiration). Finally, when energy stores are plentiful, Krebs cycle intermediates accumulate, and citrate is transported back into cytoplasm where is converted to acetyl-CoA, which is the first step of endogenous fatty acid synthesis and lipogenesis is a central abnormality in NAFLD (Figure 7 and [86]). However, this last metabolic alteration requires further investigation.

In conclusion, *M. oleifera* treatment significantly reduced acetylation of mitochondrial proteins and subsequent increase in amount of supercomplexes and Complex I activity, while it dramatically decreased UCP2 expression in high glucose treated HepG2 cells. *M. oleifera* could be a potential source of mitochondrial drugs for diabetes and NAFLD.

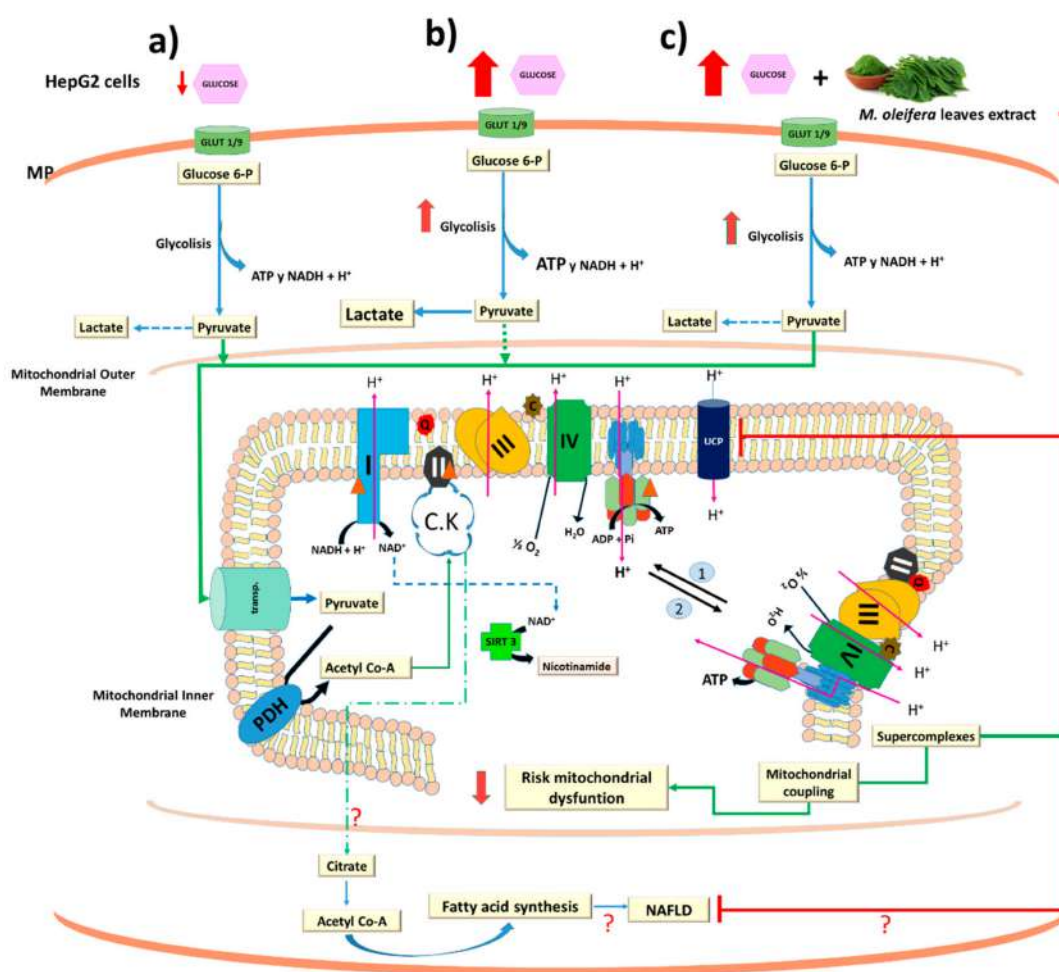


Figure 7. Proposed model for uncoupling protein 2-acetylation by sirtuins signaling pathway on HepG2 treated with high glucose and *M. oleifera* extract. The solid lines indicate carbon skeletal main flux to mitochondria (a). While that punted lines indicates the secondary pathways. PDH, pyruvate dehydrogenase; CK, Krebs cycle. The numbers 1 and 2 indicates the dissociation and association of the mitochondrial supercomplexes. Red and green lines indicate inhibition and activation of metabolic process by high glucose (b) and *M. oleifera* extract (c), respectively. Glut 1 and Glut 9 as major contributors to glucose influx in HepG2 cells [87]. MP, plasma membrane. Red triangle indicates potential site of acetylation in mitochondrial complexes.

Author Contributions: E.S.-C., M.A.V.-S., and M.B. contributed to conceptualization, literature review, and writing the original draft. J.A.S.-G. and T.Y.F.-H. conducted the cells studies and performed the experiments. G.G.G.-V., J.M.S.-P., O.F.-H., C.I.A.-D., M.B., and E.S.-C. contributed reagents/material/analysis tools. A.T.-V., J.A.S.-G., and E.S.-C. wrote the manuscript. All authors read and approved the final paper.

Funding: A.T.-V and C.A.-D. acknowledge Consejo Nacional de Ciencia y Tecnología (CONACyT) for grants No. 257848 and No. 258694, respectively.

Acknowledgments: We thank María Alejandra Sánchez-Muñoz and Jesús Ricardo Pérez-Velazquez for brilliant technical assistance. J.A.S.-G. is grateful to CONACyT, México for the financial support for his PhD studies, grant 598404. We also thank Francesca Giampieri and Massimiliano Gasparrini for helpful and insightful comments for this work. The authors are also grateful to the Mexican *Moringa oleifera* producers (Akuanandi) for providing all vegetal material for this study.

Conflicts of Interest: The authors declare no conflict of interest.

References

1. Abd Eldaim, M.A.; Shaban Abd Elrasoul, A.; Abd Elaziz, S.A. An aqueous extract from *Moringa oleifera* leaves ameliorates hepatotoxicity in alloxan-induced diabetic rats. *Biochem. Cell Biol.* **2017**, *95*, 524–530. [[CrossRef](#)] [[PubMed](#)]
2. Aa, A.B.; Om, J.; Ts, E.; Ga, A. Preliminary phytochemical screening, antioxidant and antihyperglycaemic activity of *Moringa oleifera* leaf extracts. *Pak. J. Pharm. Sci.* **2017**, *30*, 2217–2222. [[PubMed](#)]
3. Vergara Jimenez, M.; Almatrafi, M.M.; Fernandez, M.L. Bioactive Components in *Moringa Oleifera* Leaves Protect against Chronic Disease. *Antioxidants* **2017**, *6*, 91. [[CrossRef](#)] [[PubMed](#)]
4. Makkar, H.P.S.; Becker, K. Nutritional value and antinutritional components of whole and ethanol extracted *Moringa oleifera* leaves. *Anim. Feed Sci. Technol.* **1996**, *63*, 211–228. [[CrossRef](#)]
5. Tabbon, P.; Sripanidkulchai, B.; Sripanidkulchai, K. Hypocholesterolemic mechanism of phenolics-enriched extract from *Moringa oleifera* leaves in HepG2 cell lines. *Songklanakarin J. Sci. Technol.* **2016**, *38*, 155–161.
6. Barbagallo, I.; Vanella, L.; Cambria, M.T.; Tibullo, D.; Godos, J.; Guarnaccia, L.; Li Volti, G. Silibinin Regulates Lipid Metabolism and Differentiation in Functional Human Adipocytes. *Front. Pharmacol.* **2015**, *6*, 309. [[CrossRef](#)] [[PubMed](#)]
7. Brownlee, M. Biochemistry and molecular cell biology of diabetic complications. *Nature* **2001**, *414*, 813–820. [[CrossRef](#)] [[PubMed](#)]
8. Cheng, J.; Nanayakkara, G.; Shao, Y.; Cueto, R.; Wang, L.; Yang, W.Y.; Yang, X. Mitochondrial Proton Leak Plays a Critical Role in Pathogenesis of Cardiovascular Diseases. *Adv. Exp. Med. Biol.* **2017**, *982*, 359–370. [[PubMed](#)]
9. Sánchez Muñoz, A.; Valdez Solana, M.A.; Campos Almazán, M.I.; Flores Herrera, Ó.; Esparza Perusquía, M.; Olvera Sánchez, S.; Sierra Campos, E. Streptozotocin-Induced Adaptive Modification of Mitochondrial Supercomplexes in Liver of Wistar Rats and the Protective Effect of *Moringa oleifera* Lam. *Biochem. Res. Int.* **2018**, *2018*, 5681081. [[CrossRef](#)]
10. D’Onofrio, N.; Vitiello, M.; Casale, R.; Servillo, L.; Giovane, A.; Balestrieri, M.L. Sirtuins in vascular diseases: Emerging roles and therapeutic potential. *Biochim. Biophys. Acta* **2008**, *1852*, 1311–1322. [[CrossRef](#)] [[PubMed](#)]
11. Carrico, C.; Meyer, J.G.; He, W.; Gibson, B.W.; Verdin, E. The Mitochondrial Acylome Emerges: Proteomics, Regulation by Sirtuins, and Metabolic and Disease Implications. *Cell Metab.* **2018**, *27*, 497–512. [[CrossRef](#)] [[PubMed](#)]
12. Singh, C.K.; Chhabra, G.; Ndiaye, M.A.; Garcia-Peterson, L.M.; Mack, N.J.; Ahmad, N. The Role of Sirtuins in Antioxidant and Redox Signaling. *Antioxid. Redox Signal.* **2018**, *28*, 643–661. [[CrossRef](#)] [[PubMed](#)]
13. Weinberg, J.M. Mitochondrial biogenesis in kidney disease. *J. Am. Soc. Nephrol.* **2011**, *22*, 431–436. [[CrossRef](#)] [[PubMed](#)]
14. Wu, Z.; Puigserver, P.; Andersson, U.; Zhang, C.; Adelmant, G.; Mootha, V.; Spiegelman, B.M. Mechanisms Controlling Mitochondrial Biogenesis and Respiration through the Thermogenic Coactivator PGC-1. *Cell* **1999**, *98*, 115–124. [[CrossRef](#)]
15. Jing, E.; Emanuelli, B.; Hirschey, M.D.; Boucher, J.; Lee, K.Y.; Lombard, D.; Kahn, C.R. Sirtuin-3 (Sirt3) regulates skeletal muscle metabolism and insulin signaling via altered mitochondrial oxidation and reactive oxygen species production. *Proc. Natl. Acad. Sci. USA* **2011**, *108*, 14608–14613. [[CrossRef](#)] [[PubMed](#)]

16. Hirschey, M.D.; Shimazu, T.; Jing, E.; Grueter, C.A.; Collins, A.M.; Aouizerat, B.; Verdin, E. SIRT3 Deficiency and Mitochondrial Protein Hyperacetylation Accelerate the Development of the Metabolic Syndrome. *Mol. Cell* **2011**, *44*, 177–190. [[CrossRef](#)] [[PubMed](#)]
17. Ahn, B.-H.; Kim, H.-S.; Song, S.; Lee, I.H.; Liu, J.; Vassilopoulos, A.; Finkel, T. A role for the mitochondrial deacetylase Sirt3 in regulating energy homeostasis. *Proc. Natl. Acad. Sci. USA* **2008**, *105*, 14447–14452. [[CrossRef](#)] [[PubMed](#)]
18. Yang, Y.; Cimen, H.; Han, M.-J.; Shi, T.; Deng, J.-H.; Koc, H.; Koc, E.C. NAD⁺-dependent deacetylase SIRT3 regulates mitochondrial protein synthesis by deacetylation of the ribosomal protein MRPL10. *J. Biol. Chem.* **2010**, *285*, 7417–7429. [[CrossRef](#)] [[PubMed](#)]
19. Satoh, A.; Stein, L.; Imai, S. The role of mammalian sirtuins in the regulation of metabolism, aging, and longevity. *Handb. Exp. Pharmacol.* **2011**, *206*, 125–162. [[PubMed](#)]
20. Leibiger, I.B.; Berggren, P.-O. Sirt1: A metabolic master switch that modulates lifespan. *Nat. Med.* **2006**, *12*, 34–36. [[CrossRef](#)] [[PubMed](#)]
21. Milne, J.C.; Lambert, P.D.; Schenk, S.; Carney, D.P.; Smith, J.J.; Gagne, D.J.; Westphal, C.H. Small molecule activators of SIRT1 as therapeutics for the treatment of type 2 diabetes. *Nature* **2007**, *450*, 712–716. [[CrossRef](#)] [[PubMed](#)]
22. Pacholec, M.; Bleasdale, J.E.; Chrunchy, B.; Cunningham, D.; Flynn, D.; Garofalo, R.S.; Ahn, K. SIRT1720, SIRT2183, SIRT1460, and resveratrol are not direct activators of SIRT1. *J. Biol. Chem.* **2010**, *285*, 8340–8351. [[CrossRef](#)] [[PubMed](#)]
23. Liu, J.; Li, J.; Li, W.J.; Wang, C.M. The role of uncoupling proteins in diabetes mellitus. *J. Diabetes Res.* **2013**, 585897. [[CrossRef](#)] [[PubMed](#)]
24. Howitz, K.T.; Bitterman, K.J.; Cohen, H.Y.; Lamming, D.W.; Lavu, S.; Wood, J.G.; Sinclair, D.A. Small molecule activators of sirtuins extend *Saccharomyces cerevisiae* lifespan. *Nature* **2003**, *425*, 191–196. [[CrossRef](#)] [[PubMed](#)]
25. Purushotham, A.; Schug, T.T.; Xu, Q.; Surapureddi, S.; Guo, X.; Li, X. Hepatocyte-Specific Deletion of SIRT1 Alters Fatty Acid Metabolism and Results in Hepatic Steatosis and Inflammation. *Cell Metab.* **2009**, *9*, 327–338. [[CrossRef](#)] [[PubMed](#)]
26. Kim, H.Y.; Kim, K. Regulation of signaling molecules associated with insulin action, insulin secretion and pancreatic β -cell mass in the hypoglycemic effects of Korean red ginseng in Goto-Kakizaki rats. *J. Ethnopharmacol.* **2012**, *142*, 53–58. [[CrossRef](#)] [[PubMed](#)]
27. Pereira Caro, G.; Sarriá, B.; Madrona, A.; Espartero, J.L.; Goya, L.; Bravo, L.; Mateos, R. Alkyl Hydroxytyrosyl Ethers Show Protective Effects against Oxidative Stress in HepG2 Cells. *J. Agric. Food Chem.* **2011**, *59*, 5964–5976. [[CrossRef](#)] [[PubMed](#)]
28. Martín, M.A.; Ramos, S.; Granado Serrano, A.B.; Rodríguez Ramiro, I.; Trujillo, M.; Bravo, L.; Goya, L. Hydroxytyrosol induces antioxidant/detoxicant enzymes and Nrf2 translocation via extracellular regulated kinases and phosphatidylinositol-3-kinase/protein kinase B pathways in HepG2 cells. *Mol. Nutr. Food Res.* **2010**, *54*, 956–966. [[CrossRef](#)] [[PubMed](#)]
29. Kim, Y.; Choi, Y.; Ham, H.; Jeong, H.S.; Lee, J. Protective effects of oligomeric and polymeric procyanidin fractions from defatted grape seeds on tert-butyl hydroperoxide-induced oxidative damage in HepG2 cells. *Food Chem.* **2013**, *137*, 136–141. [[CrossRef](#)] [[PubMed](#)]
30. Khetani, S.R.; Berger, D.R.; Ballinger, K.R.; Davidson, M.D.; Lin, C.; Ware, B.R. Microengineered liver tissues for drug testing. *J. Lab. Autom.* **2015**, *20*, 216–250. [[CrossRef](#)] [[PubMed](#)]
31. Mordel, P.; Nowoczyn, M.; Joubert, M.; Coulbault, L.; Allouche, S. Effects of glucose fluctuations on cellular and mitochondrial functions in HL-1 cardiac cell line. *Diabetes Metab.* **2016**, *42*, 295. [[CrossRef](#)]
32. Hou, Y.; Zhou, M.; Xie, J.; Chao, P.; Feng, Q.; Wu, J. High glucose levels promote the proliferation of breast cancer cells through GTPases. *Breast Cancer Targets Ther.* **2017**, *9*, 429–436. [[CrossRef](#)] [[PubMed](#)]
33. Valdez Solana, M.A.; Mejía García, V.Y.; Téllez Valencia, A.; García Arenas, G.; Salas Pacheco, J.; Alba Romero, J.J.; Sierra Campos, E. Nutritional Content and Elemental and Phytochemical Analyses of *Moringa oleifera* Grown in Mexico. *J. Chem.* **2015**, *2015*, 860381. [[CrossRef](#)]
34. Dranka, B.P.; Hill, B.G.; Darley-Usmar, V.M. Mitochondrial reserve capacity in endothelial cells: The impact of nitric oxide and reactive oxygen species. *Free Radic. Biol. Med.* **2010**, *48*, 905–914. [[CrossRef](#)] [[PubMed](#)]
35. Brand, M.D.; Nicholls, D.G. Assessing mitochondrial dysfunction in cells. *Biochem. J.* **2011**, *435*, 297–312. [[CrossRef](#)] [[PubMed](#)]

36. Domenis, R.; Bisetto, E.; Rossi, D.; Comelli, M.; Mavelli, I. Glucose-Modulated Mitochondria Adaptation in Tumor Cells: A Focus on ATP Synthase and Inhibitor Factor 1. *Int. J. Mol. Sci.* **2012**, *13*, 1933–1950. [[CrossRef](#)] [[PubMed](#)]
37. Wittig, I.; Carozzo, R.; Santorelli, F.M.; Schägger, H. Functional assays in high-resolution clear native gels to quantify mitochondrial complexes in human biopsies and cell lines. *Electrophoresis* **2007**, *28*, 3811–3820. [[CrossRef](#)] [[PubMed](#)]
38. Jung, C.; Higgins, C.M.J.; Xu, Z. Measuring the Quantity and Activity of Mitochondrial Electron Transport Chain Complexes in Tissues of Central Nervous System Using Blue Native Polyacrylamide Gel Electrophoresis. *Anal. Biochem.* **2000**, *286*, 214–223. [[CrossRef](#)] [[PubMed](#)]
39. Kamalian, L.; Chadwick, A.E.; Bayliss, M.; French, N.S.; Monshouwer, M.; Snoeys, J.; Park, B.K. The utility of HepG2 cells to identify direct mitochondrial dysfunction in the absence of cell death. *Toxicol. In Vitro* **2015**, *29*, 732–740. [[CrossRef](#)] [[PubMed](#)]
40. Chandrasekaran, K.; Swaminathan, K.; Chatterjee, S.; Dey, A. Apoptosis in HepG2 cells exposed to high glucose. *Toxicol. In Vitro* **2010**, *24*, 387–396. [[CrossRef](#)] [[PubMed](#)]
41. Abd-Rabou, A.A.; Zoheir, K.M.A.; Kishta, M.S.; Shalby, A.B.; Ezzo, M.I. Nano-Micelle of *Moringa oleifera* Seed Oil Triggers Mitochondrial Cancer Cell Apoptosis. *West Asia Organ. Cancer Prev. (WAOCP)* **2016**, *17*, 4929–4933.
42. Madi, N.; Dany, M.; Abdoun, S.; Usta, J. *Moringa oleifera*'s Nutritious Aqueous Leaf Extract Has Anticancerous Effects by Compromising Mitochondrial Viability in an ROS-Dependent Manner. *J. Am. Coll. Nutr.* **2016**, *35*, 604–613. [[CrossRef](#)] [[PubMed](#)]
43. Kim, G.J.; Chandrasekaran, K.; Morgan, W.F. Mitochondrial dysfunction, persistently elevated levels of reactive oxygen species and radiation-induced genomic instability: A review. *Mutagenesis* **2006**, *21*, 361–367. [[CrossRef](#)] [[PubMed](#)]
44. Busik, J.V.; Mohr, S.; Grant, M.B. Hyperglycemia-induced reactive oxygen species toxicity to endothelial cells is dependent on paracrine mediators. *Diabetes* **2008**, *57*, 1952–1965. [[CrossRef](#)] [[PubMed](#)]
45. Turko, I.V.; Murad, F. Quantitative protein profiling in heart mitochondria from diabetic rats. *J. Biol. Chem.* **2003**, *278*, 35844–35849. [[CrossRef](#)] [[PubMed](#)]
46. Hwang, H.; Bowen, B.P.; Lefort, N.; Flynn, C.R.; De Filippis, E.A.; Roberts, C.; Mandarino, L.J. Proteomics Analysis of Human Skeletal Muscle Reveals Novel Abnormalities in Obesity and Type 2 Diabetes. *Diabetes* **2010**, *59*, 33–42. [[CrossRef](#)] [[PubMed](#)]
47. Sparks, L.M.; Xie, H.; Koza, R.A.; Mynatt, R.; Hulver, M.W.; Bray, G.A.; Smith, S.R. A high-fat diet coordinately downregulates genes required for mitochondrial oxidative phosphorylation in skeletal muscle. *Diabetes* **2005**, *54*, 1926–1933. [[CrossRef](#)] [[PubMed](#)]
48. Genova, M.L.; Lenaz, G. Functional role of mitochondrial respiratory supercomplexes. *Biochim. Biophys. Acta (BBA)—Bioenerg.* **2014**, *1837*, 427–443. [[CrossRef](#)] [[PubMed](#)]
49. Letts, J.A.; Fiedorczuk, K.; Sazanov, L.A. The architecture of respiratory supercomplexes. *Nature* **2016**, *537*, 644–648. [[CrossRef](#)] [[PubMed](#)]
50. Lopez-Fabuel, I.; Le Douce, J.; Logan, A.; James, A.M.; Bonvento, G.; Murphy, M.P.; Almeida, A.; Bolaños, J.P. Complex I assembly into supercomplexes determines differential mitochondrial ROS production in neurons and astrocytes. *Proc. Natl. Acad. Sci. USA* **2016**, *113*, 13063–13068. [[CrossRef](#)] [[PubMed](#)]
51. Wittig, I.; Karas, M.; Schägger, H. High Resolution Clear Native Electrophoresis for In-gel Functional Assays and Fluorescence Studies of Membrane Protein Complexes. *Mol. Cell. Proteom.* **2007**, *6*, 1215–1225. [[CrossRef](#)] [[PubMed](#)]
52. Porras, C.A.-M.; Bai, Y. Respiratory supercomplexes: Plasticity and implications. *Front. Biosci.* **2015**, *20*, 621.
53. Wu, J.; Jin, Z.; Yan, L.J. Redox imbalance and mitochondrial abnormalities in the diabetic lung. *Redox Biol.* **2017**, *11*, 51–59. [[CrossRef](#)] [[PubMed](#)]
54. Michan, S.; Sinclair, D. Sirtuins in mammals: Insights into their biological function. *Biochem. J.* **2007**, *404*, 1–13. [[CrossRef](#)] [[PubMed](#)]
55. Wu, J.; Luo, X.; Thangthaeng, N.; Sumien, N.; Chen, Z.; Rutledge, M.A.; Yan, L.J. Pancreatic mitochondrial complex I exhibits aberrant hyperactivity in diabetes. *Biochem. Biophys. Rep.* **2017**, *11*, 119–129. [[CrossRef](#)] [[PubMed](#)]
56. Saini, R.K.; Sivanesan, I.; Keum, Y.S. Phytochemicals of *Moringa oleifera*: A review of their nutritional, therapeutic and industrial significance. *3 Biotech* **2016**, *6*, 203. [[CrossRef](#)] [[PubMed](#)]

57. Al-Malki, A.L.; El Rabey, H.A. The antidiabetic effect of low doses of *Moringa oleifera* Lam. seeds on streptozotocin induced diabetes and diabetic nephropathy in male rats. *BioMed Res. Int.* **2015**, *2015*, 381040. [[CrossRef](#)] [[PubMed](#)]
58. Gibellini, L.; Bianchini, E.; De Biasi, S.; Nasi, M.; Cossarizza, A.; Pinti, M. Natural compounds modulating mitochondrial functions. *Evid.-Based Complement. Altern. Med.* **2015**, *2015*, 527209. [[CrossRef](#)] [[PubMed](#)]
59. Fiorani, M.; Guidarelli, A.; Blasa, M.; Azzolini, C.; Candiracci, M.; Piatti, E.; Cantoni, O. Mitochondria accumulate large amounts of quercetin: Prevention of mitochondrial damage and release upon oxidation of the extramitochondrial fraction of the flavonoid. *J. Nutr. Biochem.* **2010**, *21*, 397–404. [[CrossRef](#)] [[PubMed](#)]
60. Lagouge, M.; Argmann, C.; Gerhart-Hines, Z.; Meziane, H.; Lerin, C.; Daussin, F.; Geny, B. Resveratrol improves mitochondrial function and protects against metabolic disease by activating SIRT1 and PGC-1 α . *Cell* **2006**, *127*, 1109–1122. [[CrossRef](#)] [[PubMed](#)]
61. Lim, H.W.; Lim, H.Y.; Wong, K.P. Uncoupling of oxidative phosphorylation by curcumin: Implication of its cellular mechanism of action. *Biochem. Biophys. Res. Commun.* **2009**, *389*, 187–192. [[CrossRef](#)] [[PubMed](#)]
62. Ruiz, L.M.; Salazar, C.; Jensen, E.; Ruiz, P.A.; Tiznado, W.; Quintanilla, R.A.; Elorza, A.A. Quercetin Affects Erythropoiesis and Heart Mitochondrial Function in Mice. *Oxid. Med. Cell. Longev.* **2015**, *2015*, 836301. [[CrossRef](#)] [[PubMed](#)]
63. Anedda, A.; Rial, E.; Gonzalez Barroso, M.M. Metformin induces oxidative stress in white adipocytes and raises uncoupling protein 2 levels. *J. Endocrinol.* **2008**, *199*, 33–40. [[CrossRef](#)] [[PubMed](#)]
64. Lapuente Brun, E.; Moreno Loshuertos, R.; Acin Perez, R.; Latorre Pellicer, A.; Colas, C.; Balsa, E.; Enriquez, J.A. Supercomplex Assembly Determines Electron Flux in the Mitochondrial Electron Transport Chain. *Science* **2013**, *340*, 1567–1570. [[CrossRef](#)] [[PubMed](#)]
65. Shiba, S.; Ikeda, K.; Horie-Inoue, K.; Nakayama, A.; Tanaka, T.; Inoue, S. Deficiency of COX7RP, a mitochondrial supercomplex assembly promoting factor, lowers blood glucose level in mice. *Sci. Rep.* **2017**, *7*, 7606. [[CrossRef](#)] [[PubMed](#)]
66. Baeza, J.; Smallegan, M.J.; Denu, J.M. Mechanisms and Dynamics of Protein Acetylation in Mitochondria. *Trends Biochem. Sci.* **2016**, *41*, 231–244. [[CrossRef](#)] [[PubMed](#)]
67. Kim, S.C.; Sprung, R.; Chen, Y.; Xu, Y.; Ball, H.; Pei, J.; Zhao, Y. Substrate and Functional Diversity of Lysine Acetylation Revealed by a Proteomics Survey. *Mol. Cell* **2006**, *23*, 607–618. [[CrossRef](#)] [[PubMed](#)]
68. Zhao, S.; Xu, W.; Jiang, W.; Yu, W.; Lin, Y.; Zhang, T.; Guan, K.-L. Regulation of Cellular Metabolism by Protein Lysine Acetylation. *Science* **2010**, *327*, 1000–1004. [[CrossRef](#)] [[PubMed](#)]
69. Brand, M.D. The proton leak across the mitochondrial inner membrane. *Biochim. Biophys. Acta (BBA)-Bioenerg.* **1990**, *1018*, 128–133. [[CrossRef](#)]
70. Larrouy, D.; Laharrague, P.; Carrera, G.; Viguerie-Bascands, N.; Levi-Meyrueis, C.; Fleury, C.; Ricquier, D. Kupffer cells are a dominant site of uncoupling protein 2 expression in rat liver. *Biochem. Biophys. Res. Commun.* **1997**, *235*, 760–764. [[CrossRef](#)] [[PubMed](#)]
71. Toda, C.; Diano, S. Mitochondrial UCP2 in the central regulation of metabolism. *Best Pract. Res. Clin. Endocrinol. Metab.* **2014**, *28*, 757–764. [[CrossRef](#)] [[PubMed](#)]
72. Basu Ball, W.; Kar, S.; Mukherjee, M.; Chande, A.G.; Mukhopadhyaya, R.; Das, P.K. Uncoupling Protein 2 Negatively Regulates Mitochondrial Reactive Oxygen Species Generation and Induces Phosphatase-Mediated Anti-Inflammatory Response in Experimental Visceral Leishmaniasis. *J. Immunol.* **2011**, *187*, 1322–1332. [[CrossRef](#)] [[PubMed](#)]
73. Ruiz Ramirez, A.; Chavez Salgado, M.; Peneda Flores, J.A.; Zapata, E.; Masso, F.; El-Hafidi, M. High-sucrose diet increases ROS generation, FFA accumulation, UCP2 level, and proton leak in liver mitochondria. *Endocrinol. Metab.* **2011**, *301*, E1198–E1207. [[CrossRef](#)] [[PubMed](#)]
74. Castrejón Tellez, V.; Rodríguez Pérez, J.; Pérez Torres, I.; Pérez Hernández, N.; Cruz Lagunas, A.; Guarner Lans, V.; Rubio Ruiz, M. The Effect of Resveratrol and Quercetin Treatment on PPAR Mediated Uncoupling Protein (UCP-) 1, 2, and 3 Expression in Visceral White Adipose Tissue from Metabolic Syndrome Rats. *Int. J. Mol. Sci.* **2016**, *17*, 1069. [[CrossRef](#)] [[PubMed](#)]
75. Bhatt, H.B.; Smith, R.J. Fatty liver disease in diabetes mellitus. *Hepatobiliary Surg. Nutr.* **2015**, *4*, 101–108. [[PubMed](#)]
76. Baffy, G. Uncoupling protein-2 and non-alcoholic fatty liver disease. *Front. Biosci. J. Virtual Libr.* **2005**, *10*, 2082–2096. [[CrossRef](#)]

77. Su, J.; Liu, J.; Yan, X.Y.; Zhang, Y.; Zhang, J.J.; Zhang, L.C.; Sun, L.K. Cytoprotective Effect of the UCP2-SIRT3 Signaling Pathway by Decreasing Mitochondrial Oxidative Stress on Cerebral Ischemia–Reperfusion Injury. *Int. J. Mol. Sci.* **2017**, *18*, 1599. [[CrossRef](#)]
78. Serviddio, G.; Bellanti, F.; Tamborra, R.; Rollo, T.; Capitanio, N.; Romano, A.D.; Altomare, E. Uncoupling protein-2 (UCP2) induces mitochondrial proton leak and increases susceptibility of non-alcoholic steatohepatitis (NASH) liver to ischaemia-reperfusion injury. *Gut* **2008**, *57*, 957–965. [[CrossRef](#)] [[PubMed](#)]
79. Paradies, G.; Paradies, V.; Ruggiero, F.M.; Petrosillo, G. Oxidative stress, cardioprotein and mitochondrial dysfunction in nonalcoholic fatty liver disease. *World J. Gastroenterol.* **2014**, *20*, 14205–14218. [[CrossRef](#)] [[PubMed](#)]
80. Xu, J.; Li, N.; Wang, J.; Zhang, C.; Ding, S.; Jiao, Y.; Zhang, J. Effect of metformin on the expression of SIRT1 and UCP2 in rat liver of type 2 diabetes mellitus and nonalcoholic fatty liver. *J. Cent. South Univ. Med. Sci.* **2013**, *38*, 882–887.
81. Yang, Q.; Hu, S.; Zhang, Y.; Xie, W.; Li, N.; Ji, G.; Liu, H. Effect of berberine on expressions of uncoupling protein-2 mRNA and protein in hepatic tissue of non-alcoholic fatty liver disease in rats. *Chin. J. Integr. Med.* **2011**, *17*, 205–211. [[CrossRef](#)] [[PubMed](#)]
82. Rodriguez Ramiro, I.; Vauzour, D.; Minihane, A.M. Polyphenols and non-alcoholic fatty liver disease: Impact and mechanisms. *Proc. Nutr. Soc.* **2016**, *75*, 47–60. [[CrossRef](#)] [[PubMed](#)]
83. Guo, Z.; Liao, Z.; Huang, L.; Liu, D.; Yin, D.; He, M. Kaempferol protects cardiomyocytes against anoxia/reoxygenation injury via mitochondrial pathway mediated by SIRT1. *Eur. J. Pharmacol.* **2015**, *761*, 245–253. [[CrossRef](#)] [[PubMed](#)]
84. González-Castejón, M.; Rodríguez-Casado, A. Dietary phytochemicals and their potential effects on obesity: A review. *Pharmacol. Res.* **2011**, *64*, 438–455. [[CrossRef](#)] [[PubMed](#)]
85. Rafiei, H.; Omidian, K.; Bandy, B. Comparison of dietary polyphenols for protection against molecular mechanisms underlying nonalcoholic fatty liver disease in a cell model of steatosis. *Mol. Nutr. Food Res.* **2017**, *61*, 1600781. [[CrossRef](#)] [[PubMed](#)]
86. Softic, S.; Cohen, D.E.; Kahn, C.R. Role of dietary fructose and hepatic *de novo* lipogenesis in fatty liver disease. *Dig. Dis. Sci.* **2016**, *61*, 1282–1293. [[CrossRef](#)] [[PubMed](#)]
87. Takanaga, H.; Chaudhuri, B.; Frommer, W.B. GLUT1 and GLUT9 as major contributors to glucose influx in HepG2 cells identified by a high sensitivity intramolecular FRET glucose sensor. *Biochim. Biophys. Acta (BBA)-Biomembr.* **2008**, *1778*, 1091–1099. [[CrossRef](#)] [[PubMed](#)]



© 2018 by the authors. Licensee MDPI, Basel, Switzerland. This article is an open access article distributed under the terms and conditions of the Creative Commons Attribution (CC BY) license (<http://creativecommons.org/licenses/by/4.0/>).



Contents lists available at ScienceDirect

Bioorganic & Medicinal Chemistry Letters

journal homepage: www.elsevier.com/locate/bmcl

Synthesis and trypanocidal activity of novel benzimidazole derivatives



José Miguel Velázquez-López^a, Alicia Hernández-Campos^a, Lilián Yépez-Mulia^b, Alfredo Téllez-Valencia^c, Paulina Flores-Carrillo^a, Rocío Nieto-Meneses^d, Rafael Castillo^{a,*}

^a Facultad de Química, Departamento de Farmacia, Universidad Nacional Autónoma de México, México, DF 04510, Mexico

^b Unidad de Investigación Médica en Enfermedades Infecciosas y Parasitarias, IMSS, México, DF 06720, Mexico

^c Facultad de Medicina y Nutrición, Centro de Investigación en Alimentos y Nutrición, Universidad Juárez del Estado de Durango, Durango 34000, Mexico

^d Escuela Nacional de Ciencias Biológicas, Departamento de Parasitología, IPN, México, DF 11340, Mexico

ARTICLE INFO

Article history:

Received 25 June 2015

Revised 30 July 2015

Accepted 6 August 2015

Available online 8 August 2015

Keywords:

Benzimidazole derivatives

Chagas disease

Trypanosoma cruzi

Triosephosphate isomerase

ABSTRACT

The present work reports the synthesis and biological activity of a series of 14 benzimidazole derivatives designed to act on the enzyme triosephosphate isomerase of *Trypanosoma cruzi* (TcTIM). This enzyme is involved in the metabolism of glucose, the only source of energy for the parasite. In this study, we found four compounds that inhibit TcTIM moderately and lack inhibitory activity against human TIM (HsTIM). In vitro studies against *T. cruzi* epimastigotes showed two compounds that were more active than the reference drug nifurtimox, and these presented a low cytotoxic effect in mouse macrophages (J744 cell line).

© 2015 Elsevier Ltd. All rights reserved.

Chagas disease (CD), also called American trypanosomiasis, is caused by the protozoan parasite *Trypanosoma cruzi*. CD is a life threatening illness considered a Neglected Tropical Disease (NTD) by the World Health Organization (WHO).¹ The parasite is transmitted to humans through the infected feces of a blood-sucking triatomine bug, which breaks through skin or mucous membranes during the insect's bite. CD is also transmitted by the ingestion of contaminated food, infected blood transfusions, congenital transmission, or organ transplantation.² Actually, CD causes more deaths in Latin America than any other parasitic infection, affecting approximately eight million people, of whom 30–40% have or will develop cardiomyopathy, digestive megasyndromes, or both.^{3,4} In spite of this problem, no immediate prospects for vaccines have been developed. Drug therapy is the only method currently available for the treatment of Chagas disease.⁵ In this sense, only nifurtimox (NFX) and benznidazole (BZ) are widely used as treatment. However, neither of these drugs are ideal due to their side effects and variable efficacy; depending on the phase of the disease, they are only effective in the acute and early chronic phases of the infection.⁶ At the chronic phases, more than 80% of the treated patients with these drugs do not get parasitological cure. Thus, it is crucial

to continue the search for new and better drugs to treat Chagas disease chemotherapy.^{7,8}

Recently, there has been considerable interest in the inhibition of the parasite's only energy supply: the glycolytic pathway, in which triosephosphate isomerase (TIM) plays a crucial role.^{9,10} This homodimeric enzyme catalyzes the interconversion of dihydroxyacetone-phosphate (DHAP) to glyceraldehyde-3-phosphate (G3P).¹¹ Since TIM is present in both *T. cruzi* (TcTIM) and human (HsTIM) cells, and it contains a highly conserved catalytic site, the design of new drugs intended to inhibit the catalytic site must be ruled out. An alternative, extremely hydrophobic, and non-conserved site at the homodimeric interface of the enzyme has been proposed to inhibit its activity. In TcTIM, this region is constituted by aromatic residues, whereas aliphatic and aromatic residues are present in the interface of HsTIM.¹² Several efforts have been made to find a selective inhibitor of TcTIM, in which heterocyclic systems such as phenazine dioxides, thiadiazines and thiazoles have been identified as candidates by high-throughput screening.¹³ A group of amphiphilic benzothiazole derivatives were also identified by in silico studies.^{14,15} These works demonstrate the affinity of the TcTIM interface for molecules with aromatic heterocyclic systems.

Molecular modifications, such as isosteric replacement, represent a useful strategy to find new biologically active compounds and help achieve better pharmacokinetic and pharmacodynamic

* Corresponding author. Tel.: +52 55 56225287; fax: +52 55 56225329.

E-mail address: rafaelc@unam.mx (R. Castillo).

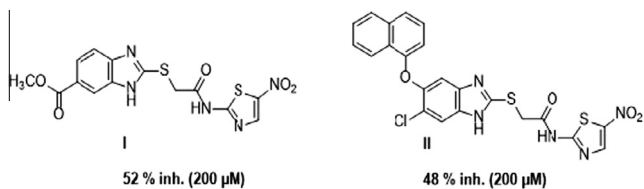
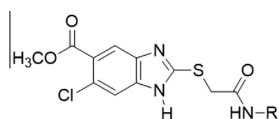


Figure 1. Benzimidazole derivatives and the inhibition presented on TcTIM.

Table 1
Chemical structure of the benzimidazole derivatives **1–14**



Compound	R	Compound	R
1	Pyridin-2-yl	8	Pyridin-4-yl
2	6-Chloropyridin-2-yl	9	Pyrimidin-2-yl
3	6-Methylpyridin-2-yl	10	Pyrazin-2-yl
4	6-Carbamoylpyridin-2-yl	11	Phenyl
5	5-Nitropyridin-2-yl	12	4-Chlorophenyl
6	5-Methoxypyridin-2-yl	13	Thiazol-2-yl
7	5-Chloropyridin-2-yl	14	5-Nitrothiazol-2-yl

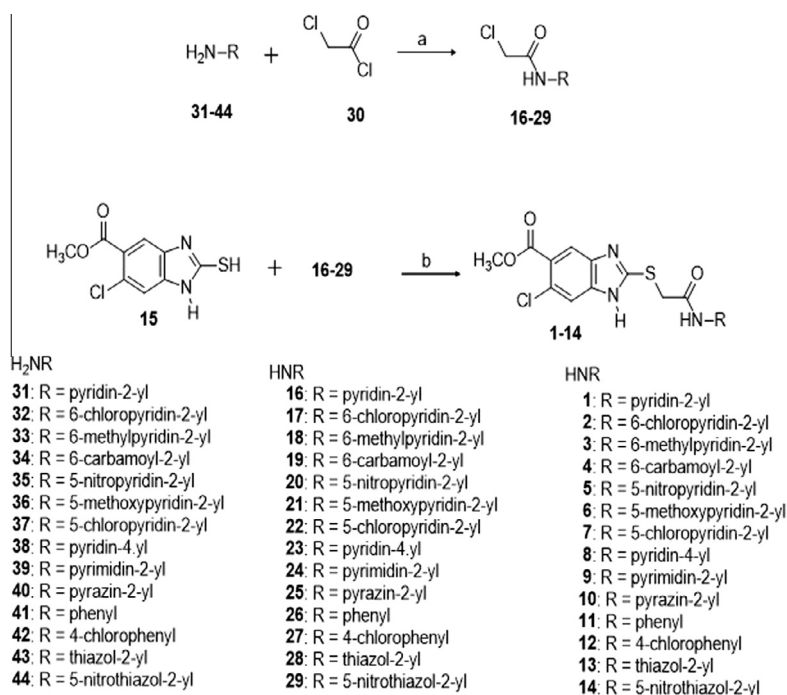
properties. Ligand-based drug design is one of the most important molecular modification tools based on the knowledge of other molecules that bind to the biological target of interest.¹⁶ In this context, our research group has synthesized a large number of benzimidazole derivatives with antiparasitic activities.^{17,18} Some of these compounds present activity as TcTIM inhibitors, such as derivatives (**I**) and (**II**) shown in **Figure 1**. These compounds presented 52% and 48% inhibition at a concentration of 200 μM , respectively.¹⁹

Based on the above study, a set of molecules designed by the isosteric replacement of the thiazole group by pyrazine, pyrimidine, substituted pyridines and substituted anilines (**Table 1**) are proposed in this work. Herein, we present the synthesis, characterization and TcTIM inhibition activities of these compounds. Furthermore, we selected the compounds which showed a significant inhibition of TcTIM to describe their anti-*T. cruzi* activity and cytotoxicity assays.

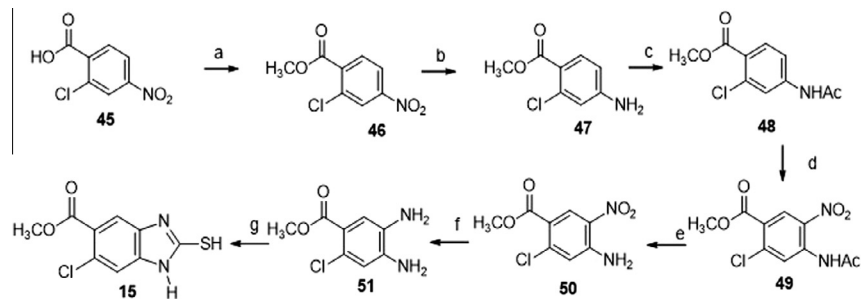
Reaction methyl 6-chloro-2-mercapto-1*H*-benzimidazole-5-carboxylate (**15**) with the appropriate 2-chloroacetamides (**16–29**) by a straightforward substitution reaction afforded the corresponding final product **1–14** as shown in **Scheme 1**. Acetone was used as the solvent and potassium carbonate as a base. The *S*-methylation reactions were carried out at low temperatures to avoid *N*-methylation. The solubility of the compounds obtained and the electronic effect of aromatic amines in the 2-chloroacetamide were decisive in the yields obtained.

In turn, 2-chloroacetamides (**16–29**) were previously synthesized by condensing 2-chloroacetyl chloride (**30**) with the appropriate aromatic amines (**31–44**). Chloroform and triethylamine were used under a N_2 atmosphere.

On the other hand, the synthesis of the common precursor **15** was carried out following the reactions outlined in **Scheme 2**. Compound **15** was prepared by methods previously described by our research group.²⁰ The synthesis started with commercially available 2-chloro-4-nitrobenzoic acid (**45**), which was treated with dimethyl sulfate to obtain methyl 2-chloro-4-nitrobenzoate (**46**). The catalytic reduction of the nitro group with H_2 and Raney nickel at room temperature afforded methyl 4-amino-2-chlorobenzoate (**47**), which upon treatment with Ac_2O led to methyl 4-(acetylamino)-2-chlorobenzoate (**48**). Then, **48** was treated with $\text{HNO}_3/\text{H}_2\text{SO}_4$ at 0–5 $^\circ\text{C}$ to give a mixture of two isomers. The required methyl 4-(acetylamino)-2-chloro-5-nitrobenzoate (**49**) was isolated from the reaction mixture by crystallization. Subsequently, the acetylamino group was hydrolyzed with KOH in EtOH , and methyl 4-amino-2-chloro-5-nitrobenzoate (**50**) was obtained. It is noteworthy that following this procedure, no hydrolysis of the



Scheme 1. Reagents and conditions: (a) NEt_3 , CHCl_3 , 0 $^\circ\text{C}$; (b) K_2CO_3 , Acetone, 0 $^\circ\text{C}$.



Scheme 2. Reagents and conditions: (a) $(\text{Me})_2\text{SO}_4$, NaHCO_3 , DMF; (b) H_2 , Raney-Ni, MeOH; (c) Ac_2O , AcOH; (d) HNO_3 , H_2SO_4 , 0–5 °C; (e) MeOH, KOH; (f) H_2 , Raney-Ni, MeOH, AcOEt; (g) CS_2 , KOH, EtOH.

methyl esters was observed. Compound (**50**) was reduced in a hydrogenation apparatus with H_2 in the presence of Raney nickel to give *o*-phenylenediamine (**51**), then upon cyclocondensation with ethyl xanthate, generated in situ, yield methyl 6-chloro-2-mercapto-1*H*-benzimidazole-5-carboxylate (**15**). The nitration and cyclocondensation reactions are the steps that reduce the total yield of this synthesis. The former gives the 4-(acetamino)-2-chloro-3-nitrobenzoate isomer as a by-product, and the latter gives relative low yields of **15** when the xanthate is generated in situ. The best yields were obtained when the xanthate was previously formed, and then added to the reaction mixture.

In vitro inhibition experiments on TIMs: Previously, it has been observed that benzimidazole derivatives **I** and **II** exhibit moderate inhibitory activity on TcTIM.²¹ In this research, these compounds were used as templates to make structural changes to determine the influence of the substituents on the inhibitory activity. Results obtained from the in vitro evaluation on recombinant TcTIM are summarized in Table 2.

The results indicate some influence of the substituents on the inhibitory activity of TcTIM. The presence of a chlorine atom at position 6(5) of the benzimidazole nucleus in compound **14** increases the inhibitory activity on the enzyme (69%) when compared with its analog compound **I** (52%). None of the substituents at position 2 of the benzimidazole nucleus was better than that with a 5-nitrothiazol-2-yl (**14**), although results obtained from the inhibition with **10** (pirazin-2-yl) and **12** (4-chlorophenyl) are considered.

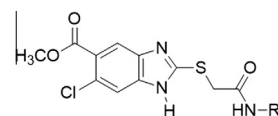
The compounds with the highest inhibition of the enzyme are those with a 4-chlorophenyl group (**12**) and the heterocyclic substituents pyrazine (**10**) and nitrothiazole (**14**); this last one being the most active inhibitor of the enzyme. Compounds having pyridines (**1**, **8**) and aniline (**11**) show low to moderate activity. Compounds **3–5**, with a 6-methylpyridin-2-yl, 6-carbamoylpyridin-2-yl, 6-nitropyridin-2-yl or pyrimidin-2-yl group (**9**), have zero inhibitory activity on the enzyme, while **2** and **7**, with chlorine attached to the pyridine ring, have moderate activity. It is worth mentioning that this group of compounds, except **9**, had low solubilities at 200 μM in DMSO. Hence the study was conducted at a lower concentration of 100 μM .

Figure 2 shows the curves of TcTIM inactivation by compounds **10** and **14**, while Table 3 shows the TcTIM and HsTIM inhibitory activity for compounds **7**, **10**, **12**, **13** and **14**. These results confirm that compound **14** has a slightly better capacity for TcTIM inhibition than compound **10**. However, compound **10** has a higher selectivity towards TcTIM than HsTIM; therefore, this compound is proposed as a potential selective TcTIM inhibitor. Although **7** and **12** have moderate to good TcTIM inhibitory activities and no activity against HsTIM, it was not possible to calculate the IC_{50} because of their low solubilities.

In vitro trypanocidal activity: In vitro trypanocidal assays were performed with compounds **7**, **10**, **12**, **13** and **14** since these

Table 2

In vitro inhibitory activity of compounds (**1–14**) on TcTIM



Compound	R	Concentration (μM)	% Inhibition TcTIM ^a
1	Pyridin-2-yl	200	10
2	6-Chloropyridin-2-yl	100	21
3	6-Methylpyridin-2-yl	100	0
4	6-Carbamoylpyridin-2-yl	100	0
5	5-Nitropyridin-2-yl	100	0
6	5-Methoxypyridin-2-yl	100	4
7	5-Chloropyridin-2-yl	100	41
8	Pyridin-4-yl	200	33
9	Pyrimidin-2-yl	200	0
10	Pyrazin-2-yl	200	68
11	Phenyl	200	33
12	4-Chlorophenyl	100	65
13	Thiazol-2-yl	200	59
14	5-Nitrothiazol-2-yl	200	69

^a Inhibition of TcTIM activity was measured indirectly quantifying the amount of NADH consumed by the reduction of DHAP by α -glycerolphosphate dehydrogenase.²²

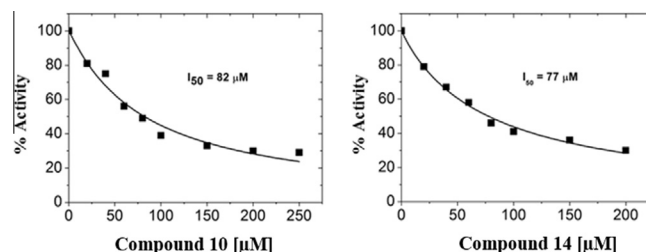


Figure 2. Inactivating curves of compounds **10** and **14**. The IC_{50} for each of the compounds tested in the inactivation of TcTIM was calculated according to Ref. 23.

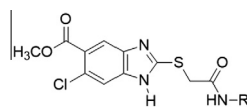
Table 3

In vitro inhibitory activity on HsTIM and TcTIM IC_{50} values

Compounds	% Inhibition TcTIM	IC_{50} TcTIM (μM)	% Inhibition HsTIM ^a
7	41 (100 μM)	—	0 (100 μM)
10	68 (200 μM)	82	6 (200 μM)
12	65 (100 μM)	—	0 (100 μM)
13	59 (200 μM)	223	0 (200 μM)
14	69 (200 μM)	77	15 (200 μM)

^a These experiments were done exactly as those carried out for the TcTIM inhibition described in Ref. 22.

Table 4
In vitro susceptibility of epimastigote to compounds **7**, **10**, **12–14** and NFX



Compound	R	IC ₅₀ INC-5 ^a (μM)	IC ₅₀ NINOA ^a (μM)	CC ₅₀ ^b (μM)
7	5-Chloropyridin-2-yl	95.049 ± 1.749	123.756 ± 2.786	82.732 ± 1.609
10	Pyrazin-2-yl	28.672 ± 0.602	98.799 ± 1.990	134.580 ± 1.995
12	4-Chloro phenyl	186.230 ± 4.103	56.967 ± 0.961	90.436 ± 1.426
13	Thiazol-2-yl	48.912 ± 0.787	119.530 ± 2.151	104.443 ± 1.326
14	5-Nitrothiazol-2-yl	42.516 ± 0.800	95.363 ± 2.143	84.895 ± 1.425
NFX	—	50.750 ± 0.839	89.804 ± 1.138	131.503 ± 0.490

^a The in vitro trypanocidal assays were carried out according to the method previously reported, with slight modifications.²⁷

^b CC₅₀: concentration that produces the cytotoxicity of 50% J774 cells.²⁸

presented the highest inhibitory action on TcTIM. The selected group of compounds was tested against two different strains of *T. cruzi*: INC-5 and NINOA isolated from Instituto Nacional de Cardiología and from a patient with Chagas disease in Oaxaca, México, respectively.²⁴ These compounds were tested against the epimastigote forms of *T. cruzi* (Table 4). Although the epimastigote is not the infective form of the parasite, the trypanocidal activity assay against this form is considered valid since several works demonstrated that the most active compounds against the epimastigote frequently correspond to the most active compounds against the infective trypomastigote.^{25,26}

As shown in Table 4, compound **10** has the best IC₅₀ against the *T. cruzi* epimastigote INC-5 strain, better than that of the reference drug, NFX. Compounds **7** and **12** were the least effective against the INC-5 strain. For this strain, the presence of the pyrazine ring in **10** increases the inhibition of the parasite considerably with respect to compounds with pyridine (**7**), aniline (**12**) and thiazole (**13**, **14**). The results obtained for the inhibition rate of TcTIM for compounds **10**, **13** and **14**, and the data obtained in the test with the parasitic INC-5 strain, it is evident that for all three compounds, there is a significant correlation between the inhibition of *T. cruzi* epimastigotes and TcTIM.

On the other hand, the NINOA strain is more resistant to NFX than the INC-5 strain. Compound **12** (with 4-chloroaniline) has the best IC₅₀ against the NINOA strain, better than that of the reference drug, NFX. Substituted compounds **7** (with pyridine), **10** (with pyrazine) and **13** and **14** (with thiazole) were not better than the reference drug.

Another important criterion in the search for molecules with antiprotozoal activity is their toxicity to mammalian cells. Hence, the *in vitro* cytotoxicity of **7**, **10**, and **12–14** was determined using mouse macrophages from the J744 cell line. As observed in Table 4, compound **10** presents a better cytotoxicity profile than NFX and the best profile in the series. The other compounds (**7**, **12–14**) present slightly higher cytotoxicity than the reference drug.

In summary, the final compounds (**1–14**) were obtained in moderate to good yields. Only four compounds (**10**, **12**, **13**, **14**) inhibited TcTIM significantly with compound **10** being distinguished from the others since it presented a good inhibition of TcTIM and a very low activity against HsTIM. Compound **10** also showed better inhibitory activity than NFX against *T. cruzi* epimastigotes of the INC-5 strain, and a more favorable cytotoxicity profile in mammalian cells.

Acknowledgments

We thank CONACyT for financing projects 168718 and 251716, and for the scholarship granted (295663/225078) to J.M.V. We are also grateful to Rosa Isela del Villar, Minerva Monroy Barreto,

Marisela Gutiérrez Franco and Georgina Duarte for the analytical support offered. We also thank Anuar Flores Gahona, Rodrigo Aguayo Ortiz from Facultad de Química, UNAM and Natalie Crespo Velasco from facultad de CIQ-UAEM for the review of this paper and the helpful suggestions.

Supplementary data

Supplementary data associated with this article can be found, in the online version, at <http://dx.doi.org/10.1016/j.bmcl.2015.08.018>. These data include MOL files and InChIKeys of the most important compounds described in this article.

References and notes

- Maya, J. D.; Cassels, B. K.; Iturriaga-Vásquez, P.; Ferreira, J.; Faúndez, M.; Galanti, N.; Ferreira, A.; Morello, A. *Comp. Biochem. Physiol. A: Mol. Integr. Physiol.* **2007**, *146*, 601.
- Kryshchshyn, A.; Kaminsky, D.; Grellier, P.; Lesyk, R. *Eur. J. Med. Chem.* **2014**, *85*, 51.
- Ribeiro, I.; Sevcsik, A.-M.; Alves, F.; Diap, G.; Don, R.; Harhay, M. O.; Chang, S.; Pecoul, B. *PLoS Negl. Trop. Dis.* **2009**, *3*, e484.
- Rassi, A.; Marin-Neto, J. A. *Lancet* **2010**, *375*, 1388.
- Papadopoulou, M. V.; Bloomer, W. D.; Rosenzweig, H. S.; Wilkinson, S. R.; Kaiser, M. *Eur. J. Med. Chem.* **2014**, *87C*, 79.
- Soeiro, M. D. N. C.; de Castro, S. L. *Open Med. Chem. J.* **2011**, *5*, 21.
- Dias, L. C.; Física, I. De; Carlos, D. S.; Paulo, U. D. S.; Sp, S. C. *Quim. Nov.* **2009**, *32*, 2444.
- Matera, R.; Alves, D. A.; Thomaz, R. P.; Almeida, E. A. *Rev. Soc. Bras. Med. Trop.* **2009**, *42*, 622.
- Lakhdar-Ghazal, F.; Casimir, B.; Willson, M.; Michels, P.; Perie, J. *Curr. Top. Med. Chem.* **2002**, *2*, 439.
- Oppendoes, F. R.; Michels, P. A. M. *Int. J. Parasitol.* **2001**, *31*, 482.
- Zomosa-Signoret, V. *Proteins Struct. Funct. Bioinf.* **2007**, *83*, 75.
- Olivares-Illana, V.; Pérez-Montfort, R.; López-Calahorra, F.; Rodríguez-Romero, A.; Gómez Puyou, A. *Biochemistry* **2006**, 2556.
- Alvarez, G.; Aguirre-López, B.; Varela, J.; Cabrera, M.; Merlino, A.; López, G. V.; Lavaggi, M. L.; Porcal, W.; Di Maio, R.; González, M.; Cerecetto, H.; Cabrera, N.; Pérez-Montfort, R.; de Gómez-Puyou, M. T.; Gómez-Puyou, A. *Eur. J. Med. Chem.* **2010**, *45*, 5767.
- Téllez-Valencia, A.; Olivares-Illana, V.; Hernández-Santoyo, A.; Pérez-Montfort, R.; Costas, M.; Rodríguez-Romero, A.; López-Calahorra, F.; De Gómez-Puyou, M. T.; Tuena; Gómez-Puyou, A. *J. Mol. Biol.* **2004**, *341*, 1355.
- Espinoza-Fonseca, L. M.; Trujillo-Ferrara, J. G. *Bioorg. Med. Chem. Lett.* **2006**, *16*, 6288.
- Guido, R. V. C.; Oliva, G.; Andricopulo, A. D. *Pure Appl. Chem.* **2012**, *84*, 1857.
- Soria-Arteche, O.; Hernández-Campos, A.; Yépez-Mulia, L.; Trejo-Soto, P. J.; Hernández-Luis, F.; Gres-Molina, J.; Maldonado, L. A.; Castillo, R. *Bioorg. Med. Chem. Lett.* **2013**, *23*, 6838.
- Navarrete-Vásquez, G.; Cedillo, R.; Hernández-Campos, A.; Valdez, J.; Castillo, R. *Bioorg. Med. Chem. Lett.* **2001**, *11*, 187.
- Romo-Mancillas, A.; Téllez-Valencia, A.; Yépez-Mulia, L.; Hernández-Luis, F.; Hernández-Campos, A.; Castillo, R. *J. Mol. Graphics Modell.* **2011**, *30*, 90.
- Perez-Villanueva, J.; Hernández-Campos, A.; Yépez-Mulia, L.; Castillo, R. *Bioorg. Med. Chem. Lett.* **2013**, *23*, 4221.
- Olivares-Illana, V.; Pérez-Montfort, R.; López-Calahorra, F.; Costas, M.; Rodríguez-Romero, A.; de Gómez-Puyou, M. T. *Biochemistry* **2006**, *45*, 2556–2560.
- In vitro inhibition TIM experiments*: Recombinant TcTIM or HsTIM at a concentration of 5 μg/mL were incubated at 36 °C in a buffer containing

- 100 mM triethanolamine, 10 mM EDTA, pH 7.4 and the compound to be tested (**1–14**) were dissolved in 10% of dimethyl sulfoxide (DMSO). After 2 h, 1 μ L was withdrawn and added to 1 mL of the reaction mixture for the activity assay. Inhibition of TcTIMs activity was measured indirectly quantifying the amount of NADH consumed by the reduction of DHAP by α -glycerolphosphate dehydrogenase. Controls were performed using enzyme alone, substrate alone, and enzyme with DMSO.
23. Téllez-Valencia, A.; Avila-Ríos, S.; Pérez-Montfort, R.; Rodríguez-Romero, A.; Tuena de Gómez-Puyou, M.; López-Calahorra, F.; Gómez-Puyou, A. *Biochem. Biophys. Res. Commun.* **2002**, *295*, 958.
 24. de Ornelas Toledo, M. J.; Bahia, M. T.; Carneiro, C. M.; Martins-Filho, O. A.; Tibayrenc, M.; Barnabé, C.; Tafuri, W. L.; de Lana, M. *Antimicrob. Agents Chemother.* **2007**, *47*, 223.
 25. Cauputto, M. E.; Ciccarelli, A.; Frank, F.; Finkielstein, L. M. *Eur. J. Med. Chem.* **2012**, *55*, 155.
 26. Carneiro, P. F.; Do-Nascimento, S. B.; Pinto, A. V.; Ferreira, V. F. *Bioorg. Med. Chem.* **2012**, *20*, 4995.
 27. *Biological assays against T. cruzi*: epimastigote forms of the NINOA and INC-5 strains (isolated from a patient with Chagas disease in Oaxaca, Mexico and Instituto Nacional de Cardiología) of *T. cruzi* were used in this study. *T. cruzi* epimastigotes were grown at 28 °C in a liquid medium containing 0.3% yeast extract, 0.9% tryptose, 0.4% dextrose, 1% disodium phosphate 2-hydrate, 0.36% sodium chloride, 0.04% potassium chloride, 0.15% powdered beef liver, 0.5% brain heart infusion, and 0.5 to 1.0 mg/100 mL hemin. Stock solutions (10 mg/mL) in DMSO of each test compound and reference drug were prepared and subsequent dilutions were done with sterile distilled water. Experiments were carried out using 96-well microplates containing 1×10^5 epimastigotes/mL. The compounds were dissolved in dimethyl sulfoxide (DMSO; final solvent concentration not greater than 1%) and were evaluated at 100, 50, 10, and 5 μ g/mL. For each experiment there were controls of parasites growing in the presence of DMSO. The different mixtures and their corresponding concentrations were added to the wells, and the plates were incubated at 28 °C for 24 h. All assays were performed in duplicate. The activity was evaluated using the resazurin. The plates were read at 535 nm em, 590 nm ex, on a multiwell plate spectrophotometer. The activity is expressed as IC₅₀ (μ M/mL).
 28. *Cytotoxicity test*: mouse macrophages from J744 cell line (J744 cells) was used to assess the cytotoxic effects on mammalian cells. The cells were cultured in standard culture medium (DMEM with 10% Fetal Bovine Serum). The cultures were incubated for 24 h at 37 °C, 5% CO₂ and 95% relative humidity with different concentrations of test compounds and reference drug. The final concentration of DMSO, used as solvent, remained below 1% in the culture medium. Untreated cells were included as controls. The cytotoxicity was determined by the resazurin method. Briefly, resazurin solution were added to each well and the plates were incubated for 3 h. The fluorescence emission was measured as indicated above, (535 nm em, 590 nm ex), on a multiwell plate spectrophotometer. Cytotoxicity was scored as a percent of metabolic reduction of treated cultures versus untreated control cells.